

Feasibility Study of a Load Alleviation Strategy on a Compound Helicopter Using Redundant Controls

MSc Thesis

L. Declerck

Delft University of Technology



Feasibility Study of a Load Alleviation Strategy on a Compound Helicopter Using Redundant Controls

MSc Thesis

by

L. Declerck

to obtain the degree of Master of Science
at the Delft University of Technology
to be defended publicly on Friday November 29, 2019 at 14:00.

Student number: 4206622
Project duration: December, 2019 – November, 2019
Thesis committee: Prof. dr. ir. C. J. Simão Ferreira, TU Delft, daily supervisor, chair
Prof. dr. ir. M. Voskuil, Ministerie van Defensie, daily supervisor
Dr. M. D. Pavel, TU Delft
Prof. dr. ir. G. Eitelberg, TU Delft

An electronic version of this thesis is available at <http://repository.tudelft.nl/>.

Preface

This report will present my thesis research as final part of my MSc in Aerospace Engineering at the Delft University of Technology. The research will investigate the feasibility of a load alleviation strategy using the redundant controls of a compound helicopter configuration.

My interest in rotorcraft sparked during my BSc thesis where I worked on the preliminary design of a sustainable coaxial helicopter. During my masters, I got introduced to the field of helicopters, a world of dynamics and applied aerodynamics with elegant mathematical tricks to capture physical phenomena. Coming back from my internship at Airbus UK where I worked on fixed wing aircraft, the rotorcraft field attracted me even more as it feels like there is still a lot to understand and optimise. During my thesis, I entered the world of rotorcraft experts and read research papers about special modelling techniques and rotorcraft optimisation on a level I did not expect. It is amazing to see how this community conquers physics and pushes for new innovations on helicopters.

The main focus of this work lies in the construction of the compound helicopter model. The goal is to provide insights into the aerodynamic and rotor flap dynamic effects that influence loads in the main rotor hub. Simple control strategies are tested and evaluated against load reduction and handling qualities. The constructed helicopter model and insights about the rotor situation can be taken to a next level by future researchers to design an optimal control strategy to alleviate loads.

I would like to express my gratitude to my supervisor Mark Voskuijl at the NLDA for answering all my technical questions and scheduling time for our meetings. I also thank Carlos Simão Ferreira, my supervisor at the TU Delft, for guiding me through the different phases of this challenging assignment. A special thank you goes to Ramon for participating in the development of the helicopter model.

Throughout my student years, I could always count on the endless support of my family. Especially my parents who always helped me to pursue my goals, therefore, a special thank you. I also thank my friends and flatmates for their support during my thesis assignment.

Laurent Declerck
Delft, November 2019

Abstract

The compound helicopter gains interest as operational needs push future rotorcraft capabilities beyond current standards. The compound helicopter is investigated as part of the Future Vertical Lift Program to replace the entire U.S. Army helicopter fleet. The compound helicopter resembles a mix between a fixed-wing aircraft and a conventional helicopter. It features a controllable rotor as well as wings, elevator, ailerons and a push propeller near the tail. Increased agility is achieved by the unique combination of controls and the maximum flying speed is expanded by unloading the rotor lift and redistributing it over the wings. However, manoeuvring at faster speeds comes at a cost. High loads in the rotor hub are expected.

Because of this unique helicopter configuration, some of the controls can be seen as redundant. This enables multiple combinations of control inputs to generate a (near) identical helicopter state. Therefore, the redundant controls can be used for a secondary objective next to manoeuvring the rotorcraft. The thesis will investigate the feasibility of using the redundant controls of a compound helicopter to alleviate loads in the rotor hub during an aggressive roll manoeuvre. This cuts down maintenance costs of highly loaded components and increases their reliability. The focus lies on understanding the physical phenomena leading up to alleviating loads.

A multi-body dynamics model of the compound UH-60A Black Hawk was constructed to simulate manoeuvring flight. The main rotor is represented as a blade element model with a Peters-He inflow model. Aerodynamic coefficients are found from quasi-steady look-up tables. Blades are assumed to be rigid and feature a feather and flap hinge. The fuselage aerodynamics are interpolated from test data. The empennage is modelled using 2D look-up tables to compute the aerodynamic coefficients. The wing and push propeller, unique to the compound helicopter type, are modelled by a non-linear lifting line and a point force acting near the tail respectively. A flight controller was implemented as the fly-to-trim method was used to find the trim condition. The model was validated against FLIGHTLAB for trim and a rolling manoeuvre. The main wing lifting line was separately validated against a vortex lattice method.

The first experiment varies the control strategy to alleviate loads during the roll doublet. Either a pure lateral cyclic, pure aileron or a 50% cyclic - 50% aileron input are investigated. When a pure lateral cyclic input is used, the rotor will lead the roll and the fuselage will follow. This effect is reversed as the rotor lags when a pure aileron input is used. The rotor smoothly follows the fuselage's roll motion when both controls are combined. This is caused by the reversed lateral flapping response switching from a pure cyclic to a pure aileron input. The combined input levels out the flapping response. As the moment measured in the hub is linked to the flap angle, loads are reduced from a factor > 7 for a pure cyclic or aileron input, to a factor ~ 2 for the combined input.

A second experiment investigates the effect of different trim settings prior to the roll manoeuvre. The horizontal tail deflection, compound thrust, rotor rpm and constant aileron input at trim are varied separately. This enables the helicopter to offload both the lifting and propulsive function of the main rotor and reduce the power required in cruise. Depending on which controls are used to achieve the trim state, loads in the hub are increased or decreased. Longitudinal hub moment loads are decreased when the required longitudinal cyclic is alleviated using the horizontal tail or compound thrust. The effect on the lateral hub moments scale with the offloading of the main rotor, except when a constant aileron input is applied at trim. A constant aileron input will lower the power required by pushing the lift more outboard over the advancing blade. The required cyclic input to counter this aileron deflection increases the lateral hub moments.

The final experiment combines the two others by defining a suboptimal trim condition and varying the control strategy during the roll doublet, according to the first experiment. It was confirmed that the 50% lateral cyclic - 50% aileron input reduces lateral blade flapping which lowers the lateral bending moment in the hub. Longitudinal bending loads are alleviated as both the lift and propulsive function of the main rotor are alleviated. This also reduces the power required in cruise. The 50% lateral cyclic - 50% aileron input increases the control power and shows to be beneficial for handling qualities.

Contents

List of Symbols	ix
Nomenclature	xi
List of Figures	xiii
List of Tables	xvii
1 Introduction	1
1.1 Compound Helicopter Definition	2
1.2 Research Objective	2
1.3 Project and Report Outline	3
2 Literature Review	5
2.1 The Compound Helicopter Through Time	5
2.2 Critical Load Situation	6
2.2.1 Rotorcraft Requirements for Future Configurations and Missions	6
2.2.2 The Break-Turn Mission Task Element	7
2.2.3 Link Between Rotor Phenomena and Critical Loads	9
2.3 Load Alleviation Strategies	10
2.3.1 Tactile Cueing on Conventional Helicopters	11
2.3.2 Structural Load Alleviation Strategies on Conventional Helicopters	11
2.3.3 Structural Load Alleviation Strategies on Compound Helicopters	12
2.3.4 Discussion of Load Alleviation Results from Literature and Link with Thesis Research. . .	13
2.4 Compound Helicopter Principles	15
2.4.1 Slower Rotor and Auxiliary Thrust Operational Envelope	15
2.4.2 Elevator Effects	15
2.4.3 Ailerons Effects	17
2.4.4 Lift Compounding Effects	18
2.4.5 Thrust Compounding Effects	19
3 Compound Helicopter Model	21
3.1 Multi-Body Dynamics General Modelling Approach	21
3.2 Structure of the Multi-Body Dynamics and Aerodynamic Model	22
3.3 Main Rotor Model.	23
3.3.1 Airloads	24
3.3.2 Induced Inflow Model	24
3.3.3 Rotor Dynamics	25
3.4 Tail Rotor Model	25
3.5 Fuselage Aerodynamic Model.	25
3.6 Horizontal and Vertical Tail Model	26
3.7 Compound Wing Model.	26
3.7.1 Non-Linear Lifting Line Model.	27
3.8 Compound Thrust Model	29
4 Flight Controller Design for Trim	31
4.1 Trim Method Approach	31
4.2 Trim Controller Architecture	32
4.3 Controller Tuning and Applicability on a Compound Helicopter Type	33

5	Model Validation	35
5.1	Model Differences Between the Constructed Multi-Body Dynamics Model and FLIGHTLAB . . .	35
5.2	Validation of the Trim Condition	36
5.2.1	Trim Validation Conventional UH-60A Model, without Inflow	36
5.2.2	Trim Validation Conventional UH-60A Model, with Peters-He Inflow	39
5.3	Validation of Roll Manoeuvre	46
5.3.1	Dynamic Response Parameter Definitions	46
5.3.2	Validation of the Response to a Lateral Input.	46
5.4	Compound Wing Model Validation	48
5.5	Validation Conclusion	49
6	Load Alleviation Experiments and Results	51
6.1	Varying the Control Strategy to Alleviate Loads in the Rotor Hub	51
6.1.1	Experiment Set-up	51
6.1.2	Results	52
6.1.3	Discussion of the Link Between Loads and Blade Flapping.	54
6.1.4	Discussion of a Pure Lateral Cyclic Input Strategy	60
6.1.5	Discussion of a Pure Aileron Input Strategy	63
6.1.6	Discussion of a 50% Lateral Cyclic - 50% Aileron Input Strategy	65
6.2	The Effect of Different Trim Settings on Loads in the Rotor Hub.	67
6.2.1	Experiment Set-up	68
6.2.2	Results	69
6.2.3	Discussion of the Effect by an Elevator Deflection at Trim	69
6.2.4	Discussion of the Effect by Compound Thrust at Trim	71
6.2.5	Discussion of the Effect by a Lower Main Rotor RPM at Trim.	72
6.2.6	Discussion of the Effect by a Constant Aileron Deflection at Trim	73
6.3	Varying the Control Strategy at a Suboptimal Trim Setting	75
7	Conclusion	79
7.1	Recommendations	81
7.1.1	Compound Helicopter model	81
7.1.2	Load Alleviation Strategy.	81
A	Reference Frames	83
B	Trim Validation Conventional UH-60A Model without Inflow Model	85
C	Trim Validation Conventional UH-60A Model with Peters-He Inflow Model	95
D	The Effect of Different Trim Settings on Loads in the Rotor Hub	107
D.1	Effect of Horizontal Tail Deflection on Responses and Loads During Roll Doublet	107
D.2	Effect of Compound Thrust on Responses and Loads During Roll Doublet	112
D.3	Effect of Lowering the Main Rotor RPM on Responses and Loads During Roll Doublet	117
D.4	Effect of a Constant Aileron Input in Trim on Responses and Loads During Roll Doublet	122
D.5	Suboptimal Cruise Condition Responses and Loads During Roll Doublet	127
	Bibliography	133

List of Symbols

b	Wing half span	[m]
D	Damage	[-]
c	Climb rate	[m/s]
C_t	Thrust coefficient	[-]
e_β	Bearing offset	[m]
F_{body}	Aerodynamic force on fuselage	[N]
F_C	Centrifugal force	[N]
F_{pk}	Peak force	[N]
F_r	Resultant force	[N]
F_{trim}	Force at trim	[N]
G	Gravitational acceleration	[m/s ²]
i_{tail}	Elevator deflection	[°]
N	Amount of cycles	[-]
$n_{z_{lim}}$	Normal load factor operational flight envelope limit	[g]
M_{body}	Aerodynamic moment on fuselage	[N]
r/R	Relative blade span location	[-]
$T_{transient}$	Transient time in sec (roll-in/out)	[sec]
V_H	Maximum flying speed at maximum continuous power	[kts]
V_i	Induced velocity	[m/s]
Q	Torque	[Nm]
Q_{xx}	Quickness (xx is generic subscript)	[-]
α	Angle of attack	[°]
α_s	Hub orientation	[°]
δ	Aileron deflection	[°]
β_0	Coning angle	[°]
β_1	First harmonic flapping	[°]
β_{1s}	Lateral flapping	[°]
β_{1c}	Longitudinal flapping	[°]
$\Delta\varphi_{transient}$	Heading angle change during transient phase in deg (roll-in/out)	[°]
γ	Flight path angle	[°]
ψ	Yaw angle	[°]
ϕ	Roll angle	[°]
ϕ_{pk}	Peak roll angle	[°]
Ω	Rotational speed , azimuth angle	[rad/s],[°]
σ	Rotor solidity	[-]
θ	Flight path angle	[°]
θ_1	Blade root pitch angle	[°]
θ_{1s}	Longitudinal cyclic	[°]
θ_{1c}	Lateral cyclic	[°]
θ_0	Collective	[°]
θ_{pk}	Peak pitch angle	[°]
θ_{TR}	Tail rotor collective	[°]
μ	Advance ratio	[-]

Nomenclature

AGL	Above Ground Level
DoF	Degrees of Freedom
FAA	Federal Aviation Administration
FCS	Flight Control System
GENHEL	U.S. Army General Helicopter Model
HQ	Handling Qualities
LAF	Load Amplification Factor
LE	Leading edge
LTI	Linear Time Invariant
LTP	Linear Time Periodic
MTE	Mission Task Element
NFAC	U.S. Airforce National Full-Scale Aerodynamics Complex
NRTC	U.S. Army's National Rotorcraft Technology Center
OFE	Operational Flying Envelope
RCAS	U.S. Army's Rotorcraft Comprehensive Analysis System
SLA	Structural Load Alleviation
TE	Trailing edge
UTTAS	Army Utility Tactical Transport Aircraft System
U.S.	United States
VNE	Velocity never to exceed

List of Figures

1.1	Airbus X ³ demonstrator [2]	2
1.2	Sikorsky X2 demonstrator [5]	2
1.3	Visual representation of the compound UH-60A modelled in this research [47]	3
1.4	Thesis project flow chart	4
2.1	Sikorsky-Boeing Defiant [48]	5
2.2	AVX Entrant [48]	5
2.3	Bell V-280 Valor [48]	5
2.4	Piasecki 16H-1A Pathfinder [48]	6
2.5	Lockheed XH-51A [48]	6
2.6	Lockheed AH-56A Cheyenne [47]	6
2.7	X-49 Speed Hawk [47]	6
2.8	Break Turn MTE visual cue in simulator [12]	7
2.9	Flap bending harmonic motions comparing the UH-60A rotor at nominal rpm (dots) with 40% of the nominal rpm (lines) for different advance ratios (μ) and thrust settings C_T/σ [17]	10
2.10	General control configuration H_∞ method [52]	12
2.11	Non-linear response roll doublet, Euler angles [44]	13
2.12	Non-linear response roll doublet, angular rates [44]	13
2.13	Control inputs during roll doublet [44]	14
2.14	Main rotor hub forces and moments during roll doublet [44]	14
2.15	Compound helicopter main rotor rpm and auxiliary thrust envelope, trim state A [42]	15
2.16	Force equilibrium trim state A [42]	16
2.17	Force equilibrium trim state B [42]	16
2.18	Compound helicopter main rotor rpm and auxiliary thrust envelope, trim state B [42]	17
2.19	Force equilibrium trim state B [42]	18
2.20	Force equilibrium trim state C [42]	18
2.21	Local angle of attack of counter clock rotating rotor, left trim state B, right trim state C [42]	18
2.22	Compound helicopter main rotor rpm and auxiliary thrust envelope, trim state C and D [42]	18
2.23	Up: fully loaded rotor, Down unloaded rotor with wings generating part of the lift	19
2.24	Effect of auxiliary lift and thrust on the blade angle of attack [45]	19
3.1	Helicopter model approach	22
3.2	Overview of multi-body model	23
3.3	Overview of aerodynamic models	23
3.4	Coupling between blade dynamics, lifting theory and inflow	25
3.5	Lifting line horseshoe vortex	28
3.6	Lifting line convergence algorithm flowchart	29
4.1	UH-60A control system overview	33
4.2	Height controller flow diagram	33
4.3	Longitudinal controller flow diagram	33
4.4	Lateral controller flow diagram	33
4.5	Directional controller flow diagram	34
5.1	Forward speed tracking during 'fly-to-trim'	36
5.2	Vehicle Euler angles during 'fly-to-trim'	36
5.3	Blade root pitch angle, no inflow model	38
5.4	Flapping angle, no inflow model	38
5.5	Total hub force: $\sqrt{F_x^2 + F_y^2 + F_z^2}$, no inflow model	39

5.6	Total hub moment: $\sqrt{M_x^2 + M_y^2 + M_z^2}$, no inflow model	39
5.7	α SimMechanics 120 kts, no inflow model	40
5.8	α Flightlab 120 kts, no inflow model	40
5.9	c_l SimMechanics 120 kts, no inflow model	40
5.10	c_l Flightlab 120 kts, no inflow model	40
5.11	c_d SimMechanics 120 kts, no inflow model	40
5.12	c_d Flightlab 120 kts, no inflow model	40
5.13	Blade root pitch angle, Peters-He inflow	42
5.14	Flapping angle, Peters-He inflow	42
5.15	Total hub force: $\sqrt{F_x^2 + F_y^2 + F_z^2}$, Peters-He inflow	43
5.16	Total hub moment: $\sqrt{M_x^2 + M_y^2 + M_z^2}$, Peters-He inflow	43
5.17	α SimMechanics 120 kts, Peters-He inflow	44
5.18	α Flightlab 120 kts, Peters-He inflow	44
5.19	c_l SimMechanics 120 kts, Peters-He inflow	44
5.20	c_l Flightlab 120 kts, Peters-He inflow	44
5.21	c_d SimMechanics 120 kts, Peters-He inflow	44
5.22	c_d Flightlab 120 kts, Peters-He inflow	44
5.23	v_i SimMechanics 120 kts, Peters-He inflow	45
5.24	v_i Flightlab 120 kts, Peters-He inflow	45
5.25	Lateral cyclic impulse of 2 seconds	47
5.26	θ response lateral impulse	47
5.27	ϕ response lateral impulse	47
5.28	ψ response lateral impulse	47
5.29	q response lateral impulse	47
5.30	p response lateral impulse	47
5.31	r response lateral impulse	47
5.32	F_{tot} response lateral impulse	48
5.33	M_{tot} response lateral impulse	48
5.34	Roll quickness lateral impulse at 45kts	48
5.35	Load quickness lateral impulse at 45kts	48
5.36	Moment quickness lateral impulse at 45kts	48
5.37	C_l wing distribution vortex lattice method against lifting line method at different α	49
5.38	C_l wing distribution vortex lattice method against lifting line method at different α and aileron deflection δ	49
6.1	Doublet input: pure lateral cyclic (lat cyc), pure ailerons and 50% lateral cyclic - 50% ailerons (combi)	52
6.2	F_y response after roll doublet	53
6.3	Forces acting on blade with flap hinge and flap hinge offset	54
6.4	F_y forces measured at the flapping hinge, modified from [42]	55
6.5	θ response roll right doublet	56
6.6	ϕ response roll right doublet	56
6.7	ψ response roll right doublet	56
6.8	p response roll right doublet	56
6.9	β_{1c} response roll right doublet	56
6.10	β_{1s} response roll right doublet	56
6.11	F_x response roll right doublet	57
6.12	F_y response roll right doublet	57
6.13	F_z response roll right doublet	57
6.14	M_x response roll right doublet	57
6.15	M_y response roll right doublet	57
6.16	M_z response roll right doublet	57
6.17	F_x quickness roll-in	58
6.18	F_y quickness roll-in	58
6.19	F_z quickness roll-in	58

6.20 M_x quickness roll-in	58
6.21 M_y quickness roll-in	58
6.22 M_z quickness roll-in	58
6.23 F_x quickness roll-out	59
6.24 F_y quickness roll-out	59
6.25 F_z quickness roll-out	59
6.26 M_x quickness roll-out	59
6.27 M_y quickness roll-out	59
6.28 M_z quickness roll-Out	59
6.29 Roll attitude quickness roll-in	60
6.30 Roll attitude quickness roll-out	60
6.31 Blade flapping during doublet using lateral cyclic or aileron input, modified from [42]	60
6.32 Absolute lateral flapping angle compared with roll angle for both lateral cyclic and aileron input doublet	61
6.33 α over the main rotor disk in trim 120 kts	62
6.34 α at max right lateral cyclic input, 2.2 s	62
6.35 α at max left lateral cyclic input, 5 s	62
6.36 α at max right aileron input, 2.2 s	62
6.37 α at max left aileron input, 5 s	62
6.38 Sideways velocity v during roll doublet	63
6.39 Lateral flapping due to roll rate (left rear view, right front view), modified from [42]	64
6.40 Lateral flap angle causing a damping moment during the rolling motion, modified from [42]	64
6.41 Incoming flow difference over left and right blade due to rolling motion, modified from [42]	65
6.42 Possible blade stall during roll-out with ailerons, c_l on left disk plot, α on right disk plot	66
6.43 Absolute lateral flapping angle compared with roll angle for roll doublet using both 50% aileron and 50% lateral cyclic input	66
6.44 Attitude quickness roll-in	67
6.45 Airbus Racer [1]	68
6.46 BELL 360 Invictus [3]	68
6.47 Sikorsky-Boeing SB>1 DEFIANT [4]	68
6.48 β_{1c} , roll doublet, 50% cyclic - 50% aileron input	69
6.49 β_{1s} , roll doublet, 50% cyclic - 50% aileron input	69
6.50 F_x , roll doublet, 50% cyclic - 50% aileron input	71
6.51 M_y , roll doublet, 50% cyclic - 50% aileron input	71
6.52 α over disk at 2.2 seconds of roll doublet, $i_{tail} = 0^\circ$	71
6.53 α over disk at 2.2 seconds of roll doublet, $i_{tail} = 5^\circ$	71
6.54 α over disk at trim, compound thrust = 0 N	72
6.55 α over disk at trim, compound thrust = 5000 N	72
6.56 F_z , roll doublet, 50% cyclic - 50% aileron input	72
6.57 M_x , roll doublet, 50% cyclic - 50% aileron input	72
6.58 Q_{F_y} , roll doublet 50% cyclic - 50% aileron input	73
6.59 Q_{M_x} , roll doublet 50% cyclic - 50% aileron input	73
6.60 β_{1c} , roll doublet, 50% cyclic - 50% aileron input	73
6.61 β_{1s} , roll doublet, 50% cyclic - 50% aileron input	73
6.62 β_{1s} , roll doublet, 50% cyclic - 50% aileron input	74
6.63 M_x , roll doublet, 50% cyclic - 50% aileron input	74
6.64 Q_{M_x} roll-in, roll doublet 50% cyclic - 50% aileron input	74
6.65 Q_{M_x} roll-in, roll doublet 50% cyclic - 50% aileron input	75
6.66 Q_{M_y} roll-in, roll doublet 50% cyclic - 50% aileron input	75
6.67 Q_p roll-in, roll doublet 50% cyclic - 50% aileron input	75
6.68 ϕ , suboptimal trim condition roll doublet	76
6.69 Q_p , suboptimal trim condition roll-out section doublet	76
6.70 M_x , suboptimal trim condition roll doublet	76
6.71 M_y , suboptimal trim condition roll doublet	76
6.72 Q_{M_x} , suboptimal trim roll-in section doublet	77
6.73 Q_{M_x} , suboptimal trim roll-out section doublet	77

List of Tables

2.1	Break Turn MTE performance standards [12]	8
2.2	UH-60A most critical manoeuvres [31]	9
2.3	Trim state details [42]	16
3.1	Main Rotor Specifications	24
3.2	Horizontal stabiliser and vertical fin specifications according to Sikorsky [27]	26
3.3	Compound Wing Specifications	27
5.1	Comparison SimMechanics/Simulink (Sim) - Flightlab (FL), no inflow model	37
5.2	Comparison of the constructed model in SimMechanics/Simulink (Sim) - Flightlab (FL), Peters-He inflow model	41
6.1	Test Matrix	68
6.2	Trim settings at different trim conditions	70

1

Introduction

The compound helicopter finds its roots in the 1950s as the U.S. military investigated combining high speed and efficient cruise capabilities with vertical take-off and hover. However, the compound helicopter never found its breakthrough as the military decided to deploy tiltrotor aircraft with better cruise performance [35].

Today, the compound helicopter concept is reviving as both civil and military organisation consider this configuration for future operations. Technology demonstrators developed over the past few years like the Airbus X³, Figure 1.1 and the Sikorsky X2 Figure 1.2 showed the impressive capabilities of this unique concept. Studies by NASA and the U.S. Army demonstrate how today's compound helicopter concept can close the performance gap between its rotary opponent, the tiltrotor [35].

In 2008, the 'Future Vertical Lift' program was started, aiming to replace all U.S. military helicopters with next generation rotorcraft [24]. Several aircraft types are considered including the compound helicopter. Rotorcraft capabilities are pushed beyond the current standards as operational needs ask for increased agility and higher flying speeds. But the improvements in performance are expected to increase the loads in the rotor system.

As part of the Vertical Lift plan, the U.S. government together with the U.S. rotorcraft industry initiated a joined program: 'Rotorcraft Handling Qualities Requirements for Future Configurations and Missions' by the US Army's National Rotorcraft Technology Center (NRTC) [12]. Within this program, new mission task elements are proposed. The thesis research will focus on the new break-turn mission task element (MTE) executed by a wing and thrust compound version of the UH-60A Black Hawk. This specific rotorcraft has also been used by recent studies to evaluate the handling quality while executing the break-turn [12]. The break-turn is an aggressive roll manoeuvre reaching a bank angle of 60 degrees.

The compound helicopter has redundant controls resulting in multiple feasible combinations of control inputs that achieve a (near-)identical helicopter state. This unique configuration comes with the opportunity of using the redundant controls for structural load alleviation purposes. Next to the primary function of the controls, they are given a second objective: reducing loads. The thesis research will investigate the feasibility of using the redundant controls of a compound UH-60A Black Hawk to alleviate loads in the main rotor hub during the execution of the break-turn MTE.

An active structural load alleviation (SLA) system strives to reduce the rotor loads over their operational lifetime. This cuts maintenance costs and improves component reliability. In the far future and depending on the applicable regulations, SLA systems can potentially be used to push rotorcraft performance even more. As loads are reduced, the rotorcraft can potentially fly manoeuvres which were previously outside its operational envelope. This opportunity has recently been demonstrated even within the civil aviation world as the FAA certified the Boeing B787-8F with a working active flutter suppression system operating within the certification envelope [19]. Without this system, FAA flutter requirements were not met.

Theoretical studies show the potential of using redundant controls to successfully alleviate loads at an acceptable degradation of handling qualities on conventional helicopters. The richer variety of redundant controls of a compound helicopter configuration is expected to alleviate loads in much more extreme conditions at a low cost of handling quality performance.

Figure 1.1: Airbus X³ demonstrator [2]

Figure 1.2: Sikorsky X2 demonstrator [5]

1.1. Compound Helicopter Definition

The compound helicopter can be seen as a mix between a helicopter and a fixed-wing aircraft. It features a fully controllable main rotor combined with fixed wings, ailerons, elevator, tail, tail rotor and an auxiliary thrust unit (propeller). There are different types of compounding: thrust and/or lift compounding. An example of a thrust compound helicopter is the Sikorsky X2 in Figure 1.2. An example of a lift and thrust compounding helicopter is the Airbus X³ in Figure 1.1. Because of its unique configuration, the compound helicopter has redundant controls and each trim or control problem becomes a control allocation optimisation problem. A (near) identical helicopter state can be accomplished by several combinations of control inputs. This presents the opportunity of using the redundant controls for a second objective next to manoeuvring the helicopter.

The compound helicopter configuration has the capability of distributing the required lift between the main rotor and fixed wings. Reducing the rotor rpm and collective setting offloads the main rotor. This reduces the retreating blade stall and advancing blade compressibility effects. The propulsive function of the main rotor can be offloaded by the auxiliary push propeller. The combination of more efficient lift generation by the fixed wings and the extra propulsion pushes airspeeds beyond conventional helicopter capabilities. Also, the unique configuration of controls enhances the rotorcraft agility. But the increase in performance comes at a cost. The combination of higher flying speeds and improved agility increases the loads in the rotor components.

1.2. Research Objective

This research is a feasibility study to investigate the potential of using the redundant controls of the compound helicopter to alleviate loads in the rotor hub. In order to investigate the potential in a realistic condition, the break-turn MTE was chosen. This manoeuvre is selected as a standard for future rotorcraft handling requirements.

The biggest part of the research consists of the construction of the compound helicopter model capable of flying break-turn MTE. The UH-60A Black Hawk helicopter was selected as a platform for the construction of the compound helicopter. Many research institutes use this helicopter type which provides a lot of available specifications. A visual representation of the compound UH-60A modelled in this thesis is presented by Figure 1.3.

The research statement consists of three parts as it relates to the set-up of the compound helicopter model, the investigation of the structural load alleviation strategy and the effect of the trim setting prior to the manoeuvre:

1. *Develop and validate a simulation model of a compound UH-60A Black Hawk helicopter capable of flying the break-turn MTE and computing the loads in the main rotor hub.*
2. *Study the feasibility of a structural load alleviation strategy by using the redundant control of a compound UH-60A Black Hawk helicopter to reduce loads in the main rotor hub during the executing of the break-turn manoeuvre and evaluate performance concerning load reduction and handling qualities.*
3. *Study the effect of different trim settings on cruise performance and steady oscillatory loads as well as the impact on loads during the break-turn manoeuvre.*

During the set-up of the simulation for this thesis research, the choice of the aerodynamics models should be well balanced to accurately capture the encountered loads during manoeuvring flight while assuring a reasonable computing cost for real-time simulations. As the model will be flown, a suitable control mechanism is required.

The compound helicopter features a rich variety of controls. The thesis will also investigate which control elements are suitable for alleviating loads during the rolling manoeuvre. Ideally, the control strategy is changed to reduce loads without negatively impacting the handling qualities of the rotorcraft. Therefore, the effect of using different control input strategies on handling qualities will also be studied.



Figure 1.3: Visual representation of the compound UH-60A modelled in this research [47]

1.3. Project and Report Outline

Figure 1.4 presents an overview of this research project. At the centre of the project is the construction of a multi-body dynamics model of the compound UH-60A model. MATLAB SimMechanics/Simulink was used for this purpose. The basis of the model was a conventional UH-60A constructed by Mark Voskuil and extended by Barend-Jan van Bruchem for his MSc thesis on tail rotor drive shaft load alleviation during hover [13]. However, the model was still far from suitable for the goal of this thesis. At the beginning, the model featured the characteristics of the body and rotor assembly with a momentum inflow model. It could hover in a way that the body was still connected to the ground. The first step was to prepare the model to enable a flying motion in 6 degrees of freedom.

The inflow model was updated to cope with manoeuvring flight at higher velocities. A fuselage drag model was added as the initial model was only used during hover. Similar to a real helicopter, some sort of mechanism is required to 'fly' the model. Therefore, a flight controller was designed to trim the model at different flying speeds before manoeuvres are initiated.

Before the model can be used for experiments, there is a very important validation step to be made. The secure validation campaign was a major part of the thesis. First, a conventional UH-60A model was validated. A copy of the helicopter model was constructed in the commercially available software FLIGHTLAB. Trim and manoeuvring flight were compared between the two models. After this step, a validated conventional UH-60A model is ready to be modified to a compound version.

The most important feature of the compound helicopter is the main wing. The main wing is represented by a lifting line model and added in the multi-body dynamics environment. An empennage model and compound thrust are also added. The extra parts were validated on a component level before the control system was updated. A module to fly different manoeuvres is added to the model.

Finally, the entire compound UH-60A model is ready and the experiments can begin. The break-turn manoeuvre is modelled as a roll doublet. Three different control strategies are investigated: a pure lateral cyclic input, a pure aileron input and a combination of both. On top of this, the effect of different trim settings prior to the manoeuvre was investigated.

Throughout this entire research, a conventional UH-60A model capable of hovering flight was updated to a full 6 degrees of freedom flying compound UH-60A model. Other helicopter models with similar capabilities do already exist but are well kept behind closed doors of research or government institutes, others are expensive. The unique implementation of the model in a SimMechanics MATLAB environment offers a great way to visualise, modify, optimise and interact with the model from a comfortable coding platform. The fact that this model is now available at the Delft University of Technology unlocks the opportunity to perform state-of-the-art research within the field of rotorcraft. A first example of an existing model used for similar

applications is the U.S. Army's Rotorcraft Comprehensive Analysis System (RCAS). Reddinger, Gandhi & Kang [43] modified this model to include wing and thrust compounding. A second example is the model by Pennsylvania State University which is used to simulate the break-tun MTE as part of the Future-Vertical-Lift [12]. This model was based on the U.S. Army General Helicopter model(GENHEL).

The manuscript starts with a literature study to introduce the fascinating world of rotorcraft in Chapter 2. The history of the compound helicopter is presented and linked to current operational needs for high speed rotorcraft. An overview of the state-of-the-art load alleviation techniques is presented. Finally, key compound helicopter principles are covered to better understand the research results.

The construction of the helicopter model is explained in Chapter 3. First, the conventional UH-60A model is updated before converted to a compound version. The design of the flight controller used to trim the aircraft is presented in Chapter 4. The step by step validation of the multi-body dynamics model with FLIGHT-LAB is covered by Chapter 5. The validation is done for trimmed and manoeuvring flight.

Once the model is ready and validated, the experiments can start. The effects of using different control strategies and trim settings on loads and handling qualities during a roll doublet are presented in Chapter 6.

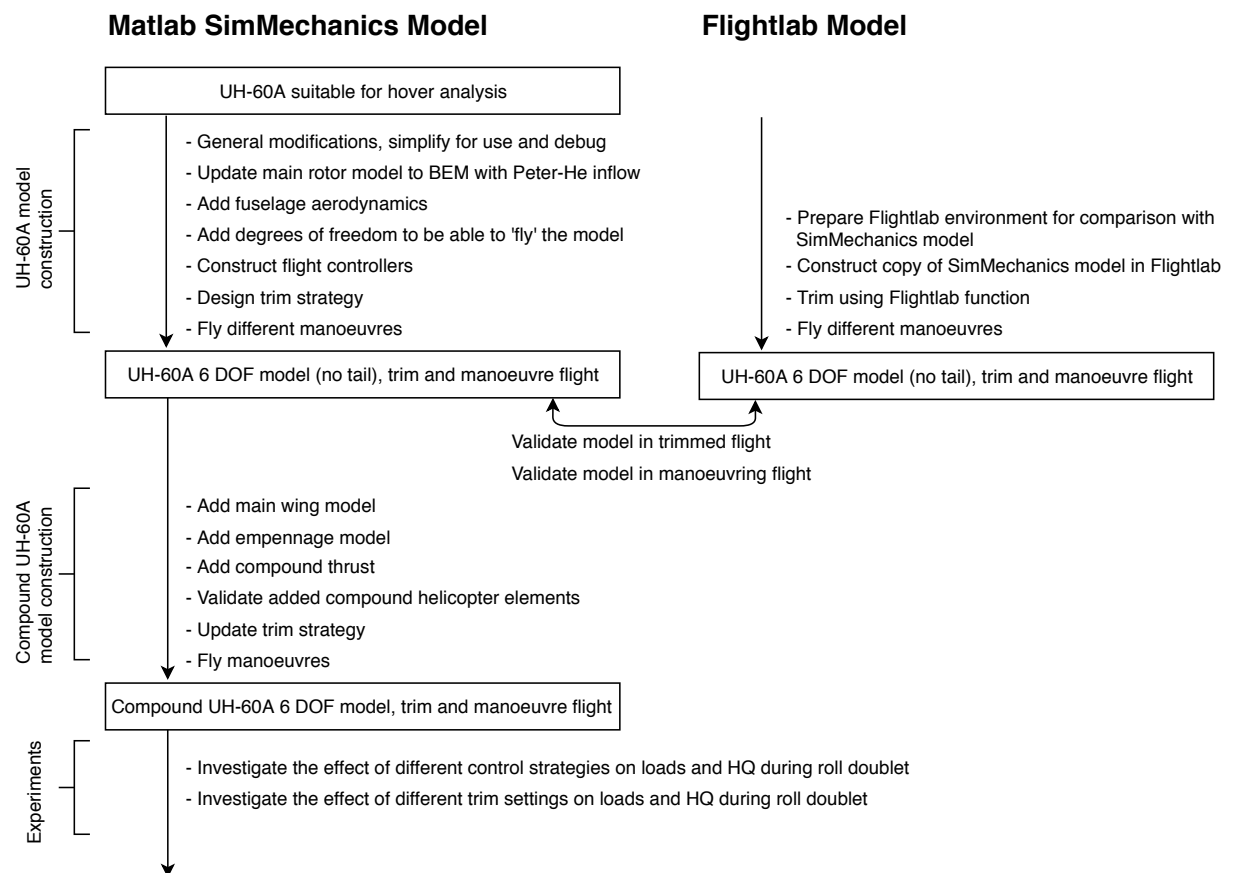


Figure 1.4: Thesis project flow chart

2

Literature Review

The literature study starts with a short history on how the compound helicopter was born, failed to deliver and is revisited today, Section 2.1. Interest to deploy compound helicopters in future missions is growing. As requirements coming from the operational needs are not gentle for the rotor hub, the link between the rotor state and the encountered loading during manoeuvres are important to understand. The in-service requirements and critical loads are covered in Section 2.2. State-of-the-art load alleviation techniques on rotorcraft are presented in Section 2.3. Compound helicopter principles and the effects of the available controls which will be varied through the load alleviation experiments, are explained in Section 2.4.

2.1. The Compound Helicopter Through Time

Understanding the principles and effectiveness of the compound helicopter is important as the concept is reviving. The U.S. Army is working on the JMR-FVL (Joint-Multi-Role and Future-Vertical-Lift) program in which multiple concepts are competing, including compound helicopter configurations. Other participants are the Sikorsky-Boeing Defiant, AVX Entrant and the Bell V-280 Valor shown in Figure 2.1 - 2.3. The DARPA (Defence Advanced Research Project Agency) X-VTOL program studies the feasibility of reaching over 75% hover efficiency combined with very high speed flying performance of 300-400 kts. Various ducted-fan and tilt-rotor concepts are considered. Although there are no compound helicopter configurations competing in this program at the moment, understanding the opportunities of mutual aspects like the redundant controls become important [48].



Figure 2.1: Sikorsky-Boeing Defiant [48]



Figure 2.2: AVX Entrant [48]



Figure 2.3: Bell V-280 Valor [48]

The first fully compounded helicopter was the Piasecki 16H-1A Pathfinder and first flew in 1962, Figure 2.4. The goal was to experiment with redistributing lift over the main rotor and fixed wings as well as sharing thrust between the main rotor and a push propeller. The lift share of the main rotor was brought down to a record of 46% of the total required lift and the propeller took up to 75% of the thrust share at high flying speeds [20].

In 1965, Lockheed developed the XH-51A compound helicopter with turbojet-engines mounted on the wings, Figure 2.5. The wing was designed to completely offload the main rotor lift and the jets also completely offloaded the main rotor propulsive function. To lower blade stress and vibrations, the collective setting was fixed above 150 kts. The XH-51A reached a top speed of 236 kts [46].

The Lockheed AH-56A Cheyenne was developed in 1967 and featured a hingeless main rotor system with variable rpm capabilities. It had a low wing configuration with a push propeller mounted near the tail, Figure



Figure 2.4: Piasecki 16H-1A Pathfinder [48]



Figure 2.5: Lockheed XH-51A [48]



Figure 2.6: Lockheed AH-56A Cheyenne [47]



Figure 2.7: X-49 Speed Hawk [47]

2.6. The Cheyenne was developed for combat purposes and showed high climb performance as well as fast acceleration and deceleration capabilities. At flying speeds above 80 kts, the collective pitch was fixed and the auxiliary thrust and vehicle pitch attitude were used to maintain airspeed and altitude. The program was canceled because of several shortcomings: high pilot workload with unacceptable lateral-directional stability, loss of control in particular cases linked to blade stall, high vibrations, difficult power management and lack of directional control in sideways flight [30].

The X-49 Speed Hawk is a compound modification of the Black Hawk helicopter, Figure 2.7. Studies were performed optimizing control allocation of four redundant controls, pushing the helicopter capabilities to achieve 177 kts in forward flight and 2 G turns at 150 kts [15].

2.2. Critical Load Situation

The U.S. Army is investigating future rotorcraft configurations as well as new mission requirements coming from the Army's operational needs. The thesis will focus on one of the new mission requirements: the break-turn mission task element (MTE). This new manoeuvre involves an aggressive 90° heading change and is described in detail in Section 2.2.2. As the break-turn MTE is executed at high speeds and high G's, high loads in the main rotor hub are expected. This defines a specific case where there is an opportunity for a SLA strategy to reduce the rotor loads. Evidence of the expected critical load cases is presented by comparing the break-turn MTE with UH-60A flight test data in Section 2.2.3.

2.2.1. Rotorcraft Requirements for Future Configurations and Missions

Current rotorcraft handling quality industry standards are documented in the ADS-33E requirements [8]. This document covers the handling requirements for conventional helicopter types during hover, low speed flight and high speed flight. This latter flying regime handling requirements are adapted from fixed-wing aircraft specifications. The U.S. Army is developing the Future-Vertical-Lift program with capabilities beyond the scope of the current industry-standard ADS-33E [12]. Therefore, the U.S. government together with the U.S. rotorcraft industry initiated a joined program: "Rotorcraft Handling Qualities Requirements for Future Configurations and Missions" by the U.S. Army's National Rotorcraft Technology Center (NRTC). This program investigates the introduction of new mission task elements coming from the U.S. Army's operational needs. Performance criteria are investigated to evaluate the handling qualities of future rotorcraft configurations.

Industry and academics put forward four future vertical take-off and landing rotorcraft and used simulator models to assess handling performance while virtually flying the new MTEs. The new rotorcraft configurations include: two tiltrotors and two compound helicopter models. The Sikorsky Aircraft Corporation evaluated the X2 Technology simulator, a coaxial thrust compounding helicopter featuring the advancing blade concept. Boeing used their tiltrotor simulation platform to fly the new MTEs. Also, Bell Helicopters tested

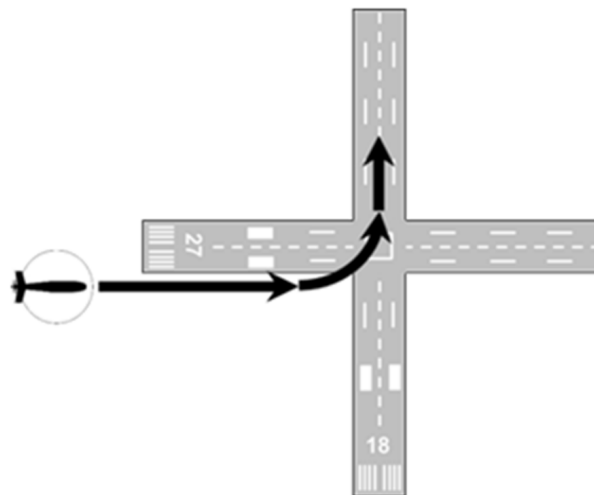


Figure 2.8: Break Turn MTE visual cue in simulator [12]

the new manoeuvres with a tiltrotor aircraft, using their generic tiltrotor simulator which was successfully used during the development of the V22 Osprey. Finally, Pennsylvania State University developed a generic compound helicopter model featuring a non-linear dynamic inversion controller. This model is based on a conventional UH-60A Black Hawk with additional wings and a push prop mounted behind the tail.

Trained pilots flew the new MTEs for each simulator model mentioned above to assess the handling qualities.

2.2.2. The Break-Turn Mission Task Element

The break-turn is an evasive combat manoeuvre involving an aggressive 90° heading change. This manoeuvre can be classified as a non-precision and aggressive manoeuvre. The pilot shall be able to execute this manoeuvre while staying within the operational flight envelope of the rotorcraft. Research by the NRTC investigated undesirable coupling effects between pitch, roll and yaw. Handling quality performance criteria were established and checked how they possibly degrade during the manoeuvre [12]. This work does not focus on the loads encountered during the manoeuvre. Since the break-turn MTE is an aggressive manoeuvre flown at high speeds, high loads in the main rotor blades and hub are to be expected. Therefore, this thesis research will propose a load alleviation strategy to reduce loads seen during the executing of the break-turn MTE.

Manoeuvre Description

Within the simulator environment, to provide a visual cue to the pilot, the helicopter is lined up with the runway. The pilot is required to execute a 90° heading change and line up with the intersecting runway as shown in Figure 2.8

The rotorcraft flies wings level at 300 ft AGL at $0.8V_H$ when the pilot initiates the 90° heading change. The use of auxiliary thrust and pedal inputs are allowed. The manoeuvre shall be performed as quickly as possible until wings level is achieved after rolling out of the turn. Since this is a non-precision/aggressive manoeuvre, certain variations are allowed in final heading change, airspeed and altitude as summarized in Table 2.1. These performance variations are categorized in desired targets and adequate targets. The key performance measure for this manoeuvre is the time till completion. The time target is defined as a ΔT being the difference between the total completion time and an ideal turning time T_{ideal} , equation 2.1. The ΔT will act as the actual performance target and will be the same for each evaluated rotorcraft. Values of ΔT are set to 3.5 sec for the desired performance and 7.0 sec for adequate performance as explained in [12] and presented in Table 2.1. The T_{ideal} is defined as an ideal completion time of a 90° heading change according to equation 2.2. The ideal turn is split-up in a transient roll-in/roll-out and a steady turn. $T_{transient}$ and $\Psi_{transient}$ stand for the time it takes to roll-in or roll-out and the associated heading change. The roll acceleration/deceleration is assumed constant according to the time-to-bank requirements by the MIL-STD-1797B Section 5.2.3.5 [34]. The bank angle is restricted to the maximum allowed load factor within the rotorcraft's operation flight envelope.

$$\Delta T = T - T_{ideal} \quad (2.1)$$

$$T_{ideal} = \frac{\pi V(45 - \Delta\Psi_{transient})}{90g\sqrt{n_{z_{lim}}^2 - 1}} + 2T_{transient} \quad (2.2)$$

Table 2.1: Break Turn MTE performance standards [12]

Criteria	Desired	Adequate
Complete manoeuvre within time $T < \Delta T + T_{ideal}$	$\Delta T = 3.5 \text{ sec}$	$\Delta T = 7.0 \text{ sec}$
Final change in directional flight path shall be at least 85° and no more than X degrees	95°	105°
When rolling out to wings-level attitude, the overshoot in roll attitude shall not exceed X degrees	5°	10°
Final airspeed loss shall be no more than X% of initial airspeed ($0.8V_H$)	10%	20%
Maintain altitude within $\pm X$ feet	75 ft	150 ft
Any oscillations or inter- axis coupling shall not be	Undesirable	Objectionable

The ideal manoeuvre used to calculate the T_{ideal} as described above, is summarized below. The turn is split-up into a transient roll-in/roll-out phase and a steady turn. The UH-60A compound helicopter falls under the Class I, Category A according to MIL-STD-1797B Section 5.2.3.5 [34]. This sets the time-to-bank requirement to 60° in 1.3 sec which fixes the roll acceleration. The maximum load factor was set to $n_{z_{lim}} = 2.5$ G which leads to a maximum bank angle of 66.42° . To arrive at the maximum bank angle with zero rotational speed, a step function is used with a positive followed by a negative constant acceleration. The time it takes to perform this transient roll-in (and roll-out) manoeuvre and the associated heading changes are given below [12]. The analysis made by Penn State University uses $0.8V_H = 160 \text{ kts}$ for the rotorcraft flying speed. Plugging these values into Equation 2.2 results in an ideal time given below and the according desired and adequate executing time as defined by Table 2.1.

$$T_{transient} = 1.93 \text{ sec} \quad (2.3)$$

$$\Delta\Psi_{transient} = 11.7^\circ \quad (2.4)$$

$$T_{ideal} = 7.1 \text{ sec} \quad (2.5)$$

$$T_{desired} = 10.6 \text{ sec} \quad (2.6)$$

$$T_{adequate} = 14.1 \text{ sec} \quad (2.7)$$

As the break-turn manoeuvre needs to be simulated for the design of the SLA strategy, this simplification of the MTE into a transient roll-in/roll-out and steady turn is suitable. Therefore, the considered break-turn MTE which will be used for computing the loads, designing the SLA strategy and assessing the handling qualities is defined below:

1. **Roll-in** manoeuvre, transient phase 1.93 sec, constant roll acceleration from the MIL-STD-1797B Section 5.2.3.5 [34], max bank angle reached at zero rotational speed 66.42° , 11.7° heading change
2. **Steady turn**, 2.5 G at 66.42° bank angle constant turn for 4.42 sec
3. **Roll-out** manoeuvre, transient phase 1.93 sec, constant roll acceleration from the MIL-STD-1797B Section 5.2.3.5 [34], bank angle from 66.42° to wings level, 11.7° heading change.

Table 2.2: UH-60A most critical manoeuvres [31]

Manoeuvre	Count	Rank Order					
		Pitch link load	Torsion Moment r/R = 0.30	Flap bending r/R=0.113	Flap bending r/R=0.60	Chord bending r/R=0.113	Chord bending r/R=0.60
RTTURN, 140 KIAS, 60° AOB	11680	1	1	15	4	1	14
UTTAS PULL-UP, 130 KIAS, 2.1G	11029	3	8	1	15	8	4
RTTURN, 140 KIAS, 55° AOB	11679	2	2	23	7	23	15
DIVE ROLL PULLOUT, 120 KIAS	11028	6	5	8	23	3	22
PULL-UP, 120 KIAS, 2.25G	11023	10	7	2	26	4	25
LTTURN, 130 KIAS, 60° AOB	11686	9	3	7	17	12	15
DESCENT, 186 KIAS (VNE)	11682	24	24	28	1	21	2
LTTURN, 120 KIAS, 60° AOB	11660	8	4	13	14	7	6
RTTURN, 130 KIAS, 60° AOB	11672	13	6	10	18	5	8
UTTAS PULL-UP, 130 KIAS, 1.8G	11031	4	14	5	13	11	9

2.2.3. Link Between Rotor Phenomena and Critical Loads

Since the above described MTE is meant for future rotorcraft, there is no available flight test data. This means there is no direct evidence of high loads encountered during the break-turn. However, studies on conventional helicopters show critical load cases during similar manoeuvres. These studies will form the basis of showing the opportunities to minimize loads during the execution of the break-turn MTE.

Kufeld and Bousman focus on the most critical load conditions coming from the NASA/Army UH-60A Airloads Program, a total of 68 classic and air-to-air combat manoeuvres were flown and investigated [31]. Tests were done with a UH-60A helicopter with highly-instrumented blades to measure pitch link loads, torsion moments, flap bending and blade chord bending. Kufeld and Bousman present a list with the top 10 critical loads in Table 2.2. The counter represents an overall ranking, higher count means more critical manoeuvre. The numbers under each load case indicate the criticality of the manoeuvre for that particular load case ex: UTTAS pull-up is the number one critical manoeuvre for flap bending at r/R=0.113 as indicated by the number one. Note that r/R stands for the relative blade span location.

In order to form an idea about which kind of load cases will be critical during the break-turn, one can look at the individual sub-manoevres as stated above in Section 2.2.2. In short, the break-turn can be seen as a roll-in/roll-out manoeuvre and a steady turn at high G's.

Comparing these MTE segments with the tested manoeuvres listed in Table 2.2, one can recognize commonalities. The transient roll-in, roll-out and steady turn manoeuvres pop-up in the top 10 list under "RT TURN" and "LT TURN" in Table 2.2. The goal of the break-turn MTE is to change heading as fast as possible. This means initiating the turn by rolling-in, followed by a tight turn, pulling hard on the stick and therefore increasing the G's. The effect of the increased load factor can be seen in the pull-up manoeuvres as presented in Table 2.2.

It was decided to study main rotor hub forces, moments and flapping in this thesis. These load cases pop-out as critical for the above listed manoeuvre elements and are expected to behave similarly during the execution of the break-turn MTE.

It is crucial to understand what causes these high loads. Work done by Yeo, Bousman & Johnson [55] and Yeo & Johnson [54] state the relationship between the 1/rev blade flapping motion and main rotor loads with the associated shaft bending. The shaft moments M_{Hs} are related to main rotor hub moments M_H . These latter are linked to the blade flapping and approximated by Equation 2.8. F_c is the centrifugal force, e_β the bearing offset and β_1 the first harmonic flapping. Also Kufeld et al. [41] use blade flapping to calculate shaft bending based on flight tests of the UH-60A airloads program. Later in this report, several SLA strategies will be presented reducing the hub loads and moments by reducing blade flapping. For example by using the elevator to offload part of the longitudinal cyclic input to initiate a pull-up. Hence reducing flapping.

$$M_H \cong M_{Hs} \quad M_H \cong M_{H\beta} \cong 2e_\beta F_c \sin\beta_1 \quad (2.8)$$

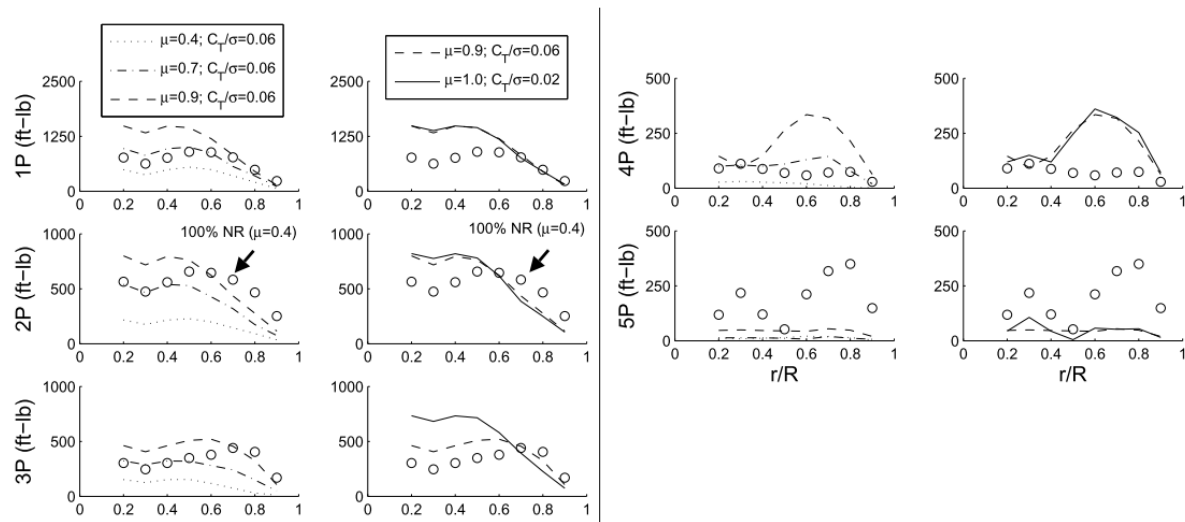


Figure 2.9: Flap bending harmonic motions comparing the UH-60A rotor at nominal rpm (dots) with 40% of the nominal rpm (lines) for different advance ratios (μ) and thrust settings C_T/σ [17]

To achieve high speeds, the compound helicopter can slow down the main rotor and generate a part of the required lift by the wings. The operation of a slowed rotor at high flying speeds is still a new area of research. In order to acquire insights about the behaviour of slowed rotors, extensive testing has been done at the U.S. Airforce National Full-Scale Aerodynamics Complex (NFAC). Datta, Yeo & Norman present the test results of a full-scale UH-60A rotor wind tunnel test, investigating the rotor loading and aerodynamic effects for advance ratios reaching a value up to 1.0 [17].

Results from the slowed rotor test show bending and torsion loads to be similar or significantly higher compared to when the rotor operates at its nominal rpm. This is linked to the higher differential loading between the rotor's inboard and outboard sections. The differential loading is a consequence of the larger reverse flow area over the retreating blades which requires more negative (higher) longitudinal cyclic input to trim the helicopter. This in combination with the high twisted blades (the UH-60A rotor was not modified for better performance at high speeds) causes the supersonic flow to be located more inboard on the advancing blades, compared to a non-slowed rotor. This creates larger elastic twist deformation causing an increased negative lift section outboard of the advancing blade and increases differential loading [17]. Figure 2.9 presents the first up to the fifth harmonic motion, comparing the slowed rotor with the nominal rotor for different levels of advance ratio and thrust. The left column of plots shows the influence of changing the advance ratio while keeping a constant thrust coefficient. In the right column, also the thrust coefficient is changed. The dots represent the nominal rotor while the lines are the slowed rotor. Investigating the 1P and 2P harmonics, one can clearly see a 50 – 100% increase in load over the inboard 70% of the blade span. For the 1P and 2P motions, the increased loading also seems little depending on the thrust values, as can be seen in the upper 2 right plots for 1P and 2P harmonics, Figure 2.9.

Note that during these tests, the UH-60A rotor was slowed down to an 'extreme' case of 40% of its nominal rotating speed. Comparing this to Thorsen [48], who used a compound version of the UH-60A flying at 90% of the nominal rpm to model the break-turn. Proven concepts also operate at a higher rpms: Sikorsky's X2 at $\mu = 0.8$ at 80% nominal rpm and the Airbus X³ at $\mu = 0.6$ at 78% nominal rpm, [17].

2.3. Load Alleviation Strategies

Various studies and flight tests show high loads during manoeuvres, especially in combination with high speeds [31] [16]. Since future rotorcraft operational needs are demanding higher speeds and more aggressive manoeuvres like the break-turn MTE, load alleviation or mitigation can become more important. Also more and more hingeless rotor concepts are installed to improve the controllability and manoeuvrability performance of the helicopter. Hingeless rotors enable large control moments on the blades to be transferred to the fuselage, improving the agility as well as increasing the required structural strength. Gotzfried describes this challenge during the TIGER helicopter development in [21], where structural re-enforcement was required to handle the loads in the hingeless rotor.

A first technique to avoid high loads is to limit the angular accelerations of the helicopter. This strategy was implemented on the RAH-66 Comanche helicopter [50]. Secondly, the pilot can be warned when a violation of the structural operational flight envelope will follow. Loads are mitigated as the pilot can react before limits are exceeded. This technique is called tactile cueing and the challenge lies in the prediction of load exceedances. A more detailed discussion on tactile cueing is presented in Section 2.3.1. Instead of restricting or warning the pilot, structural load alleviation can be implemented. The rotorcraft's response is actively manipulated by deflecting control surfaces with the goal of reducing the loads. Loads are reduced but not mitigated as exceedances are still possible in extreme situations. State of the art SLA strategies on conventional helicopters are discussed in Section 2.3.2, steps towards SLA systems on compound helicopters are discussed in Section 2.3.3.

The above mentioned strategies only focus on the avoidance of lower order mode loads. Another cost driving and performance limiting factor are the high vibrations experienced in rotorcraft. Research by Reddinger, Gandhi & Kang [43] and Sekula & Gandhi [45] investigate vibration reduction using redundant controls of the compound helicopter in the trim conditions. Saetti & Horn [44] look at pitch link vibratory load reduction during pitch-up and rolling manoeuvres. This latter research comes close to the goal of this thesis as the redundant controls are used to change how the helicopter executes the manoeuvres while reducing loads.

2.3.1. Tactile Cueing on Conventional Helicopters

Tactile cueing is used to warn the pilot for an upcoming flight envelope violation. This requires evaluating if the extra stick input by the pilot will cause an envelope excursion and therefore, a load predicting algorithm is needed. Sahani & Horn presented a tactile cueing system implemented on the UH-60A Black Hawk which uses a fixed linear model of the helicopter onboard to predict load exceedances [26]. The system is capable of avoiding static load exceedances on the main rotor hub by cueing lateral and longitudinal cyclic limits to the pilot.

Research by Horn, Calise & Prasad increased the accuracy of these predictions by adding a neural network algorithm to the rotorcraft model [25]. This enables the algorithm to learn about the helicopter's behaviour to control inputs and increase the accuracy of the predictions.

Flight tests showed that implementing tactile cueing increased the agility of the flight manoeuvres as the pilots were more confident to approach flight envelope limits.

2.3.2. Structural Load Alleviation Strategies on Conventional Helicopters

Several flight control systems (FCS) have been investigated or developed in order to alleviate loads in the tail rotor drive train, reduce rotor torques and minimize pitch link loads, hub moments and blade flapping. Also studies at the Delft University of Technology in the Netherlands investigated the feasibility of SLA strategies applied on the UH-60A Black Hawk.

In 2017, van Bruchem supervised by Voskuil presented an SLA technique to alleviate loads in the UH-60A tail rotor drive train [13]. High dynamic loads in this part of the drive train were seen during pedal inputs initiating a left turn in hover. Loads in the tail rotor drive train were directly linked to the tail rotor collective setting. A control strategy was presented reducing 30% of the loads while still complying with level 1 handling qualities.

Also at the Delft University of Technology, Verhagen supervised by Voskuil studied the feasibility of a mixed control SLA scheme using the UH-60A variable horizontal stabilizer to reduce rotor shaft bending loads during a UTTAS pull-up manoeuvre [49]. This particular manoeuvre can be found in the top most critical manoeuvres in Table 2.2. The pitch command is distributed over a longitudinal cyclic pitch and horizontal stabilizer deflection through a speed-dependent gearing ratio. Control gains related to the longitudinal cyclic and stabilizer pitch output of the load alleviation module are kept constant. These gains are found using the weighted pseudo-inverse (WPI) method as described by Bordignon [10]. The research uses a linearised model of the UH-60A extracted from a non-linear multi-body dynamics model in FLIGHTLAB. Partial derivatives linking rotor loads to the control inputs required for the WPI method are found by exciting the helicopter model for longitudinal pitch θ_{1s} and stabilizer angle i_{tail} . A 50% reduction in main rotor shaft bending is claimed at 1.8 G pull-up/pushover manoeuvres at 130 kts as well as the reduction of other hub forces and moments. This was achieved while keeping the handling qualities nearly identical. Only the small amplitude flight path angle response lies lower when the SLA system is activated. This can be linked to the overall change in lift as the stabilizer produces negative lift at the tail to initiate the pitch.

Earlier work by Voskuil, Walker & Manimala [52] demonstrated the opportunities of load alleviation using

active control to reduce pitch link loads also applied to the UH-60A Black Hawk helicopter. The collective and longitudinal cyclic inputs were used to reduce loads seen during high speed longitudinal manoeuvres. An H_∞ optimization technique was used to find a stabilizing controller for a cost function which includes both load alleviation performance objectives and HQ objectives such as pitch attitude tracking error. Figure 2.10 shows a general control overview with a plant P and a feedback controller K , $\bar{\mathbf{w}}$ is the reference signal, $\bar{\mathbf{z}}$ the error vector, $\bar{\mathbf{v}}$ the feedback states and $\bar{\mathbf{u}}$ the input variables. The H_∞ optimization finds a stabilizing controller while minimizing the energy gain between the reference signal $\bar{\mathbf{w}}$ and the error signal $\bar{\mathbf{z}}$. Load alleviation and handling performance objectives are included in the error signal $\bar{\mathbf{z}}$. The SLA uses more longitudinal cyclic and an opposite collective to execute the pitch-up manoeuvre resulting in a significant decrease in pitch link loads. However, higher blade flapping angles are observed during the manoeuvre. Charging the longitudinal cyclic leaves less margin with respect to the actuator limits, increasing the chance of running against these limits during more aggressive manoeuvres. This is a known drawback of using the H_∞ method. It was shown that with the SLA system implemented, the helicopter could obtain a flight path angle which is a few degrees lower compared to the conventional control system, meaning less altitude is gained during the pull-up manoeuvre. This is seen as a reduction in handling qualities. Note that work by Verhagen, earlier mentioned in this section, looked at reducing blade flapping to lower rotor shaft moments while the described H_∞ method suggests one degree more flapping to alleviate pitch link loads. Whether the increased flapping is significant in terms of higher hub loads is not stated by the research.

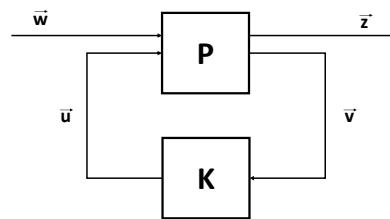


Figure 2.10: General control configuration H_∞ method [52]

In 2005, an H_∞ controller was implemented on a Bell 412 helicopter with the goal of testing handling quality requirements, a load alleviation strategy and flight envelope protections [53]. As part of this project, Voskuijl worked on the first steps towards using the H_∞ model for load alleviation purposes applied on pitch links [51].

2.3.3. Structural Load Alleviation Strategies on Compound Helicopters

Seatti & Horn looked at reducing vibratory pitch link loads by using the redundant controls of the compound helicopter [44]. A wing only compound version of the UH-60A was used for this study. Since the study focuses on higher frequency vibratory loads, the required level of modelling will be significantly different compared to this thesis research. In contrary to the work of Seatti & Horn, the thesis will focus on main rotor hub forces and moments which are mainly linked to the lowest order blade flap mode. However, Seatti & Horn also briefly show a reduction of lower order loads and the potential of using the redundant controls to achieve this.

Higher than 1/rev vibratory loads are well captured by linear time periodic (LTP) models instead of the more common linear time invariant models (LTI). However, Seatti & Horn approximate the LTP model by a decomposition of several high order LTIs where the higher frequency harmonics are captured into states of an LTI state space model. This method is called harmonic decomposition.

A non-linear FLIGHTLAB model of the UH-60A was used featuring flexible blades, a 6 state Pit-Peters inflow model combined with fully non-linear aerodynamic look-up tables. Note that flexible blades were used to capture higher frequency vibrations. The FLIGHTLAB model is linearised into a LTP model at 120 kts flying speed.

Next, the harmonic decomposition is applied to get from a LTP system to several LTI systems using Fourier analysis. When a set of LTI systems is achieved, residualisation is performed. The singular perturbation theory is used and the reader is referred to the paper by Seatti & Horn [44] for a more detailed description of this method. In short, this method simplifies systems having different levels of dynamic motions divided into slow and fast dynamics. It decouples the slow from the fast dynamics. The slow dynamics are solved

while the fast dynamics are assumed to quickly reach their steady-state. Body states and 0^{th} order flapping are considered slow states. Higher order flapping states have small amplitudes compared to the 0^{th} order and are truncated in this research. Note that higher order pitch link harmonics are kept to capture the influence of body states and controls on the vibratory loads.

A Weighted pseudo-inverse strategy is used for the control allocations as earlier described in this chapter referring to the work of Verhagen [49]. Unfortunately, the objective matrix which can include both manoeuvring as well as load reduction targets is not stated by the paper.

Seatti & Horn compare the baseline controller (using rotor controls only) with the load alleviation controller using the pseudo-inverse technique. The load alleviation module was implemented in the non-linear model. Simulations were done with and without rotor state feedback. A roll doublet at 120 kts with a roll rate of 0.2 rad/s was modelled. Figure 2.11 and 2.12 show the manoeuvre with 'LA PI' being the load alleviation module with pseudo-inverse and the 'LA PI RFB' the module which also includes rotor feedback. Figure 2.13 shows how the lateral cyclic input θ_{1c} is reallocated over the ailerons (left aileron δ_l and right aileron δ_r). The effect on main rotor hub forces and moments can be seen in Figure 2.14. The study claims up to 17% peak-to-peak pitch link load reduction by the pseudo-inverse SLA. The rotor feedback is found to have no beneficial effects.

Next to the reduced pitch link loads, Seatti & Horn show the potential of using the redundant controls to alleviate hub loads by offloading the lateral cyclic input during a roll doublet, Figure 2.14. It is claimed that the pseudo-inverse method is an effective way to do so. Assessing the HQ, the study states an improvement of HQ according to the ADS-33E-PRF regulations for target acquisition and tracking.

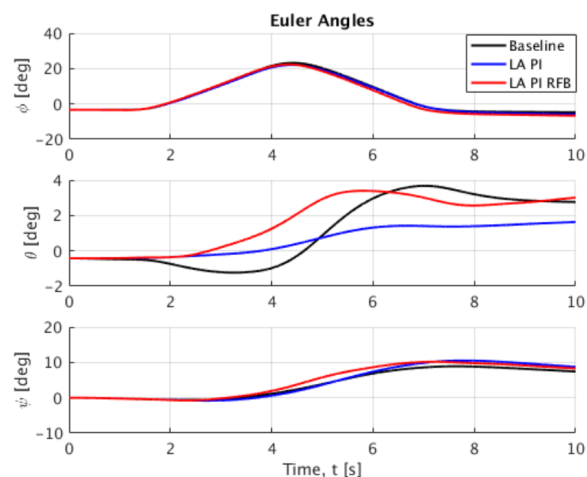


Figure 2.11: Non-linear response roll doublet, Euler angles [44]

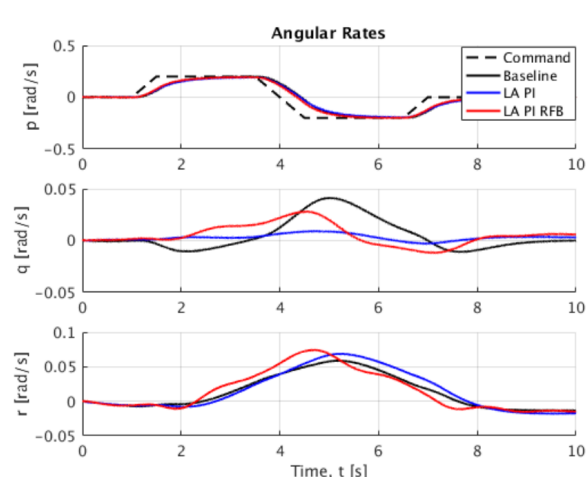


Figure 2.12: Non-linear response roll doublet, angular rates [44]

2.3.4. Discussion of Load Alleviation Results from Literature and Link with Thesis Research

There is little data available on using the redundant controls of the compound helicopter to reduce main rotor hub loads and moments. Therefore, this section will discuss how the results of the previously discussed studies performed by Verhagen & Voskuijl [49] and Seatti & Horn [44] can be applicable for the this thesis work.

To better understand which effects influence the loads on the hub, Verhagen presents a detailed study linking rotor phenomena to each force and moment. The longitudinal cyclic is partly replaced by a horizontal tail input to fly the pull-up manoeuvre. The following phenomena are observed over the rotor disk. Starting with the hub forces, F_x is reduced as using the elevator to initiate the pitch-up manoeuvre requires less longitudinal cyclic, hence less flapping. This force is linked to the rotation of lift- and drag vector in the xz -plane. F_y is also reduced and influenced by two different phenomena: structural lead-lag in the xy -plane and lateral cyclic in the yz -plane. As blades lag over regions of high angle of attack reaching a maximum at the right and left side of the rotor, a force in the y -direction appears. When the SLA system is active, less longitudinal cyclic is required, less coupling with the lateral motion of the rotor exists and spikes in F_y are reduced. F_z mainly follows the load factor and has a lift and drag component along the z -axis. Spikes along this axis are removed

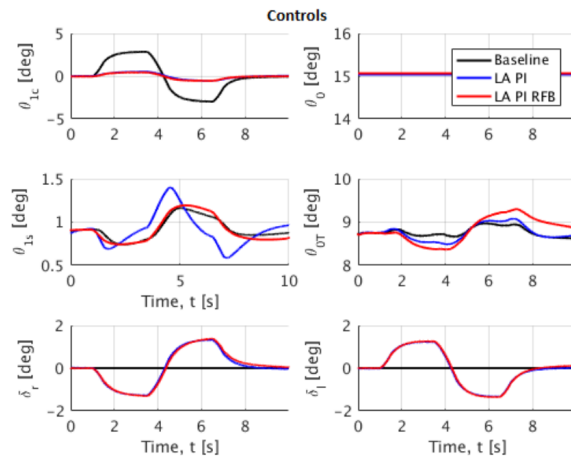


Figure 2.13: Control inputs during roll doublet [44]

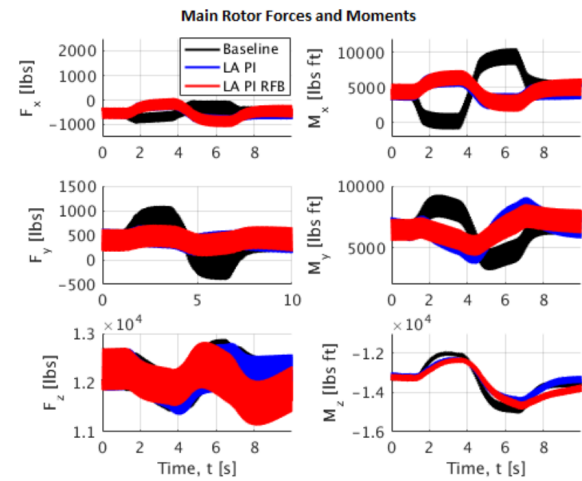


Figure 2.14: Main rotor hub forces and moments during roll doublet [44]

due to less longitudinal cyclic input. For the moments, M_x along the rolling axis is also reduced as less longitudinal cyclic is linked to less roll-coupling. M_y is important in this study since high moments around the y-axis are expected during pitch manoeuvres. When only longitudinal cyclic is used, large blade flapping will cause the blades to reach a max flapping angle in front and minimum in the back of the rotorcraft. Flapping can be linked to high moments. Using the elevator to initiate the pitch-up decreases flapping hence decreasing hub loading. Increasing the blade angle of attack at high flying speeds by using the longitudinal cyclic can also lead to retreating blade stall. This stall effect can be decreased by using the elevator to initiate the pitch-up manoeuvre and more opportunities are seen on compound helicopter configurations as they can offload the main rotor.

Relevant results linked to this thesis presented by Seatti & Horn [44] are given in Figure 2.14. The thesis will focus on the break-turn MTE which reaches a higher bank angle. Unfortunately, the flapping angles are not given in the paper by Seatti & Horn. These are interesting as they are linked to the hub loads and moments.

Changing the input strategy from a pure lateral cyclic input to a pure aileron input mainly affects the F_y and M_x as shown in Figure 2.14. The F_y force is lower with the SLA active, Figure 2.14. Less cyclic input leads to less lift tilt in the yz-plane. M_x shows an opposing main rotor moment response when the SLA is active. This moment can be linked to the lateral cyclic input to roll and associated blade flapping. Here, one can see a significant difference between the two rolling strategies. The difference in M_x response is linked to the absence of lateral cyclic input but also by a reversed flapping phenomena when the SLA is active. It seems that the rolling motion, when initiated by the ailerons, is causing the left blade to flap down and right blade to flap up in case of this right turn. This flapping motion has a damping effect on the rolling motion initiated by the ailerons. This will be an interesting subject to investigate further during the thesis as well as how it relates to physical flapping angle constraints during the break-turn MTE. F_x and M_y are related to the longitudinal input and the cross coupling effect between lateral and longitudinal helicopter motions.

The pseudo-inverse control allocation strategy is proposing an almost pure aileron deflection without lateral cyclic to roll the helicopter, Figure 2.13. As mentioned before, this inverts the response of the M_x moment. Depending on how the pseudo-inverse control allocation problem was set in terms of objective and weighted matrix, a combination of controls is suggested. In this case, purely using the ailerons came out as the optimum solution. This thesis will investigate mixing the lateral cyclic and ailerons to initiate rolling and further improve load alleviation. This can potentially change the response of the M_x moment to an almost straight line instead of a waving inverted behaviour as achieved with the active SLA by Seatti & Horn [44], shown in the top right of Figure 2.14.

2.4. Compound Helicopter Principles

In order to discover the true potential of the redundant controls to alleviate loads, one should understand their individual effects. This section will briefly present the effects of the different controls on the helicopter behaviour and more specifically on the main rotor state. The theory presented in this section comes from the work done by Reddinger, Ganhi & Kang [42] and Sekula & Ganhi [45]. They investigated the potential of using the redundant controls of a compound helicopter to reduce power required and main rotor vibrations. Note that this research focuses on trim state conditions and not manoeuvring.

2.4.1. Slower Rotor and Auxiliary Thrust Operational Envelope

The compound helicopter is flown with a variable lift share between the main rotor and wings combined with a thrust setting of the auxiliary propeller. Lift unloading is done by reducing the main rotor rpm (and/or collective) and loading the fixed wings. To give a first idea about the compound helicopter trim settings and limits, the operational envelope being a function of the main rotor rpm and the auxiliary thrust setting is presented in Figure 2.15. This plot was made for a compound version of the UH-60A flying at 225 kts as described by Reddinger & Ganhi [42]. Point A indicated the starting point and trim data are summarized in Table 2.3. Note that parameters like the redundant control inputs, flapping and lift share will be important throughout this chapter. The curved lines on the plot in Figure 2.15 show the total power required (main rotor + auxiliary prop). Also, four limits can be observed:

- No trim solution: the main rotor rpm is too low for the forward speed flown. The forward speed can be linked to the auxiliary thrust.
- Minimum collective pitch: the offloaded rotor, to sustain rotation, a minimum collective pitch is required (comparable to pitch setting required to sustain auto-rotation)
- Max tip speed: mach effects constraining the max tip speed
- Minimum blade flapping: maximum blow back of the rotor without aft blade hitting the airframe or tail boom.

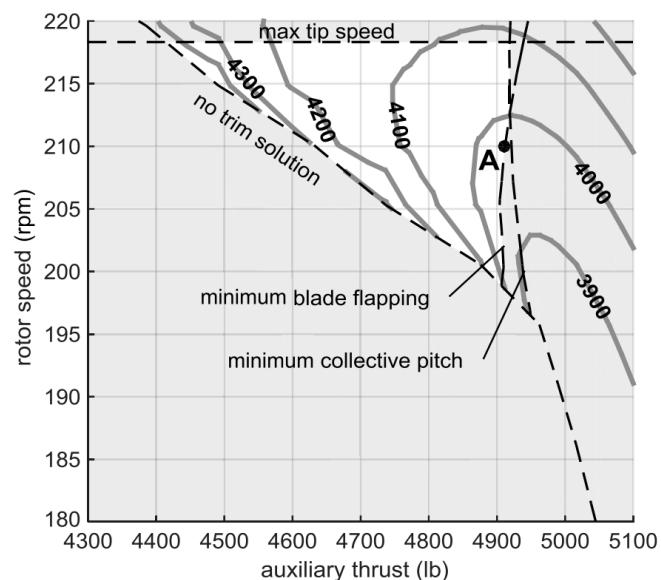


Figure 2.15: Compound helicopter main rotor rpm and auxiliary thrust envelope, trim state A [42]

2.4.2. Elevator Effects

The effect of the elevator on a compound helicopter can be observed moving from trim state A to state B, summarized in Table 2.3. Reducing the upwards lift generated by the elevator brings the helicopter in a more nose-level position. This increases the angle of attack of the wings which causes the lift share of the wing to

Table 2.3: Trim state details [42]

	Trim point			
	A	B	C	D
Total power, hp	4,073	3,820	3,716	3,455
Main rotor power, hp	61	426	414	219
Propulsor power, hp	4,011	3,395	3,302	3,236
Advance ratio	0.64	0.64	0.64	0.73
Wing-lift share, %	37.2	66.9	67.0	66.7
Rotor lift share, %	60.9	31.9	31.7	32.1
Wing L/D	29.3	35.5	35.5	35.5
Rotor L/D_e	7.9	5.1	5.7	8.2
Total L/D	3.4	3.6	3.7	4.0
Rotor lift offset	0	0.01	0.11	0.10
Rotor Z force, lb	12,187	6,401	6,384	6,488
Rotor H force, lb	1,941	731	627	555
Rotor roll moment, lb · ft	-97	1,848	18,487	16,609
Propulsor thrust, lb	4,912	4,247	4,143	4,069
Revolutions per minute, rpm	210	210	210	186
Stabilator pitch, deg	3.9	1.3	1.3	1.3
Aileron deflection, deg	0	0	0.53	0.53
Collective pitch (0.75R), deg	0.7	0.4	0.4	2.7
Lateral pitch, deg	-0.7	0.01	6.9	8.1
Longitudinal pitch, deg	2.8	-0.1	0.2	-2.6
Vehicle pitch attitude, deg	-2.3	-0.7	-0.7	-0.7
Roll angle, deg	0.1	-0.8	1.5	2.4
Rotor coning, deg	2.2	0.9	0.9	0.7
Lateral flapping, deg	-1.9	-0.6	6.6	7.3
Longitudinal flapping, deg	-8.0	-2.4	-1.7	-1.5
Minimum flapping, deg	-6.0	-1.6	-5.9	-6.0

increase and the rotor to be further unloaded. Since wings are a more efficient way to produce lift (higher L/D), less auxiliary power is required to propel the helicopter. When the helicopter is brought to a more nose-level state, the rotor goes from an almost auto-rotation state to a higher power state, Figure 2.16 and 2.17. The large blow back which was initially driving a large part of the rotor is now gone. Due to the decrease in blow back, the H -forces decrease which eventually leads to less rotor drag and less required auxiliary thrust. The main rotor itself, however, operates at a higher power state and higher torque level at trim setting B. Overall, a decrease in total power is observed moving from trim state A to B.

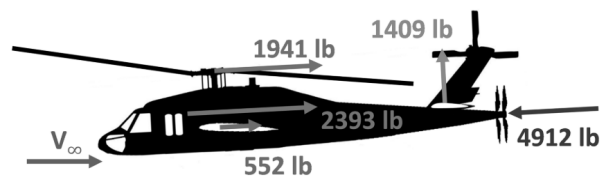


Figure 2.16: Force equilibrium trim state A [42]

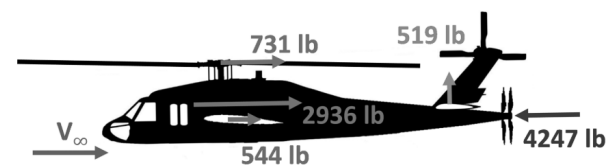


Figure 2.17: Force equilibrium trim state B [42]

The change in elevator pitch also has an effect on the limits presented in Section 2.4.1. The minimum blade flapping limit is pushed to the right due to the reduction in flapping. The no trim boundary comes down as more lift is generated by the wings. A new limit is introduced at very low auxiliary thrust settings as the longitudinal forward disc tilt reaches a maximum of 16° in this case. The updated envelope is shown in Figure 2.18.

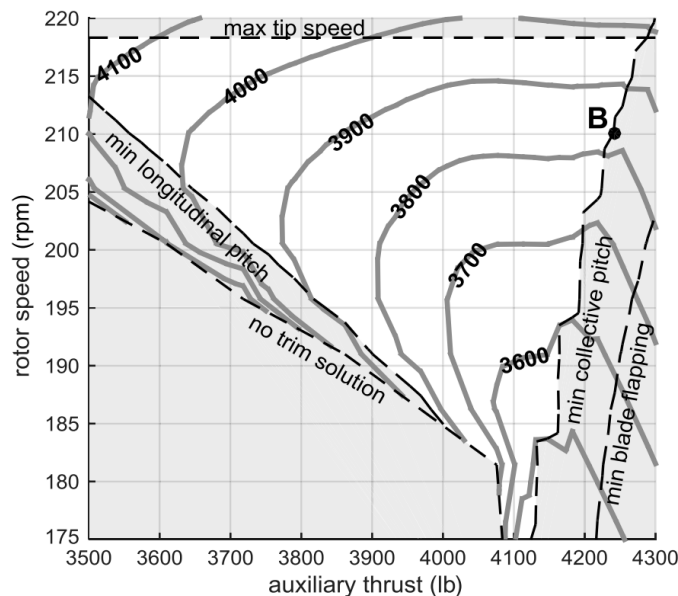


Figure 2.18: Compound helicopter main rotor rpm and auxiliary thrust envelope, trim state B [42]

2.4.3. Ailerons Effects

The effect of using the ailerons (differential flaperons) can be seen by moving from trim state B to trim state C according to table 2.3. The Sikorsky X2 helicopter shown in Figure 1.2 features the lift-offset Advancing Blade Concept. Most of the rotor lift is generated over the advancing blade side. This is impossible for a conventional helicopter since it would cause an unrecoverable rolling motion. Because the X2 has a coaxial rotor system (two counter-rotating rotors), the moment created by lift-offset over the advancing blade of the upper rotor cancels out with the moment of the lower rotor. The efficiency of the rotor is increased since generating lift at higher dynamic pressure is more efficient.

This principle does not work on a conventional helicopter since there is no means to create this lift-offset without rolling the helicopter. The compound helicopter, however, can use its ailerons mounted on the wings. From trim state B to C, the aircraft is flown with an aileron deflection generating a differential lift over the wings as presented in Figure 2.19 and 2.20. The rolling moment generated by the ailerons increases the later flapping and a lateral cyclic input is required to trim the helicopter level, Table 2.3. Also the longitudinal pitch is increased which means higher angles of attack are seen over the advancing side of the rotor creating more lift, hence more lift-offset. This effect can clearly be seen in Figure 2.21 (rotors spins counter clock). The local angle of attack can be linked to the generation of lift. One can see that the aileron deflection creates a large section of positive lift over the advancing side.

The use of ailerons has a positive effect on the power required. Lift is generated over a more efficient part of the rotor at higher dynamic pressures, the rotor lift-over-drag-ratio increases. The reduction in total power required (main rotor and auxiliary power) is mainly linked to the reduction in H-forces by the increased longitudinal pitch and the smaller region of negative lift over the tip of the advancing blades, as the lift-offset is increased. The effect of ailerons in trim state C on the rpm and auxiliary thrust envelope is shown in Figure 2.22. The minimum blade flapping and collective pitch boundary are coinciding for this case.

Note that the increase in flapping is beneficial for the power required but can cause increased blade loads and vibrations.

The work of Reddinger & Kang [42] looked at using the redundant control for power minimisation. Therefore, a fourth trim state D was presented according to Table 2.3, reducing the main rotor rpm to further decrease the power required as can be seen in Figure 2.22, point D.

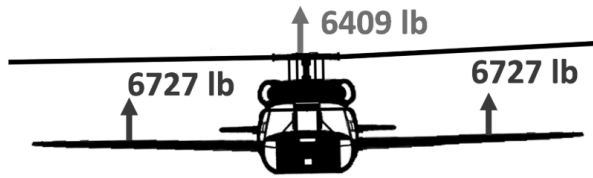


Figure 2.19: Force equilibrium trim state B [42]

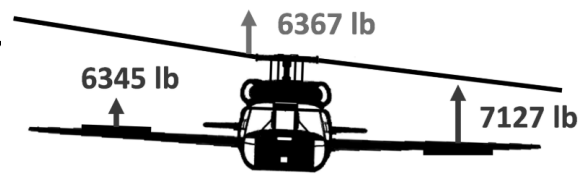


Figure 2.20: Force equilibrium trim state C [42]

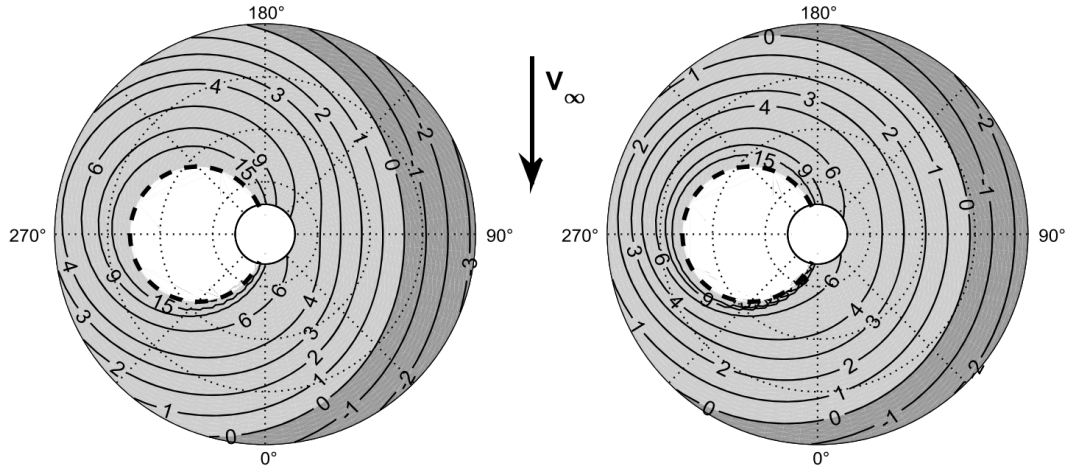


Figure 2.21: Local angle of attack of counter clock rotating rotor, left trim state B, right trim state C [42]

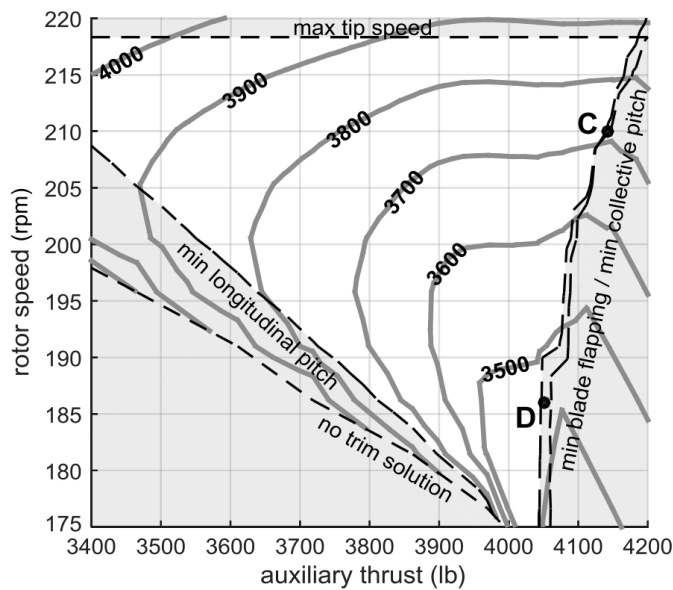


Figure 2.22: Compound helicopter main rotor rpm and auxiliary thrust envelope, trim state C and D [42]

2.4.4. Lift Compounding Effects

The investigation of individual effects of lift compounding and thrust compounding (in next section) comes from the work by Sekula & Ganhi [45]. They looked at reducing vibrations during the trim state by using auxiliary lift and propulsion. Implementing auxiliary lift and thrust introduces moments changing the vehicle's attitude and required control inputs such that vibrations can be minimised.

In the case of a helicopter configuration with only additional wings and no additional thrust, the wings contribute to the total lift and the main rotor generates all the propulsive force. When offloading the rotor, an increased forward longitudinal input or a more nose down attitude is required to keep the rotor propulsive component the same, Figure 2.23. The main rotor is offloaded so F_r decreases and the propulsive force

$\sin(\alpha_s)F_r$ is kept constant by increasing α_s .

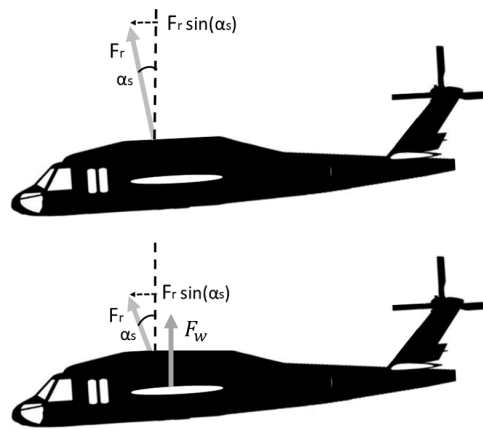


Figure 2.23: Up: fully loaded rotor, Down unloaded rotor with wings generating part of the lift

As α_s is increased, the inflow through the rotor increases. This decreases the angle of attack on the blades shown in Figure 2.24. The reduction in angle of attack means a reduction in generated thrust. When off-loading the main rotor, one expects a significant reduction in required collective setting as the rotor's main function is to generate the propulsive force instead of propulsive and lift force. The collective pitch setting decrease is smaller than expected due to the effect in Figure 2.24.

Higher blade flapping can be expected by the increased longitudinal input to maintain the forward thrust component of the main rotor.

2.4.5. Thrust Compounding Effects

The effect of thrust compounding will be discussed in this section. The lift is generated by the rotor and the propulsive force mainly comes from the propeller installed in the back. The auxiliary thrust tilts the rotor backwards reducing the inflow, Figure 2.24. This reduces the induced drag and the rotor goes to an almost auto-rotation state where the airflow partly drives the main rotor.

The rotor tilts back due to the pitch up moment generated by the auxiliary thrust. The required longitudinal cyclic input pushing the rotor forward to sustain forward flight without auxiliary thrust is partly alleviated.

If thrust compounding is combined with lift compounding, the rotor will tilt even more backwards as the rotor is also unloaded. There is more upwash and negative inflow (coming from underneath the rotor) which drives the rotor and decreases the required power and torque. The rotor will operate even closer to an auto-rotation state.

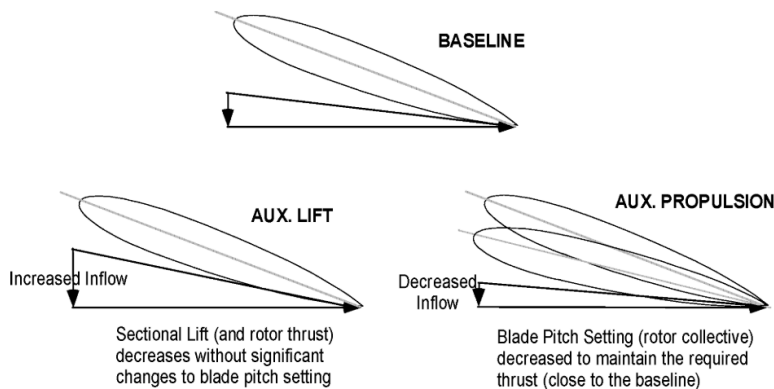


Figure 2.24: Effect of auxiliary lift and thrust on the blade angle of attack [45]

3

Compound Helicopter Model

This chapter will present all the elements of the compound helicopter model. The general modelling strategy used for this research is presented in the Section 3.1. A visual overview of the multi-body dynamics model and linked aerodynamic models are presented in Section 3.2.

The rest of the chapter will cover each of the aerodynamic models separately, which together capture the aerodynamics of the compound helicopter. The main rotor blade element and inflow model is presented in Section 3.3. The model used for the tail rotor is presented in Section 3.4. A function fit on experimental data is used to model the aerodynamics of the helicopter's fuselage, Section 3.5. The modelling of the main wing and compound thrust which differ the compound helicopter from a conventional type are presented in Section 3.7 and Section 3.8.

3.1. Multi-Body Dynamics General Modelling Approach

The most basic representation of the model used for this thesis research is shown in Figure 3.1. The helicopter model consists of 2 main type of components: aerodynamic models and several bodies. The helicopter is build up using several bodies each having their own dimensions, mass and inertia. These bodies are for example the entire fuselage, rotor shaft, swashplate... and are joined together using constraints in the multi-body dynamics model. A complete overview of the multi-body model build-up is presented in the next section. Secondly, the aerodynamic models compute the forces and moments generated by the airflow and act on the different helicopter bodies. The aerodynamic models include for example the main rotor blade element and inflow model, fuselage drag model... The helicopter states like angle of attack and flying speed are measured on the helicopter bodies and passed to the aerodynamic models to compute the forces and moments which then act on specified locations of the bodies. Note that the gravity acceleration is defined as a constant in the model and acts directly on the CG of each body using its mass.

The aerodynamic models and bodies define the physics of the helicopter model. In order to fly the model, a control system of some sort is required. The control system will use the state feedback to suggest a set of control inputs in order to fly a certain mission or manoeuvre. These control inputs are translated into aerodynamic forces and moments which act on the helicopter bodies changing its states.

The entire model is constructed in a MATLAB SimMechanics/Simulink environment. One can make the analogy with building a multi-body model in a CAD software. Each component is given dimensions, mass and inertia. Next, the different bodies are joined using specified constraints. Similar to a CAD program, these constraints are for example a weld (fixed joint) or allow a certain degree of freedom (joints, bearings, rotating axis...). As this model needs to represent a flying object through space, the helicopter in constraint using a 6 degrees of freedom joint with respect to a ground reference plane. This allows the aerodynamic forces to fly the bodies around in 6 degrees of freedom. The reference system used to construct the model is presented in Appendix A.

The multi-body dynamics model allows to introduced several body sensors at certain locations in order to measure states. A crucial sensor will be placed at the CG of the helicopter reading states important for the flight dynamics analysis. Forces and moments are passed on to the bodies in vector formulation by actuating-blocks at certain locations.

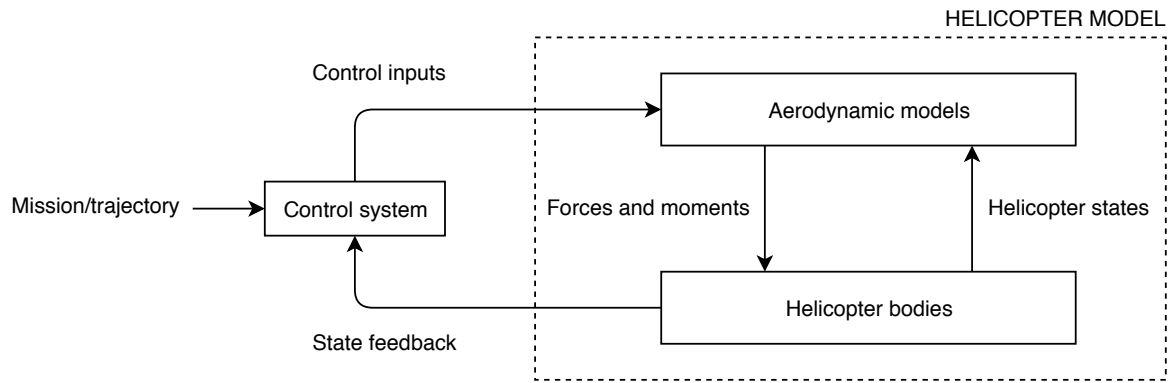


Figure 3.1: Helicopter model approach

When all physics models and interactions are defined in the multi-body dynamics environment, the program will solve the equations of motion. Therefore, there is no need to manually write down and compute the equations of motion. This allows for a very efficient construction and visual representation of a dynamic model. On the other hand, as a lot of computations are happening in the background of the multi-body dynamics software, it might be trickier to troubleshoot.

3.2. Structure of the Multi-Body Dynamics and Aerodynamic Model

A graphical overview of the multi-body structure is presented in Figure 3.2. In the center is the fuselage, which has the mass and inertia of the real UH-60A fuselage. The simplest connections are the welds. These are found between the fuselage CG and the main wing, the fuselage CG and main rotor gear box and at the vertical tail. A 1 DoF hinge allows the horizontal tail to deflect. The helicopter is allowed to freely move through space by the 6 DoF joint connecting the body CG with the ground (earth reference system).

It does get more complicated if the focus shifts towards the entire rotor hub assembly. Working from bottom to top, the body CG is connected to the main gearbox. This is where the main rotor shaft is held up and allowed to rotate all the way through the main rotor hub assembly. In the real UH-60A helicopter, the non-rotating swashplate is connected to the fuselage through pitch links. Separately moving these pitch links up and down pivots the non-rotating swashplate around the x- and y-axis defining cyclic inputs. Collective inputs are handled by moving all pitch links up and down at the same time. Because these rods are not modelled here, the non-rotating swashplate's orientation and height is directly set as a control input. The 2 DoF joint allows for the pivoting and the single translation DoF for moving up and down, Figure 3.2.

Moving up, one encounters the rotating swashplate. Actually, the non-rotating swashplate and rotating swachplate are 'mated' together. They lie on top of each other with the difference that the upper one spins with the main rotor shaft. In the real UH-60A, the spinning of the rotating swashplate is caused by a scissor link, connected to the main rotor shaft. This link is not modelled here.

The rotating swashplate is connected through 4 pitch links to the pitch horns. These are connected to the blade axis and allows to set the blade pitch by rotating around the feathering hinge. Another 1 DoF hinge allows the blade to flap up and down.

A graphical overview of the different aerodynamic models is presented in Figure 3.3. A blade element model using 10 equi-annular sections in combination with a Peters-He [38] inflow model is used for the main rotor aerodynamics. A non-linear lifting line model is used to model the main wing. The lifting line incorporates the effect of ailerons by applying different airfoils at the aileron location. Simple 2D wing models are used to represent the horizontal and vertical tail. The tail rotor is modeled as stated by Hilbert [23]. Finally, the compound thrust is modelled by a point force.

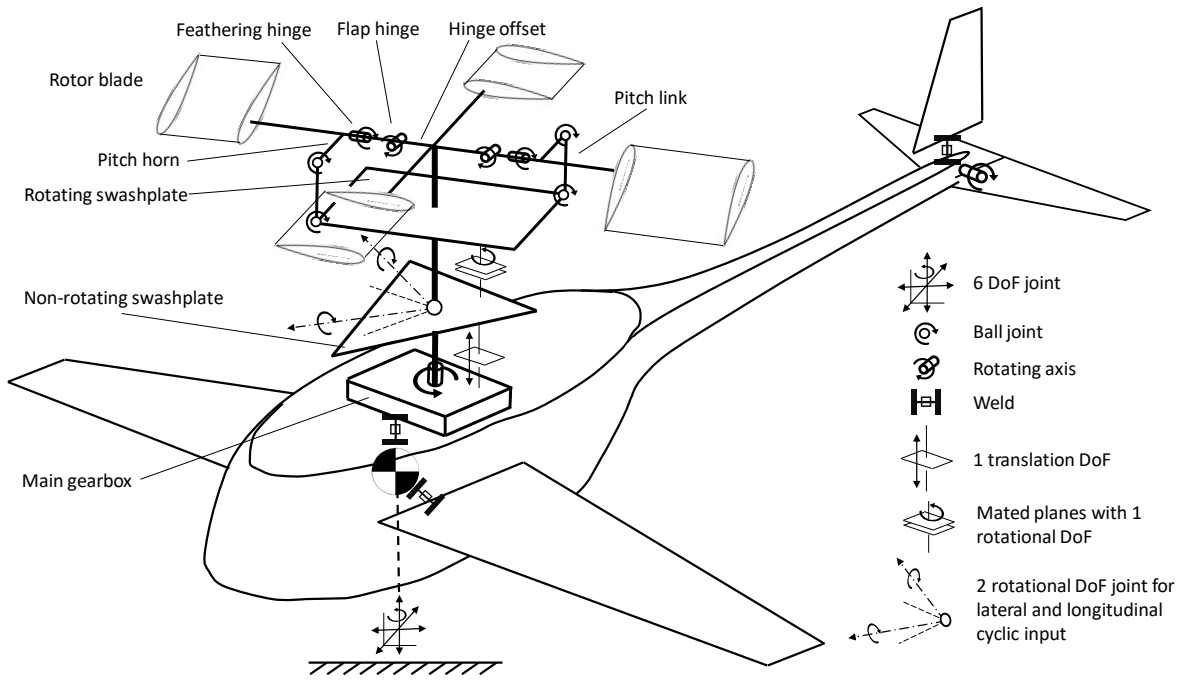


Figure 3.2: Overview of multi-body model

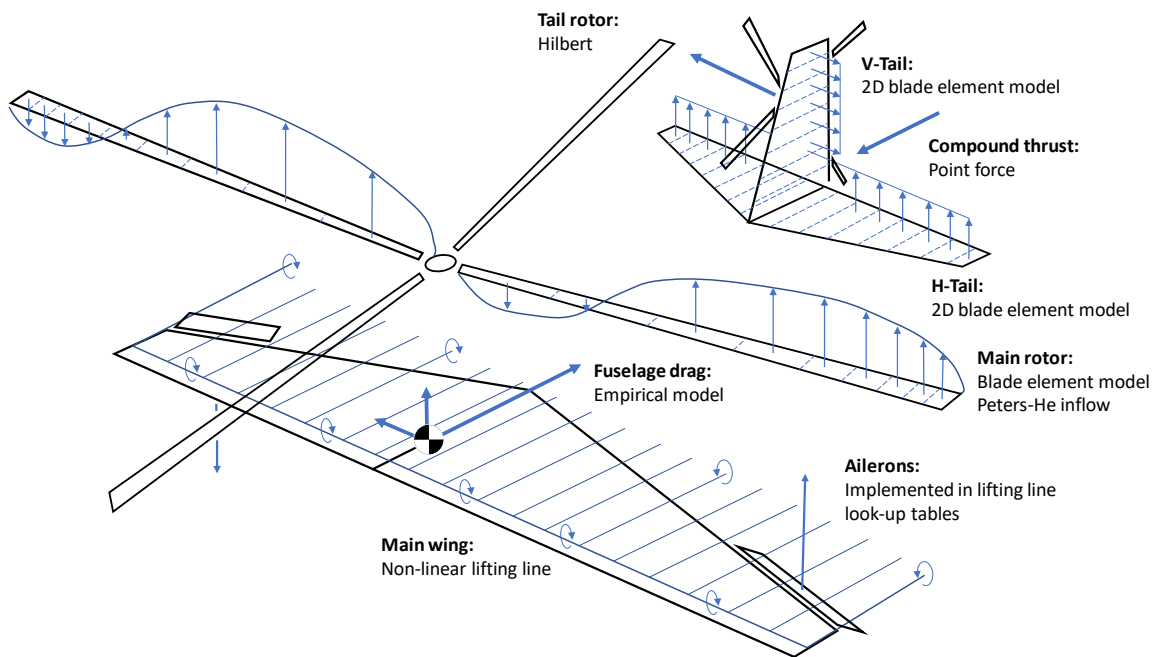


Figure 3.3: Overview of aerodynamic models

3.3. Main Rotor Model

Modelling of the main rotor is a complex task and crucial to this research as aerodynamic phenomena over the rotor will drive the loads in the blades. Modelling of the rotor is split up in 3 different domains:

1. Airloads: which couple the local angle of attack with the aerodynamic coefficients (c_l , c_d , c_m)
2. Induced velocity: computes the local angle of attack taking into account the inflow over the main rotor
3. Rotor dynamics: coupling between aerodynamics and blade motion which links to the blade loads

In order to choose a suitable model for this research, it is important to understand which phenomena need to be captured and which can be neglected. The thesis will investigate the effect of using different control input strategies on hub loads and handling qualities. This research will specifically look at forces and moments in the rotor hub during a roll doublet manoeuvre. The manoeuvres are performed at a flying speed of 120 kts.

The main rotor specifications are presented in Table 3.1.

Table 3.1: Main Rotor Specifications

Main rotor specifications	
Airfoil	NACA0012
Number of blades	4
Radius [<i>m</i>]	8.1778
Solidity [–]	0.0821
Blade mass [<i>kg</i>]	127.8
Flap inertia [<i>kg m²</i>]	0.3056
Rotor forwards tilt [°]	3

3.3.1. Airloads

The blade is divided into 10 equi-annular spaced elements. The airloads acting on each section are found through quasi-steady look-up tables linking the local angle of attack with the aerodynamic coefficients (c_l, c_d, c_m). These look-up tables are generated by wind tunnel test of the NACA0012 for an angle of attack range from -180° till 180° to take into account regions of reversed flow area of the disk. The look-up tables are made for different Mach numbers to correct for comparability effects and include stall. A dynamic stall model was not added to this model, which will be discussed in the results chapter.

Furthermore, losses near the blade tips are not corrected over the aerodynamic coefficients but taken into account in the inflow model.

3.3.2. Induced Inflow Model

Another challenge is the accurate modeling of the local angle of attack which is a function of time, radius and azimuth angle, Equation 3.1.

$$\alpha(\psi, r, t) = a_{pitch} + \alpha_{twist} + \alpha_{flap} + \alpha_{wh} + \alpha_{inflow} \quad (3.1)$$

a_{pitch} is the physical pitch setting of the blade, α_{twist} is the static and dynamic blade twist. α_{flap} is the influence caused by the flapping motion. α_{wh} stands for the inclination of the flow at the hub and α_{inflow} the inflow angle.

The goal of this research is to minimise hub forces and moments which are mainly caused by the 1/rev flapping. Therefore, Hamers & Basset [22] suggest using a dynamic finite-state inflow model suitable for manoeuvring flight modelling. Dynamic inflow models take into account the time lag between the build up of the induced velocity and changes in inflow state. Instead of modelling the vortices of the wake, finite-state models use a time constant to simulate the induced velocity build-up and are suitable for real-time simulations as stated by Chen [14] (computationally efficient). Hamers & Basset [22] suggest the Pitt-Peters or Peters-He inflow model which show similar performance, however, the latter gives better results in terms of vibrations and aeroelastic effects. The Peters-He inflow model was selected for this thesis. This can be seen as an overkill as the Pit-Peters is sufficient. But this specific rotor model offers flexibility to use the constructed model for a wider range of applications. So it is a practical decision to chose the Peters-He model over the Pit-Peters model. These type of inflow models are also used by load alleviation studies discussed in the literature study, Chapter 2.

Inflow models used for rotorcraft applications decompose the blade dynamics, lifting theory and inflow. The coupling between these three elements, as implemented in the main rotor model, is shown by Figure 3.4 and linked to Equation 3.1. The Peters-He inflow model computes the induced flow by a distribution function over the rotor radius which changes over the azimuth. The theory is based on the acceleration potential equations and only compute the inflow perpendicular to the disk. For a detailed description of the Peter-He inflow model used for this thesis, the reader is referred to the work by Peters and He [38].

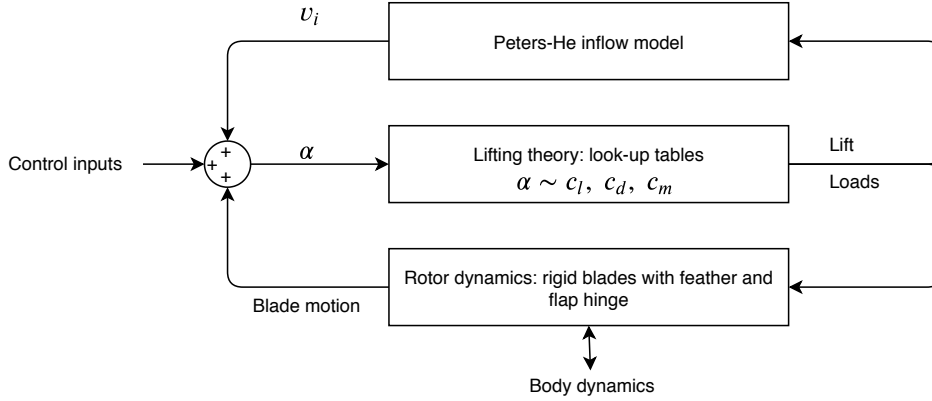


Figure 3.4: Coupling between blade dynamics, lifting theory and inflow

3.3.3. Rotor Dynamics

The performance of the load alleviation strategy will be measured by the reduction in rotor hub loads. Padfield [36] describes different levels of rotor modelling. In the lowest level, rigid blades are assumed for calculating blade flap, lag and torsion. In terms of modelling the flexibility of the blades, Padfield states the higher the mode, the less significant. If the blade loading distribution is close to the shape of the first flap-bending mode, modelling only the first mode should be sufficient. Although this is generally not the case, the first flap mode often results in a good approximation of the zero and 1/rev blade dynamics and hub moments. This phenomenon can be explained by the first flap mode frequency always being close to the 1/rev frequency [36]. Note that this is specific to an articulated rotor system which is used on the UH-60A.

3.4. Tail Rotor Model

The tail rotor acts as the main rotor anti-torque mechanism. The tail rotor will not be used for any other tasks in this research and therefore does not required a very high fidelity model.

The tail rotor model is based on work done by Hilbert [23]. The model is similar to the widely used Bailey model [9] but extended to compute the rotor torque and in-plane rotor forces next to thrust. The inputs of the model are the collective setting of the tail rotor blades, the tail rotor shaft speed and the body velocities measured at the tail rotor position. The tail rotor shaft speed is directly linked to the main rotor shaft speed through a 1/4.6122 gear ratio. The computed forces and moments are placed at the tail rotor location on the vertical tail. Note that the interference effects of the tail and main rotor wake were not taken into account for this research.

3.5. Fuselage Aerodynamic Model

The aerodynamic forces and moments generated by the fuselage are found using data regressions of wind tunnel experiments as described by Hilbert [23]. The forces and moments depend on the fuselage angle of attack and side slip angle measured at the nose, defined by Equation 3.2 - 3.7. These forces and moments are transformed into the body reference system and applied at the helicopter's CG. For this research, interference effects of the main rotor onto the fuselage were not taking into account.

$$\text{Drag: } \frac{D}{q} = 90.0555 \sin^2 \alpha - 41.5604 \cos \alpha + 2.94684 \cos 4\beta - 103.141 \cos 2\beta - 0.535350 \times 10^{-6} \beta^4 + 160.2049 \quad (3.2)$$

$$\text{Lift: } \frac{L}{q} = 29.3616 \sin \alpha + 43.4680 \sin 2\alpha - 81.8924 \sin^2 \alpha - 84.1469 \cos \alpha - 0.0821406\beta + 3.00102 \sin 4\beta + 0.0323477\beta^2 + 85.3496 \quad (3.3)$$

$$\text{Sideforce: } \frac{Y}{q} = 35.3999 \sin \beta + 71.8019 \sin 2\beta - 8.04823 \sin 4\beta - 0.980257 \times 10^{-12} \quad (3.4)$$

$$\text{Pitching: } \frac{M}{q} = 2.37925\alpha + 728.026 \sin 2\alpha + 426.760 \sin^2 \alpha + 348.072 \cos \alpha - 510.581 \cos^3 \beta + 56.111 \quad (3.5)$$

$$\begin{aligned} \text{Rolling: } \frac{\ell}{q} &= 614.797 \sin \beta + \frac{\beta}{|\beta|} (-47.7213 \cos 4\beta - 290.504 \cos^3 \beta \\ &\quad + 735.507 \cos^4 \beta - 669.266) \quad 25^\circ < |\beta| \leq 90^\circ \\ \frac{\ell}{q} &= \frac{\beta}{|\beta|} (455.707 \cos^4 \beta - 428.639) \quad 10^\circ < |\beta| \leq 25^\circ \\ \frac{\ell}{q} &= 0.0 - 10^\circ \leq \beta \leq 10^\circ \end{aligned} \quad (3.6)$$

$$\begin{aligned} \text{Yawing: } \frac{N}{q} &= 220.0 \sin 2\beta + \frac{\beta}{|\beta|} (671.0 \cos^4 \beta - 429.0) \quad 20^\circ < |\beta| \leq 90^\circ \\ \frac{N}{q} &= -278.133 \sin 2\beta + 422.644 \sin 4\beta - 1.83172 \quad -20^\circ \leq \beta \leq 20^\circ \end{aligned} \quad (3.7)$$

3.6. Horizontal and Vertical Tail Model

The vertical tail acts as a mechanism to counter side slip angles. The vertical tail will not be used for any other purposes in this research and therefore allow for a simple model representation. A sensor placed in the multi-body dynamics model measures the local flow conditions on the tail to compute the angle of attack. Look-up tables are used to link the angle of attack with the aerodynamic coefficients. The tail surface is divided into elements and lift is found using the conventional lift formula with the c_l from look-up tables and the area of each wing element. The model does not take into account 3D effects.

A similar approach is implemented for the horizontal tail. Additionally, the horizontal tail features a hinge to allow control inputs to deflect the tail. As the flow sensor is mounted onto the tail, it is not required to change the model as previously discussed for the vertical tail. This level of modelling is adequate as only trim settings and low frequency deflections are to be expected for this research.

The horizontal stabiliser and vertical fin are defined according to the specs given by Sikorsky in [27], Table 3.2.

Table 3.2: Horizontal stabiliser and vertical fin specifications according to Sikorsky [27]

Horizontal tail specifications			
Area [m^2]	4.18	Station Line Position 0.25c [m]	-17.79
Span [m]	4.39	Butt Line Position 0.25c Right Wing [m]	0
c_{root} [m]	1.12	Water Line Position 0.25c [m]	-6.20
c_{tip} [m]	0.77	Airfoil	NACA 0012
Vertical fin specifications			
Area [m^2]	3	Station Line Position 0.25c [m]	-17.65
Span [m]	2.49	Butt Line Position 0.25c Right Wing [m]	0
c_{root} [m]	1.83	Water Line Position 0.25c [m]	-6.93
c_{tip} [m]	0.86	Airfoil	NACA 0012

3.7. Compound Wing Model

For this specific application, the wing shall fulfill the following set of functions:

1. The wing shall create lift to carry a part of the weight of the helicopter and offload the main rotor.
2. The wings are a platform for mounting the ailerons which are the redundant controls of the compound helicopter and crucial for this research.
3. The wings shall have a damping effect during helicopter manoeuvres (ex. during rolling). Therefore a realistic modelling of the lift is required.

The wing will be constructed within the multi-body dynamics environment as a solid body. Sensors placed on this body will read the different states which are used as an input to calculate the aerodynamic forces and moments.

The wing used for this research will be the same as presented by Thorsen [47]. Thorsen describes the modified UH-60A model from Pennsylvania State University which is used for research concerning new helicopter configurations in the Future-Vertical-Lift program [12]. The main wing design is a compromise between induced drag and manoeuvrability capabilities. The wing area is set to 10% of the main rotor disk area. The characteristics of the wing are summarized in Table 3.3. The wing position is defined according to the model reference frame presented in Appendix A.

The appropriate aerodynamic model needs to be constructed. First, the unsteadiness of the model is investigated. As stated by Leishman [29], this can be done by computing the reduced frequency k with ω being the wing pitching frequency, Equation 3.8. For this research, a forward velocity between 45kts-180kts can be assumed, the chord is set to the wing MAC and the wing oscillations during manoeuvres will not exceed 1Hz. Using Equation 3.8, the maximum reduced frequency of the wing for this research will be $k = 0.0171$. As this number is well below 0.05 at which unsteady aerodynamics needs to be considered according to Leishman [29], assuming steady aerodynamics can be justified.

As stated above, realistic wing damping behaviour during roll manoeuvres will be required for this research. Therefore, a 3D representation of the wing is necessary. A lifting line model is chosen as it offers a good trade-off between computational efficiency and accuracy. The lifting line is extended to use look-up tables to link the airfoil's aerodynamic coefficients with the angle of attack instead of assuming a linear lift curve. This also allows to compute the aerodynamic coefficients in terms of Mach number and offers a convenient method to switch airfoil, add stall models... if required.

Note that the interactions of the rotor with the main wing are not modelled as experiments will be done at a flying speed of 120 kts. The wake skew angle is large enough and the rotor wake will not impinge on the main wing.

$$k = \frac{\omega c}{2V} \quad (3.8)$$

Table 3.3: Compound Wing Specifications

Compound Wing Specifications			
Effective Area [m^2]	20.90	Wing Incidence [$^\circ$]	4
Effective Span [m]	13.716	Station Line Position 0.25c [m]	-9.0932
MAC [m]	1.524	Water Line Position 0.25c [m]	-6.477
c_{root} [m]	1.675	Airfoil	NACA 63-412
c_{tip} [m]	1.373	Taper [-]	1.22

3.7.1. Non-Linear Lifting Line Model

The lifting line model is based on the work presented by Phillips and Snyder in [39] and extends the classic Prandtl's lifting line to a fully three-dimensional vortex lifting line. This means the model can cope with wing sweep and dihedral. As this aerodynamic model will run through time and therefore converge for each time step, the non-linear lifting line offers a good trade-off between computational costs and accuracy.

A visual representation of the lifting line model is presented by Figure 3.3 and in more detail by Figure 3.5.

The lifting line model consists of a set of horseshoe vortices defined as bound vortices located on the quarter chord line and 2 trailing vortices. The horseshoe elements are placed on the wing forming a vortex distribution so each trailing vortex coincides with the trailing vortex of the neighbouring horseshoe. These counter rotating vortices partly cancel each other and only the difference in vorticity is shed from the wing along the trailing vortices.

The velocity effect of an individual vortex line at an arbitrary point in space can be calculated using the Biot-Savart law, Equation 3.9. The effect of an entire horseshoe element consisting of a bound and two trailing vortices can be written according to the Biot-Savart rule, Equation 3.10.

$$\mathbf{V} = \frac{\Gamma}{4\pi} \frac{\mathbf{r}_1 \times \mathbf{r}_2}{|\mathbf{r}_1 \times \mathbf{r}_2|^2} \mathbf{r}_0 \cdot \left(\frac{\mathbf{r}_1}{r_2} - \frac{\mathbf{r}_2}{r_1} \right) \quad (3.9)$$

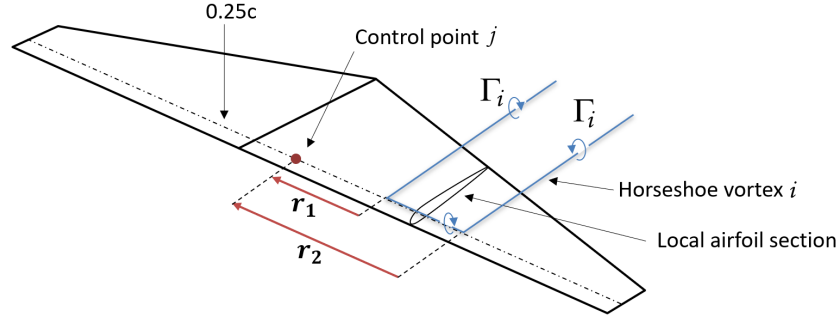


Figure 3.5: Lifting line horseshoe vortex

$$\mathbf{V} = \frac{\Gamma}{4\pi} \left[\frac{\mathbf{u}_\infty \times \mathbf{r}_2}{r_2 (r_2 - \mathbf{u}_\infty \cdot \mathbf{r}_2)} + \frac{(r_1 + r_2)(\mathbf{r}_1 \times \mathbf{r}_2)}{r_1 r_2 (r_1 r_2 + \mathbf{r}_1 \cdot \mathbf{r}_2)} - \frac{\mathbf{u}_\infty \times \mathbf{r}_1}{r_1 (r_1 - \mathbf{u}_\infty \cdot \mathbf{r}_1)} \right] \quad (3.10)$$

The total velocity at an arbitrary control point placed along the quarter chord of the wing is the sum of $v_{\infty j}$ and the induced velocity generated by each vortex horseshoe element, Equation 3.11. Note that $v_{\infty j}$ stands for the local freestream velocity at control point j . In trimmed flight, this velocity is the same for every element but changes when the aircraft starts to roll.

$$\mathbf{V}_j = \mathbf{V}_{\infty j} + \sum_{i=1}^N \frac{\Gamma_i \mathbf{v}_{ij}}{\bar{c}_i} \quad (3.11)$$

\mathbf{v}_{ij} is the dimensionless velocity induces by vortex j at control point i . Applying the Biot-Savart law for horseshoe vortex segment, \mathbf{v}_{ij} can be written according to Equation 3.12. Note that if $i = j$, the downwash effect of the bound vortex is excluded as the control point lies on top of the bound vortex.

$$\mathbf{v}_{ij} = \begin{cases} \frac{\bar{c}_i}{4\pi} \left[\frac{\mathbf{u}_\infty \times \mathbf{r}_{i2j}}{r_{i2j}(r_{i2j} - \mathbf{u}_\infty \cdot \mathbf{r}_{i2j})} + \frac{(r_{i1j} + r_{i2j})(\mathbf{r}_{i1j} \times \mathbf{r}_{i2j})}{r_{i1j} r_{i2j} (r_{i1j} r_{i2j} + \mathbf{r}_{i1j} \cdot \mathbf{r}_{i2j})} - \frac{\mathbf{u}_\infty \times \mathbf{r}_{i1j}}{r_{i1j}(r_{i1j} - \mathbf{u}_\infty \cdot \mathbf{r}_{i1j})} \right] & , i \neq j \\ \frac{\bar{c}_i}{4\pi} \left[\frac{\mathbf{u}_\infty \times \mathbf{r}_{i2j}}{r_{i2j}(r_{i2j} - \mathbf{u}_\infty \cdot \mathbf{r}_{i2j})} - \frac{\mathbf{u}_\infty \times \mathbf{r}_{i1j}}{r_{i1j}(r_{i1j} - \mathbf{u}_\infty \cdot \mathbf{r}_{i1j})} \right] & , i = j \end{cases} \quad (3.12)$$

The local angle of attack, being the effect of the freestream velocity and the downwash effects, is calculated by Equation 3.13

$$\alpha_j = \tan^{-1} \left(\frac{w_j}{u_j} \right), \quad \mathbf{V}_j = (u_j, v_j, w_j) \quad (3.13)$$

In order to extend to model by Phillips and Snyder [39] to regions of non-linear lift, look-up tables are used to link the local angle of attack α_j with the aerodynamic coefficients of the airfoil. These look-up tables were constructed in XFOIL [33] for different Mach numbers. On top of this, a stall model is added as presented by Thorsen [47] for this exact wing, Equation 3.14-3.16. This model is applied at angles above the stall angle of attack. The ailerons are implemented into the lifting line model as different airfoils over a certain span section of the wing. An airfoil with a flap at different deflection angles are models in XFOIL and stored in the look-up tables. Finally, the aerodynamic coefficients are found by interpolating the look-up tables for angle of attack, Mach number and aileron deflection angle.

$$c_l = 1.6 \sin(2\alpha) \quad (3.14)$$

$$c_d = -1.3 \cos \left(-2\alpha + \frac{\pi}{10} \right) + 1.31 \quad (3.15)$$

$$c_m = 0.08 \sin^3(1.1\alpha + \pi) - 0.03 \quad (3.16)$$

Since lift is now non-linear, the Jacobian method used by Phillips and Snyder [39] to find the set of vortex strengths does not work anymore. Therefore, another numerical scheme similar to the method presented by Anderson [6] was used. A flowchart of the convergence algorithm to find the lift distribution is presented in Figure 3.6. For this application, the wing was split in 40 sections according to a cosine-distribution.

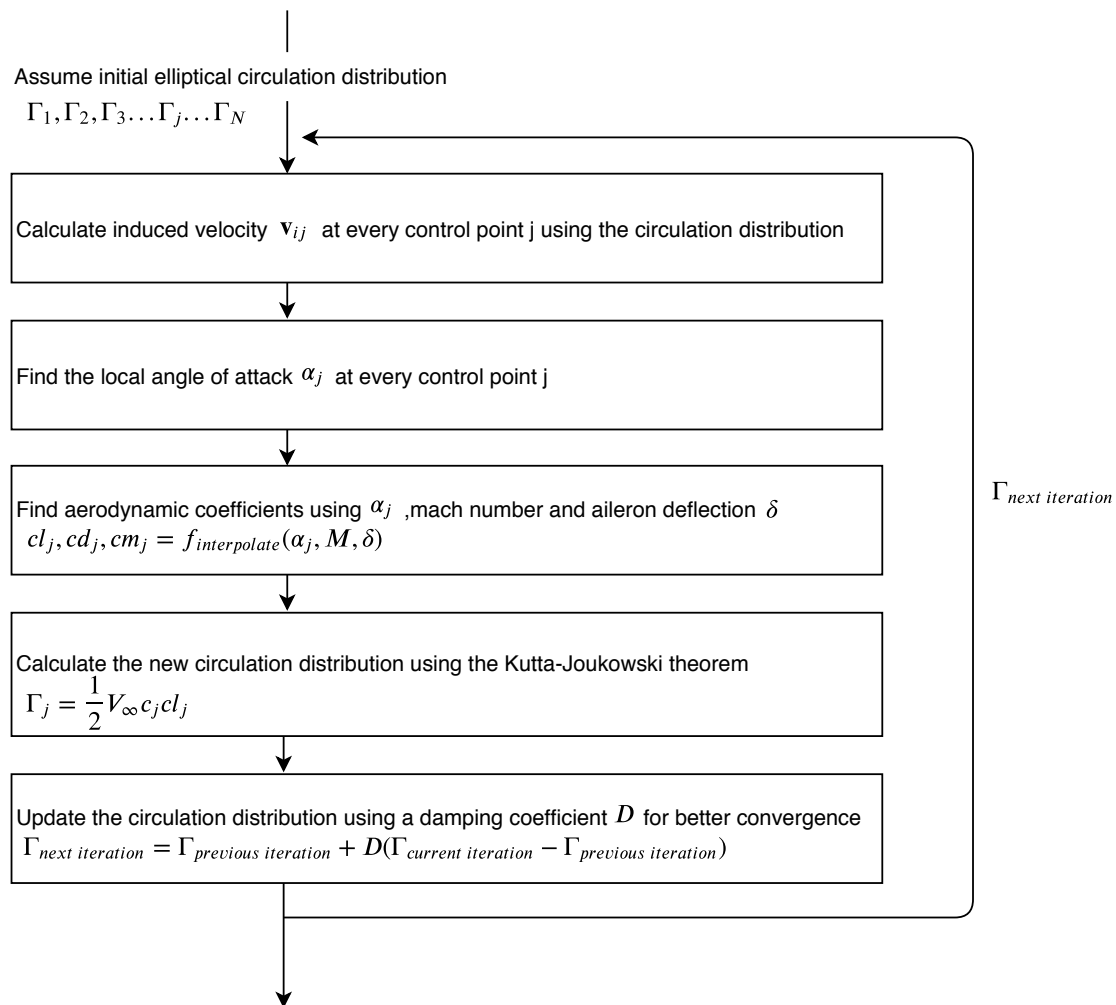


Figure 3.6: Lifting line convergence algorithm flowchart

3.8. Compound Thrust Model

The compound thrust will be used to put the compound helicopter in a different trim effect and learn how this might affect loads and handling qualities. Therefore, there is no real need for a complicated propeller model. The compound thrust is modelled as a point force which acts at the tail location. The force is aligned with the fuselage CG and does not create a pitching moment. If one wants to know the power required of the compound thrust, it can be calculated in post-processing.

4

Flight Controller Design for Trim

Experiments using the helicopter model will always start from a trimmed flight situation. Also during the development of the model, trimmed flight is needed to validate new changes and functionalities. An efficient and robust trim method is required capable of handling changes in the model characteristics. Several trim techniques were tested and explained in 4.1. In the end, a flight controller was used to 'fly' the helicopter to a desired trim situation. This method was proven to be fast and robust. The layout of the controller is presented in Section 4.2. Tuning of the control gains and its applicability to a compound helicopter configuration is covered by Section 4.3.

4.1. Trim Method Approach

The goal of a trim algorithm of a 6 DoF model is to pull the vehicle's 3 linear accelerations and 3 angular accelerations to zero to achieve a steady flight condition. These 6 accelerations are given in Equation 4.1. The available control inputs for the conventional UH-60A are the main rotor controls: collective and cyclic, the tail rotor collective and the body Euler angles θ and ϕ , Equation 4.2. Note that θ and ϕ define the direction of the gravity vector and cannot be controlled directly by the pilot. However, they are defined as controls as a 6 DoF model requires an equal amount of controls [18]. The trim problem can be stated as finding a set of control inputs which drive all body accelerations to zero. Or, if an initial control input guess is used, find a delta control input which needs to be added to the initial guess to pull the accelerations to zero. Note that only the controls of a conventional helicopter are listed here. This is because the model was updated from a conventional UH-60A towards a compound version requiring a control system using the inputs as stated below. In this research, the controls specific to the compound helicopter were varied during trim but did not require an update of the control system as will be explained in Section 4.3.

$$a = [\ddot{u} \ \ddot{v} \ \ddot{w} \ \dot{p} \ \dot{q} \ \dot{r}] \quad (4.1)$$

$$c = [\theta_0 \ \theta_{1s} \ \theta_{1c} \ \theta_{TR} \ \theta \ \phi] \quad (4.2)$$

The 'fly-to-trim' method was selected. An initial trim guess is required, after which the model is 'flown' towards a desired steady condition within one simulation. This is done by using a closed-loop control system allowing the control inputs to change in order to capture a prescribed steady flight reference signal. Trim is reached during a single run of the model as the body accelerations converge to zero through the simulation time. This is different from other trim methods which often require several runs of the model as will be explained later.

However, the 'fly-to-trim' method was discouraged by Dreier [18] stating numerous disadvantages. Dreier stated the 'fly-to-trim' method will only be applicable for a specific situation like straight and level flight. For this project, only a level flight trim situation is required for validation purposes and to set the initial condition prior to executing a manoeuvre. A second problem mentioned by Dreier is the robustness of this method, risking it would only work for one specific aircraft configuration. However, the flight controller showed no difficulties coping with model updates like different inflow models, changes in main rotor location, the addition of compound wings and CG changes, without changing the architecture. It should be noted that there can be a risk of losing the trimming capabilities of the controller if specific model variables are updated. For

example, it was observed that the system is sensitive to changes in the blade inertia and CG location, causing the model to be untrimmable with the initial controller. In the best case, the gains require retuning, in the worst case, the architecture needs an update. Dreier also states two additional practical challenges. The first one being the fact that the feedback states are not available at time zero at the initiation of the simulation. This was solved by switching the trim controller ON after a short amount of time (0.2-1 sec). This also avoided the controller to over-correct the 'extreme' transient response at the initiation of the model as rotor states like flap angle are settling. Finally, Dreier states the challenge of designing the controllers to change the vehicle's accelerations which have unfamiliar units and therefore complicate the tuning process. The controllers were set up to capture a reference state by controlling the Euler angles through controlling the body rates. For example, the forward speed [m/s] is controlled by the pitch angle [$^\circ$] by controlling the pitch rate [$^\circ/s$], avoiding the unfamiliar units of the body accelerations. This principle will be discussed in the control architecture in the next section.

Before the 'fly-to-trim' method was selected, two other trim methods were attempted. Initially, the Jacobian method was used to try and trim the model. The Jacobian method approximated the helicopter response by a Taylor expansion, ignoring terms higher than first order. This can be seen as a sort of linearisation. The Jacobian-matrix J needs to be constructed which contains the links between the inputs and model outputs in the form of partial derivatives. These partial derivatives are found by exciting the model for each control input and locally approximating the response as linear. If a central difference formulation for the local derivatives is used, 72 runs of the model are required to construct the J matrix. Also, the initial condition needs to be carefully defined taking the outcome from the previous iteration. The model is specifically sensitive to the rotor position and flapping degrees of freedom. Because of the number of required runs and the sensitivity to the initial conditions, this method was found to be less practical for this multi-body dynamics environment. The Jacobian method uses a fairly simple convergence method to pull the body accelerations towards zero. In order to improve this, a second trim approach was attempted. This time, the trim problem was stated as a weighted optimisation problem. The *Fminsearch* function in MATLAB was used to change the controls. This method showed improved convergence but did not perform better than the 'fly-to-trim' method.

4.2. Trim Controller Architecture

The 'fly-to-trim' uses the 4 conventional helicopter control inputs: main rotor collective θ_0 , cyclic input θ_{1s} , θ_{1c} and the tail rotor collective θ_{TR} . Each input has its designated controller which controls the vehicle's response to a reference signal using the state feedback of the model. An overview of the set-up is presented in Figure 4.1. The two additional inputs to be able to control a 6 DoF model are the vehicle's pitch and roll angle. Note that the pitch and roll angle have no designated controller but are allowed to settle throughout the simulation. The control system is designed as a sequence of P(I) controllers according to the time-separation principle. Each controller is build up using a set of inner loops. Each inner loop will control one order at the time. For example in Figure 4.3 from right to left, the pitch rate is controlled by θ_{1s} , pitch angle is controlled by the pitch rate and the forward speed is controlled by the pitch angle. This assures robustness over directly controlling the forward speed by θ_{1s} .

The controllers were build up step by step. Within the model, the link between the helicopter and world (ground) is a custom joint with the capability of defining the degrees of freedom. This allows to freeze certain motions and gradually build up the controllers.

First, the height controller was designed by allowing the helicopter to translate freely along the z-axis. The height is controlled by the desired climb rate which is changed by the main rotor collective input. The height controller is presented in Figure 4.2. A sequential P + PI controller assures good height tracking performance.

The longitudinal controller was designed by allowing the helicopter to translate along the x-axis and pitch around the y-axis. The forward speed of the helicopter being a combination of u and w is controlled by a desired pitch angle θ which is controlled by a desired pitch rate as a result of a longitudinal input θ_{1s} , Figure 4.3. Good forward speed tracking was achieved by implementing a sequential PI + P + PI controller.

Next, the vehicle is allowed to move along the y-axis and roll around the x-axis. In order to achieve symmetric straight and level flight, a lateral controller was implemented tracking a 0 m/s sideways speed reference signal, $v = 0m/s$. This is achieved by setting a desired roll angle ϕ , through a desired roll rate p by controlling the lateral cyclic θ_{1c} . A PI - PI - PI sequence was implemented as shown in Figure 4.4.

Finally, the last DoF was unfrozen to allow the helicopter to rotate around the z-axis. The direction is set by controlling ψ by a desired yaw rate r , by the tail rotor collective input θ_{TR} . This controller is shown in Figure 4.5.

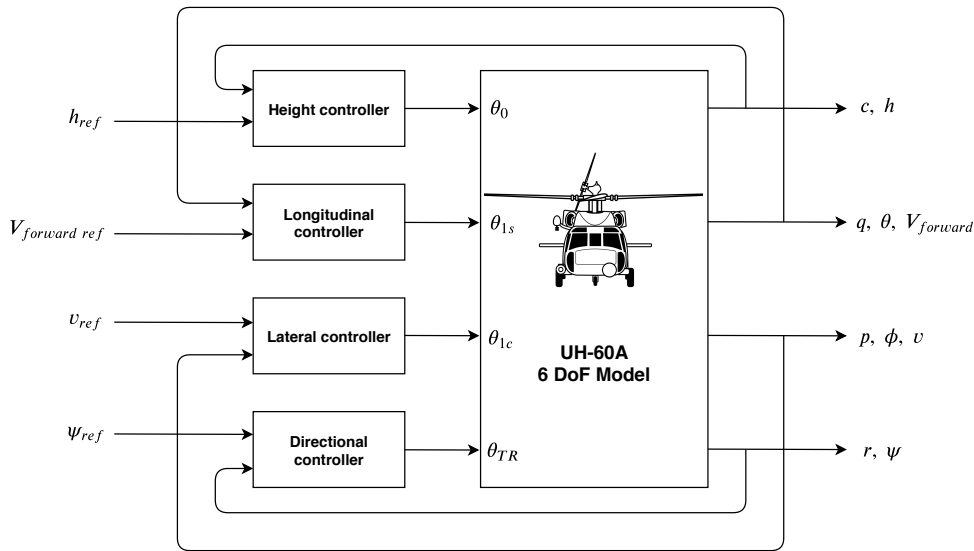


Figure 4.1: UH-60A control system overview

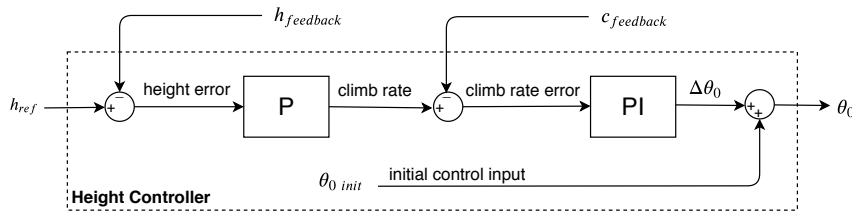


Figure 4.2: Height controller flow diagram

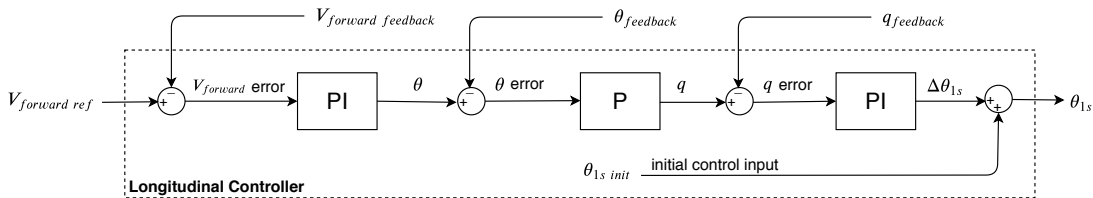


Figure 4.3: Longitudinal controller flow diagram

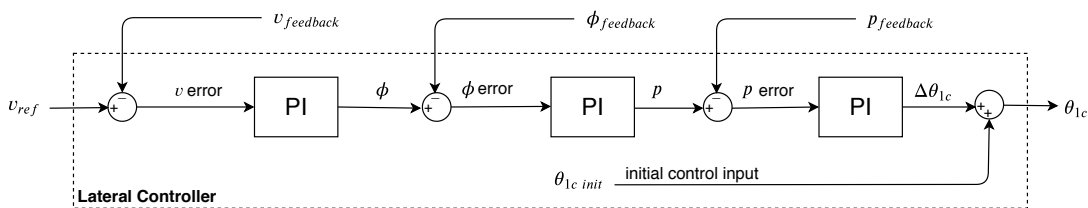


Figure 4.4: Lateral controller flow diagram

4.3. Controller Tuning and Applicability on a Compound Helicopter Type

In this research, the controller is solely used as a 'fly-to-trim' method to achieve a level flight condition. This is required to define the initial condition prior to the load alleviation experiments but also during the development of the model to be able to validate a realistic flying situation. This means the controller is not required to handle abrupt flight path trajectory changes but shall cope well with changes to the aircraft model. This requires the design of a robust controller. Robustness is assured by designing the controller according to the

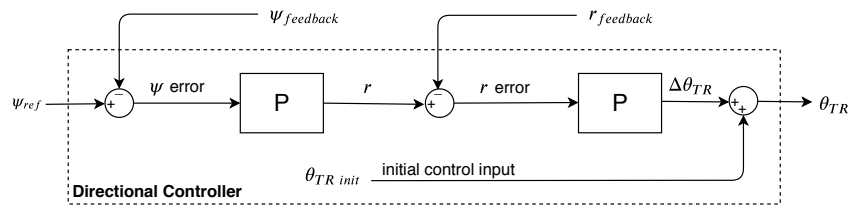


Figure 4.5: Directional controller flow diagram

time-separation principle as discussed earlier.

The controllers are tuned using the response to a step reference signal, working from the inner loop towards the outer control loop. For example, the longitudinal controller shown in Figure 4.3, first the response to a pitch rate step q was manually tuned until satisfying tracking performance was achieved. Gains were implemented in a PI controller. Next, satisfying tracking performance to a pitch angle step θ reference signal was assured by the P controller. Finally, a step on the forward speed was used to tune the last PI-controller. This process was repeated throughout the entire control system. The I-element was only added if a P controller was not sufficient and compensation for a steady state error was required.

The same control system was used for both the conventional as well as the compound version of the model. The control system used for this research only needs to provide trimmed level flight. This research will investigate the effect of using different control strategies to roll the aircraft. Each of these control strategies is a predefined control input through time. No state feedback is required and all other controls are frozen at their trim values to clearly isolate the effect of using different control strategies. The thesis will also investigate the effect of different trim settings prior to the rolling manoeuvre. The trim settings are set to vary controls typical for the compound helicopter configuration: horizontal tail deflection, compound thrust, reduced main rotor rpm and constant aileron deflection during trim. Each of these listed controls are varied separately outside the control system. For example the horizontal tail deflection was set to $i_{tail} = 5^\circ$ and the 'fly-to-trim' controller is allowed to change conventional helicopter controls to achieve trim in this condition. The control system only required returning to cope with the changes between the conventional and compound version of the UH-60A model.

5

Model Validation

Before the compound helicopter model will be used to conduct a series of experiments, an elaborate model validation campaign is required. This validation step took a major part of the time allocated for this thesis research. To perform a secure step by step validation, the constructed multi-body dynamics model was cross-checked with a commercially available software FLIGHTLAB at different stages of complexity. So next to the model construction described in the previous chapters, the entire model was also replicated in the FLIGHTLAB software.

It is important to understand that it is not possible to create the exact same model in FLIGHTLAB. The main differences between the the constructed model and FLIGHTLAB are presented in Section 5.1.

The validation process is divided into 3 steps. First, the trim condition is analysed. To start simple, the conventional UH-60A model without inflow model is compared with its equivalent in FLIGHTLAB. When a close match is assured, the Peters-He inflow model is added and a second comparison is done for trimmed flight. The trim validation is presented in Section 5.2. As this research focuses on load reduction during manoeuvres, the dynamics responses need to be validated. The response to a lateral cyclic input was compared between the constructed multi-body dynamics model and FLIGHTLAB in Section 5.3. After the conventional UH-60A model was upgraded to the compound version, the non-linear lifting line model for the main wing was validated against a vortex-lattice method AVL [32] in Section 5.4. Differences found in the results are linked with the differences between the constructed model and FLIGHTLAB in the validation conclusion, Section 5.5.

5.1. Model Differences Between the Constructed Multi-Body Dynamics Model and FLIGHTLAB

The main difference between the the developed model and FLIGHTLAB is the entire hub assembly model. In the model developed for this research, the entire hub and swashplate system are represented by several bodies linked to each other, as previously explained. FLIGHTLAB does not feature an actual representation of the entire assembly and rotor control inputs directly change the blade pitch. FLIGHTLAB also features a different fuselage drag model. The drag model used for this thesis is presented in Section 3.5 and based on test data. Both models feature a Peters-He inflow model. As a wide range of variations of this inflow model exist, differences between the two models are expected. Unfortunately, this cannot be checked as there is no access to the source code of FLIGHTLAB.

The parameters used to construct the multi-body dynamics model are loaded from separate specification files per helicopter component. For example, all rotor specs are saved in one file, all fuselage specs in another file... In order to ensure a close match between the two models, FLIGHTLAB uses this same files to define the helicopter model.

Note that only a conventional UH-60A helicopter model was validated with FLIGHTLAB. This was done before the model was further modified towards a compound version of the UH-60A. The focus of the validation with FLIGHTLAB lies on the correct rotor responses. When this is guaranteed, the rotor is expected to behave correctly when the model is modified to a compound version. There are no differences in rotor specification between the normal UH-60A model and the compound version.

5.2. Validation of the Trim Condition

For validation purposes, the model was trimmed at different flying speeds to compare the states with FLIGHT-LAB. Figure 5.1 shows how the model is flown to different flying speeds by following a forward speed reference signal. Figure 5.2 shows how the Euler angles settle at different flying speeds. The measurements to evaluate the trim condition are taken when the states are fully settled as indicated in Figure 5.1. During the actual measurements, the control inputs are frozen for a short amount of time to avoid the interference of slightly oscillating control inputs. Note that β shows an oscillating response when the helicopter reaches zero air-speed as β is measured as the angle between the forward and sideways speed.

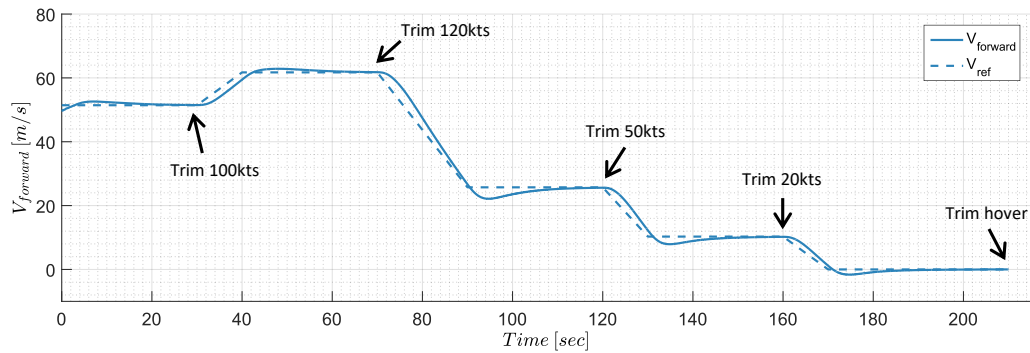


Figure 5.1: Forward speed tracking during 'fly-to-trim'

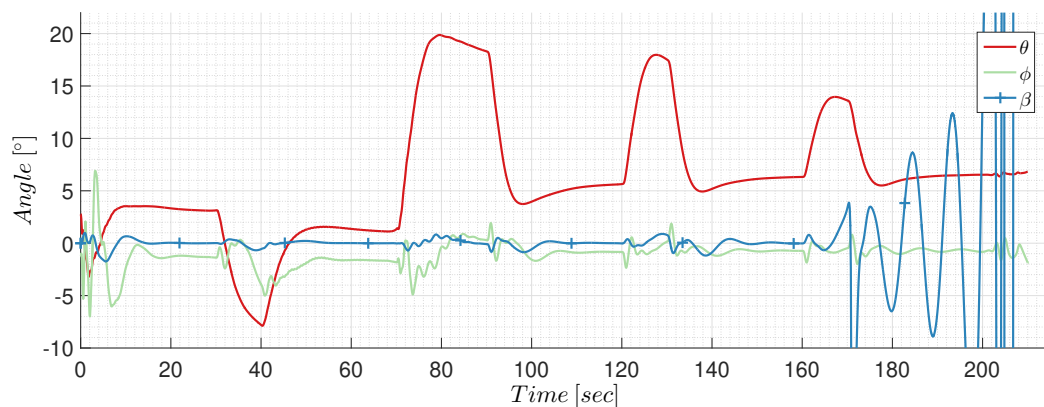


Figure 5.2: Vehicle Euler angles during 'fly-to-trim'

The trim condition of a UH-60A without inflow model at hover, 20 kts, 50 kts, 100 kts and 120 kts are compared with FLIGHTLAB in Table 5.1 and Figure 5.3-5.12. The same analysis is done for a UH-60A model with Peters-He inflow model in Table 5.2 and Figure 5.13-5.22. Note that the situation over the rotor is only plotted at 120 kts, all other flying cases are presented in Appendix B and C.

5.2.1. Trim Validation Conventional UH-60A Model, without Inflow

Starting with the model without inflow model, parameters presented in Table 5.1 provide a good insight into the helicopter and rotor situation during trim. The controller implemented in the constructed model puts the helicopter in almost the exact same condition in terms of speeds and Euler angles compared to FLIGHT-LAB. Speed differences are smaller than 1 m/s and attitude differences smaller than 1 degree (except θ at 120 kts, 1.18°). Control inputs are also in good agreement. One can only note a few degrees offset between the longitudinal cyclic angles at hover. However, both models seem to be in a very similar hover situation looking at the attitude angles. An explanation might be that hover is a fairly unstable situation and control inputs are required to keep the helicopter in place. The controls are frozen to make the measurements presented in this table but still, the controller could have been busy keeping the helicopter in hover when the control angles

were measured, resulting in a difference only for the hover situation. Flap angles also match which is important for the upcoming research. Total forces and moments are measured at the rotor hub and averaged over one rotor revolution. The goal of the thesis is to reduce these loads, so a good validation is required. Differences in average loads are found to be acceptable and within 3%. Moments however, show a mismatch at low speed with differences up to almost 30%, but seem to match better at higher speeds with only 2% difference at 120 kts. Thrust generated by the tail rotor matches for both models. Differences in fuselage aerodynamic forces are expected as a different model is used. However, they seem to have a minor influence on the aircraft controls and flying attitude at trim.

Table 5.1: Comparison SimMechanics/Simulink (Sim) - Flightlab (FL), no inflow model

Variable	0 kts		20 kts		50 kts		100 kts		120 kts	
	Sim	FL	Sim	FL	Sim	FL	Sim	FL	Sim	FL
u [m/s]	0	0	10.23	10.14	25.46	25.6	51.43	51.32	61.79	61.56
v [m/s]	-0.02	0	0	0	0	-0.01	0	-0.03	0	0.01
w [m/s]	0	0	1.12	1.19	2.5	2.62	2.79	2.16	1.24	0
θ [°]	6.72	6.78	6.31	6.64	5.61	5.85	3.11	2.42	1.16	-0.02
ϕ [°]	-1.07	-0.63	-0.73	-0.65	-0.83	-0.78	-1.35	-1.31	-1.76	-1.66
θ_0 [°]	12.6	12.92	12.64	12.95	12.85	13.18	13.89	14.53	14.76	15.59
θ_{1s} [°]	-5.57	-3.71	-4.0	-4.25	-4.68	-5.06	-5.51	-5.86	-5.52	-5.75
θ_{1c} [°]	-0.52	-0.44	-0.38	-0.39	-0.33	-0.32	-0.30	-0.34	-0.34	-0.44
β_0 [°]	1.86	2.42	1.85	2.415	1.83	2.38	1.74	2.30	1.74	2.31
β_{1s} [°]	-0.14	-0.19	0.02	0.02	0.26	0.32	0.55	0.63	0.58	0.63
β_{1c} [°]	-3.85	-3.77	-3.77	-3.79	-3.77	-3.8	-3.24	-3.00	-2.49	-2.02
$F_{hub_{tot}}$ [N]	68286	67407	68167	67335	67840	66949	65814	66363	65077	66796
$M_{hub_{tot}}$ [Nm]	22260	17232	22098	17361	22632	18075	24719	22154	26877	26359
$F_{tail_{tot}}$ [N]	1112	1103	1171	1146	1307	1273	2025	2129	2628	2796
$F_{x_{bodyaero}}$ [N]	0	0	-108	-146	-679	-909	-2770	-3603	-4004	-5072
$F_{y_{bodyaero}}$ [N]	0	0	-0.4	0	-1	2	3	16	-0.6	-9
$F_{z_{bodyaero}}$ [N]	0	0	-92	-97	-522	-535	-1268	-956	-856	-210
$M_{x_{bodyaero}}$ [Nm]	0	0	0	0.2	0	-0.4	0	-3	0	2
$M_{y_{bodyaero}}$ [Nm]	0	0	102	72	433	289	-1224	-1899	-5069	-5931
$M_{z_{bodyaero}}$ [Nm]	0	0	-4	-0.2	-24	5	-78	37	-123	-20

The blade root pitch angle over one rotor revolution is plotted in Figure 5.3. One can clearly see how more input is required to achieve higher speeds. Differences between FLIGHTLAB and the constructed model are growing at higher speeds but stay within one degree (except just over one degree peak at 120 kts). The blade flapping over one rotor revolution is presented in Figure 5.4. Once again, data from FLIGHTLAB and the developed model match well. The biggest difference in flapping is seen over the front of the rotor (180°) at 120 kts. This is also the point where the biggest differences in fuselage pitch angle is observed.

The evolution of the hub forces over one rotor revolution are presented in Figure 5.5. Differences can be observed but note the small scale on the y-axis. If flying speed increases, forces start to oscillate more. The developed model shows a higher amplitude when comparing the forces. It is very difficult to pinpoint what exactly causes this difference. It might be triggered by a slightly different situation over the rotor. One also has to bear in mind that the entire hub assembly is different in FLIGHTLAB and the reaction forces are very sensitive to where they are measured. Figure 5.6 shows the hub moments over one rotor revolution. Larger

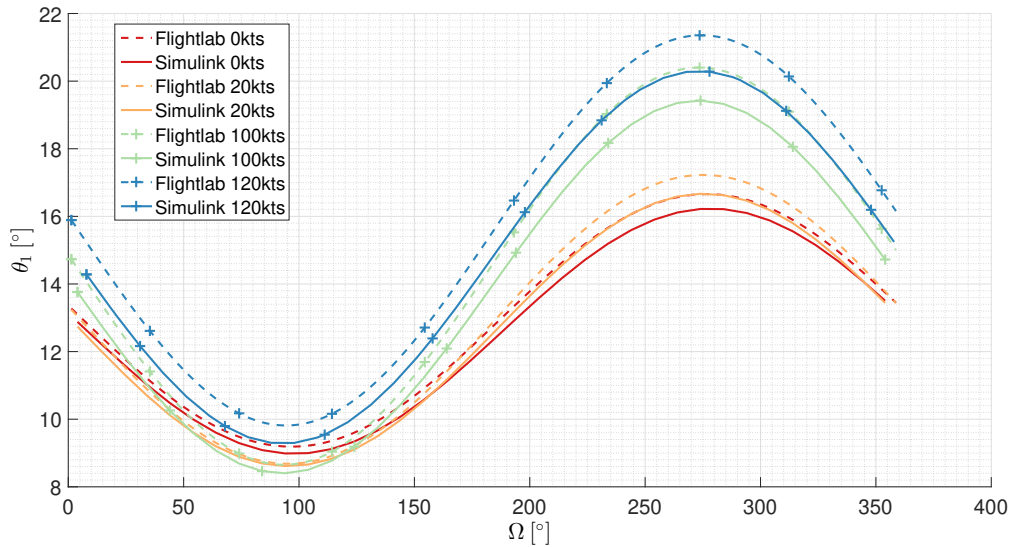


Figure 5.3: Blade root pitch angle, no inflow model

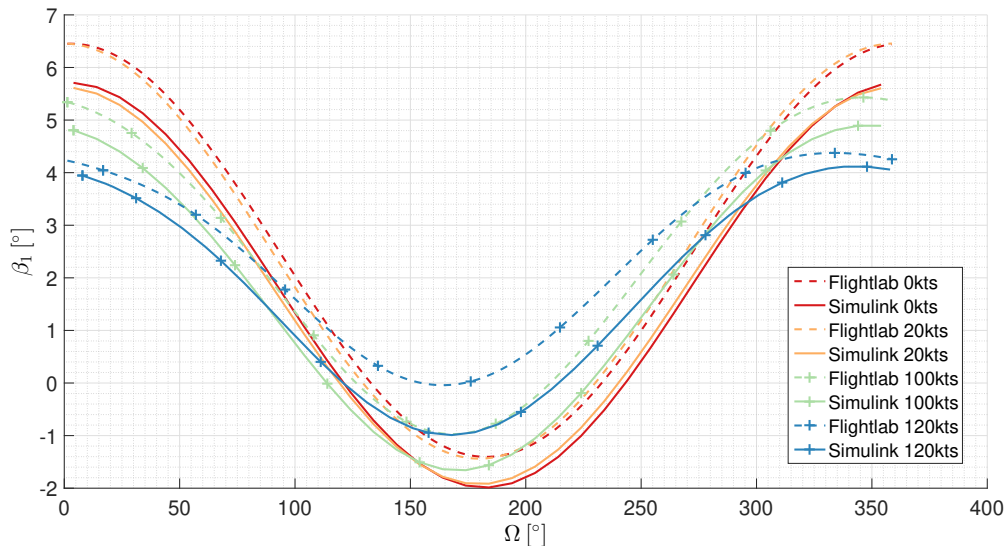


Figure 5.4: Flapping angle, no inflow model

differences between the two models at low speeds were already mentioned before. One can see how the moments close in at higher speeds. At 120 kts, they almost exactly match.

The situation over the rotor disk is studied by plotting α , c_l and c_d over the disk at 120 kts for both models, Figure 5.7 - 5.12. A much more elaborate comparison is included in Appendix B for different flying speeds and extra parameters like $c_l M^2$ and $c_d M^2$. The 120 kts situation is shown here as experiments later in this project will be done at this flying speed.

One has to carefully study these plots to find differences between the rotor disk situation of the two models, meaning they look alike. Regions of high angle of attack and the associated increase in lift and drag coefficient match. The real difference between these plots is the reversed flow area, indicated by the white spot over the retreating side of the rotor (white as angles are very negative and fall outside the colour scale). An explanation for this effect might be the difference in rotor blade resolution near the root. The only real difference noted at 120 kts in Table 5.1 is the difference in collective setting which is higher for FLIGHTLAB. The longitudinal inputs are the same, but the same longitudinal input on a higher collective results in higher blade pitching over the retreating side. This might also influence why FLIGHTLAB shows slightly higher α 's

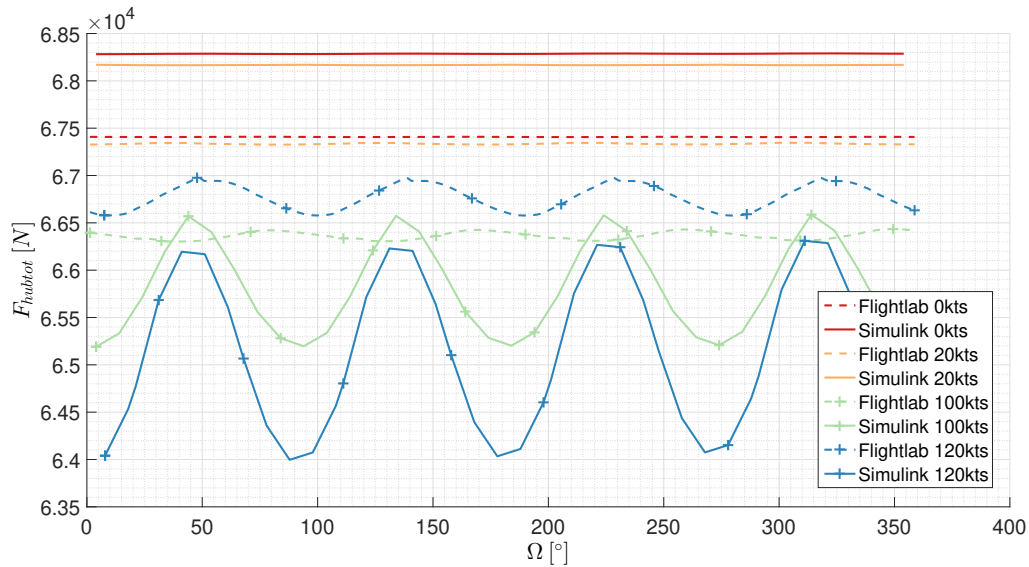


Figure 5.5: Total hub force: $\sqrt{F_x^2 + F_y^2 + F_z^2}$, no inflow model

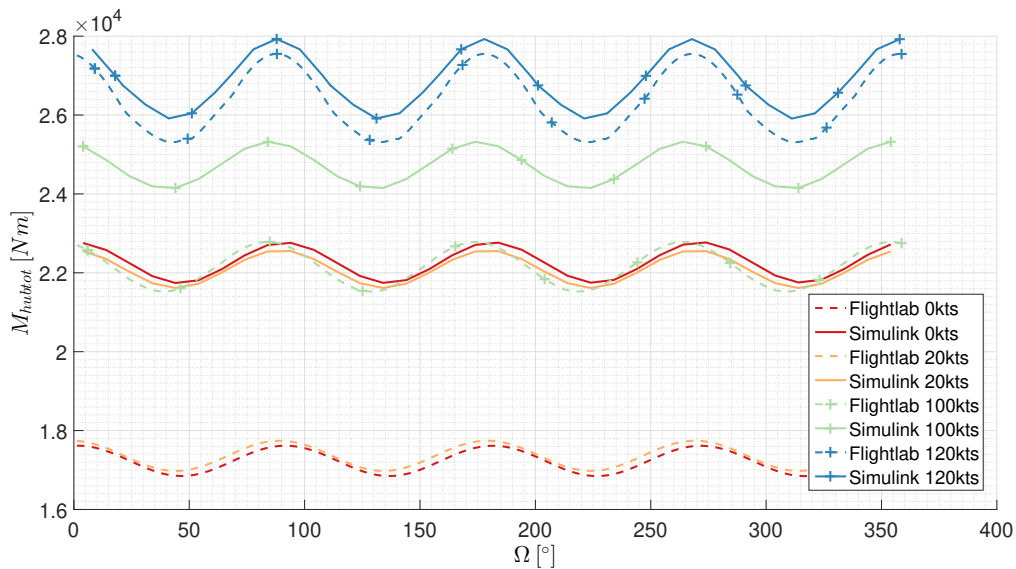


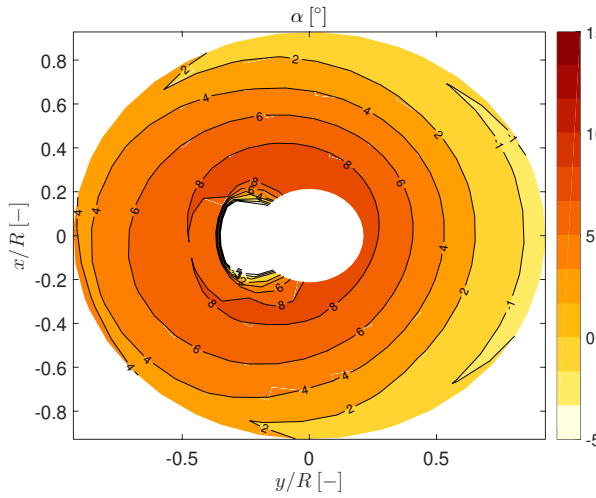
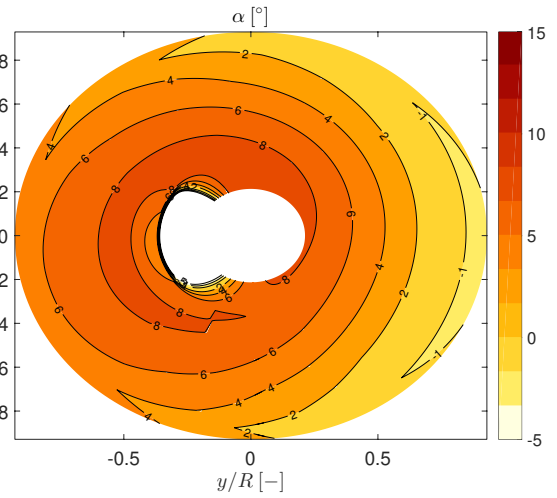
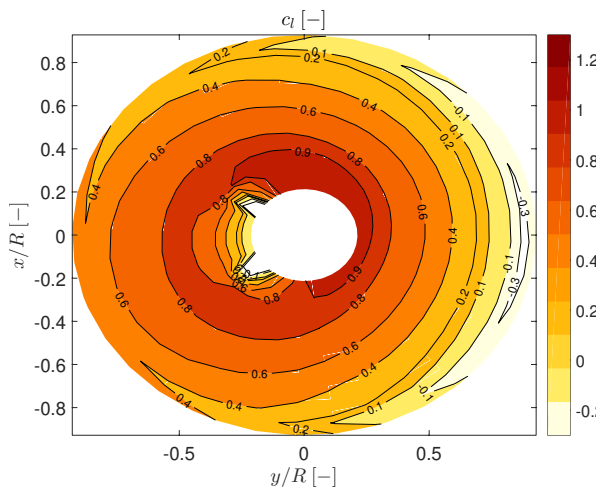
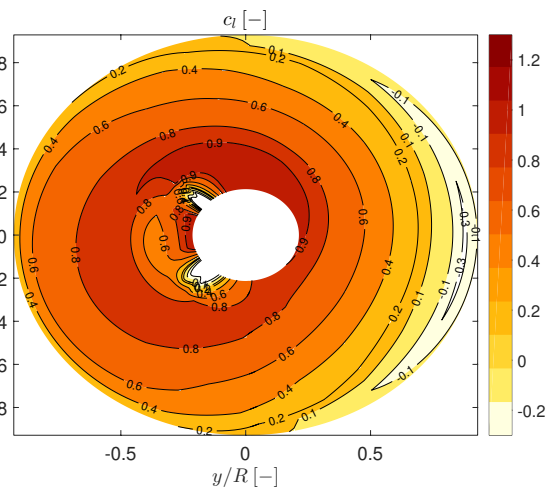
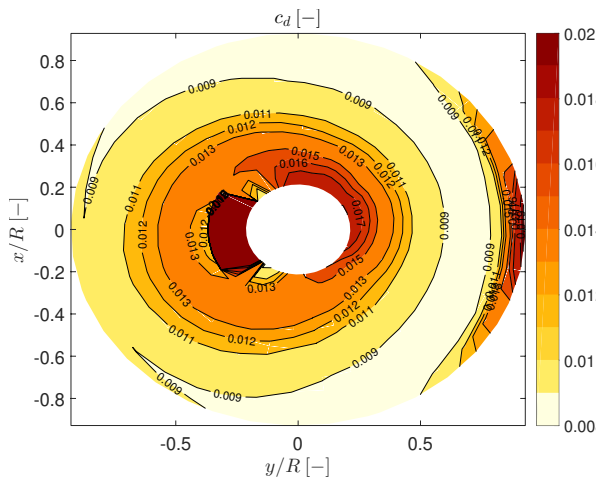
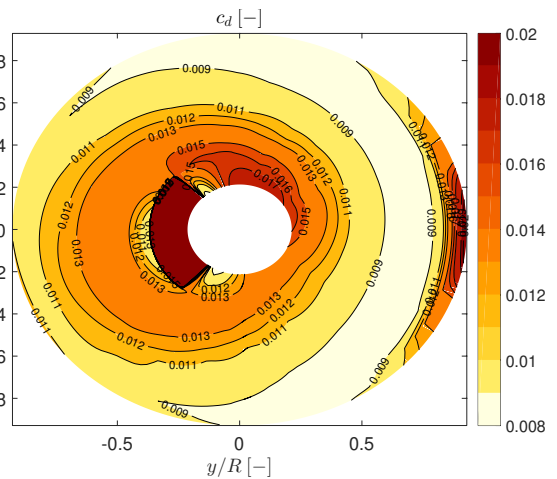
Figure 5.6: Total hub moment: $\sqrt{M_x^2 + M_y^2 + M_z^2}$, no inflow model

over the retreating side and the reversed flow area is more outboard.

5.2.2. Trim Validation Conventional UH-60A Model, with Peters-He Inflow

During the second stage of the trim validation, the Peter-He inflow model was added to both the model developed for this thesis as well as FLIGHTLAB. Table 5.2 presented the important flying parameters. Again, both models are trimmed in a very similar flight condition as flying speeds match and the difference between the attitude angles are in the order of 1 degree.

The collective settings shows a maximum delta of 1.58° at 120 kts. This is not an alarming difference but moving 1.58° up the lift curve will results in a noticeable increase in lift. The rotor disk will be studied later in this section to try and explain this difference. Both lateral and longitudinal cyclic input between the two models are aligned. Also flapping is checked in Table 5.2 and matches for both models. Forces measured over one rotor revolution show a maximum difference of 2%. Moments on the rotor hub are significantly higher when the inflow model is added. Moments at low speed show a good match while a 15% difference is

Figure 5.7: α SimMechanics 120 kts, no inflow modelFigure 5.8: α Flightlab 120 kts, no inflow modelFigure 5.9: c_l SimMechanics 120 kts, no inflow modelFigure 5.10: c_l Flightlab 120 kts, no inflow modelFigure 5.11: c_d SimMechanics 120 kts, no inflow modelFigure 5.12: c_d Flightlab 120 kts, no inflow model

observed at 120 kts. Differences in body drag are noted but do not have a major influence on the results.

The blade pitch angle over one rotor revolution is plotted in Figure 5.13. Generally, the blade pitch of the FLIGHTLAB model lies higher. The shapes match well, certainly at higher speeds. The blade flap angles

Table 5.2: Comparison of the constructed model in SimMechanics/Simulink (Sim) - Flightlab (FL), Peters-He inflow model

Variable	0 kts		20 kts		50 kts		100 kts		120 kts	
	Sim	FL	Sim	FL	Sim	FL	Sim	FL	Sim	FL
u [m/s]	0	0	10.16	10.26	25.49	25.65	51.46	51.35	61.81	61.55
v [m/s]	-0.1	0	0	-0.02	0	-0.03	0.07	-0.02	0.06	-0.02
w [m/s]	0	0	0.93	0.86	2.25	2.09	2.31	1.41	0.64	-1.00
θ [°]	5.13	4.58	5.26	4.73	5.04	4.64	2.52	1.56	0.55	-0.95
ϕ [°]	-2.48	-2.57	-0.95	-1.77	-0.76	-1.00	-1.21	-1.38	-1.59	-1.66
θ_0 [°]	16.77	17.64	15.12	16.89	13.92	15.48	14.65	16.09	15.5	17.08
θ_{1s} [°]	-2.14	-1.58	-3.27	-2.75	-4.69	-4.55	-5.80	-5.89	-5.87	-5.75
θ_{1c} [°]	-0.79	-1.02	-2.76	-2.08	-1.94	-2.69	-1.32	-2.13	-1.30	-2.08
β_0 [°]	2.20	2.79	2.10	2.74	1.99	2.64	1.92	2.61	1.92	2.63
β_{1s} [°]	-0.54	-0.83	0.10	-0.29	0.24	0.26	0.37	0.37	0.36	0.29
β_{1c} [°]	-2.34	-1.69	-2.77	-1.99	-3.39	-2.74	-2.98	-2.24	-2.19	-1.11
$F_{hub_{tot}}$ [N]	66164	66014	66915	66265	67188	66370	65730	66085	65172	66406
$M_{hub_{tot}}$ [Nm]	41518	42812	32178	38018	26118	29006	27636	30246	30180	34760
$F_{tail_{tot}}$ [N]	4334	4690	3126	4101	2128	2955	2526	3184	3088	3778
$F_{x_{bodyaero}}$ [N]	0	0	-108	-146	-680	-907	-2773	-3584	-4009	-5072
$F_{y_{bodyaero}}$ [N]	0	0	-0.7	1.9	-2.6	6	-39	6	-41	-19
$F_{z_{bodyaero}}$ [N]	0	0	-78	-70	-475	-429	-1062	-674	-535	-106
$M_{x_{bodyaero}}$ [Nm]	0	0	0	0.3	0	-1	0	-1	0	4
$M_{y_{bodyaero}}$ [Nm]	0	0	52	11	266	38	-1929	-2669	-6139	-7610
$M_{z_{bodyaero}}$ [Nm]	0	0	-5	4	-26	13	-166	13	-206	-44

over one rotor revolution are shown in Figure 5.14. The biggest difference in flap angle is noted over the nose of the helicopter. This is the result of the sum of the differences between the longitudinal flap angle and coning angle presented in Table 5.2. Remember the difference in collective setting discussed earlier. FLIGHTLAB shows a higher collective setting which lifts up the blades and increases the coning angle. Also, less longitudinal flapping for the FLIGHTLAB model can be the result of a more nose down flight condition with less longitudinal input. Note that these last discrepancies are small. This combined effect might explain the difference in flapping angle over the nose of the helicopter.

Figure 5.15 compares the forces in the hub. One can see how the general trend matches throughout the different flying speed and maximum encountered forces almost lie on top of each other. The minimum encountered forces lie lower for the FLIGHTLAB case. An explanation for this difference will be presented later when the disk plots are investigated. Moments over one rotor revolution are shown in Figure 5.16. An offset in the mean moment, as well as a higher amplitude for the moment measured in FLIGHTLAB is visible.

The situation over the rotor disk is investigated by plotting α , c_l and c_d at a flying speed of 120 kts. This time, also the induced inflow over the rotor is plotted, Figure 5.23, 5.24. Again, extra plots for a detailed analysis can be found in Appendix C showing other flying speeds and parameters like $c_l M^2$ and $c_d M^2$. When the disk situation in the developed model is compared with FLIGHTLAB, the same trends are noted. Areas of high angle of attack match and therefore also areas of high c_l , c_d and inflow. But one can also note the same differences as discussed earlier when the two models without inflow model were discussed. A higher overall angle of attack over the disk in FLIGHTLAB is observed. This links to the higher lift-, drag coefficient and inflow shown for the FLIGHTLAB model. The effect of the higher α is most visual over the retreating side of

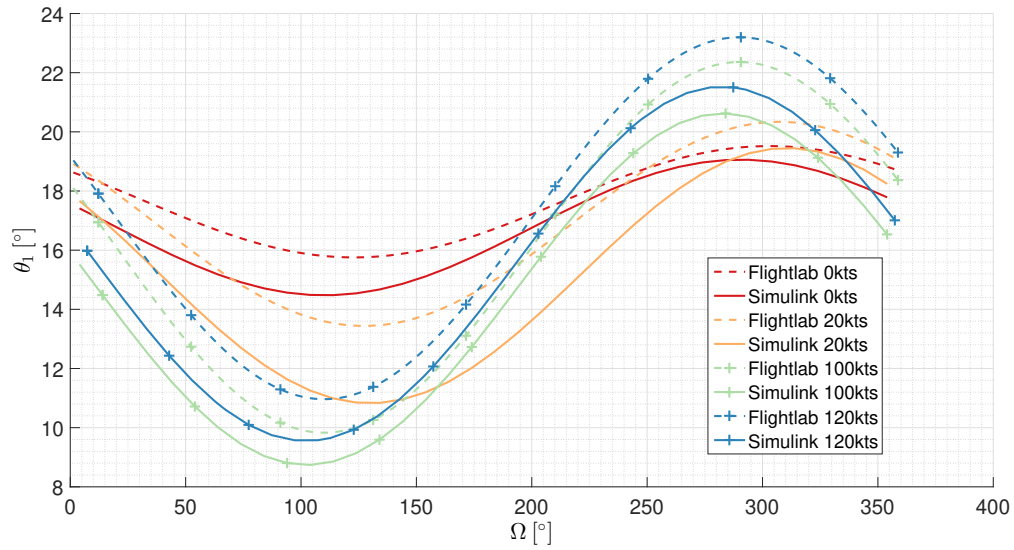


Figure 5.13: Blade root pitch angle, Peters-He inflow

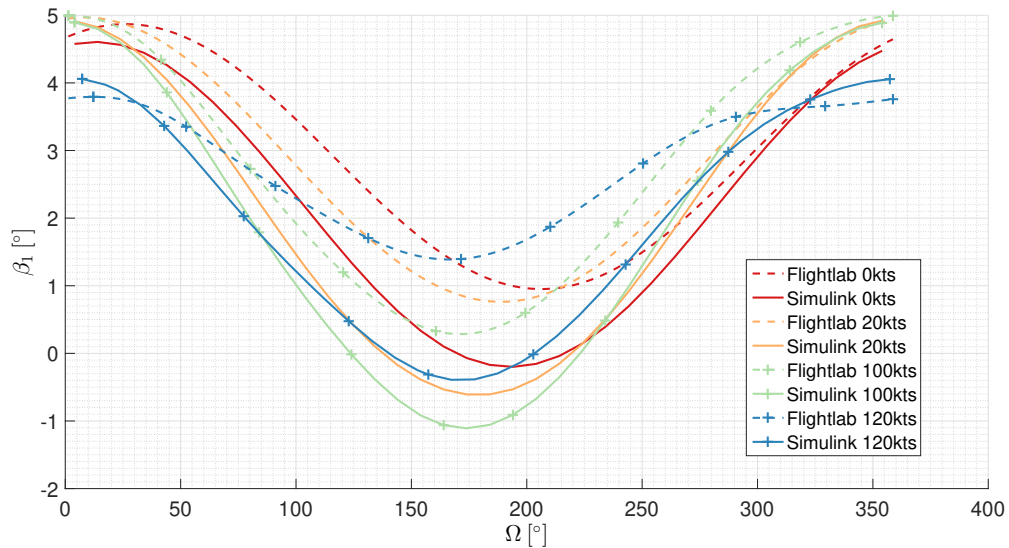


Figure 5.14: Flapping angle, Peters-He inflow

the disk. As α depends on several variables, there are a few observations that can be made which might effect the differences. At a 270° location over the retreating side of the rotor, Figure 5.13 shows a $\pm 2^\circ$ difference in blade pitch at 120 kts between both models. If Figure 5.17 and 5.18 are studied closely. At 270° , if the $\pm 2^\circ$ of blade pitch difference is added to the α distribution of the constructed model, one could argue that the results look like the FLIGHTLAB disk. A higher α over the retreating side can also explain the larger reverse flow area in FLIGHTLAB. However, this is not a direct link as α also depends on the inflow and flapping velocity. The discrepancies in loads can come from the slightly different situation over the rotor and reversed flow area.

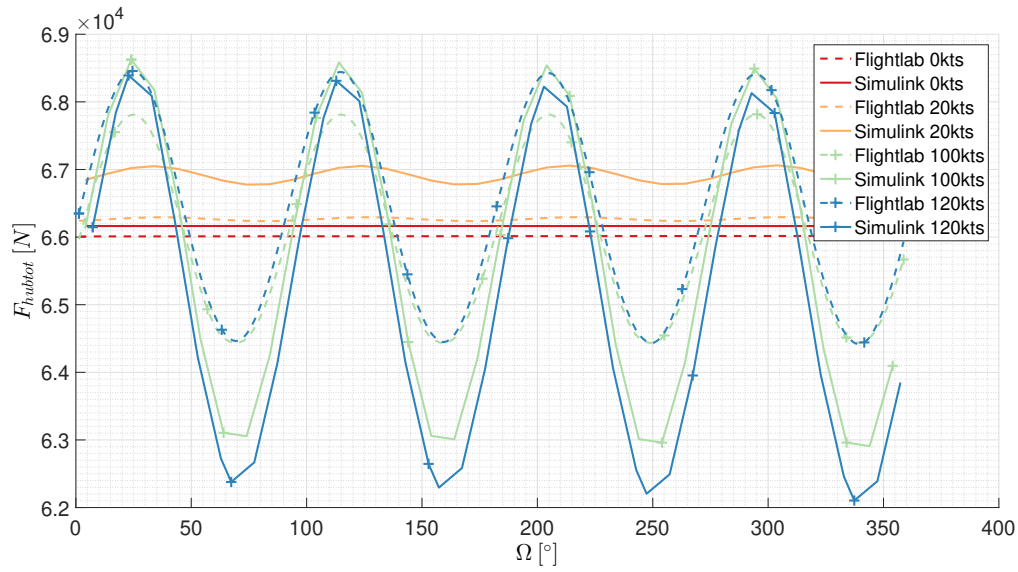


Figure 5.15: Total hub force: $\sqrt{F_x^2 + F_y^2 + F_z^2}$, Peters-He inflow

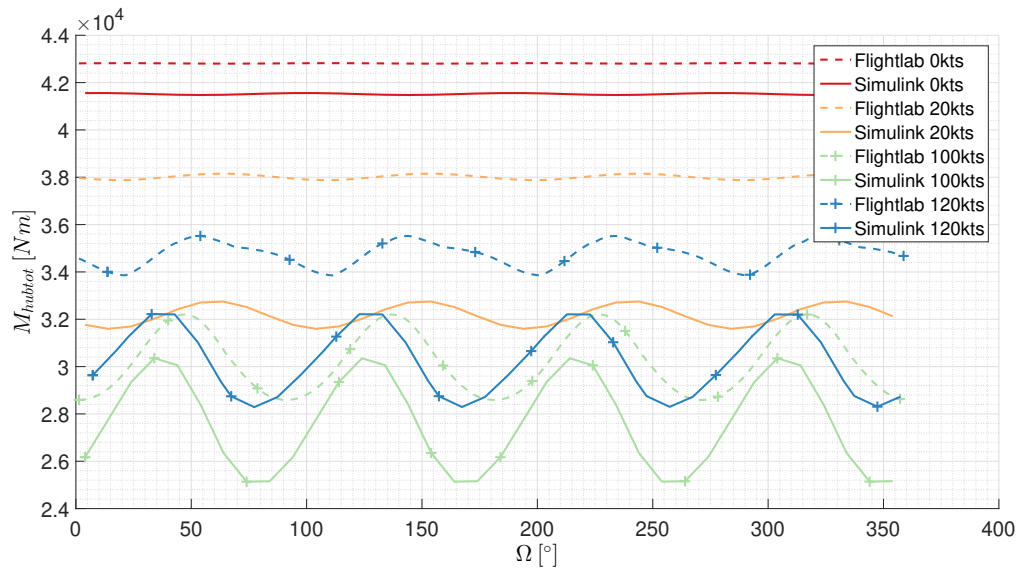


Figure 5.16: Total hub moment: $\sqrt{M_x^2 + M_y^2 + M_z^2}$, Peters-He inflow

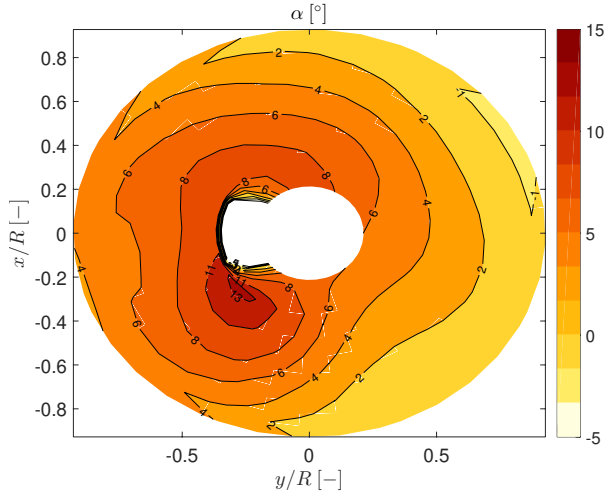


Figure 5.17: α SimMechanics 120 kts, Peters-He inflow

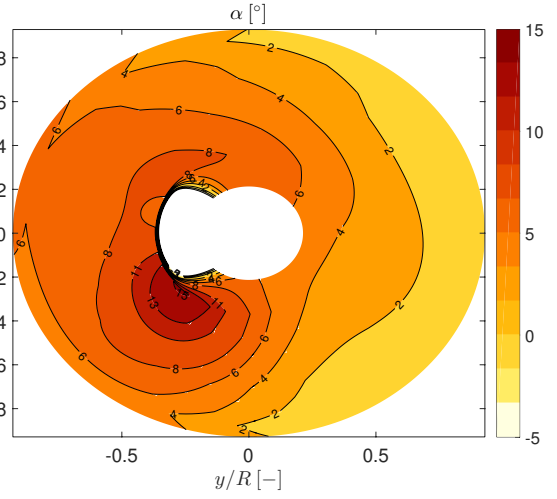


Figure 5.18: α Flightlab 120 kts, Peters-He inflow

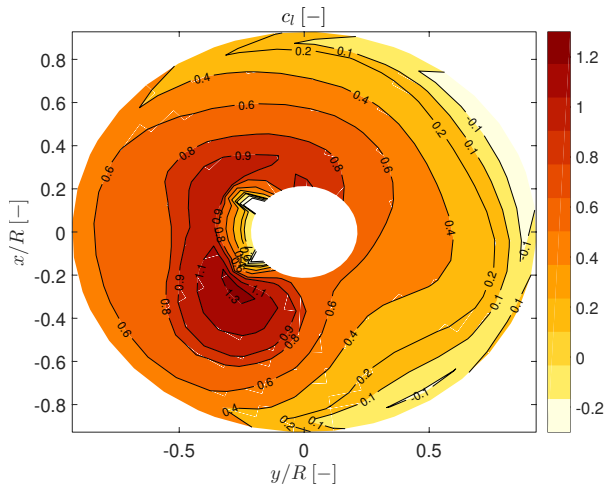


Figure 5.19: c_l SimMechanics 120 kts, Peters-He inflow

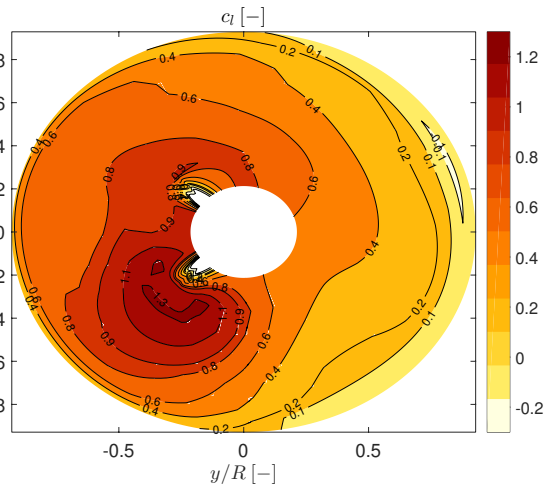


Figure 5.20: c_l Flightlab 120 kts, Peters-He inflow

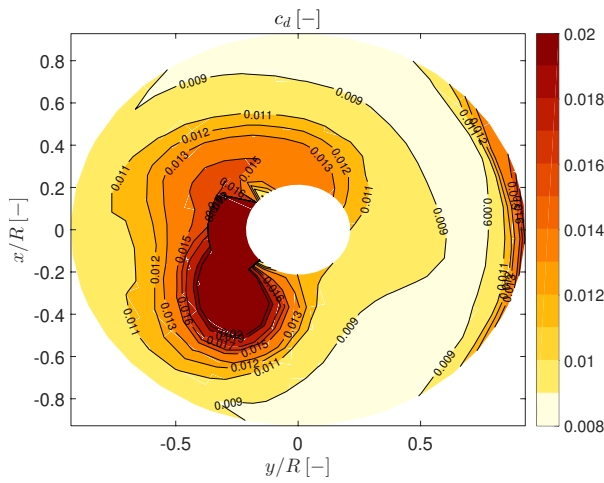


Figure 5.21: c_d SimMechanics 120 kts, Peters-He inflow

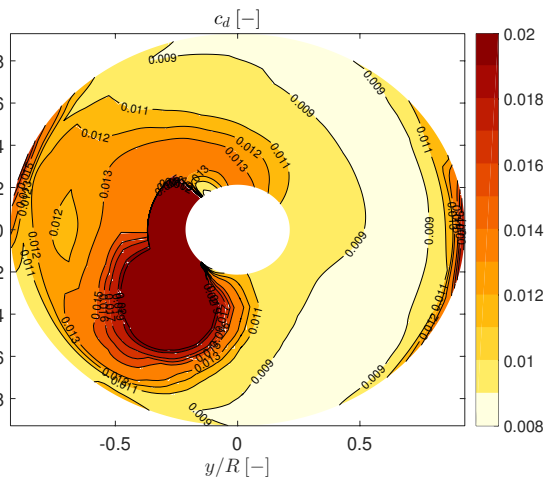
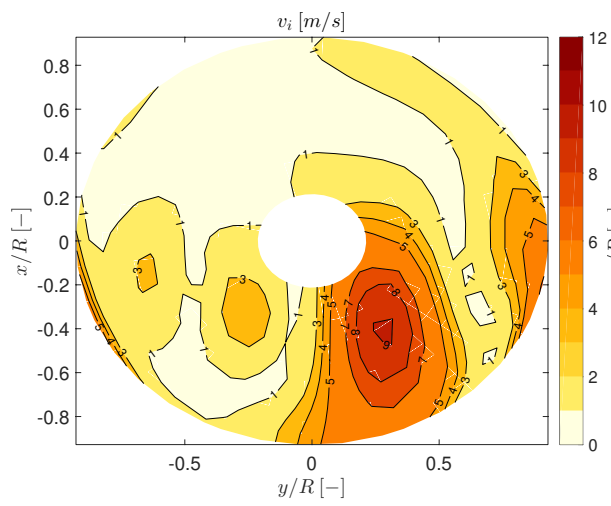
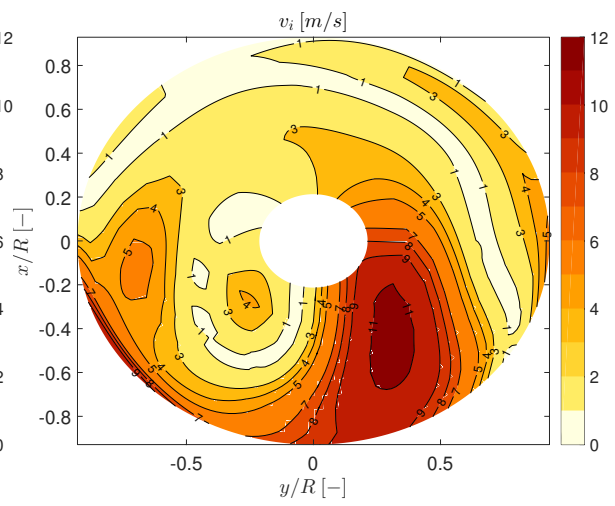


Figure 5.22: c_d Flightlab 120 kts, Peters-He inflow

Figure 5.23: v_i SimMechanics 120 kts, Peters-He inflowFigure 5.24: v_i Flightlab 120 kts, Peters-He inflow

5.3. Validation of Roll Manoeuvre

After the trimmed flight is validated, dynamic responses to control inputs need to be checked. The thesis focuses on load reduction and its effects on handling performance. In order to quantify these behaviours, a set of parameters is defined in Section 5.3.1. It is important the developed multi-body dynamics model shows a correct response to these parameters as they will later be used to assess the performance of the structural load alleviation capabilities. The dynamic validation is done for a lateral control input as a roll manoeuvre is flown during the load alleviation experiments.

5.3.1. Dynamic Response Parameter Definitions

A parameter is required to show peak loads during the manoeuvres and give insights about flying qualities. Both aspects are quantitatively captured by a set of quickness metrics introduced below.

The attitude quickness parameters are used by the ADS33 [8] to evaluate handling qualities and are presented by Equations 5.1. Attitude quickness is measured during a series of impulse responses of varying time but with an equal magnitude. Attitude quickness is plotted against $\Delta\phi_{min}$ which is defined as the angle at which the attitude rate of change p reaches 10% of its peak value triggered by the impulse control input, as described by Pavel and Padfield in [37].

In order to measure the load changes during the response, load quickness can be used which is an extension of the attitude quickness, proposed by Pavel and Padfield in [37] and also used by Voskuijl et al. [52]. These load (and moment) quickness parameters are defined by Equation 5.2 and also measured during an impulse response.

The off-axis responses are measured using the parameters suggested by the ADS-33 [8] and defined by Equation 5.3. The peak off-axis response is measured over the first 4 seconds following a step input and divided by the primary response at 4 seconds following the input.

$$Q_p = \frac{p_{pk}}{\Delta\phi_{pk}} \quad (5.1)$$

$$Q_F = \frac{F_{pk}}{F_{trim}\Delta\phi_{pk}} \quad Q_M = \frac{M_{pk}}{M_{trim}\Delta\phi_{pk}} \quad (5.2)$$

$$\frac{\Delta\phi_{pk}}{\Delta\theta_4} \quad (5.3)$$

5.3.2. Validation of the Response to a Lateral Input

The response to a pure lateral impulse is compared between the constructed model and FLIGHTLAB. As discussed above, the impulse duration is varied from 0.5 to 2 seconds with equal magnitude in order to generate the quickness plots. The magnitude of the impulse is chosen to reach a maximum roll angle of 30 degrees to keep the helicopter at a realistic flying condition. The 2 seconds lateral input for both FLIGHTLAB and the developed model is shown in Figure 5.25. Note that Figure 5.25 shows the lateral cyclic angle measured at the blade root. This is important as FLIGHTLAB directly controls the blade root pitch while in the constructed model, an appropriate pitch link deflection of the non-rotating swashplate is required to match the same cyclic input on the blades. A small offset between the control angles at trim exists. Therefore, the FLIGHTLAB signal is not exactly matched upon the input signal of the constructed model but the θ_{1c} deflection is kept the same. The small observed spike might be linked to the fact that the constructed model requires the entire swashplate to rotate to control the blade pitch while the blades are controlled directly in FLIGHTLAB. It was also carefully checked to not have any mechanical coupling between the lateral cyclic and longitudinal cyclic input. The model was adapted to have a swashplate phase angle of 0 degrees. Coupling effects due to aerodynamic, inertia and centrifugal forces over the blades are still free to settle.

The dynamic validation presented in this report is done at a flying speed of 45 kts. This ensures both models to stay within a realistic flying condition. One has to keep in mind that at this stage of the project, a conventional UH-60A is validated featuring a main rotor with inflow model, fuselage and tail rotor as presented in the project overview, Figure 1.4 (no vertical nor horizontal tail). A model of this configuration shows very abrupt responses to inputs at high flying speeds which makes it difficult to validate. This motivates why the 45kts was selected.

The attitude response, angular velocity response, force and moment response to 2 seconds impulse are presented in Figure 5.26 - 5.33. The primary response ϕ and p are shown to be in good agreement. Differences

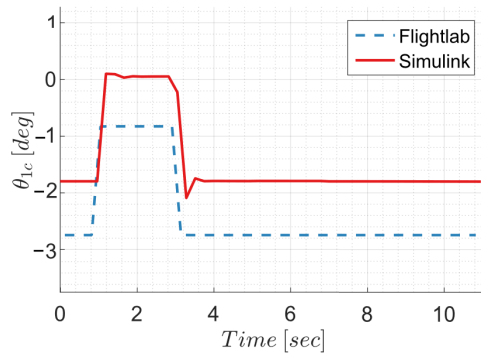


Figure 5.25: Lateral cyclic impulse of 2 seconds

start to occur when the input is released. The yaw response also indicated a very similar response looking at ψ and r . The yaw response is quite aggressive and therefore small changes in r will quickly cause a difference in ψ over time. The pitch response is comparable between the two models, however the research model does reach a higher pitch off-axis response after the control input is released. The force and moment responses show some discrepancies and are likely linked to the differences in motion response and differences in modelling. FLIGHTLAB shows a wider oscillation band for the hub moments. This might be linked to the larger reversed flow area generally observed in FLIGHTLAB as discussed earlier.

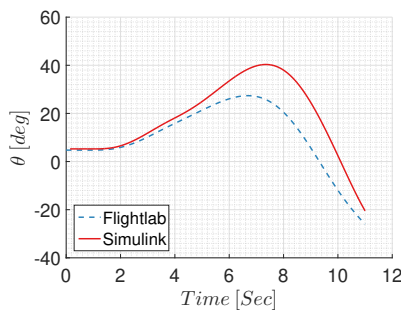


Figure 5.26: θ response lateral impulse

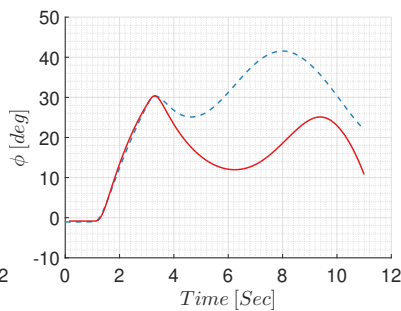


Figure 5.27: ϕ response lateral impulse

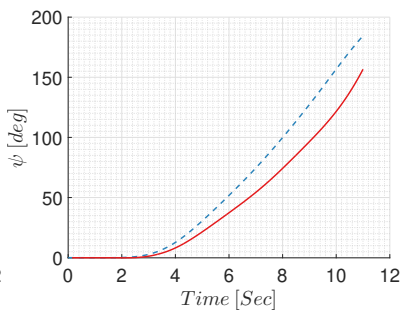


Figure 5.28: ψ response lateral impulse

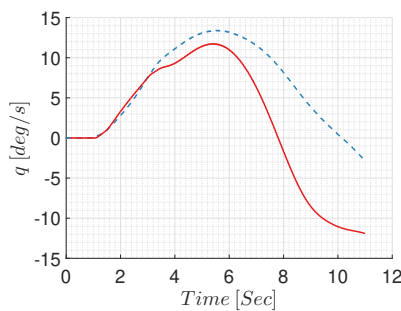


Figure 5.29: q response lateral impulse

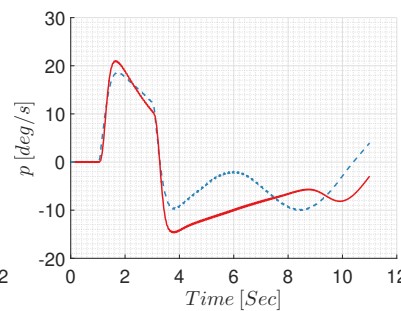


Figure 5.30: p response lateral impulse

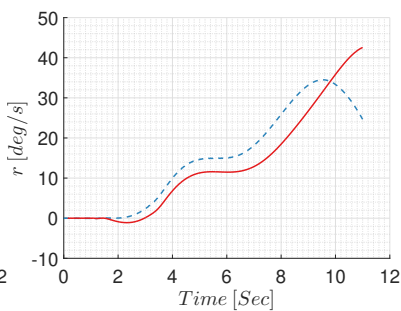


Figure 5.31: r response lateral impulse

The roll quickness for an impulse of 0.5, 1, 1.5 and 2 seconds is shown in Figure 5.34 and shows a good agreement between the two models. This is key as roll quickness will be used during the experiments to evaluate handling qualities.

The load and moment quickness are shown in Figure 5.35 and 5.36. These plots enable a fair comparison between the encountered loads as it corrects for the differences in motion (divided by peak roll angle) of the two models after the same input. Both force and moment quickness plots show good agreement suggesting the difference shown in the actual load response (Figure 5.32 and 5.32) are caused by a different motion of the helicopter. A reasonable difference in pitch due to roll off-axis response is found comparing $\Delta\theta_{pk}/\Delta\phi_4 = 0.3288$ for the developed model and $\Delta\theta_{pk}/\Delta\phi_4 = 0.2621$ for FLIGHTLAB.

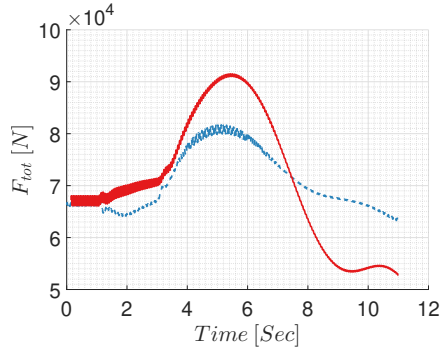
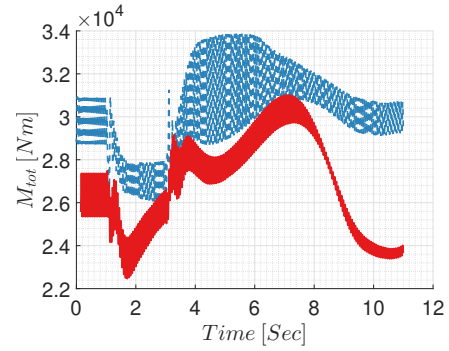
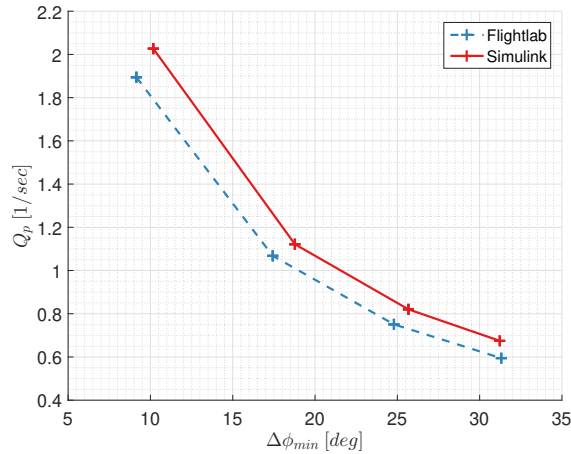
Figure 5.32: F_{tot} response lateral impulseFigure 5.33: M_{tot} response lateral impulse

Figure 5.34: Roll quickness lateral impulse at 45kts

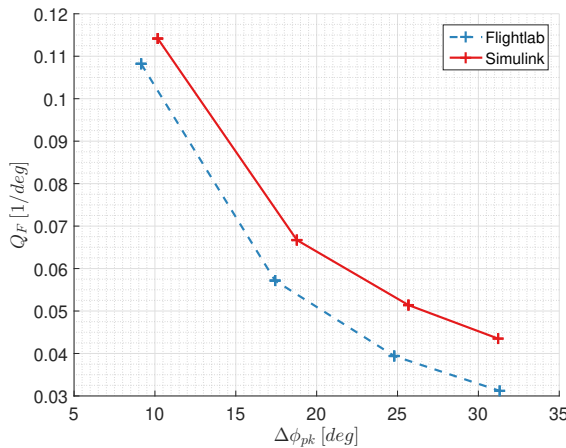


Figure 5.35: Load quickness lateral impulse at 45kts

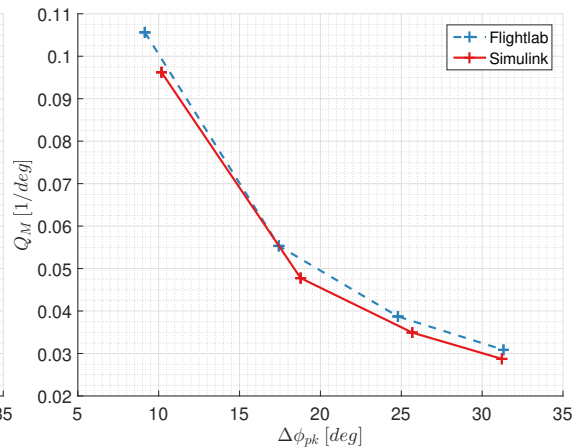


Figure 5.36: Moment quickness lateral impulse at 45kts

5.4. Compound Wing Model Validation

A key part specific to the compound helicopter is the main wing. This component was validated separately. The lifting line presented in Section 3.7 is checked against the open source vortex lattice method AVL [32]. First, the c_l -distribution of the compound wing without aileron deflection is compared at different angles of attack, presented in Figure 5.37. Secondly, different ailerons deflections at several angles of attack are compared in Figure 5.38. An almost perfect match can be observed. Note that the drag coefficient is not compared as the modelling basis between the lifting line used for this thesis and AVL is substantially different. The non-linear lifting line uses XFOIL [33] look-up tables including viscous effect while AVL is inviscid.

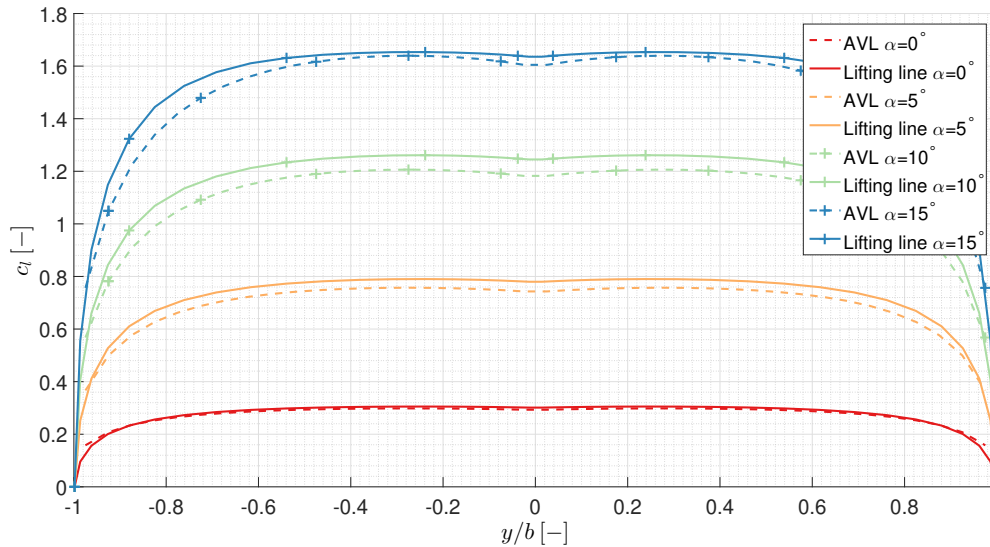


Figure 5.37: C_l wing distribution vortex lattice method against lifting line method at different α

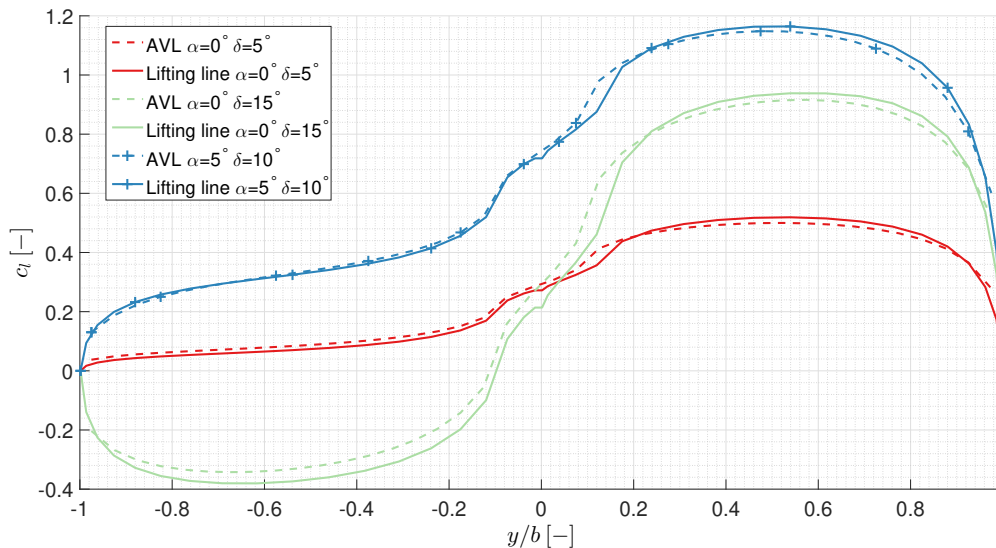


Figure 5.38: C_l wing distribution vortex lattice method against lifting line method at different α and aileron deflection δ

5.5. Validation Conclusion

The validation step should assure the constructed model is suitable for the upcoming experiments. This is why the validation step was tailored to the flight conditions of the experiments. In the next chapter, load alleviation opportunities will be tested with the compound UH-60A flying trimmed at 120 kts before executing a roll doublet. Exactly these two aspects were tested against FLIGHTLAB, a trimmed flight at 120 kts and a roll manoeuvre using the lateral cyclic. Next to using the lateral cyclic, the ailerons will also be used to roll. The aileron model was validated separately in this chapter.

The trim conditions with and without inflow model show a very good match comparing the thesis model with FLIGHTLAB. Especially note how the Euler angles and control inputs lie very close to each other suggesting the general flight situation of both models is similar. Some differences are noted especially when studying the aerodynamic situation over the main rotor disk. However, loads at a flying speeds of 120 kts lie close enough to accept the model for this thesis research.

Attitude quickness and load quickness were introduced to make a fair comparison to validate the roll

response. These metrics are in good agreement between both models. Initially, a good match for the roll response is observed. Pitch response is overestimated and yaw response slightly underestimated by the constructed model, but the differences are acceptable. As expected, the responses do drift away as the control input is released because the difference in orientation between both models grows. It was concluded that the model is also suitable to fly roll manoeuvres during the experiments.

6

Load Alleviation Experiments and Results

The potential of using the redundant controls of the compound helicopter to alleviate loads is studied in this chapter. Simulations are set-up to represent the break-turn MTE. The manoeuvre is modelled by a roll doublet. In order to understand how different control inputs affect the response and loads of the compound helicopter during the doublets, three experiments were set-up.

First, the control input strategy is varied to alleviate loads during the roll manoeuvre. A baseline trim configuration of the compound helicopter is defined. From trim, roll doublets are executed using either a pure lateral cyclic input, a pure aileron input or a combination of both (50% lateral cyclic - 50% ailerons). The rotor dynamics are investigated and linked to the encountered hub loading. The findings of changing the control strategy are presented in Section 6.1.

Secondly, the effects of different trim settings prior to the doublet manoeuvre are investigated. The trim settings are varied according to a test matrix and focus on changing the redundant controls of the compound helicopter: horizontal tail setting, compound thrust, changing the main rotor rpm and applying a constant aileron input at trim. The 50% lateral cyclic - 50% ailerons control strategy from the first experiment showed great potential and was used to fly the doublet for each trim settings. Results of the trim settings are presented in Section 6.2.

Finally, experiment one and two are combined. A suboptimal trim condition is defined by combining the trim settings which were separately varied during the second experiment. All three control strategies from the first experiment are used to fly the doublet in order to discover the true load alleviation potential applied on a typical compound helicopter trim condition. The findings are presented in Section 6.3.

6.1. Varying the Control Strategy to Alleviate Loads in the Rotor Hub

The compound helicopter features redundant controls meaning a (near) identical manoeuvre can be flown using different control strategies. The different control strategies are investigated in this experiment.

6.1.1. Experiment Set-up

The first set of experiments are flown at sea level, 120 kts with a baseline main rotor rpm of 257 (27 rad/s), advance ratio of $\mu = 0.28$. A doublet manoeuvre will be flown using different input strategies in order to investigate the effect on hub loads. The roll handling qualities are kept constant for the different simulations in order to solely investigate the effect on loads for the same manoeuvre. The experiment is conducted according to the following sequence:

1. The compound helicopter controls are set according to the baseline configuration, shown in Table 6.1 in the next section. Other control inputs are allowed to settle and achieve a trimmed situation using the 'fly-to-trim'-method. Trim is defined upon convergence of the body accelerations and rates. The baseline trim condition is presented in Table 6.2 in the next section.
2. After trim, a lateral cyclic doublet input is executed while all other controls are frozen at their trim value. The doublet input is presented in Figure 6.1 and designed to achieve a roll angle of 60° in 2 seconds. This manoeuvre is comparable to the 'roll-in/roll-out' section of the break-turn MTE.

3. A second run is initiated but this time, the ailerons are used to achieve the roll angle of 60° .
4. A third run combines the previous two strategies and used a 50% lateral cyclic input with a 50% aileron input, Figure 6.1. Again, a 60° bank angle is achieved.
5. The different control strategies are compared in terms of body responses, rotor dynamics and hub loads.

Note that each control strategy uses the same signal input shape, but scaled to reach a bank angle of 60 degrees in 2 seconds and resemble the break turn MTE.

The input signal shape might be the same, differences in the helicopter response will appear as a completely different sort of input is used. In order to make a fair comparison between different control strategies, quickness terms are introduced. These metrics are discussed below in Results 6.1.2.

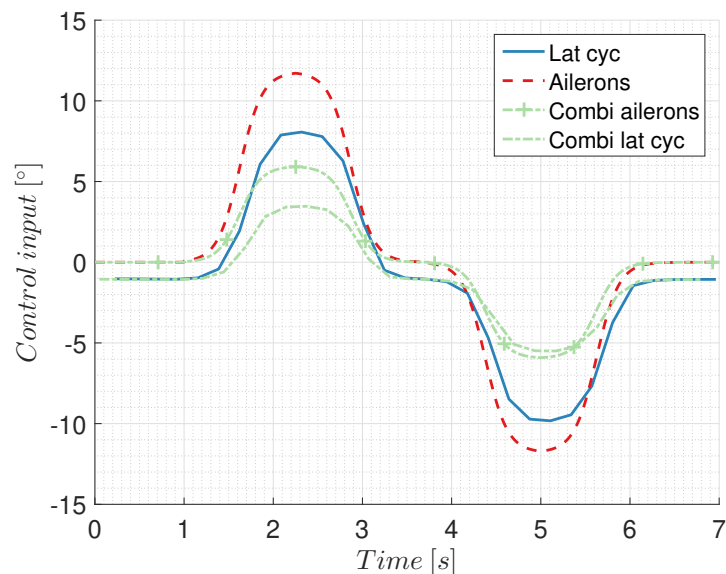


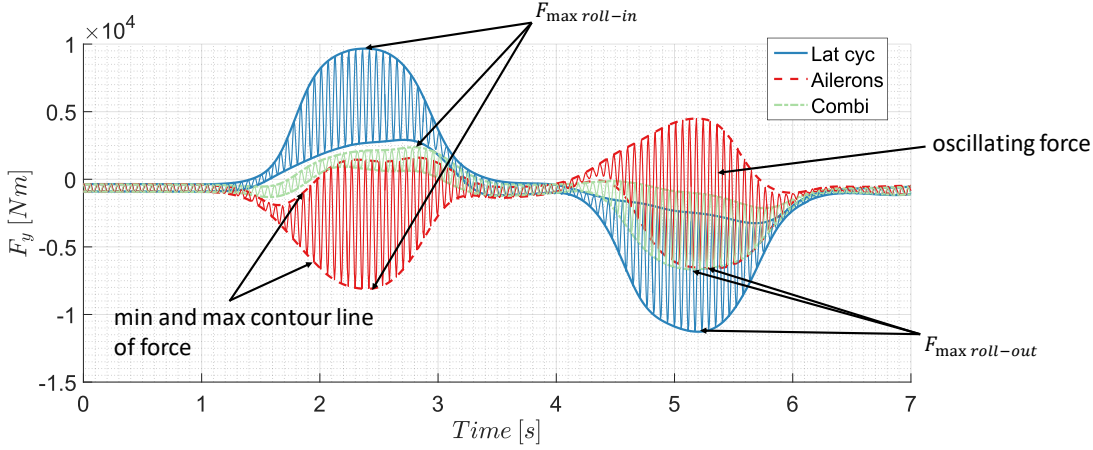
Figure 6.1: Doublet input: pure lateral cyclic (lat cyc), pure ailerons and 50% lateral cyclic - 50% ailerons (combi)

6.1.2. Results

Before one can interpret the results, there are important notes and definitions to be introduced. Different types of results will be presented in this report:

- Response through time of the Euler angles, flapping angles, angular rates, Figure 6.5 - 6.10
- Forces and moment responses, Figure 6.11 - 6.16
- Force and moment quickness (load quickness) plots for the roll-in motion, Figure 6.17 - 6.22 and the roll-out motion, Figure 6.23 - 6.28
- Attitude quickness plots, roll-in Figure 6.29 and roll-out Figure 6.30

As an example, Figure 6.2 shows the load response during a roll doublet with inputs according to Figure 6.1. One can observe how the response of the force oscillates at two different frequencies. The lowest frequency can be matched to the input signal and the attitude changes of the aircraft. For this particular case, when a lateral cyclic input is used, F_y is tilted to the right to roll-in and back to the left to roll-out to wings level. The high frequency oscillations correspond to the frequency of the main rotor blade rotation. Later in this section, the forces and moments in the hub will be linked to blade flapping, which oscillates at a frequency very close the rotor revolution. In order to clearly represent the response of the forces and moments, the high frequency oscillations will be removed in the coming plots and only the contour lines as shown in Figure 6.2 will be presented.

Figure 6.2: F_y response after roll doublet

Loads are measured in the multi-body dynamics model at the main rotor hub. These represent the reaction forces and moments encountered in the hub's structural component and are passed to the fuselage through the rotor shaft. All Euler angles are measured at the CG of the helicopter. Blade flap angles are measured at the flap hinge itself relative to the body. Positive longitudinal flapping is defined as the blades flap up over the nose, positive lateral flapping is defined as the blades flap up over the retreating blade side.

Attitude quickness, load quickness and moment quickness are defined according to Equations 6.1 and computed for both the roll-in as well as the roll-out section of the doublet manoeuvre.

$$Q_p = \frac{p_{pk}}{\Delta\phi_{pk}} \quad Q_F = \left| \frac{F_{pk}}{F_{trim}\Delta\phi_{pk}} \right| \quad Q_M = \left| \frac{M_{pk}}{M_{trim}\Delta\phi_{pk}} \right| \quad (6.1)$$

Studying the Euler angle responses in Figure 6.5-6.8, one can observe how the attitude changes are very similar for the three control strategies. A 60° bank angle is reached in 2 seconds and hold for about 1 second before returning to wings level. Larger differences appear after the rolling out, deviating from a wings level flight. This is not seen as a problem as the real break-turn MTE also allows deviating from a perfect wing-level condition during the roll-out. Reasonable pitch response is shown for the aggressive motion in roll. The longitudinal flapping follows the shape of the control input, Figure 6.9. The longitudinal flapping shows a similar trend for all control strategies but varies in magnitude. This is not the case for the lateral flapping, which is a crucial finding for the load alleviation as will be explained later. Changing between using the lateral cyclic to roll and the ailerons, reverses the lateral flapping behaviour, Figure 6.10. Using a combination of both almost levels the lateral flapping response.

The forces and moments are studied in Figure 6.11 - 6.16. The biggest difference caused by changing the control strategy is found in F_y and M_x , as expected for a rolling motion. The response of M_x but also F_y is linked to the lateral flapping β_{1s} . An opposite response of this force and moment is observed between a pure cyclic and pure aileron input. When both controls are combined, F_y and M_x are decreased. M_y but also F_x can be linked to the longitudinal flapping and show smaller differences when the control inputs are varied. F_z and M_z represent the main rotor lift and torque.

The load quickness plots offer a fair comparison between the different control strategies, Figure 6.17 - 6.28. The load amplification factors (LAF) are plotted as a reference onto the load quickness plots. The load amplification factor is a metric to evaluate how many times the load grows compared to its trim value. As the definition for load quickness used in this thesis is normalised with the trim load, the LAF is stated by the following equation with N the amplification factor:

$$LAF = N \frac{1}{\Delta\phi_{pk}} \quad (6.2)$$

The biggest effect of changing the control strategy is observed for M_x and F_y . Studying Q_{f_y} , the lateral cyclic shows the highest load quickness for both roll-in and roll-out motion. The difference between the pure aileron and mixed input is smaller for Q_{f_y} . The mixed control input shows a significantly lower load quickness

for Q_{M_x} . Load quickness Q_{F_z} , Q_{M_z} , Q_{M_y} almost completely overlap. Q_{F_x} does show some differences but are very small taking into account the scale of the plots.

The attitude quickness is plotted in figure 6.29 and 6.30 against the flying quality levels for roll attitude quickness for utility helicopters defined by the ADS-33 [8]. Only very small differences in attitude quickness are observed as the goal of this research is to perform the roll manoeuvre using different control strategies at the same level of handling qualities.

6.1.3. Discussion of the Link Between Loads and Blade Flapping

As the hub loads are linked to the flapping motion, it is crucial to understand the fundamentals of blade flapping before discussing any results. Prouty [40] has a very clear chapter on blade dynamics, the basics are presented below.

The flapping moment of the blade can be triggered by two different phenomena. The first one is a cyclic control input by the pilot. The second one is a stability response of the blades itself, no input from the pilot.

Controlling the helicopter is done by applying a moment over the CG which triggers an angular acceleration. Using an articulated rotor, there are two ways a moment around the CG can be created. The first one is by pivoting the total force generated by the rotor which stands perpendicular on the tip-path-plane and acts on the rotor hub. By pivoting this force, a moment arm will be created around the CG which lies lower in the fuselage. The tilting of the forces also creates a translating motion. A second moment is introduced by blade flap. The centrifugal forces of the opposing blades will create a moment around the flap hinge offset as the blades flap up or down. This moment is transferred through the rotor shaft and rotates the helicopter. Figure 6.40 further in the report helps to visualise this phenomenon.

When the rotor is not controlled and the pilot holds the stick fixed, flapping of an articulated rotor will have a stabilising effect. A blade with a flap hinge degree of freedom will strive to a zero moment condition. In order to balance the aerodynamic, inertial and centrifugal forces, a flapping motion appears.

Chopra and Datta [28] clearly describe all the forces acting on the blades to find the moment around the flap hinge featuring a flap hinge off-set (no torsional spring in the flap hinge), Figure 6.3. Note that m is the mass per unit of blade length and small angles are assumed.

1. Blade inertia forces: $m dr (r - e) \ddot{\beta}$, with arm around flapping hinge: $(r - e)$
2. Blade centrifugal forces: $m dr \Omega^2 r$, with arm around flapping hinge: $(r - e)\beta$
3. Blade aerodynamic forces: $F_{aero} dr$, with arm around flapping hinge: $(r - e)$

The moment around the flapping hinge can be written as:

$$\int_e^R m(r - e)^2 dr \ddot{\beta} + \int_e^R m \Omega^2 r (r - e) dr \beta - \int_e^R F_{aero} (r - e) dr = 0 \quad (6.3)$$

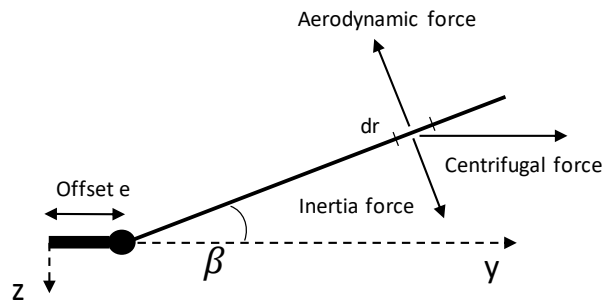


Figure 6.3: Forces acting on blade with flap hinge and flap hinge offset

A measurement at the flap hinge location in the multi-body dynamics model confirms how the hub moments are mainly related to the centrifugal forces. Figure 6.4 shows the F_z forces measured at the flapping hinge when the rotor moves over the nose ($\Omega = 180^\circ$) and tail ($\Omega = 0^\circ/360^\circ$) of the helicopter. The blade reaches a flap angle of 0.84° over the front and 3.3° over the rear section of the disk. The centrifugal force

of the blade is $F_C = 478140N$. Multiplying the centrifugal force with $\sin(\beta)$ results in $F_{z\text{hinge}\Omega=180} = 7001N$ and $F_{z\text{hinge}\Omega=0} = -27524N$. Note that these values lie close to the actual forces measured in the z-direction as indicated in Figure 6.4. This suggests that the moment generated around the hub is mainly a result of the centrifugal forces. The moment around the hub can be approximated by $M_{hub} \approx 2eF_C \sin(\beta)$ as earlier stated in the literature study by Yeo, Bousman & Johnson [55] [54]. If the flapping angle is small, the role of the aerodynamic and inertia forces becomes more important.

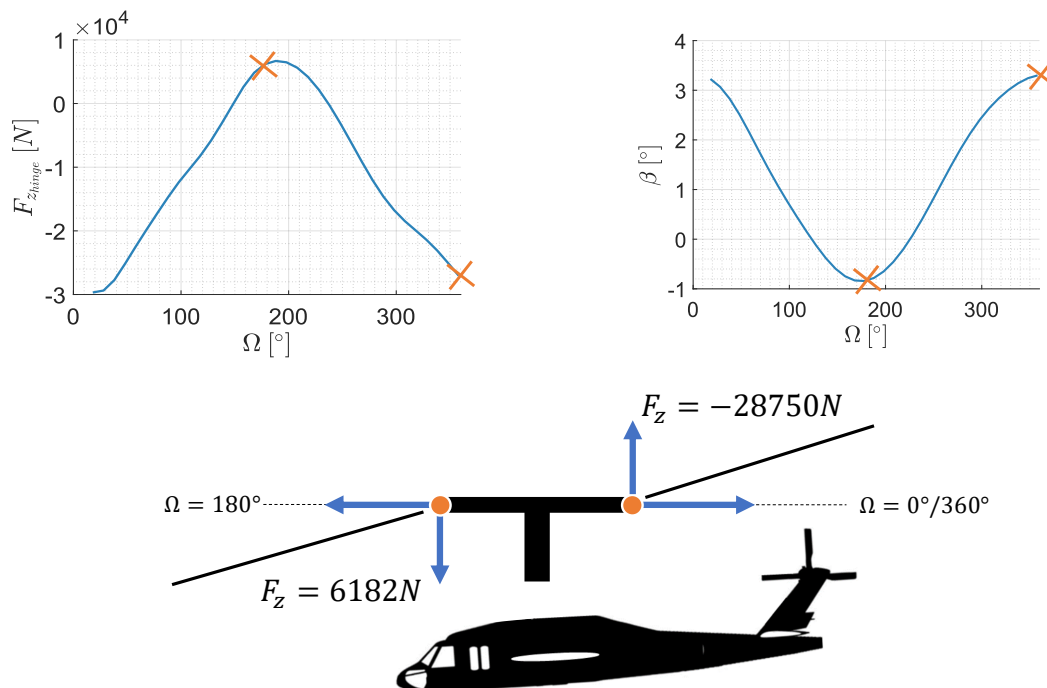


Figure 6.4: F_y forces measured at the flapping hinge, modified from [42]

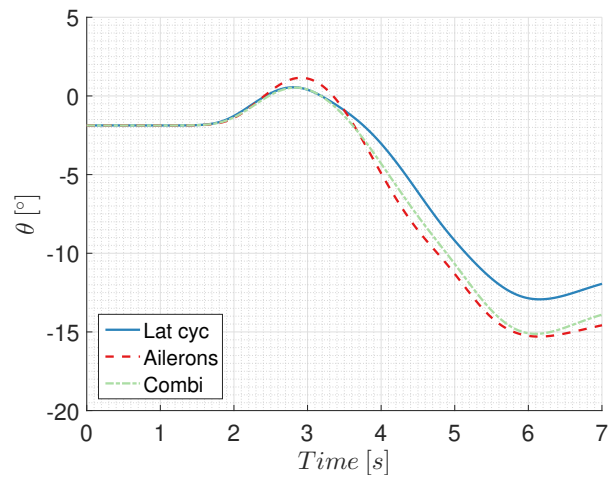


Figure 6.5: θ response roll right doublet

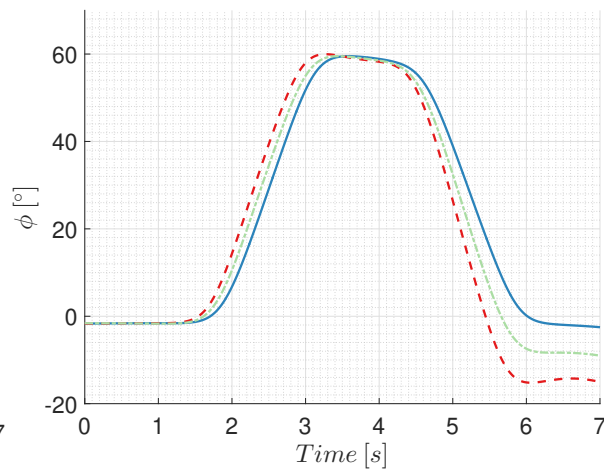


Figure 6.6: ϕ response roll right doublet

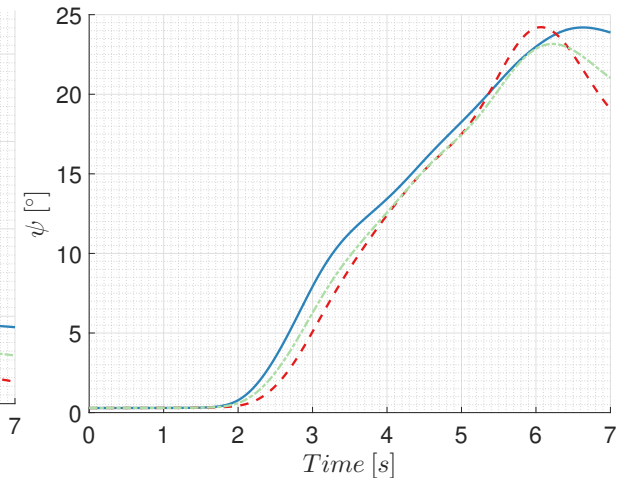


Figure 6.7: ψ response roll right doublet

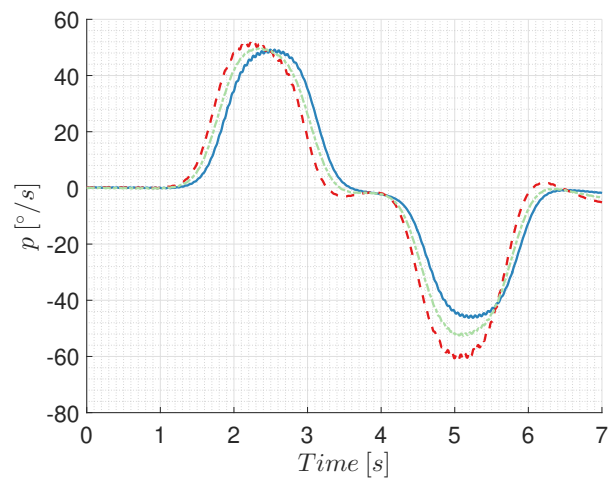


Figure 6.8: p response roll right doublet

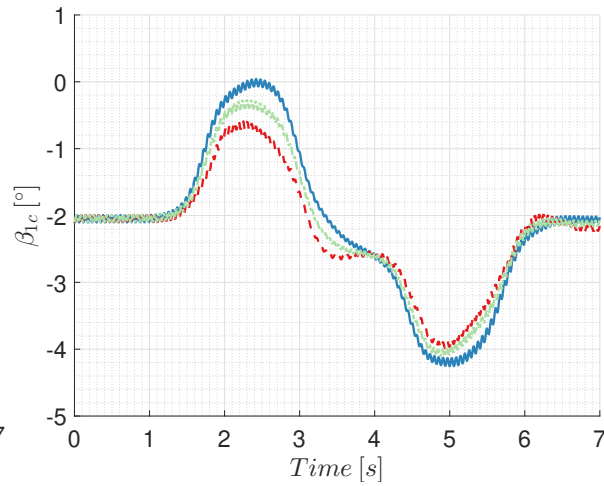


Figure 6.9: β_{1c} response roll right doublet

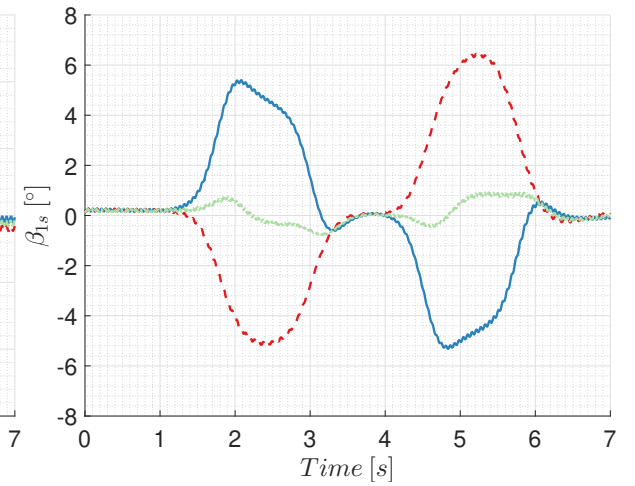


Figure 6.10: β_{1s} response roll right doublet

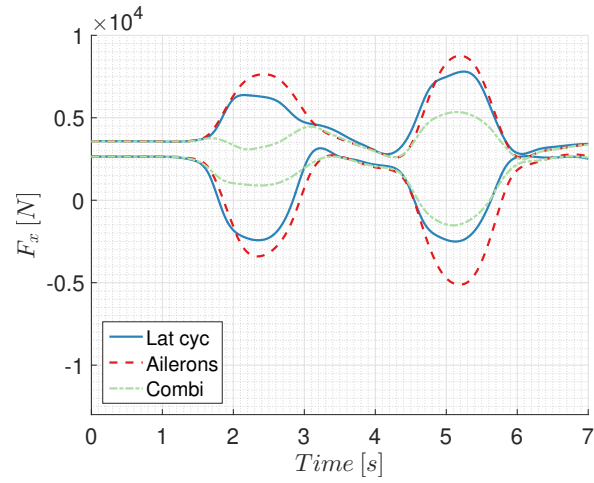


Figure 6.11: F_x response roll right doublet

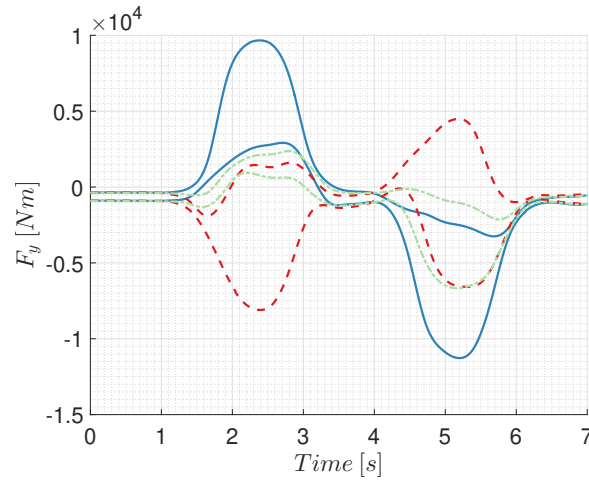


Figure 6.12: F_y response roll right doublet

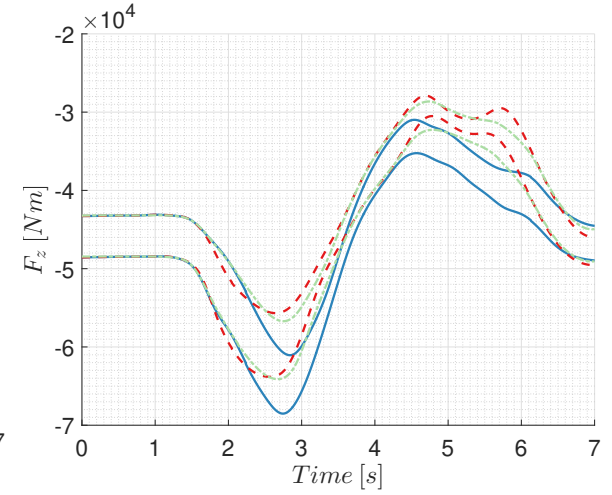


Figure 6.13: F_z response roll right doublet

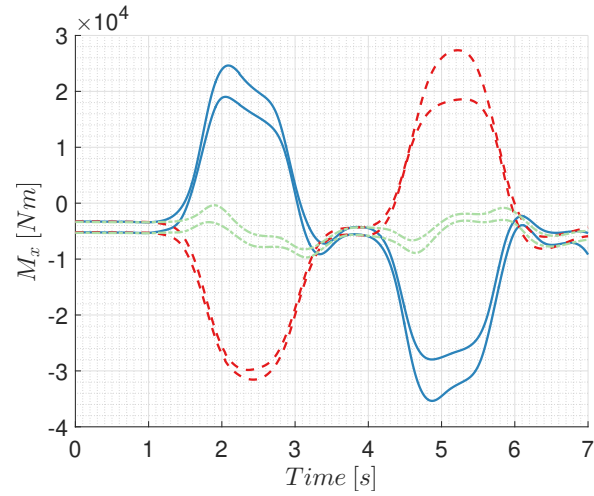


Figure 6.14: M_x response roll right doublet

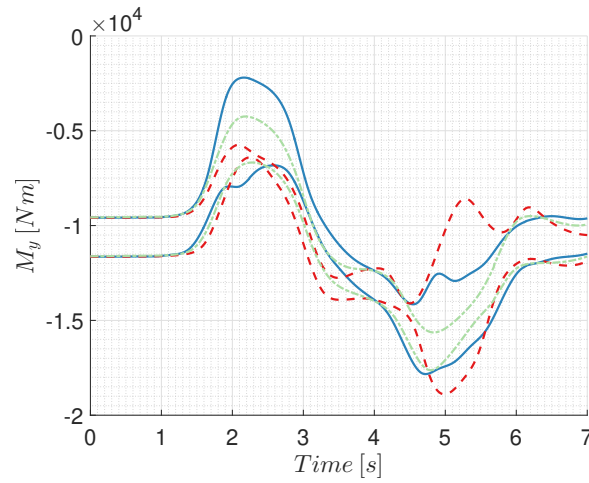


Figure 6.15: M_y response roll right doublet

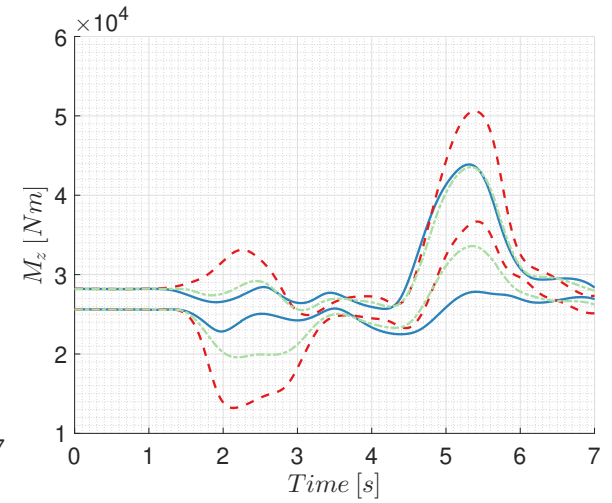


Figure 6.16: M_z response roll right doublet

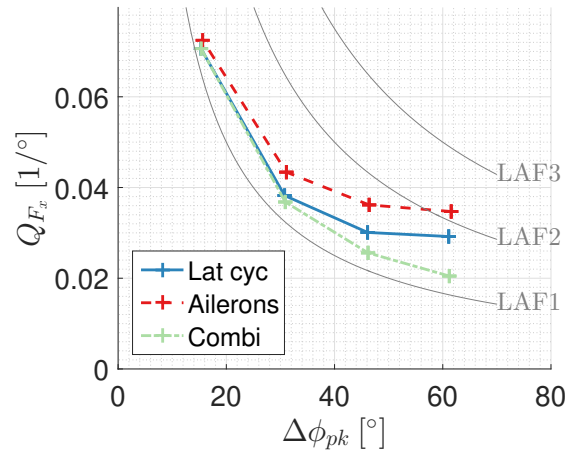


Figure 6.17: F_x quickness roll-in

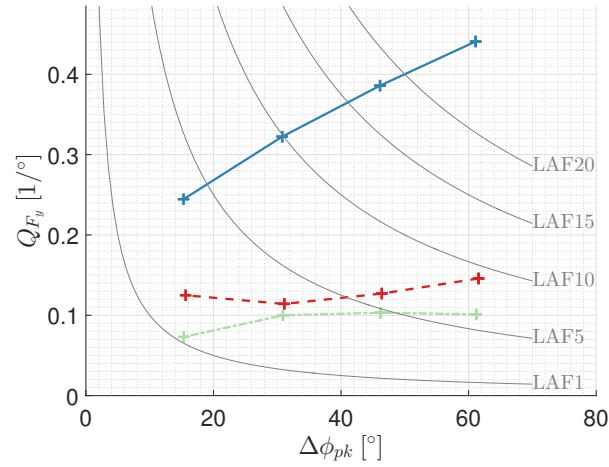


Figure 6.18: F_y quickness roll-in

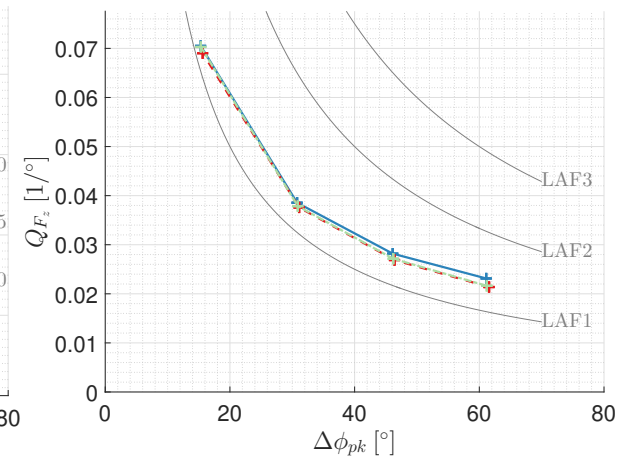


Figure 6.19: F_z quickness roll-in

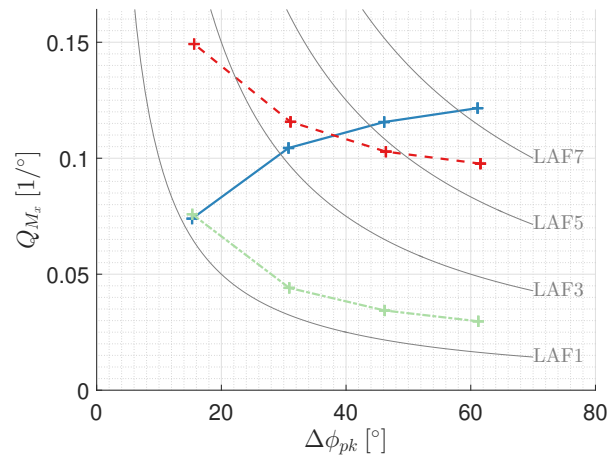


Figure 6.20: M_x quickness roll-in

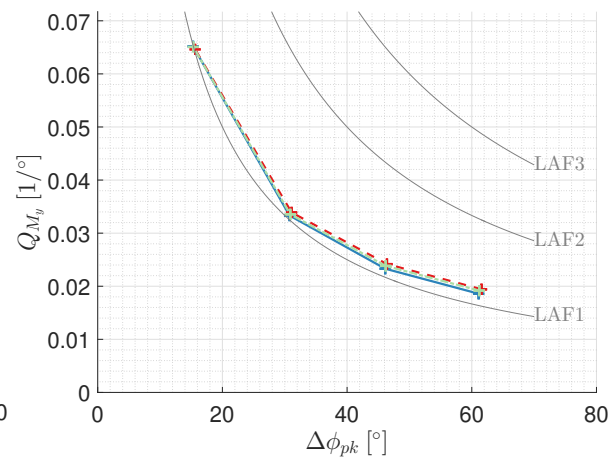


Figure 6.21: M_y quickness roll-in

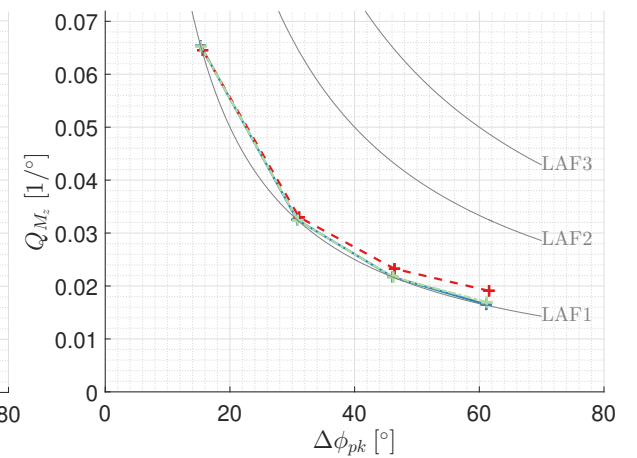


Figure 6.22: M_z quickness roll-in

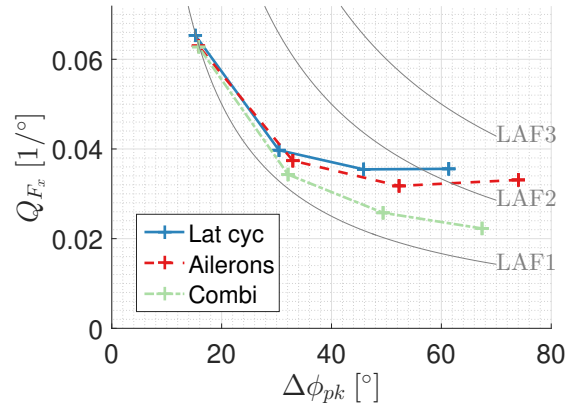


Figure 6.23: F_x quickness roll-out

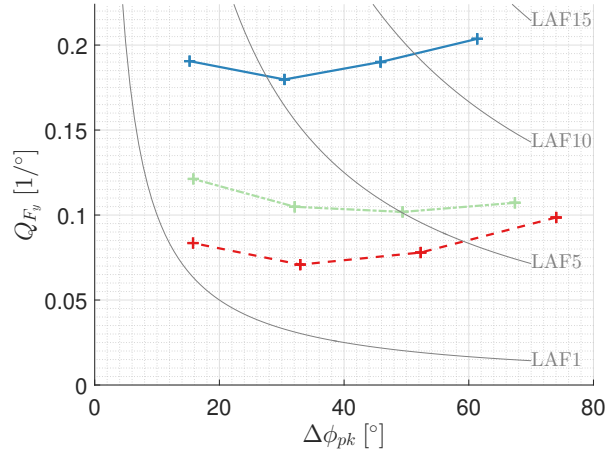


Figure 6.24: F_y quickness roll-out

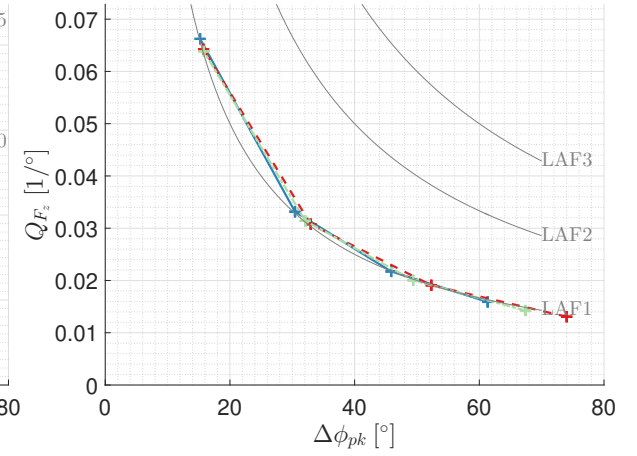


Figure 6.25: F_z quickness roll-out

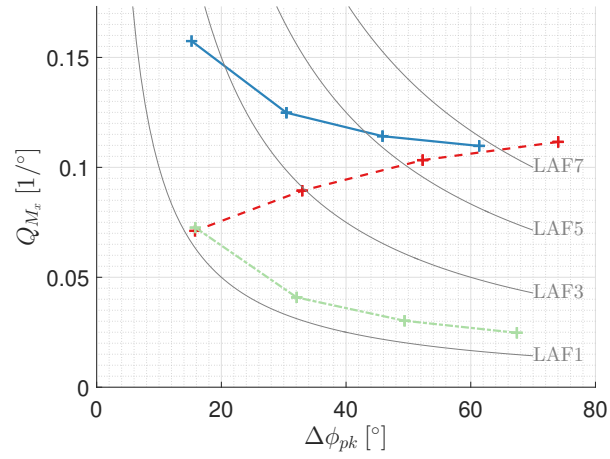


Figure 6.26: M_x quickness roll-out

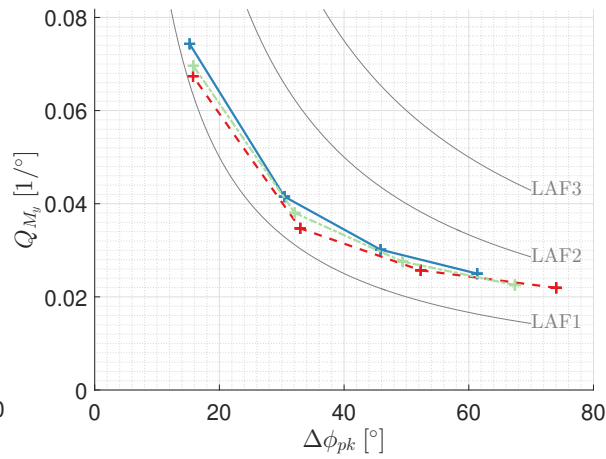


Figure 6.27: M_y quickness roll-out

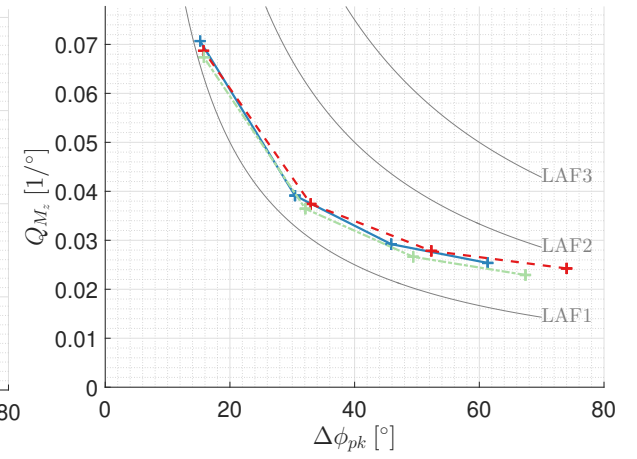


Figure 6.28: M_z quickness roll-out

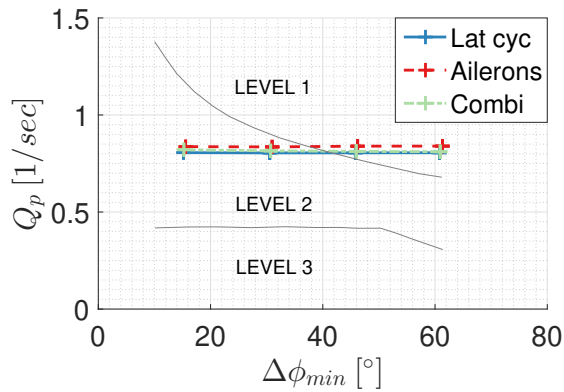


Figure 6.29: Roll attitude quickness roll-in

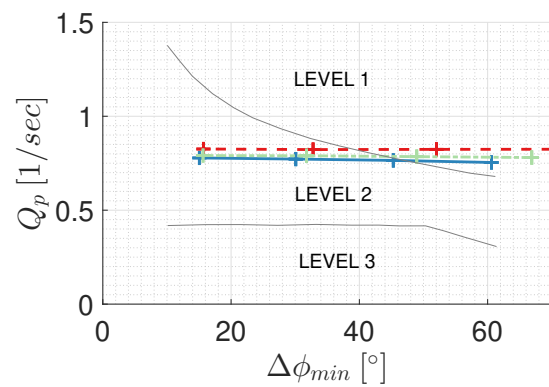


Figure 6.30: Roll attitude quickness roll-out

6.1.4. Discussion of a Pure Lateral Cyclic Input Strategy

As previously mentioned, loads in the main rotor hub can be associated with blade flapping. Different flapping phenomena will be encountered during the roll doublet. Therefore, each flapping motion is discussed separately.

Lateral Flapping due to Later Cyclic Input

First, the situation for a pure lateral cyclic input is explained. The motion and associated lateral flapping for a doublet using the lateral cyclic is shown in Figure 6.31. Figure 6.33 shows the angle of attack over the rotor disk during trim at 120 kts. Figure 6.34 and 6.35 show the effect of changing the lateral cyclic to roll. These figures are snapshots taken at 2.2 and 5 seconds where the maximum control input is applied as presented in Figure 6.1. A cyclic input to roll right will deflect the swashplate to increase the blade angle of attack over the front of the rotor. As the angle of attack increases, the lift over the blade increases causing a flap up motion. A maximum flap angle is achieved over the left side of the rotor disk. This describes the typical $\sim 90^\circ$ delay in blade flapping seen over a disk when the blade pitch is changed. This effect is caused by the balance between the applied aerodynamic forces, centrifugal and inertia forces on the blade. The maximum flap angle achieved over the left side of the rotor allows the centrifugal force to create a moment around the flap hinge off-set. This moment around the x-axis on the hub rolls the helicopter. A minimum flap angle is achieved over the right, advancing side.

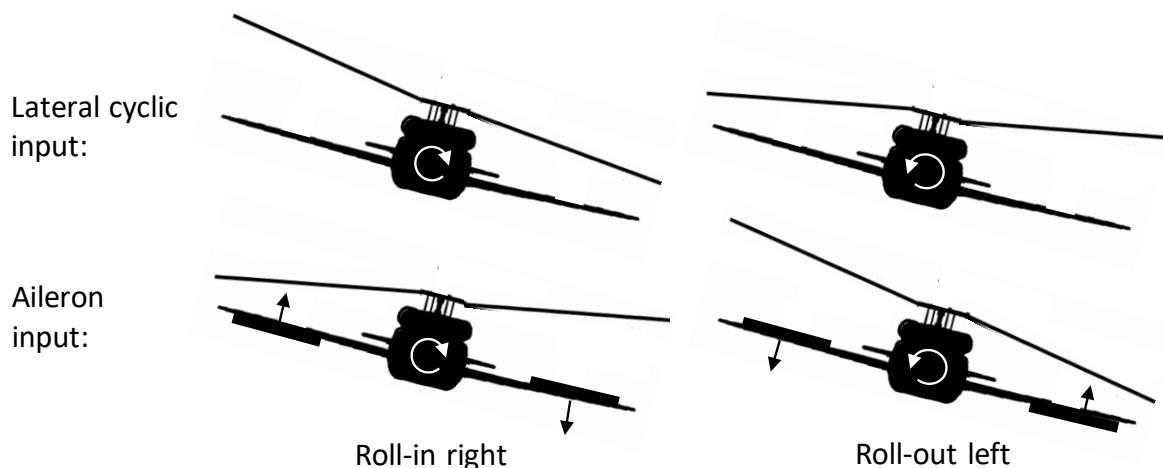


Figure 6.31: Blade flapping during doublet using lateral cyclic or aileron input, modified from [42]

Blade flapping causes the entire lift vector to point into the direction of the turn. The lift tilt will also create a rolling moment around the CG. It can be seen in Figure 6.31 how the lateral cyclic tilts the disk to the right. When lateral cyclic is used, the rolling motion is initiated over the rotor disk and passed through the hub to roll the fuselage. This means the rotor rolls first and the body follows. This leading rotor and following body

effect can clearly be observed when the roll angle and lateral flap angle are plotted with respect to an absolute world reference frame, Figure 6.32. The blue dotted line shows how the rotor rolls first and the blue solid line how the fuselage follows.

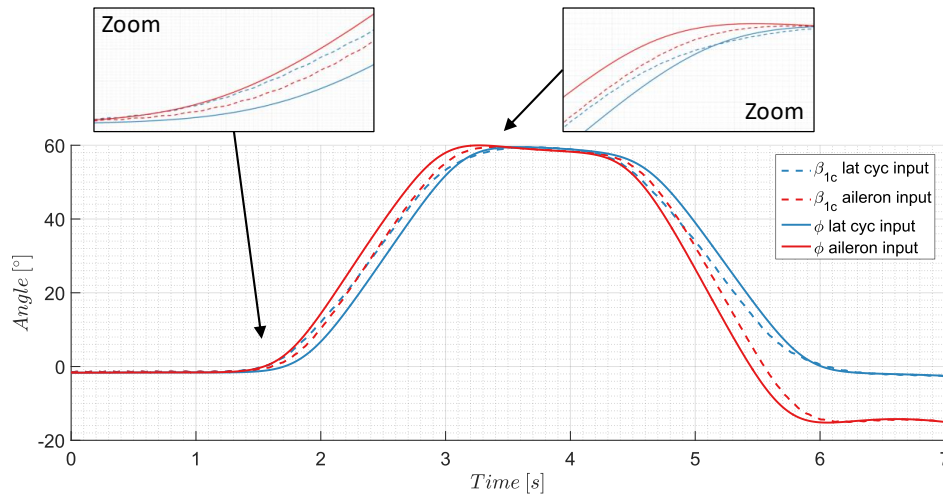


Figure 6.32: Absolute lateral flapping angle compared with roll angle for both lateral cyclic and aileron input doublet

Longitudinal Flapping due to Lateral Cyclic Input

A lateral cyclic input for an articulate rotor with no hinge off-set will cause the blades to find a balance ($\sum M = 0$) between the aerodynamic, inertial and centrifugal forces at exact 90° later. For a roll right, the blade pitch is maximum over the front of the disk and flapping finds it maximum at the left side of the disk. But the UH-60A rotor features a flap hinge off-set, causing the phase delay to be slightly smaller than 90° . A cross-coupling effect between lateral input and longitudinal motion appears. This motion is called 'acceleration cross-coupling' and only happens during a control input, or when an acceleration is applied [40]. As the peak flap angle is not exactly found over the left side of the disk but slightly forward, a longitudinal blade flap is noted. This explains the flap up motion β_{1c} of the blade during the roll-in manoeuvre, Figure 6.9. M_y follows the trend of the longitudinal flapping, Figure 6.15.

Longitudinal Flapping due to Roll Rate

Because the rotor is rolled to the right, the blades at the right side will see the flow coming from below and the opposite happens for a blade over the left side of the disk. This is visualised in Figure 6.41. Note that this figure shows a roll initiated by the ailerons but this should have no effect on this principle.

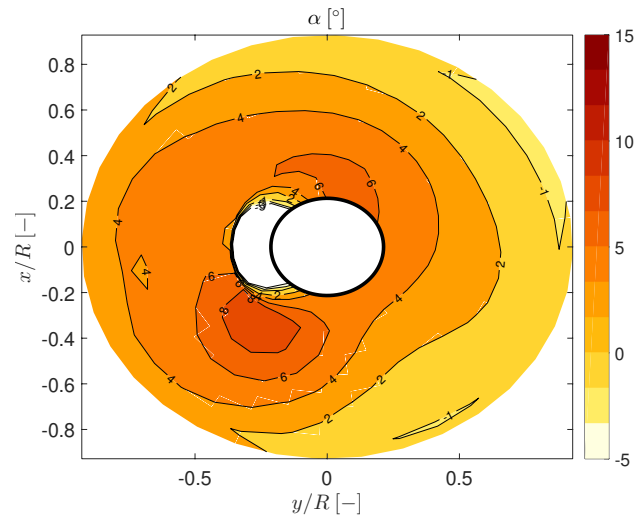
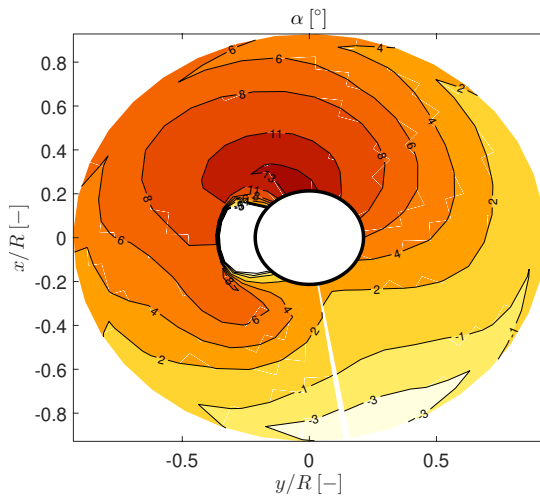
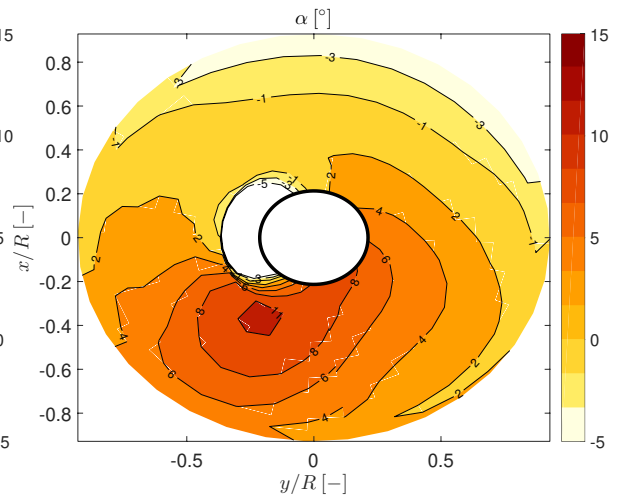
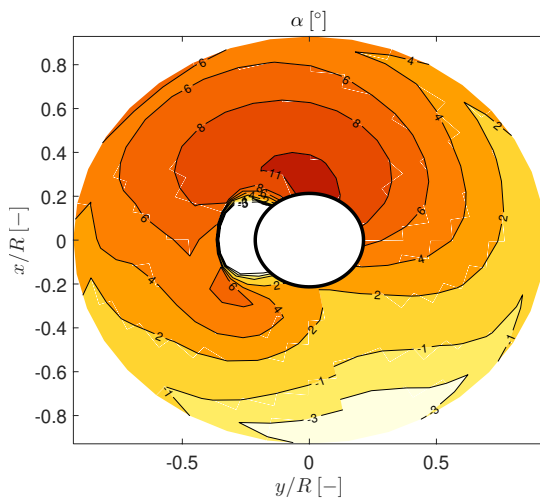
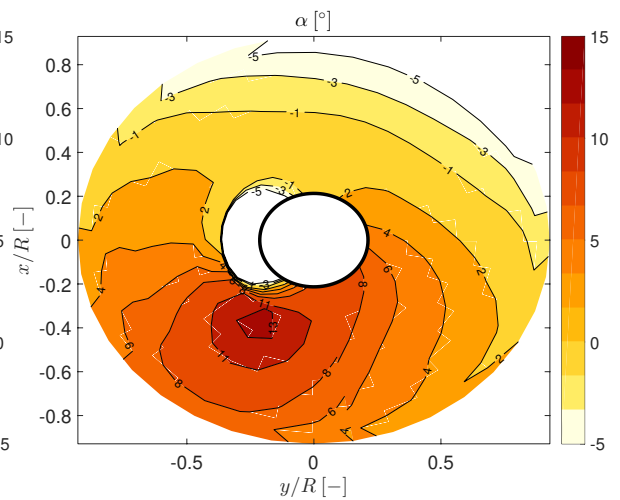
The flapping will immediately correct for the difference in flow situation over the left and right side of the rotor. The right side will flap up and the left down, reaching a maximum flap angle over the nose of the aircraft, β_{1c} .

Lateral Flapping due to Sideways Translation

As a result of the rolling motion, the helicopter will also translate, mainly into the direction of the roll angle over the time of the doublet. Sideslip will also have an effect on lateral flapping. For a right translation, the blade over the tail of the helicopter will see an increased flow and flaps up, the opposite will happen for the blade moving over the nose. Flapping due to this effect will peak over the right side for a right sideways motion. The tip-path-plane is tilted left which damps the sideways translation. Sideways velocity v is visualised in Figure 6.38. The sideways motion is small compared to the forward velocity of the helicopter and this effect is assumed to have little influence on the rotor state.

Rotor Lead-Lag and the Response of F_z and M_z

F_x is found to be growing and crimping, Figure 6.11. Note that the model does not feature a lead-lag hinge in the rotor assembly. Blades tend to lag over areas with high angle of attack and lead over disk areas with lower angles of attack. The biggest influence of this effect is normally seen in F_x for a rolling manoeuvre. Rolling with lateral cyclic increases α over the front of the rotor delaying the blade while it leads over the rear section

Figure 6.33: α over the main rotor disk in trim 120 ktsFigure 6.34: α at max right lateral cyclic input, 2.2 sFigure 6.35: α at max left lateral cyclic input, 5 sFigure 6.36: α at max right aileron input, 2.2 sFigure 6.37: α at max left aileron input, 5 s

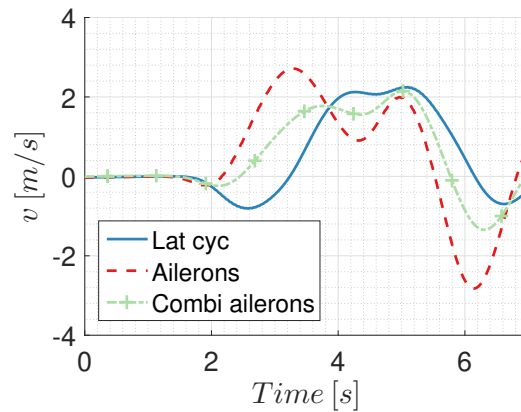


Figure 6.38: Sideways velocity v during roll doublet

of the disk. The transition from lead to lag happens around the sides of the rotor disk causing an effect in F_x . This effect is not modelled for this research and assumed less important as the real gain in load reductions are expected for F_y and M_x for a rolling manoeuvre.

Furthermore, F_z represents the lift vector and is affected by the load factor during the manoeuvre. M_z represents the main rotor torque and is affected by the blade lift and drag component in the xy -plane.

6.1.5. Discussion of a Pure Aileron Input Strategy

Studying Figure 6.31, the exact opposite flapping motion with respect to the fuselage can be observed when ailerons are used to roll the aircraft. The key to understanding this opposite motion lies in the situation over the main rotor disk. Although the lateral flapping and associated forces and moments are very different when using the ailerons instead of a cyclic input, the situation over the rotor disk seems very similar. This can be seen by comparing Figure 6.34 and 6.35 with Figure 6.36 and 6.37. The regions of higher angles of attack match for both roll-in and roll-out when the two input strategies are compared. However, a small difference in absolute value of α is noted.

Lateral Flapping due to Roll Rate

Figure 6.39 visualises what happens to the lateral flapping when the helicopter is rolled using the ailerons. The blades are exaggerated to clearly show the effects. This figure shows both the rear (left) and front (right) view of the helicopter during a roll-right manoeuvre. Starting from a wings level situation. No cyclic input means the swashplate's orientation is kept unchanged with respect to the fuselage, hence blade pitch is kept unchanged.

When the helicopter rolls to the right using the ailerons ($p > 0$), the entire hub assembly will roll with it. The main rotor can be seen as a gyroscope which will try to hold its orientation [40]. Figure 6.39 shows how the rotor lags the fuselage motion. While the blades still rotate in the horizontal plane, the blade pitch with respect to the horizontal plane points nose down (rear view) due to the rotation of the entire fuselage and hub assembly. This results in a negative angle of attack over the rear of the disk, pointing lift downwards. The negative angle over the rear side of the disk can be seen in Figure 6.36. The rotor will find itself in an unbalanced situation ($\sum M \neq 0$) and will work itself towards a balance by starting a flapping motion. Blades over the rear of the disk will flap down. Investigating the front of the helicopter, the opposite effect will take place. The rolling motion of the fuselage increases the angle of attack with respect to the lagging rotor plane. The increase in α causes a flap up motion over the front of the helicopter. The high regions of α over the front of the disk are visualised in Figure 6.36.

The rotor quickly compensates the unbalance by the flapping motion and follows the motion of the fuselage (rotor follows the motion of swashplate, constant to the motion of the fuselage in this case). This will cause the rotor to lag the fuselage motion as can be seen in Figure 6.32. It is very important to understand that the flap angle is measured at the flap hinge in body reference system in Figure 6.10. This is why an opposite β_{1s} response is seen for the aileron input compared to a cyclic input. However, for both input strategies, the rotor will tilt right during the roll-in measured in the absolute world frame. Flapping is often defined with respect to the control plane, the swashplate. With respect to the swashplate, both input strategies will see a

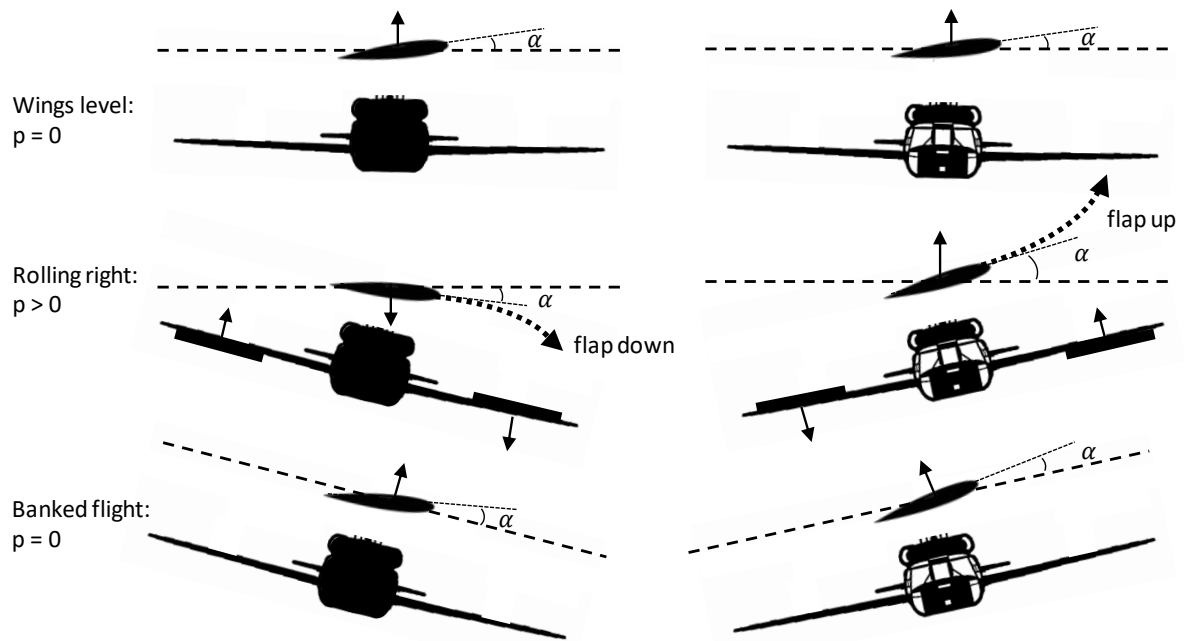


Figure 6.39: Lateral flapping due to roll rate (left rear view, right front view), modified from [42]

similar flapping motion (not opposite), but with a time delay. Reviewing Figure 6.10, the analogy can be made that for a lateral input, the rotor is tilted while the reference system (body) lags behind. While the reference system (body) is rolled and the rotor stays behind when ailerons are used.

As the reaction forces in the hub are also measured in the body reference system, the change in flapping response will invert M_x , Figure 6.14. F_y in Figure 6.12 is the result of the lift tilt perpendicular to the tip-path-plane measured in body axis, hence opposite response is observed comparing both input strategies.

M_x is a moment created by the flapping motion. The centrifugal forces of the opposing blades will create a moment around the flap hinge offset on top of the hub. This moment will damp the rolling motion when ailerons are used to roll. Figure 6.40 shows the moment created by the ailerons and lateral flapping during a roll right. An easy way to visualise the moment created by the blades is the picture pulling the two dotted arrows which represent the centrifugal forces of the blades. In order to avoid any misconceptions, the ailerons do not transfer a moment from the fuselage into the hub as the flap hinge can not pass through moments.

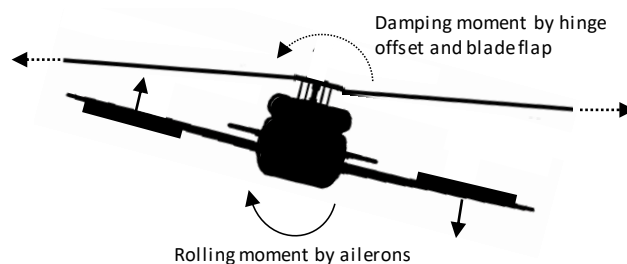


Figure 6.40: Lateral flap angle causing a damping moment during the rolling motion, modified from [42]

Longitudinal Flapping due to Blade Pitch

The analogy can be made with a cyclic input, the cyclic increases the blade pitch over the front of the disk by tilting the washplate. The aileron deflection has the same effect on the blade pitch but instead of tilting the washplate, the entire fuselage is rolled. Therefore the same coupling effect with the longitudinal flapping exists as previously described.

Longitudinal Flapping due to Roll Rate

As for a lateral cyclic input, the roll rate generated by the ailerons also produces another longitudinal flap response. The effect of the different inflow direction over the right and left blades is visualised in Figure 6.41.

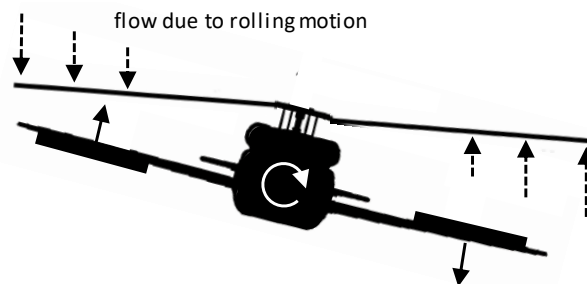


Figure 6.41: Incoming flow difference over left and right blade due to rolling motion, modified from [42]

Lateral Flapping due to Sideways Translation

The longitudinal flapping effect caused by the sideways translation explained under the results of a lateral input also holds here. However, the sideways velocity is small as shown in Figure 6.38 and this effect is assumed to have minor influences on the rotor.

Blade Stall Effects

For both a lateral cyclic and aileron input, the response of the moments and forces look fairly symmetric for the doublet. This means the roll-in response looks similar to the roll-out response. However, when closely investigating the M_x and M_y when ailerons are used, one notices a section of higher amplitudes during the roll-out, Figure 6.42. This effect can be linked to higher angles of attack and high c_l values over the disk at this moment. It is believed that the raise in moment response is caused by blades approaching stall over the indicated area on the disk, Figure 6.42. Blade stall will have a significant effect on the loading and might be responsible for the observed growing of the moment amplitude band.

6.1.6. Discussion of a 50% Lateral Cyclic - 50% Aileron Input Strategy

With the goal of reducing loads in mind, a 50% lateral cyclic and 50% aileron input strategy is investigated. As expected, this results in a rotor situation which lies between the previously presented cases (pure cyclic or pure aileron input). A pure lateral cyclic causes the rotor to lead compared to the fuselage and a pure aileron input has a lagging rotor, Figure 6.32. Combining both inputs results in a body which 'perfectly follows' the rotor motion, visualised in Figure 6.43. The reaction forces caused by a lead or lag effect are therefore alleviated. M_x and F_y shown in Figure 6.14 and 6.12 'level out'.

As F_x shows a growing and crimping response, combining the ailerons decreases the encountered force, Figure 6.11. M_y shows a cycling nature and the response by the combined cyclic-aileron input falls between the two others, showing minor improvements compared to a pure lateral cyclic, Figure 6.15. F_z and M_z follow a similar response for all control strategies, Figure 6.13, 6.16.

Load Quickness

Load quickness is studied during the roll-in section of the doublet. Note that both roll-in and roll-out quickness plots are presented in this report for completeness. The roll-in section is studied below as this is the 'cleanest' part of the manoeuvre (wings level to 60° bank angle instead of 60° bank angle to more or less wings level).

The load quickness plots confirm the benefit of using a combination of a cyclic and aileron input to alleviate loads during a rolling manoeuvre. The rolling moment quickness Q_{M_x} is decreased from a value above $LAF > 7$ for a pure cyclic or aileron input to a value around $LAF \approx 2$ for a mixed input, Figure 6.20. The large LAF scale on the F_y quickness plot in Figure 6.18 is the result of almost no force in the y-direction during trim compared to tilting the entire lift vector for rolling. Q_{F_y} is found to be lower when both cyclic and ailerons are used. The mixed input also shows a positive effect on the Q_{F_x} although the benefit becomes smaller as the magnitude of the control input is decreased, Figure 6.17.

The input strategy has almost no effect on the load quickness Q_{F_z} , Figure 6.19. The longitudinal flapping response of the mixed control input lies between the response of the two others, the same trend is seen in

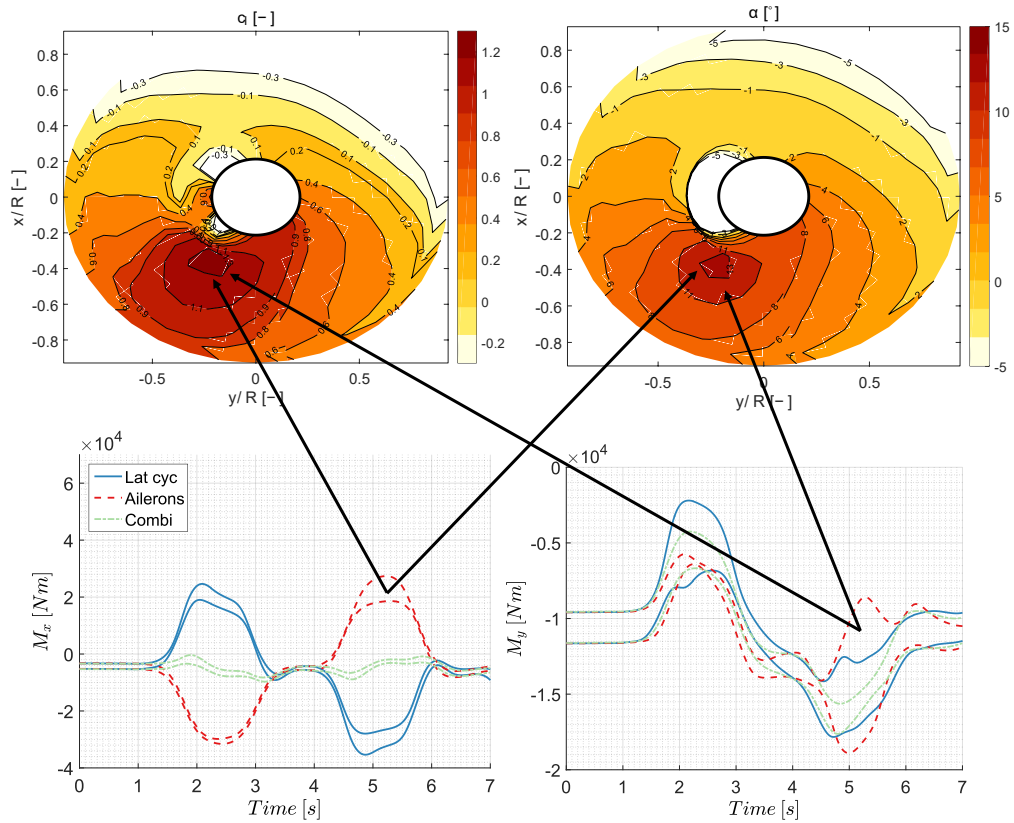


Figure 6.42: Possible blade stall during roll-out with ailerons, c_l on left disk plot, α on right disk plot

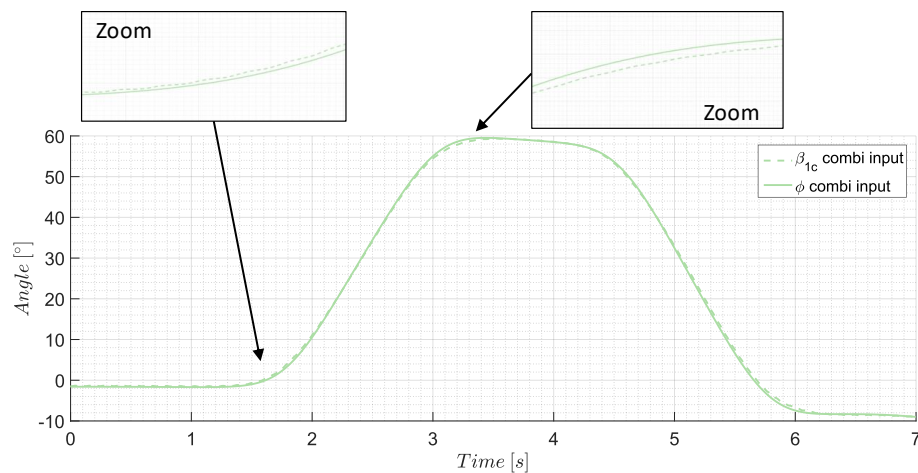


Figure 6.43: Absolute lateral flapping angle compared with roll angle for roll doublet using both 50% aileron and 50% lateral cyclic input

Figure 6.21 for Q_{M_y} . Differences in load quickness Q_{M_y} are small. Also, Q_{M_z} shows minimal changes when switching to another control strategy.

As the combined input shares the control power over the lateral cyclic and ailerons, the risk of running into blade stall decreases. This can avoid a sudden rise in loads linked to blade stall.

Attitude Quickness

The experiments were conducted at the same level of attitude quickness as shown in Figure 6.44. The input signal shape is kept constant but the magnitudes of the control inputs are scaled in order to achieve a 60° bank angle, shown in Figure 6.1. Looking at the control input presented in Figure 6.1 and roll response in Figure 6.6, two observations can be made.

Achieving a 60° bank angle in such a short time is a demanding manoeuvre for the aircraft. For both a pure cyclic or pure aileron input, the controls will operate at a high saturation level. When a combined input is used, both control inputs will operate at a lower saturation level. This means there is an opportunity to reach a higher roll quickness when both cyclic and ailerons are used. It is believed that the attitude quickness can be increased to achieve the LEVEL 1 handling requirements for all angles as shown in Figure 6.44.

Secondly, it can be observed how the helicopter reacts faster to a roll input using the ailerons compared to a pure lateral cyclic input. This might suggest the aileron input has a larger bandwidth compared to a cyclic input making it easier for the pilot to track a reference signal (for example easier to exactly achieve the 60° bank angle, or exact wings level).

It is concluded that using a combination of the ailerons and lateral cyclic input to fly a roll doublet offers the opportunity to alleviate loads and potentially increase handling quality performance.

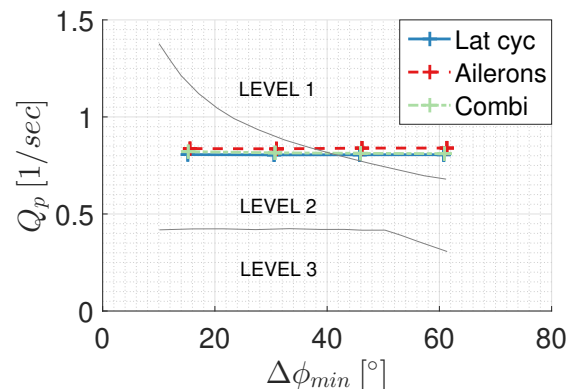


Figure 6.44: Attitude quickness roll-in

6.2. The Effect of Different Trim Settings on Loads in the Rotor Hub

In the previous section, it was concluded that using a 50% lateral cyclic - 50% aileron control input strategy results in lower loads in the main rotor hub during a roll doublet. This chapter will investigate the effect of different trim settings prior to the execution of the roll doublet.

During the literature study, it was presented how the compound helicopter achieves an increased cruising efficiency and higher flying speeds by offloading both the lifting and propulsive function of the main rotor. This can be done using the rich variety of controls of the compound type as described in Section 2.4 Compound Helicopter Principles. The study by Reddinger & Ganhi [42] presented in Section 2.4 focuses on cruise efficiency by varying trim settings to minimise power required. However, the study does not look at the effect on rotor loads.

Reddinger & Ganhi [42] achieve an optimal cruise condition by changing the horizontal tail deflection, wing lift, rotor rpm, compound thrust and aileron input during trim. This thesis will vary the compound trim settings according to the same principles but focus on the impact on rotor loads.

Varying the trim settings will change the lift share as well as the propulsive function of the rotor. This is achieved by different control mechanisms at trim which will define the test matrix of this experiment. Each of these mechanisms can be linked to future compound helicopter types as different concepts feature different control systems. The Airbus Races[1] in Figure 6.45 features a main wing and two propellers as well as an adjustable horizontal stabiliser and ailerons. All these control elements can be used to trim the helicopter in a cruise optimal setting. Bell recently introduced the Bell 360 Invictus [3], Figure 6.46. This helicopter type does not feature an extra propulsive unit and relies on the main rotor for forward speed. However, the rotor lift can be offloaded to the main wing. The Boeing-Sikorsky Defiant SB>1 [4] features a coaxial rotor system making it fundamentally different from the model constructed for this research, Figure 6.47. However, this helicopter type uses a technology called 'the advancing blade concept (ABC-concept)' initially tested on the Sikorsky X2 shown in Figure 1.2. The lift is pushed more outboard of the advancing blade increasing its efficiency as lift is generated at higher dynamic pressures. As this creates a high moment, a counter mechanism is required. This is one of the reasons the Sikorsky X2 and the Boeing-Sikorsky SB>1 feature a coaxial rotor to cancel out this moment. The same principle is impossible to achieve on a conventional helicopter but as a

compound helicopter features a main wing, the ailerons can be used to counter the moment of the rotor. This was also presented by Reddinger & Ganhi [42] and discussed in detail in Section 2.4.3. This condition will be particularly interesting as it will affect the lateral motions like the roll doublet.



Figure 6.45: Airbus Racer [1]



Figure 6.46: BELL 360 Invictus [3]



Figure 6.47: Sikorsky-Boeing SB>1 DEFILANT [4]

6.2.1. Experiment Set-up

The trim conditions are varied using settings of the compound helicopter controls as summarised in the test matrix Table 6.1. The model will again be flown at 120 kts, before executing a roll doublet. The input strategy to fly the roll doublet is fixed for this experiment to a 50% lateral cyclic and 50% aileron input as shown in Figure 6.1.

Table 6.1: Test Matrix

Trim condition:	Baseline	HT.1	HT.2	CT.1	CT.2	RPM.1	RPM.2	AA.1
Horizontal tail deflection [$^{\circ}$] (HT.)	0	5	-5	0	0	0	0	0
Compound thrust [N] (CT.)	0	0	0	2500	5000	0	0	0
Main rotor revolution [rad/s] (RPM.)	27	27	27	27	27	24.3	21.6	27
Constant aileron deflection [$^{\circ}$] (AA.)	0	0	0	0	0	0	0	3

The motivation to vary the compound helicopter's trim settings according to the test matrix Table 6.1 are presented per control input below:

Horizontal Stabiliser Settings

The functions of the horizontal stabiliser are listed in the UH-60A operation manual [7] and are linked to the aircraft's flying speed and control inputs. At low speeds, the elevator is deflected LE up in order to align the wing surface with the main rotor wake to minimise the pitch up tendency caused by the wake impingement on the horizontal tail. During forward flight, the angle of attack of the horizontal tail is decreased to improve static stability, depending on the flying speed. The incidence angle is also used to improve the dynamic response of the aircraft. The tail is linked to the main rotor collective to counter the change in pitch angle when adjusting the collective setting. The tail is also adjusted to provide a pitch rate feedback which improves the dynamic stability. Finally, a side slip to pitch coupling helps to reduce the aircraft's response to gusts.

An advance ratio of 0.28 set by the baseline condition dictates a stabiliser setting of 0° as defined by the UH-60A stabiliser incidence speed scheduling given by Bousman and Kufeld [11]. Test are done at $+5^{\circ}$ and -5° angle setting of the tail to capture the effect of both an upwards as well as downwards facing force near the tail section.

As the deflection of the horizontal tail will affect the pitch angle, this mechanism is also used unload the main rotor as the angle of attack over the main wing increases, generating more lift.

Compound Thrust Settings

The compound thrust setting increased to a maximum of 5000 N which counters the drag generated by the helicopter's fuselage. Results will show how the propulsive function of the main rotor is almost completely replaced by the compound thrust at a setting of 5000 N.

Rotor RPM Settings

The rotor rpm is lowered to 90% and 80% of its baseline setting. It was observed that the model struggled to find a trim solution for rpm settings lower than 80% of its baseline setting without changing the fuselage pitch angle to increase the lift share of the main wing.

Aileron Setting

As previously explained in this chapter, the ailerons can be used to improve cruise efficiency. A 3° aileron deflection was chosen to lower the main rotor power required and achieve a significant change in lateral blade flap and fuselage roll angle in trim.

6.2.2. Results

Each condition as specified in test matrix Table 6.1 results in a different trim setting as presented in Table 6.2. Note that the variables presented in the table are averaged over one rotor revolution. Also, lift share over the rotor and wing does not add up to 100 % as components like fuselage or tail also produce lift (upwards or downwards) which means the rotor and wing lift need to compensate for these phenomena.

After trim is achieved, the roll doublet is initiated using a 50% cyclic - 50% aileron input. A complete overview of the rotorcraft attitude, flapping and load responses during the roll right doublet at each trim setting as given by Table 6.2, is presented in Appendix D. Only the most relevant plots will be shown and discussed in this section. Note that the load quickness definition is slightly changed for this experiment. As each trim condition is different, load quickness is not scaled (divided by) the load at trim.

$$Q_F = \left| \frac{F_{pk}}{\Delta\phi_{pk}} \right| \quad Q_M = \left| \frac{M_{pk}}{\Delta\phi_{pk}} \right| \quad (6.4)$$

The effect of each of the control inputs as specified in the test matrix on trim and the roll doublet are discussed separately below. Table 6.2 shows an overview of all trim settings according to the test matrix while below, only condition HT.1, CT.2, RPM.2 and AA.1 are compared against the Baseline condition. SO. stands for the suboptimal trim condition and is discussed in the final Section 6.3.

6.2.3. Discussion of the Effect by an Elevator Deflection at Trim

Condition HT.1 where the elevator is deflected 5° TE down is compared against the Baseline condition. The elevator can be used to alleviate longitudinal control inputs. As shown in Table 6.2, when the elevator is deflected down (positive), it creates a nose down moment which tilts the helicopter to a more nose down attitude. Without horizontal tail, the longitudinal cyclic is required to tilt the lift vector forward and generate a forward speed. One notices a much smaller θ_{1s} input when the elevator is deflected down. As this is coupled to the longitudinal flapping, the sign is reversed and rotor blow back is noted when $i_{tail} = 5^\circ$, Figure 6.48. Due to the change in pitch angle, the main wing sees a smaller angle of attack and the lift share of the rotor increases. More lift over the main rotor will increase the coning angle.

The difference in longitudinal input linked to longitudinal flapping has a significant impact on M_y , Figure 6.48, 6.51. Deflecting the elevator with 5° leads to a 29% lower average M_y load in trim and it is noted how the entire M_y response during the roll doublet is shifted. The average F_x is reduced when the tail is deflected down, Figure 6.50. The elevator deflection has little influence on the lateral flapping and therefore also M_x , Figure 6.49. F_z is found to be lower when the main rotor is more offloaded at $i_{tail} = 0^\circ$.

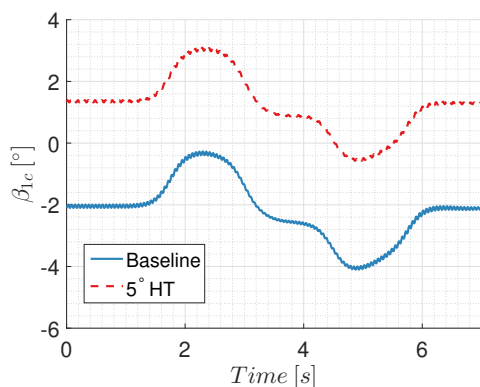


Figure 6.48: β_{1c} , roll doublet, 50% cyclic - 50% aileron input

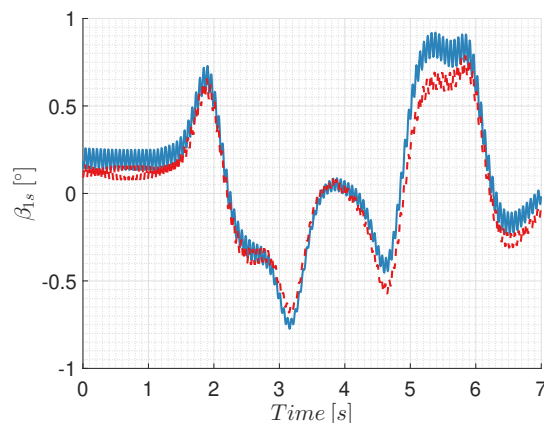


Figure 6.49: β_{1s} , roll doublet, 50% cyclic - 50% aileron input

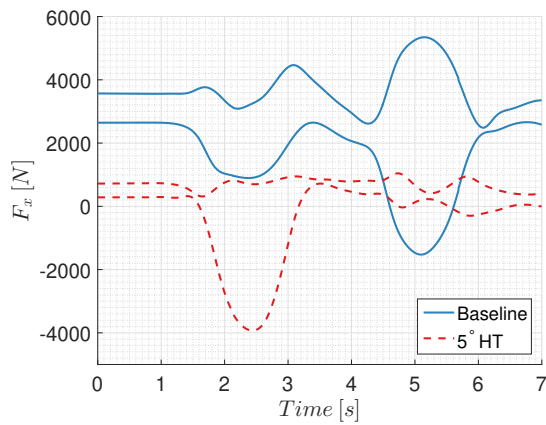
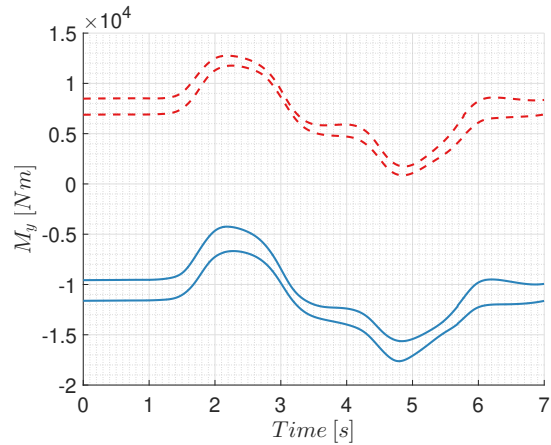
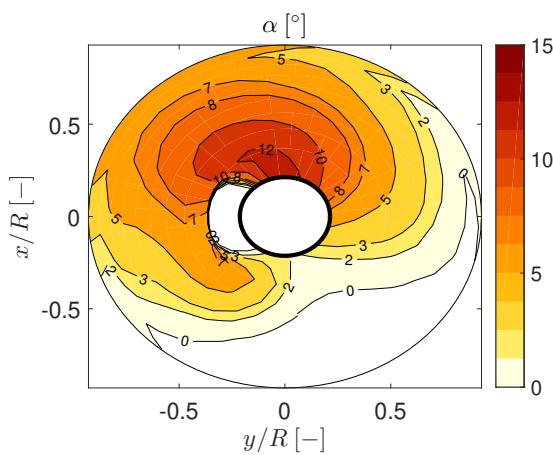
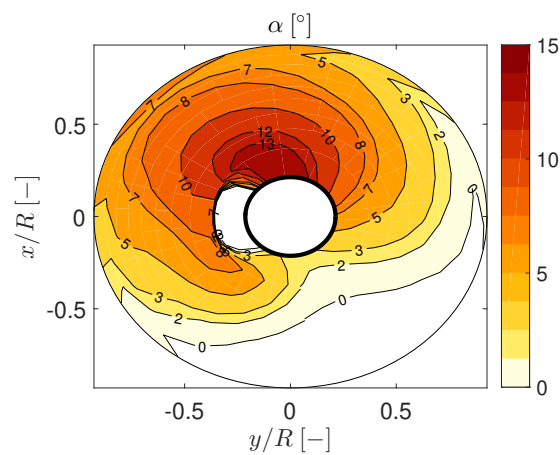
Table 6.2 shows how the collective settings stays the same while the rotor is offloaded by 13%. This might be linked to the orientation of the tip-path-plane. If the fuselage pitch angle and longitudinal flapping are

Table 6.2: Trim settings at different trim conditions

Variable	Baseline	HT.1	HT.2	CT.1	CT.2	RPM.1	RPM.2	AA.1	SO.
θ [°]	-1.87	-4.25	0.47	-0.84	0.59	-1.69	-1.58	-1.80	0.94
ϕ [°]	-1.61	-1.70	-1.41	-0.95	-1.22	-1.29	-1.79	0.41	1.34
θ_0 [°]	15.26	15.40	15.41	14.07	12.11	16.40	17.99	15.21	13.01
θ_{1c} [°]	-1.06	-0.94	-1.08	-1.02	-0.48	-1.21	-1.48	-3.52	-3.92
θ_{1s} [°]	-5.08	-2.04	-8.78	-3.56	0.97	-6.16	-7.71	-4.95	-1.80
i_{tail} [°]	0.00	5.00	-5.00	0.00	0.00	0.00	0.00	0.00	0.00
Compound thrust [N]	0.00	0.00	0.00	2500	5000	0.00	0.00	0.00	5000
Ω [rad/s]	27.00	27.00	27.00	27.00	27.00	24.30	21.60	27	21.60
δ [°]	0.00	0.00	0.00	0.00	0.00	0.00	0.00	3.00	3.00
Rotor-lift share [%]	0.68	0.81	0.55	0.60	0.47	0.65	0.68	0.67	0.46
Wing-lift share [%]	0.34	0.18	0.49	0.40	0.50	0.36	0.35	0.35	0.52
β_0 [°]	1.26	1.55	1.01	1.02	0.57	1.63	2.11	1.24	1.62
β_{1c} [°]	-2.04	1.34	-6.11	-1.01	0.82	-2.08	-2.01	-2.29	1.29
β_{1s} [°]	0.21	0.15	0.34	0.17	0.29	0.28	0.39	-2.38	-3.27
$F_{hub_{xmean}}$ [N]	3115	540	5006	1707	132	3344	3325	3152	43
$F_{hub_{xampl}}$ [N]	467	227	427	353	281	608	762	524	310
$F_{hub_{ymean}}$ [N]	629	810	576	474	205	658	797	2759.3	2327
$F_{hub_{yampl}}$ [N]	271	116	596	148	218	385	498	345.	317
$F_{hub_{zmean}}$ [N]	45900	54902	37191	40507	31576	45695	44051	45658	31002
$F_{hub_{zamppl}}$ [N]	2635	1996	2074	2687	2664	3106	2596	2568	2601
$F_{hub_{totmean}}$ [N]	46012	54910	37530	40547	31579	45826	44188	45856	31094
$F_{hub_{totamppl}}$ [N]	2658	1998	2091	2699	2661	3137	2629	2578	2570
$M_{hub_{xmean}}$ [Nm]	4255	4299	4223	3772	2499	4090	4048	17986	14822
$M_{hub_{xamppl}}$ [Nm]	969	611	2627	970	961	792	468	1239	692
$M_{hub_{ymean}}$ [Nm]	10615	7564	29926	5173	4810	8553	6377	11226	5081
$M_{hub_{yampl}}$ [Nm]	1027	805	2561	1098	1178	695	436	1183	764
$M_{hub_{zmean}}$ [Nm]	26916	27980	26649	21777	15632	25591	25430	25796	9025
$M_{hub_{zamppl}}$ [Nm]	1289	1643	3597	694	1159	973	512	3499	2294
$M_{hub_{totmean}}$ [Nm]	29214	29267	40469	22769	16451	27293	26479	33322	18230
$M_{hub_{totamppl}}$ [Nm]	1116	1631	1202	588	1012	916	574	2992	878
P_{totreq} [kW]	727	755	720	742	730	623	549	697	504

taken into account, one will find a more nose down orientation of the tip-path-plane for the case with 0° tail deflection. As the rotor is tilted more into the freestream, the inflow will be higher. An increased inflow will lower the overall angle of attack meaning the collective setting cannot significantly be reduced, even when the rotor is unloaded, as a certain thrust needs to be guaranteed. The effect of the increased inflow on the angle of attack over the blade is visualised in Figure 2.24.

An abrupt increase in amplitude is noted for F_x during the roll-in section of the doublet, Figure 6.50 between 2 and 3 seconds. It is difficult to exactly pinpoint what causes this increase in amplitude but a possible explanation might be high α 's over the rotor reached at this time. It can be observed that the longitudinal flap angles reach a much higher value when the elevator is deflected, Figure 6.48. Even when taking into account the difference in fuselage pitch and coning angle, the rotor will have a significantly smaller angle with the freestream between 2 and 3 seconds when $i_{tail} = 5^\circ$. When the rotor is placed more horizontal in the stream, the inflow through the rotor is decreased which raises the blade angles of attack pushing it closer to the stall point, associated with an increase in drag (and lift). The α distributions for the baseline case and 5° tail deflection case at 2.2 seconds into the manoeuvre are shown in Figure 6.52 and 6.53. This effect might explain why the F_x amplitude grows.

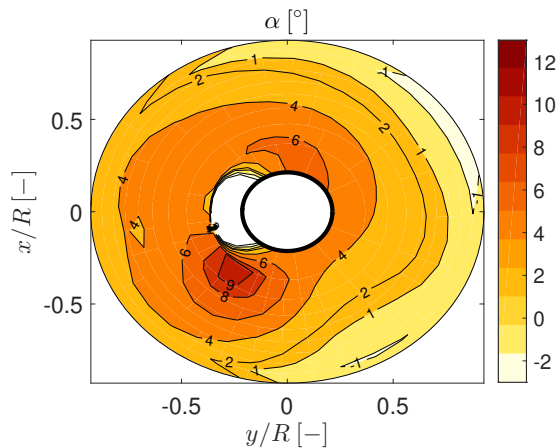
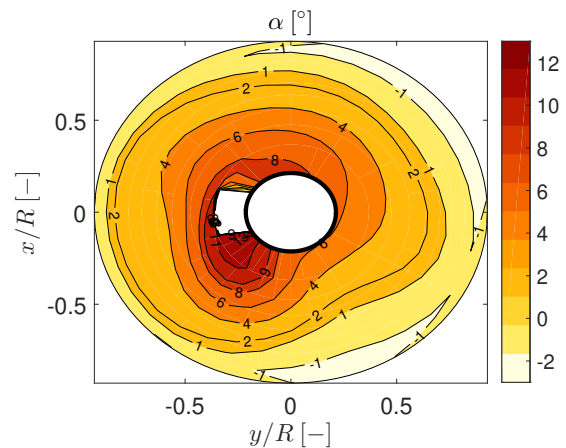
Figure 6.50: F_x , roll doublet, 50% cyclic - 50% aileron inputFigure 6.51: M_y , roll doublet, 50% cyclic - 50% aileron inputFigure 6.52: α over disk at 2.2 seconds of roll doublet, $i_{tail} = 0^\circ$ Figure 6.53: α over disk at 2.2 seconds of roll doublet, $i_{tail} = 5^\circ$

To conclude the effect of the horizontal tail, it was found that this control input has limited effect on lateral flapping, F_y and M_x . The TE down tail deflection does alleviate the longitudinal cyclic to maintain forward speed. This effects the longitudinal flapping and lower the F_x - and M_y -loads. As the sign of M_y can be reversed for significant tail inputs, the roll direction will also have influence whether the load in the hub are increased or decreased during the manoeuvre, Figure 6.51. If the horizontal tail input is relaxed from $i_{tail} = 5^\circ$ to $i_{tail} = 0^\circ$, the total required power is reduced by 3.9%. However a higher longitudinal cyclic input will increase the loads in the hub.

6.2.4. Discussion of the Effect by Compound Thrust at Trim

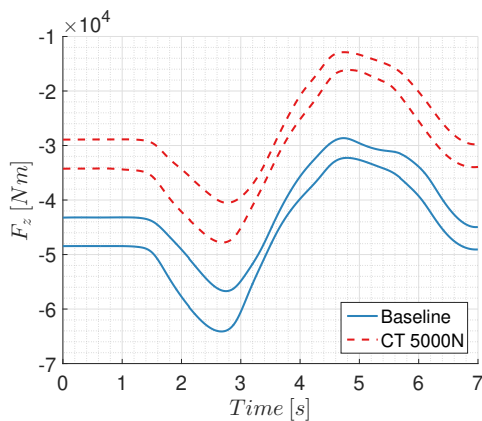
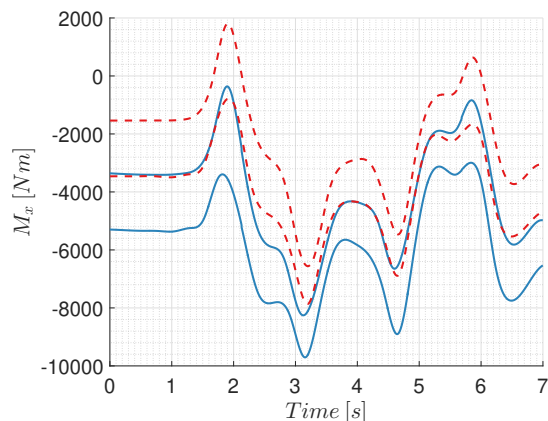
The thrust setting is set to 5000 N in condition CT.2 and compared against the Baseline. The compound thrust takes away the propulsive function of the main rotor, normally generated by a longitudinal cyclic input. The longitudinal input is noted to be reduced and the helicopter flies at a higher pitch angle. This also has an effect on the longitudinal flapping. One notices a blow back situation of the rotor when 5000N of compound thrust is added. The nose up attitude also changes the angle of attack over the wing and offloads the lifting function of the main rotor. As the disk itself flies at a smaller angle with the freestream, there will be less inflow through the rotor. This phenomenon increases the angle of attack seen by the blade. Combined with the offloaded rotor, this allows for a lower collective setting to generate the appropriate amount of rotor thrust. This effect is visualised in Figure 2.24 and explained in Section 2.4.5. The lower collective setting is also noted when plotting the angle of attack over the rotor blade in trim, Figure 6.54 and 6.55. The reverse flow area is observed to be smaller when compound thrust is added and the collective setting is adapted.

Adding the compound thrust will have a very similar effect on the flapping as applying a TE down horizontal tail deflection. The added thrust will shift β_{1c} upwards comparable to Figure 6.48 and has little effect

Figure 6.54: α over disk at trim, compound thrust = 0 NFigure 6.55: α over disk at trim, compound thrust = 5000 N

on β_{1s} , comparable to Figure 6.49. Appendix D includes all response plots for this specific trim condition.

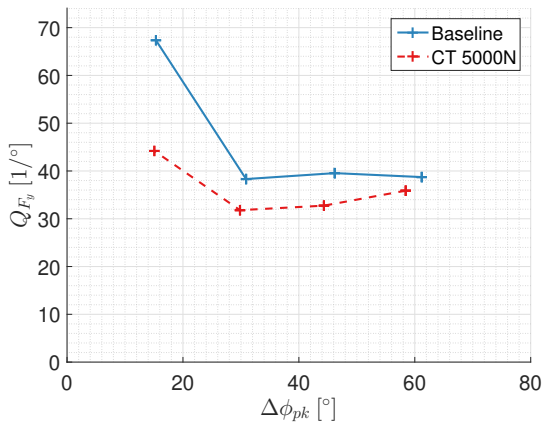
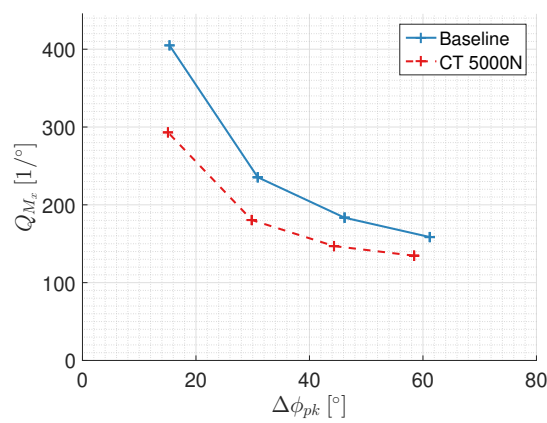
As both the lifting and propulsive function of the rotor are alleviated, the overall loads in the hub will be much lower. The effects on F_x and M_y are similar to applying a horizontal tail deflection, comparable to Figure 6.50 and 6.51. The entire response of these loads is shifted as the propulsive function of the main rotor is alleviated by the compound thrust. The effect of the rotor lift unloading is clearly visible in Figure 6.56. The M_x response is observed to be translated while the general shape stays the same, Figure 6.57. Note that previously, the changes in hub moment M_x were directly coupled to the moment created by the blade centrifugal force over the flap hinge offset due to the flap angle. Comparing trim values of the Baseline and CT.2, the lateral flap angle is almost identical. It is believed that the decrease in M_x is not linked to the centrifugal forces (as they create a small moment as β_{1s} is small) but linked to the coupling effect of the longitudinal rotor offloading. Aerodynamic and inertial forces become more dominant at small flap angles. This explains the decrease in M_x while the lateral flap angle remains the same.

Figure 6.56: F_z , roll doublet, 50% cyclic - 50% aileron inputFigure 6.57: M_x , roll doublet, 50% cyclic - 50% aileron input

As this study focuses on a roll manoeuvre and associated loads, the improvements of adding 5000 N of compound thrust on the load quickness for F_y and M_x are shown in Figure 6.58 and 6.59. Other load quickness plots are added in Appendix D. During compound helicopter operations, compound thrust is added to boost the flying speed or to achieve accelerations and decelerations without significant fuselage pitch. The power required for the main rotor is found to be decreased but the total power required is 2% higher when 5000 N of compound thrust is added.

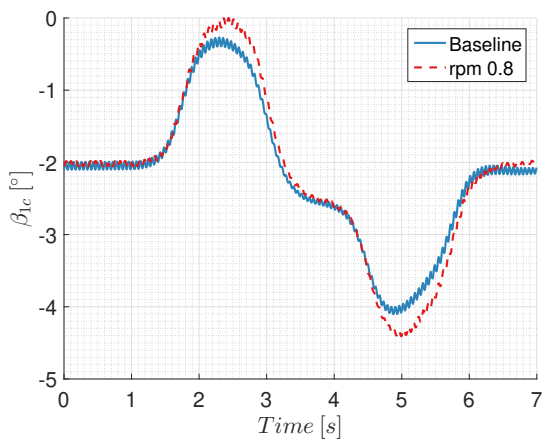
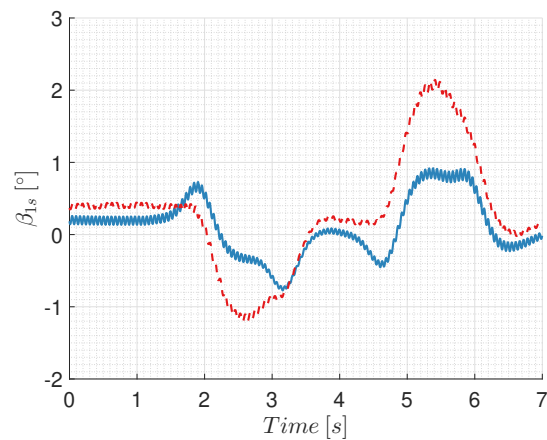
6.2.5. Discussion of the Effect by a Lower Main Rotor RPM at Trim

The rotor rpm is lowered to 80% of its nominal value in trim setting RPM.2 and compared against the Baseline. As rpm is decreased, the fly-to-trim controller wants to increase the collective setting to maintain altitude.

Figure 6.58: Q_{F_y} , roll doublet 50% cyclic - 50% aileron inputFigure 6.59: Q_{M_x} , roll doublet 50% cyclic - 50% aileron input

This results in limited rotor offloading. The current control system does not feature the capabilities to change the attitude angle of the compound helicopter to increase the angle of attack over the main wing and the lift of the main wing will stay almost unchanged.

The combination of lower rpm and higher collective increases the coning angle. The centrifugal forces are decreased allowing the higher flap angles, also seen in the longitudinal and lateral flap Figure 6.60, 6.61. When lateral cyclic input is used, a combination of the lateral flap angle and the centrifugal force determine the magnitude of the rolling moment. If the same rolling manoeuvre is flown, more flapping will be required to achieve the same rolling moment as the centrifugal force is reduced at a lower rpm. As for this experiment, the ailerons are also used to roll. One can reason that the lateral cyclic part of the combined aileron-cyclic-input becomes less effective. The overall observed effect is little change in the F_y quickness and a slight improvement of the M_x quickness. Lowering the rpm to 80% of its nominal value reduces the power required with 24%.

Figure 6.60: β_{1c} , roll doublet, 50% cyclic - 50% aileron inputFigure 6.61: β_{1s} , roll doublet, 50% cyclic - 50% aileron input

6.2.6. Discussion of the Effect by a Constant Aileron Deflection at Trim

A constant aileron deflection at trim in condition AA.1 is compared to the Baseline. Previous trim settings had a major influence on the longitudinal condition of the helicopter. Cruise performance is improved by alleviating the lift and thrust of the rotor by the main wing and compound thrust. Section 2.4.3 describes another option to boost cruise performance. A constant roll right aileron input is applied. To counter the rolling moment, a lateral cyclic is required which pushes the lifting section of the advancing blade more outboard where it operates at a higher dynamic pressure, hence higher efficiency. This resembles the advancing blade concept as described at the beginning of this section.

The effect of a 3° aileron input is presented in Table 6.2. Compared to the Baseline, the trim fuselage roll angle is turned to the right and an increased cyclic input is observed which tilts the rotor (β_{1s}) to the left.

Effects on pitch angle and longitudinal cyclic input are very small. A 4% decrease in total required power is achieved.

Similar to applying a horizontal tail deflection affecting β_{1c} , the constant rolling moment by the ailerons shifts the β_{1s} response, Figure 6.62. This is associated with a shift in rolling moment M_x , Figure 6.63. Note that in order to increase cruise efficiency, only a right rolling moment is beneficial, towards the side of the advancing blade.

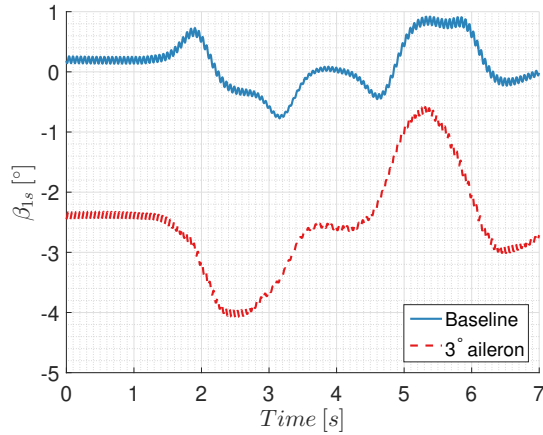


Figure 6.62: β_{1s} , roll doublet, 50% cyclic - 50% aileron input

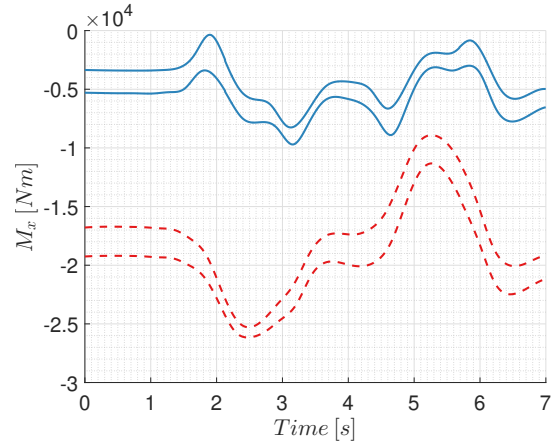


Figure 6.63: M_x , roll doublet, 50% cyclic - 50% aileron input

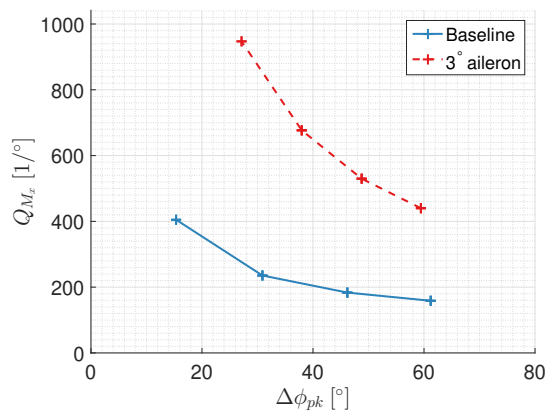


Figure 6.64: Q_{M_x} roll-in, roll doublet 50% cyclic - 50% aileron input

The constant rolling moment applied by the ailerons and countered by the lateral cyclic will cause a different response between a right or left turn. When the helicopter is turned to the left, the lateral cyclic will first have to fight the right rolling moment created by the ailerons in trim. It will take some time for the aileron deflection to go from its roll right deflection to roll left deflection, helping the lateral cyclic (50% cyclic - 50% aileron input). This effect increases the moment in the hub when turning left. This is visible in the load quickness plots of M_x and M_y for the roll-in section of a right and left doublet, Figure 6.65, 6.66. The control inputs were tweaked to achieve the same roll angle during the roll left and right. However, a small decrease in attitude quickness is noted for the roll left motion in Figure 6.67, caused by the same principle as motioned above.

In order to create these quickness plots, the magnitude of the control input was varied. The far most right data point corresponds to a roll-in motion to achieve a 60° bank angle. The far most left data point uses 25% of the control magnitude required to achieve the 60° . When a constant right aileron deflection is applied in trim, a small input will not be enough to create a significant rolling motion to the left. For this situation, the lateral cyclic is just fighting the opposite aileron rolling moment. This explains the peaks for the far most left data point in the plots Figure 6.65, 6.66 (off the scale for load quickness). These quickness peaks are high, not because high loads are achieved, but because of a very small achieved roll angle according to the quickness definitions, equation 6.1.

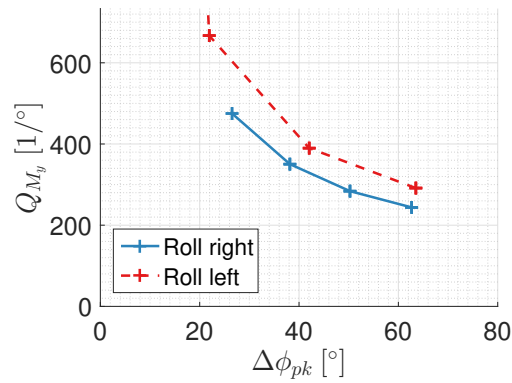
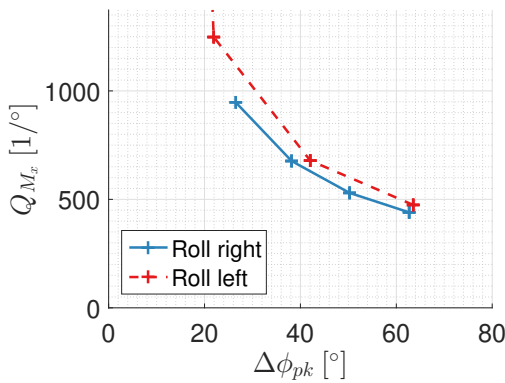


Figure 6.65: Q_{M_x} roll-in, roll doublet 50% cyclic - 50% aileron input Figure 6.66: Q_{M_y} roll-in, roll doublet 50% cyclic - 50% aileron input

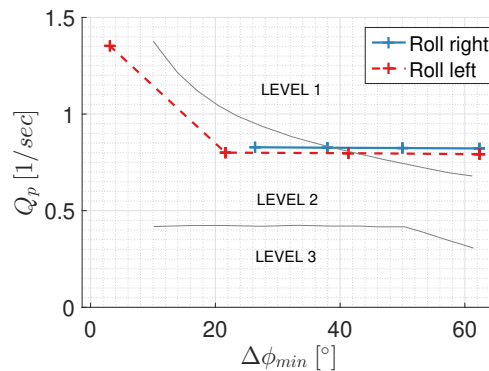


Figure 6.67: Q_p roll-in, roll doublet 50% cyclic - 50% aileron input

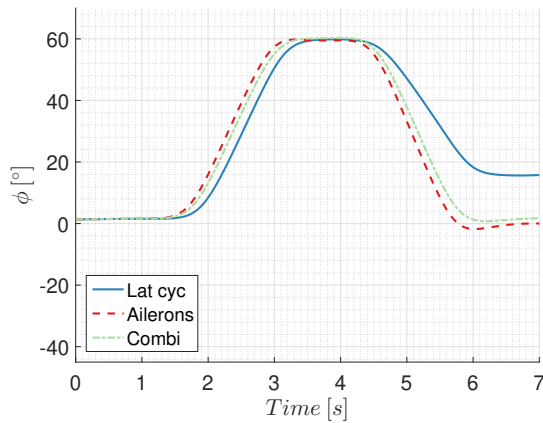
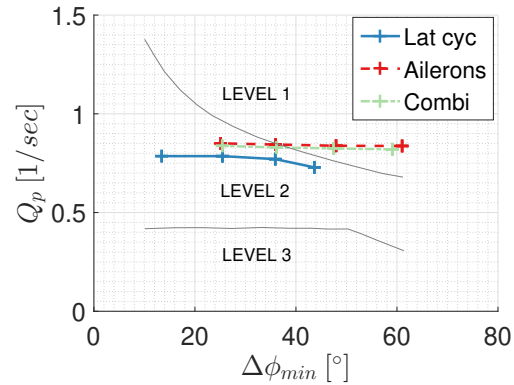
6.3. Varying the Control Strategy at a Suboptimal Trim Setting

In the previous section, each control input typical to the compound helicopter configuration is varied separately. Here, a suboptimal trim condition is proposed combining the settings described above. The trim settings are chosen to improve cruise performance for a compound helicopter flying at 120 kts. It is not the intention of this research to perfectly tweak these control settings to minimise power required as focus lies on investigating the loads. The compound thrust is set to 5000 N, the main rotor rpm is lowered to 80% of its nominal values and a 3° constant aileron input is applied. The trim condition is presented in the last column (SO.) in Table 6.2. The total power required is reduced by 31%.

To fully understand the potential of using a different control strategy to roll, the pure cyclic, pure aileron or mixed input were used to fly a right doublet at this suboptimal trim setting. Figure 6.68 shows how a pure lateral cyclic struggles to roll back to a wings level condition as it needs to fight the constant 3° roll right aileron deflection. The attitude quickness plot shown in Figure 6.69 confirms the lower roll quickness for a pure lateral cyclic input during the roll-out. The pure lateral cyclic asks for a high blade pitch setting which exceeds stall. Lift over the blade is lost and the required roll rate is not achieved. The effects of blade stall are also noted by the increase in amplitude of hub moments M_x and M_y in Figure 6.70 and 6.71.

As discussed for the baseline condition, a combined cyclic and aileron input 'levels out' the M_x response during the roll doublet. Comparing the baseline, Figure 6.14 with the suboptimal trim, Figure 6.70, it can be observed how the constant aileron deflection translates the entire M_x response. Therefore, when the combined input is used, the M_x will slightly vary around the non-zero trim value for the suboptimal trim case. However, when a pure lateral cyclic is used during the roll right section and a pure aileron input during the roll left, the M_x moment in the hub can potentially be lower compared to the combined input strategy.

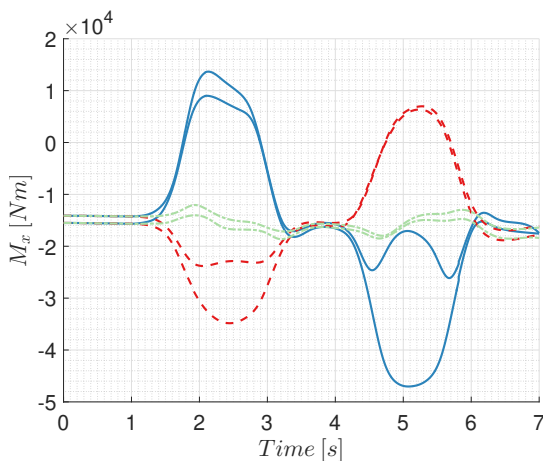
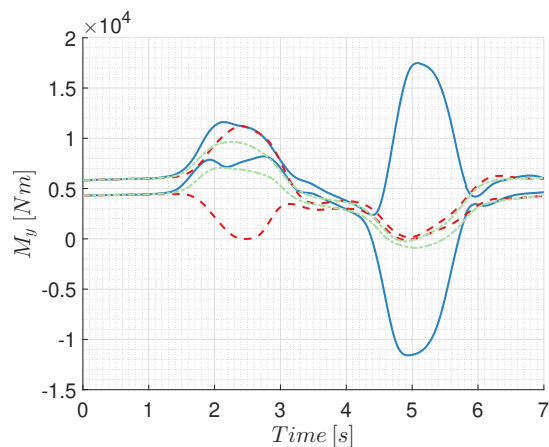
This effect is also observed in the load quickness plots, Figure 6.72 and 6.73. When a combined input strategy is used, the roll direction has little effect on M_x . However, this is not true for the other two strategies. The quickness plots show how the lateral cyclic is lower for the roll right (roll-in) and how the ailerons cause lower loads when used during the roll left. This suggests a fourth control strategy where pure lateral cyclic

Figure 6.68: ϕ , suboptimal trim condition roll doubletFigure 6.69: Q_p , suboptimal trim condition roll-out section doublet

is used for the rolling right and pure ailerons are used to roll left. However, it also introduces a loading-unloading cyclic which might affect the fatigues life of the component. It also has to be investigated if this strategy is practical from a control point of view as it introduces a degree of asymmetry. Finally, the load alleviation capabilities of this fourth strategy are similar to a combined 50% cyclic - 50% aileron input. More research is required if this fourth strategy is beneficial.

Investigating the M_y moment response between the baseline in Figure 6.14 and the suboptimal trim in Figure 6.71, it can be noted that the entire response is reduced. Mainly due to the offloading of the longitudinal cyclic input, the M_y response is translated downwards as explained earlier in this section.

This concludes how the rotor lift and thrust can be offloaded to reduce the power required in cruise. As this also alleviates the required longitudinal cyclic to maintain the forward speed, the M_y load in the hub is decreased. The 50% lateral cyclic - 50% aileron input strategy to fly the doublet minimises blade flapping and levels out the M_x response. However, the constant 3° aileron deflection at trim, used to reduce power, shifts the entire M_x response which increases its trim value. Control saturation levels are shown to be lower when the 50% lateral cyclic - 50% aileron input strategy is used. This lowers the risk of running into blade stall which can potential cause an abrupt rise in loads. Also, the control power to roll is higher which can lead to an increase in roll quickness.

Figure 6.70: M_x , suboptimal trim condition roll doubletFigure 6.71: M_y , suboptimal trim condition roll doublet

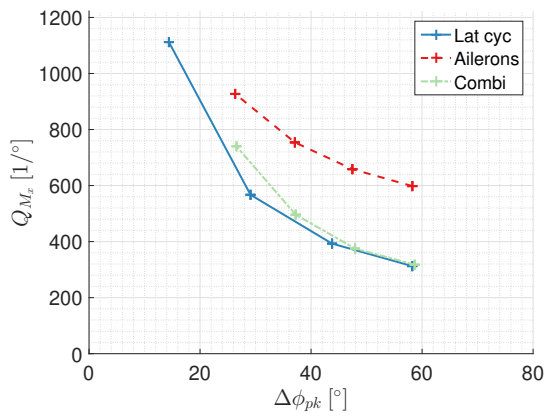


Figure 6.72: Q_{M_x} , suboptimal trim roll-in section doublet

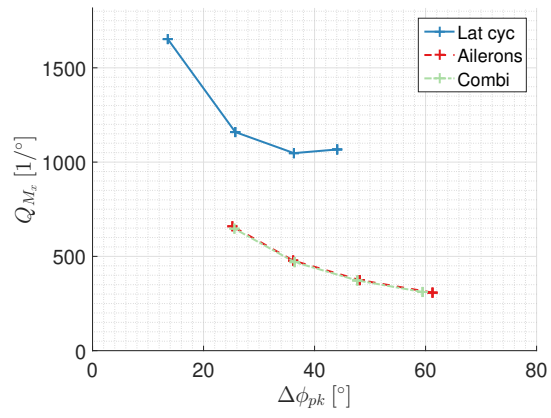


Figure 6.73: Q_{M_x} , suboptimal trim roll-out section doublet

7

Conclusion

The thesis investigated how the redundant controls typical to the compound helicopter configuration can alleviate loads during an aggressive manoeuvre. A compound version of the UH-60A Black Hawk was modelled during this research. It features a main wing and push propeller mounted near the tail. This specific helicopter type is also used for theoretical studies within the 'Future-Vertical-Lift program' which revisits the potential of compound helicopter configurations [12]. Focus will be on the break-turn manoeuvre coming from rotorcraft operational needs. The break-turn is modelled as an aggressive roll doublet at 120 kts, causing high loads in the rotor hub.

Research performed within the NASA/Army Airloads Program [31] and work by Yeo, Bousman & Johnson [55] and Yeo & Johnson [54] show how high loads in the rotor hub are expected during the manoeuvre and linked to the 1/rev blade flapping. The potential of load alleviation strategies was already demonstrated in studies on conventional helicopters. This thesis investigates load alleviation opportunities on compound configurations, the research goals are concluded below:

Develop and validate a simulation model of a compound UH-60A Black Hawk helicopter capable of flying the break-turn MTE and computing the loads in the main rotor hub.

A multi-body dynamics 6 degrees of freedom model of a compound UH-60A Black Hawk was constructed. The main rotor is modelled by a blade element method combined with a Peters-He [38] inflow model. Quasi-steady look-up from wind tunnels tests are used to link the blade angle of attack to the aerodynamic coefficients. The hub system features a feathering hinge, flap hinge and a flap hinge offset. Blades are assumed to be rigid. These main rotor model choices are tailored to well capture first order flapping motions during manoeuvring flight at low frequency control inputs, typical for flight dynamics applications. The empennage is represented by wing sections using 2D look-up tables to compute the aerodynamic coefficients and the tail rotor is modelled according to Hilbert [23]. To correctly capture the 3D effects of the main wing and provide a platform for the ailerons, a non-linear lifting line model is used, modified from Phillips and Snyder [39]. Compound thrust is defined as a force acting near the tail of the helicopter with a line of action through the fuselage CG. Fuselage drag was implemented by interpolating test data as described by Hilbert [23]. A controller was designed to achieve trimmed flight using the 'fly-to-trim' method. A sequence of P(I) controllers are used according to the time-scale-separation principle.

The model was built step by step and validated along the way. First, a conventional UH-60A model was compared with FLIGHTLAB. This was done for both trim and a rolling manoeuvre. A close match between the trim settings of both models was found flying at 120 kts. A slightly higher angle of attack over the rotor disk was noted for FLIGHTLAB, best seen over the retreating side of the disk. Also, a larger reversed flow area is noted. It is believed that the discrepancies in results are linked to the different version of the Peters-He inflow model and body aerodynamics model used by FLIGHTLAB. The rolling manoeuvre is compared, a good match for the roll rate is found during the initial response. As expected, the models do drift away eventually as differences in orientation grow over time. FLIGHTLAB does not feature a mechanical representation of the hub assembly with swashplate which might also explain discrepancies in roll response. The load quickness metric is introduced as the peak load divided by the peak roll angle encountered during the manoeuvre. This allows for a fair comparison of loads even when the flying manoeuvre is slightly different. Attitude quickness and load quickness show a good match between both models which gives confidence as these metrics are

crucial for the load alleviation experiments. The main wing lifting-line was validated against a vortex lattice method in AVL [32], showing a close match.

Study the feasibility of a structural load alleviation strategy by using the redundant control of a compound UH-60A Black Hawk helicopter to reduce loads in the main rotor hub during the executing of the break-turn manoeuvre and evaluate performance concerning load reduction and handling qualities.

The first experiment investigates the effect of different control strategies. The break-turn is modelled as a roll doublet reaching a bank angle of 60° in 2 seconds at 120 kts with advance ratio 0.28. The manoeuvre is initiated by either a pure lateral cyclic input, a pure aileron input or a 50% cyclic-50% aileron input. The attitude quickness is kept constant for all control strategies. Studying the rotor hub, the largest share of bending moments (M_x , M_y) are generated by the blade centrifugal forces which create a moment over the flap hinge offset as the blades flap up or down.

Using a pure lateral cyclic input on a counter-clockwise rotating rotor to roll right, the blade pitch is increased over the nose of the aircraft. At $\sim 90^\circ$ later, the blade reaches its maximum flap angle over the left side of the aircraft which allows the centrifugal force to create a moment over the flap hinge offset and roll the fuselage. The rotor tilts right and leads the roll while the fuselage follows. When the control strategy is changed to a pure aileron input, the fuselage will roll first and the rotor will lag because of its inertia. This causes an angle of attack between the blades and the blades' plane of rotation, similar to a cyclic input, instead, the entire fuselage is rolled with no input to the swashplate. Also similar to a cyclic input, the angle of attack is increased over the front and decreased over the rear of the disk. The $\sim 90^\circ$ lateral flapping phase shift again rolls the rotor. Measured in the body reference frame, the difference in lead or lag of the rotor during roll will invert the lateral flapping response and therefore also the lateral hub moment M_x . This effect can cleverly be used as combining the cyclic input with the ailerons will 'level out' the response of M_x . The lead or lag effect of the rotor disappears and it smoothly follows the fuselage's motion, alleviating the M_x loads. The M_x loading is reduced from > 7 times the trim loading for a pure cyclic or aileron control to a value of ~ 2 times the trim load for a 50% cyclic-50% aileron input. F_y is also reduced by the combined control strategy, effects on other loads are small compared to M_x and F_y .

A pure cyclic or pure aileron input is observed to have a high control saturation level to reach the 60° in 2 seconds. Although attitude quickness is kept constant during the experiment, the 50% lateral cyclic-50% aileron input would allow increasing roll quickness as more control power to create the rolling motion is available.

Study the effect of different trim settings on cruise performance and steady oscillatory loads as well as the impact on loads during the break-turn manoeuvre.

The second experiment varies the trim settings prior to the roll doublet, the manoeuvre is flown using a 50% cyclic - 50% aileron input. The effect of varying the elevator deflection, compound thrust, rotor rpm and constant aileron input at trim, are investigated separately.

If the horizontal stabiliser input is relaxed to generate less upwards lift, the fuselage will fly more nose-up and the angle of attack of the main wing is increased. The lift share of the main rotor decreases and the total power required drops with 3.9%. However, an increased longitudinal cyclic is required to tilt the rotor lift vector forward to sustain speed. This leads to larger longitudinal flapping and raises longitudinal hub moment M_y and load F_x , both for trimmed and rolling flight. Little effect on lateral flapping and therefore also the lateral hub moment M_x is noted during the doublet.

The compound thrust is set to 5000 N to counter the fuselage drag. Both the propulsive and lifting function of the main rotor are alleviated. The longitudinal rotor loading F_x and M_y are reduced as the compound thrust alleviates the longitudinal cyclic, rotor lift and torque are lower due to nose-up attitude which unloads the rotor. Little effect is seen on the lateral flapping throughout the doublet. Therefore, the reduction of lateral hub moment M_x is believed to be caused by coupling effects. Compound thrust is used to push rotorcraft performance, the main rotor power required is reduced but the total power required increases with 0.4%.

The rotor rpm is set to 80% of its nominal value. The fly-to-trim does not feature a mechanism to change the pitch angle to load the main wing and therefore, the collective setting is increased to maintain altitude. Centrifugal forces of the blades are lowered allowing the flap angles to increase. However, the lateral hub moment M_x at trim and during the doublet are decreased as it is believed the lower centrifugal forces have a bigger effect on the reduction of M_x compared to the small increase in flap angles. The power required is reduced by 24%.

A constant right aileron input at trim allows the lift generated over the advancing side to be pushed more

outboard, similar to the Advancing Blade Concept by Sikorsky [5]. The lift is generated over a disk region seeing a higher dynamic pressure, hence increasing the efficiency. The lateral cyclic required to counter the roll right moment by the ailerons tilts the rotor to the left and increases the flapping at trim. The entire flapping response during the doublet is therefore shifted leading to an increase in loads M_x . Due to the constant M_x and rotor orientation at trim, rolling left will see higher loads compared to a roll right. The power required is lowered by 4.3%.

A third experiment combines the two first ones and investigates using the different control strategies to roll the aircraft from a suboptimal trim condition defined as: 5000 N compound thrust, 80% of nominal rotor rpm and 3° right aileron at trim. The total power required is reduced by 31%. A pure lateral cyclic control strategy struggles to roll left as it fights the constant 3° aileron input. High blade pitch is required causing blade stall, the amplitude of the bending moments at the hub increase. The 50% cyclic - 50% aileron input strategy lowers the control saturation levels and avoids blades stall. Using the combined input, the lateral moment load M_x response 'levels out' around the non-zero M_x trim value due to the constant aileron input. The longitudinal hub moment M_y at trim is reduced as the longitudinal cyclic and rotor lift are offloaded.

To conclude, using the 50% lateral cyclic - 50% aileron input, instead of a pure cyclic or aileron input, levels out the lateral hub moment response and loads are decreased. Control power is increased and attitude quickness can potentially be raised using the combined input. The control saturation levels are decreased which lowers the risk of blade stall. The compound helicopter can offload the lifting and propulsive function of the main rotor to lower its power required at cruise. When the required longitudinal cyclic is offloaded, the longitudinal hub moment at trim is reduced. A constant aileron deflection will also reduce the power required but increase the lateral hub moment at trim.

7.1. Recommendations

The goal of this thesis was to investigate the rotor dynamics following different input strategies and trim settings during the execution of a roll doublet. The thesis links physical effects happening over the main rotor with the alleviation of loads. Recommendations for future research are divided into upgrades to the compound UH-60A model and the further development of the load alleviation strategy.

7.1.1. Compound Helicopter model

It has been found that a part of the blades is found in stall when executing the roll doublet. The current model does not feature a dynamic stall model. It would be interesting to see if the increased lift, abrupt stall and raise in drag typical for dynamic stall will influence the results.

The current model does not feature a lead-lag hinge. Implementing this hinge will affect loads in the main hub and more closely resemble the real UH-60A.

Blade twist was not adapted for the compound helicopter flying conditions. Slowed rotor operations at higher flying speeds ask for a different rotor blade twist which is a significant design variable.

Interaction effects between the main rotor and any other part of the helicopter are not modelled. Interactions unique to the compound helicopter type are the rotor wake effect on the main wing and rotor wake interactions with the compound thrust. The current study assumes the wake skew angle to be high enough so the rotor wake does not hit the wing when flying at 120 kts. This is not valid when the rotorcraft is slowed down. Interaction effects can be added in the future depending on the application.

7.1.2. Load Alleviation Strategy

The input strategy suggested in this thesis offers a proof of concept but can still be improved. The helicopter model and acquired knowledge on blade dynamics phenomena which lead to a reduction in loads can be used to design an optimal load alleviation strategy.

The research can be extended to the full break-turn MTE including the coordinated turn part. This will require an update of the control system to neatly fly the helicopter through this manoeuvre.

When the optimal load alleviation system is in place, a more detailed analysis can be done concerning the handling qualities. During this thesis, the loads were investigated while the handling qualities are kept constant. As already mentioned, there is a potential of improving the handling qualities when different control strategies are used. Requirements for handling qualities are stated by the ADS-33 [8] and include metrics like bandwidth. Also, failure conditions of the load alleviation system and the effect of different configurations like CG location can be checked.

The compound helicopter has the capabilities to slow down the main rotor, load the wing and push the airspeed above conventional helicopter capabilities. Loads are expected to grow with flying speed. It would be interesting to test the performance of the load alleviation strategy at higher speeds.

The thesis research investigates loading measured at the main rotor hub. High loads in the blade itself are also expected when aggressive manoeuvres are performed. Future studies can investigate loads over the blade structure. Blades are assumed to be rigid. When loads in the blades are measured, this assumption might need a careful review.

A

Reference Frames

The helicopter reference system is presented in Figure A.1. The body CG reference system is used to measure flight dynamic variables like attitude and angular rates. The aircraft reference system is used to construct the model. An arbitrary reference point is defined on the symmetry plane in front of the helicopter. Station line (SL), water line (WL) and but line (BL) are used to position all components in the multi-body dynamics environment. For the model used in this research, the CG lies at $SL_{CG} = -9.13m$, $WL_{CG} = -6.25m$ and $BL_{CG} = 0m$. The rotor system is defined by Figure A.2.

Longitudinal flapping is defined positive as the rotor flaps up over the nose. Lateral flapping is defined positive as the blade flaps up over the retreating side, tilting the disk right.

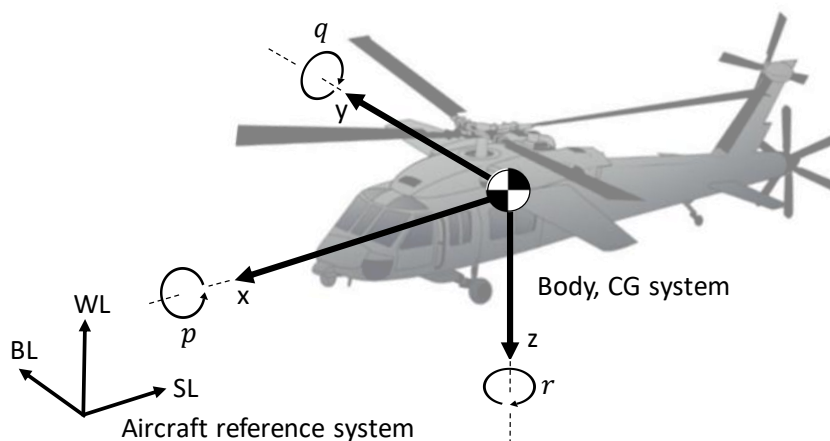


Figure A.1: Reference system, figure modified from [47]

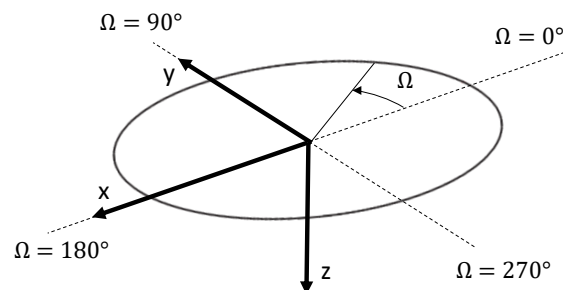


Figure A.2: Rotor axis system

B

Trim Validation Conventional UH-60A Model without Inflow Model

The situation over the rotor disk is compared between the constructed model and FLIGHTLAB for α , c_l , $c_l M^2$ and $c_d M^2$ at different flying speeds. Note that this validation is without inflow model implemented.

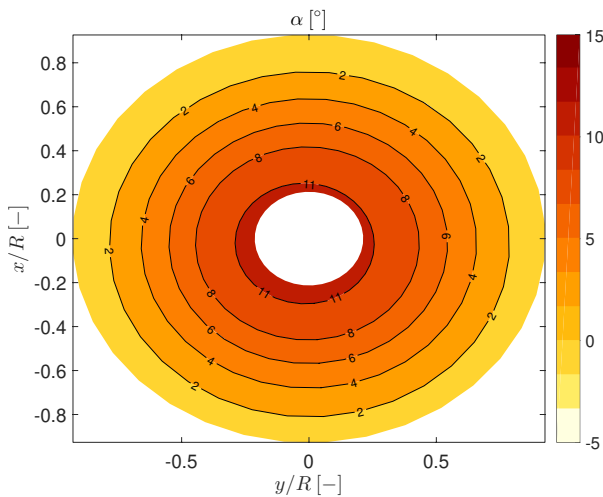


Figure B.1: α SimMechanics 0 kts

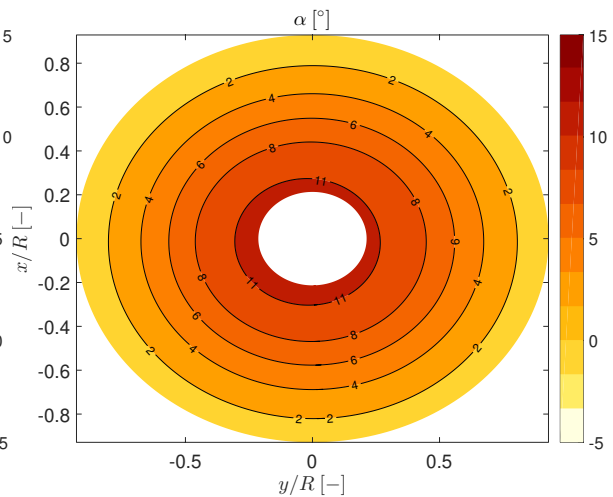
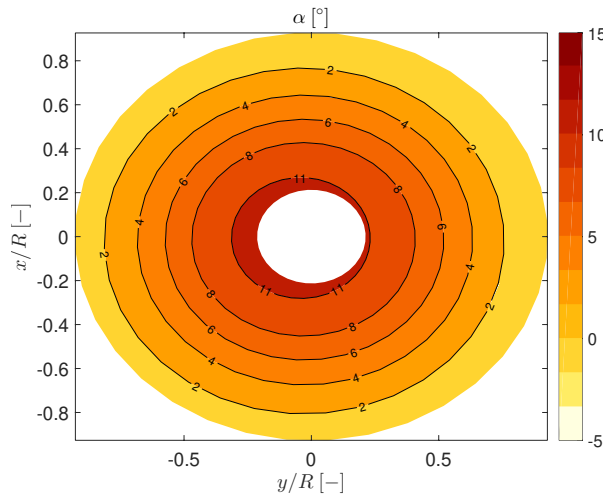
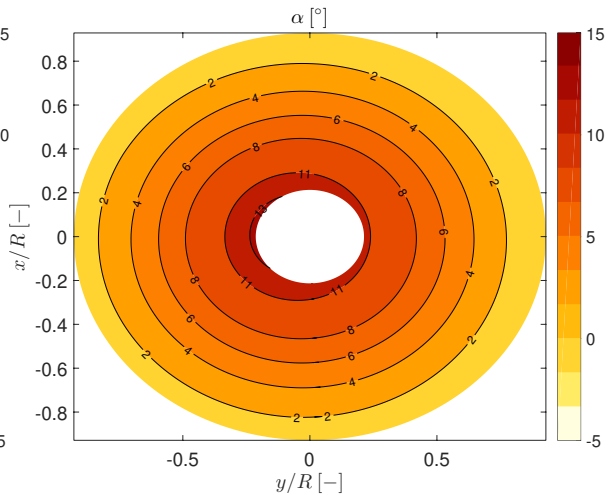
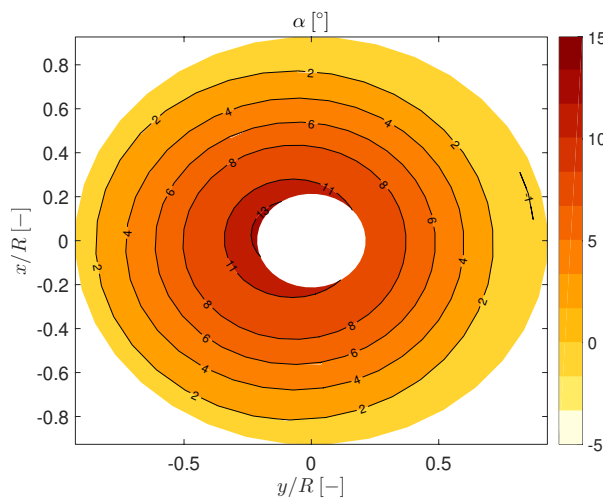
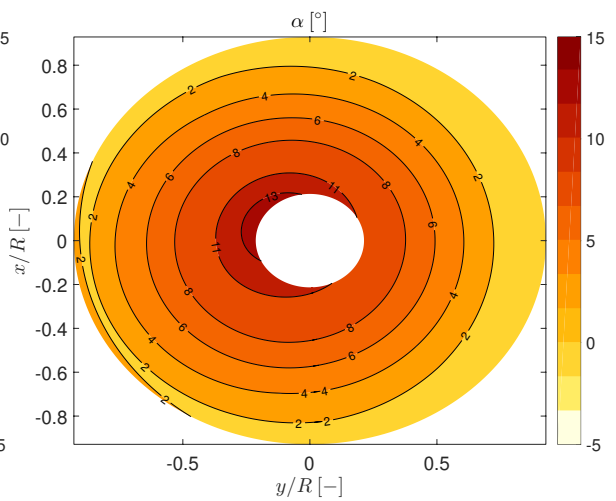
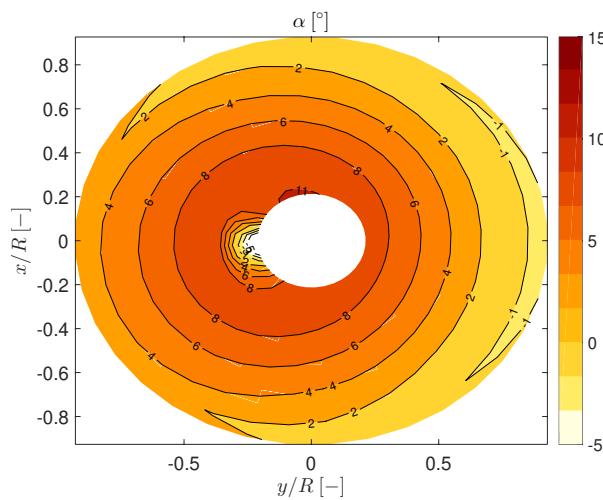
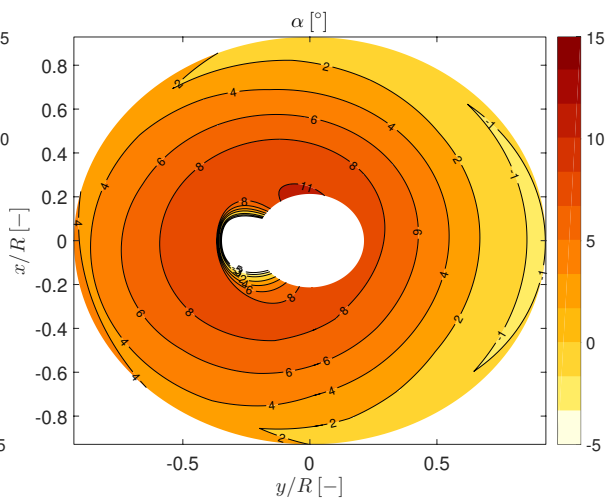
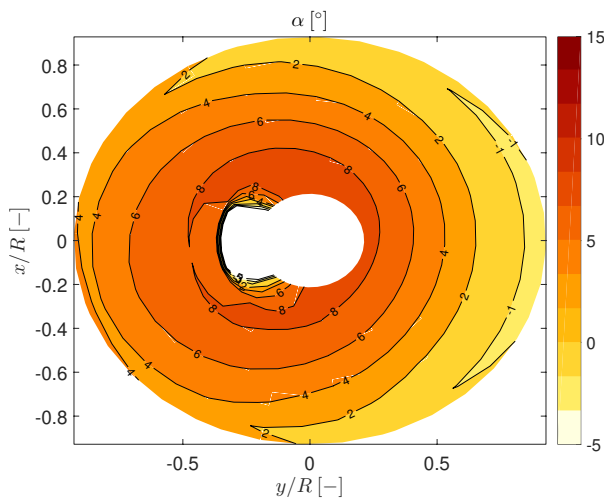
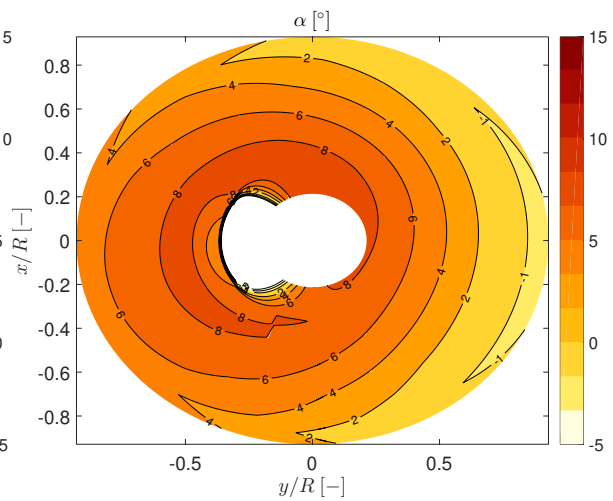
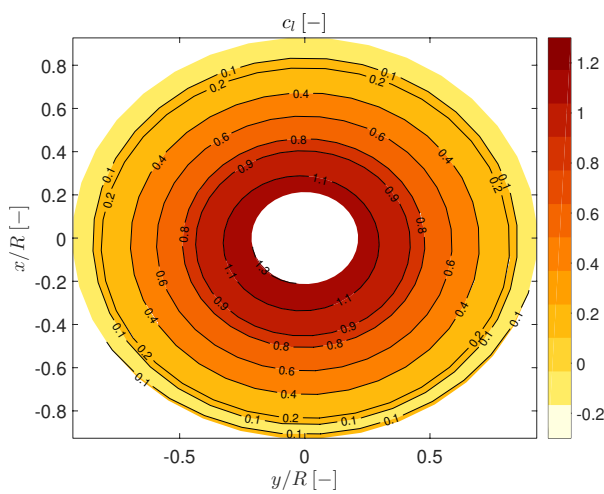
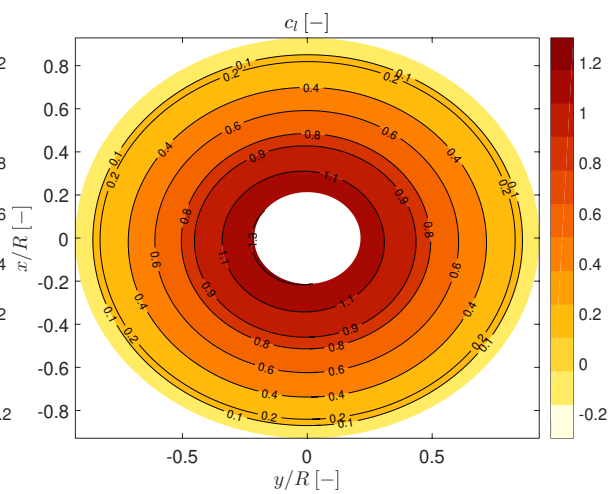
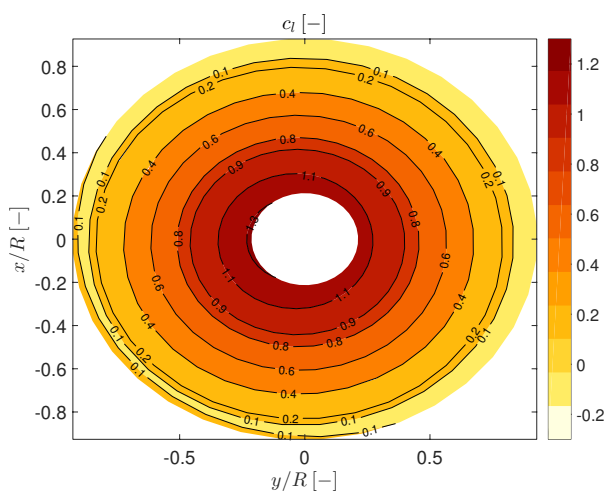
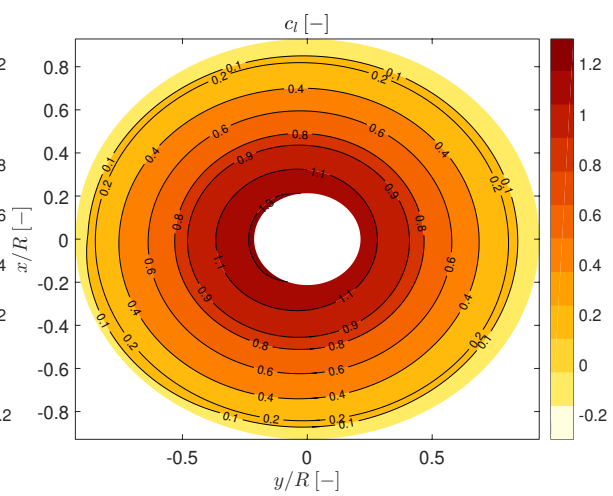
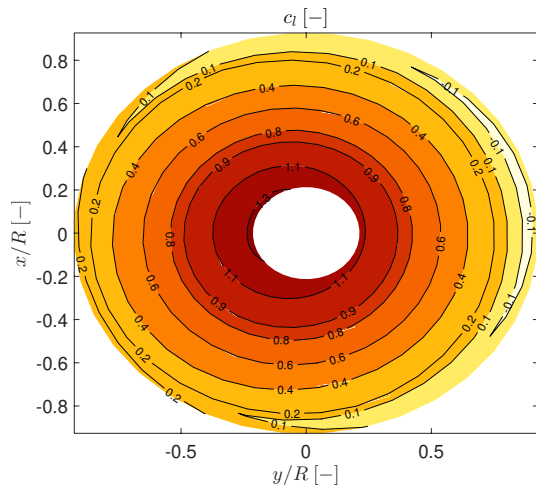
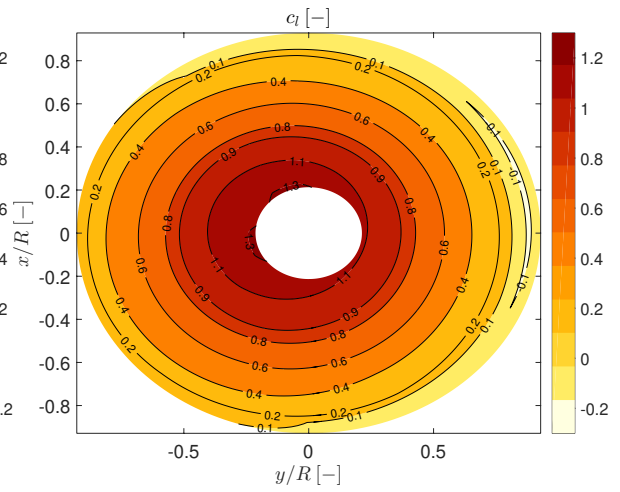
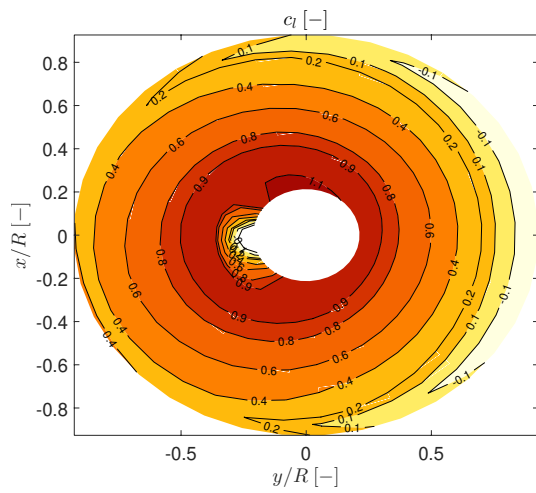
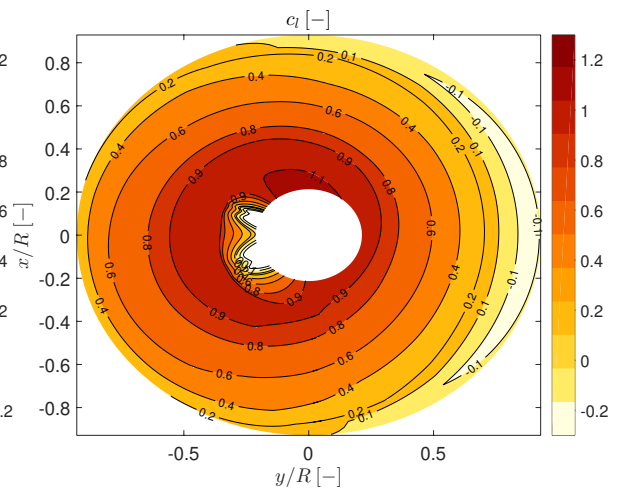
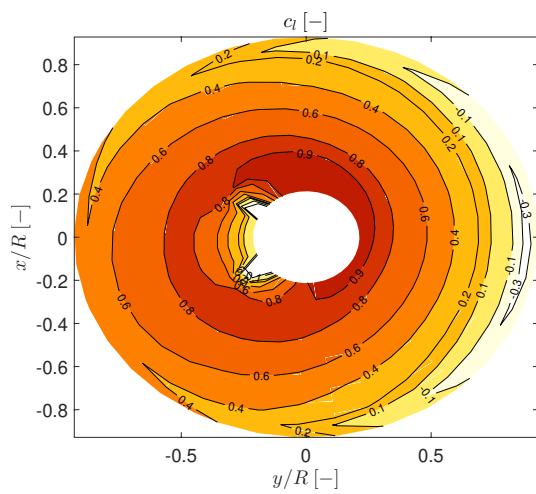
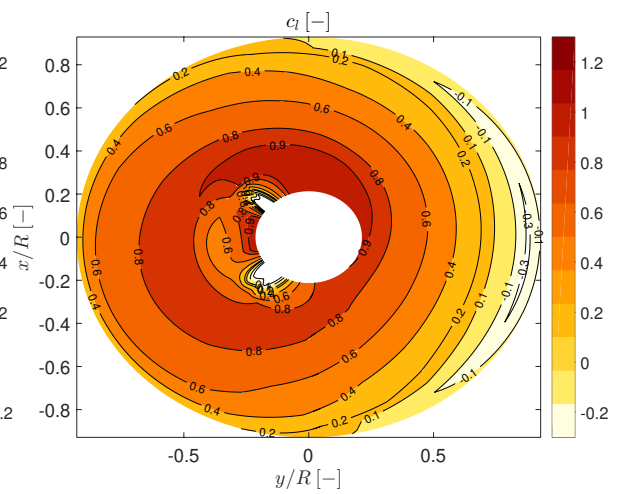
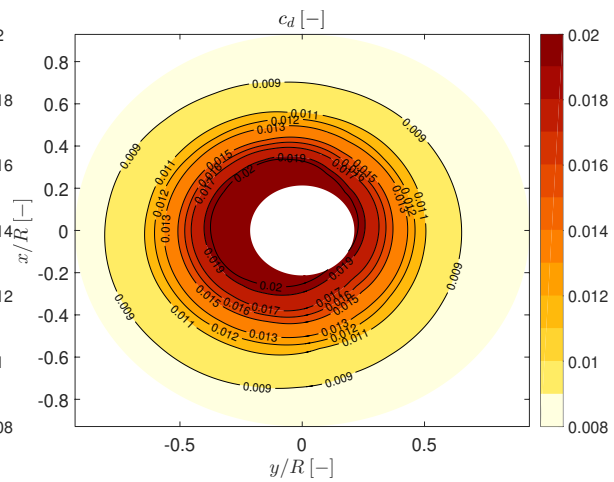
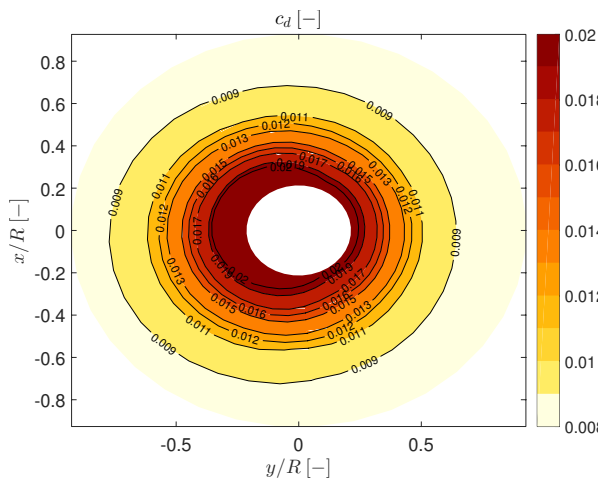
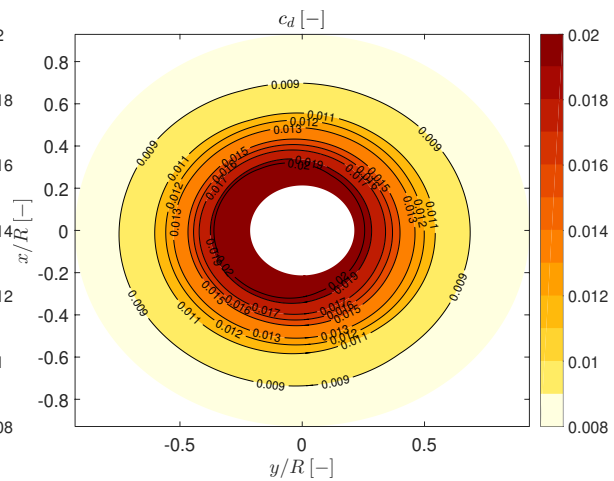
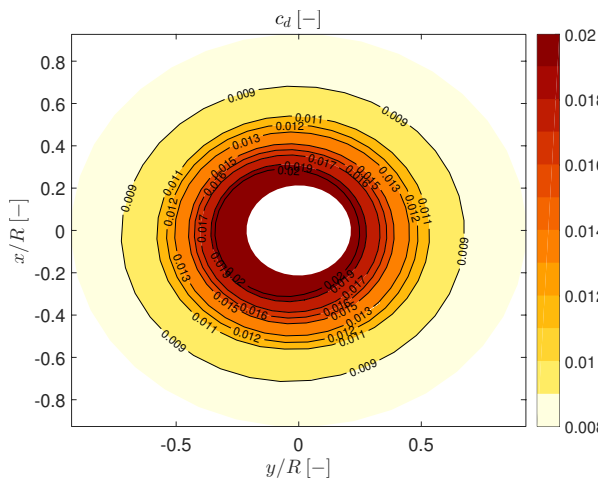
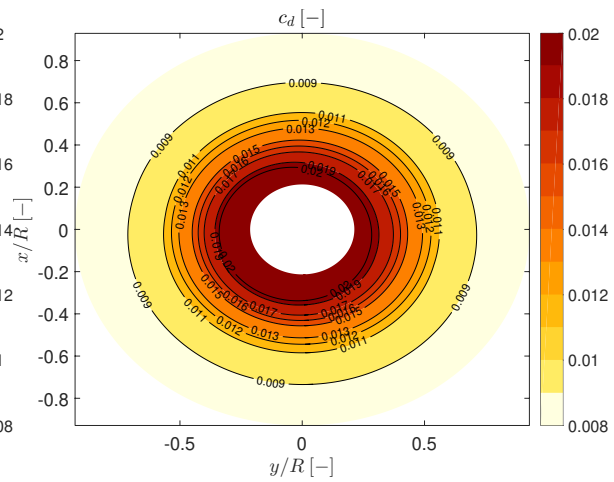
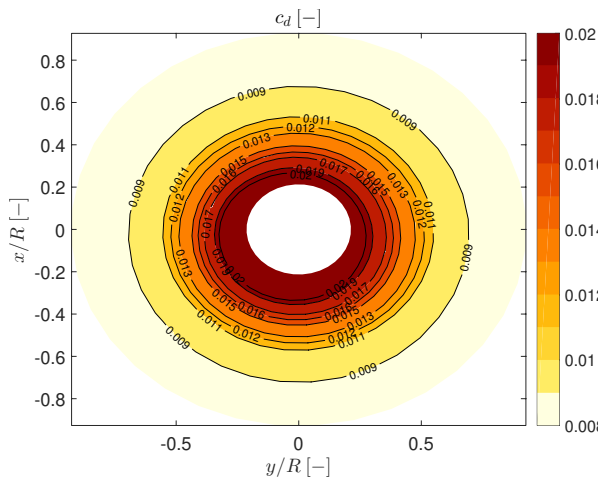


Figure B.2: α Flightlab 0 kts

Figure B.3: α SimMechanics 20 ktsFigure B.4: α Flightlab 20 ktsFigure B.5: α SimMechanics 50 ktsFigure B.6: α Flightlab 50 ktsFigure B.7: α SimMechanics 100 ktsFigure B.8: α Flightlab 100 kts

Figure B.9: α SimMechanics 120 ktsFigure B.10: α Flightlab 120 ktsFigure B.11: c_l SimMechanics 0 ktsFigure B.12: c_l Flightlab 0 ktsFigure B.13: c_l SimMechanics 20 ktsFigure B.14: c_l Flightlab 20 kts

Figure B.15: c_l SimMechanics 50 ktsFigure B.16: c_l Flightlab 50 ktsFigure B.17: c_l SimMechanics 100 ktsFigure B.18: c_l Flightlab 100 ktsFigure B.19: c_l SimMechanics 120 ktsFigure B.20: c_l Flightlab 120 kts



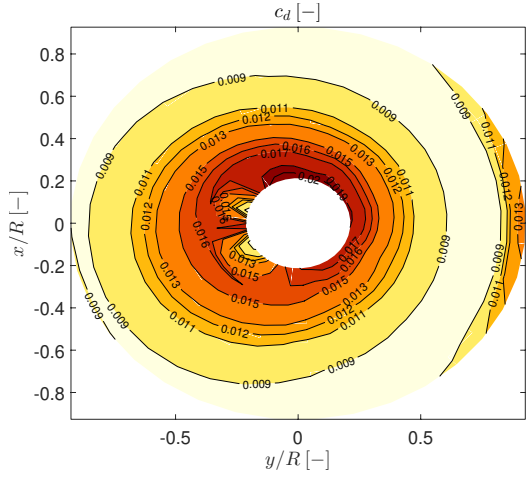


Figure B.27: c_d SimMechanics 100 kts

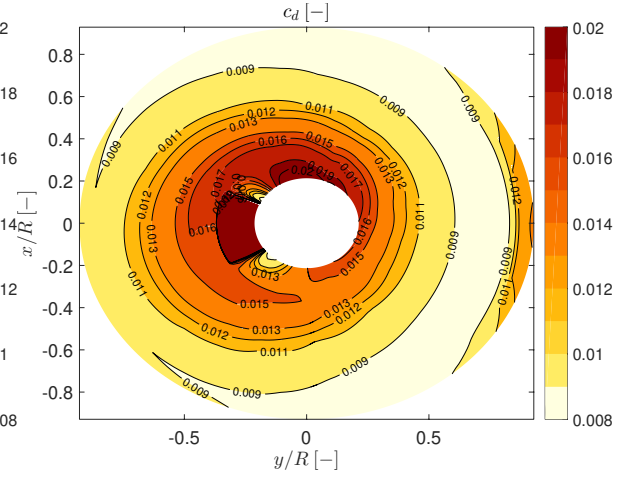


Figure B.28: c_d Flightlab 100 kts

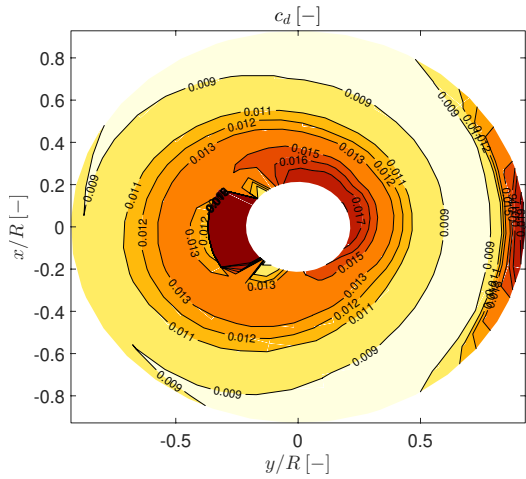


Figure B.29: c_d SimMechanics 120 kts

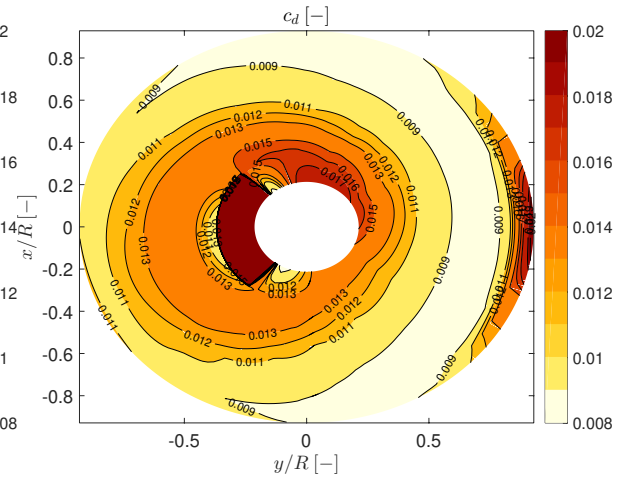


Figure B.30: c_d Flightlab 120 kts

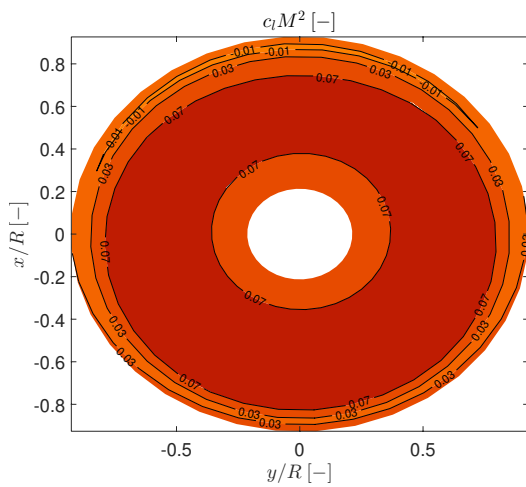


Figure B.31: $c_l M^2$ SimMechanics 0 kts

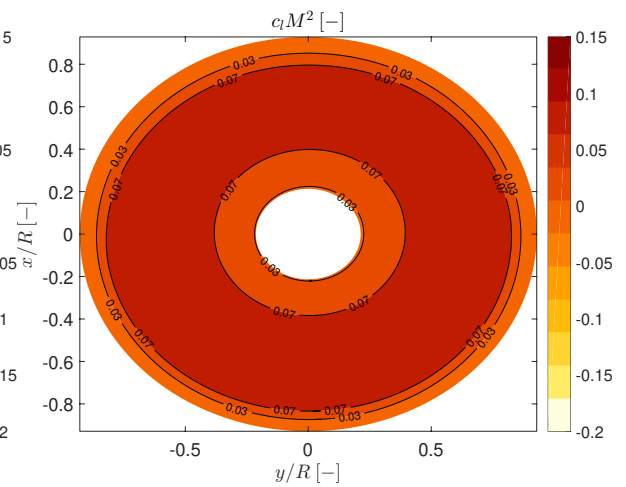
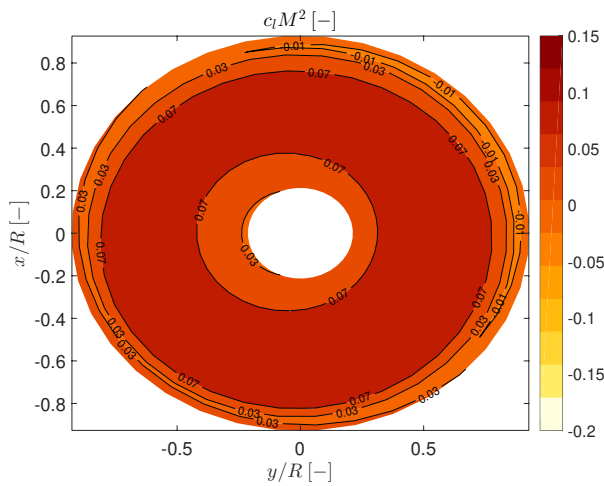
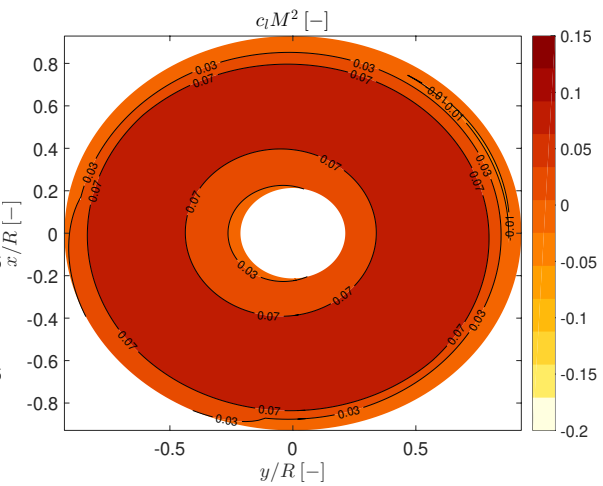
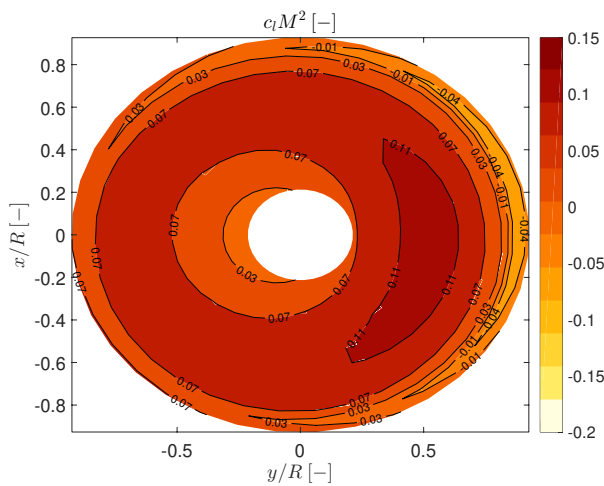
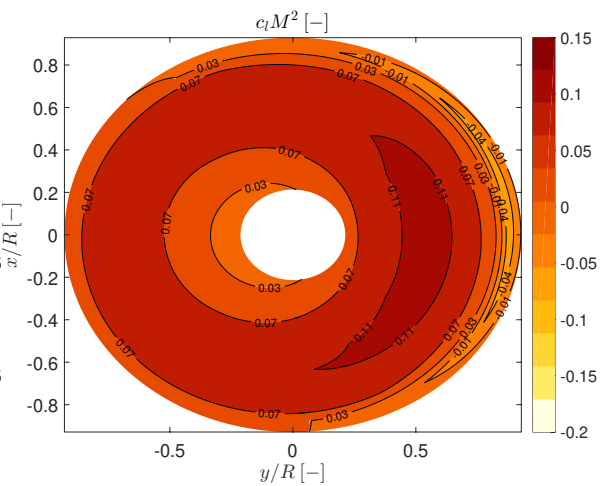
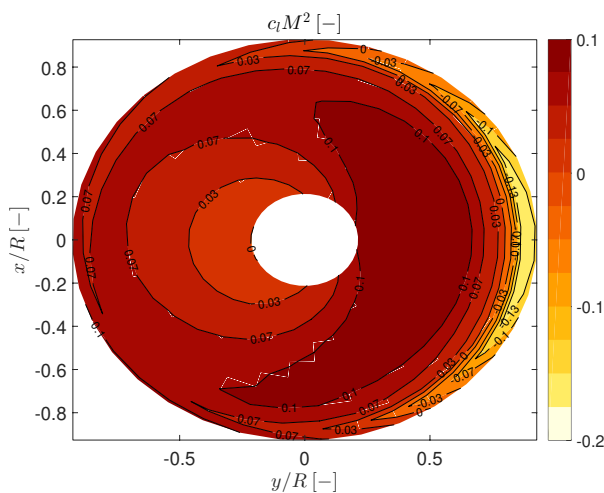
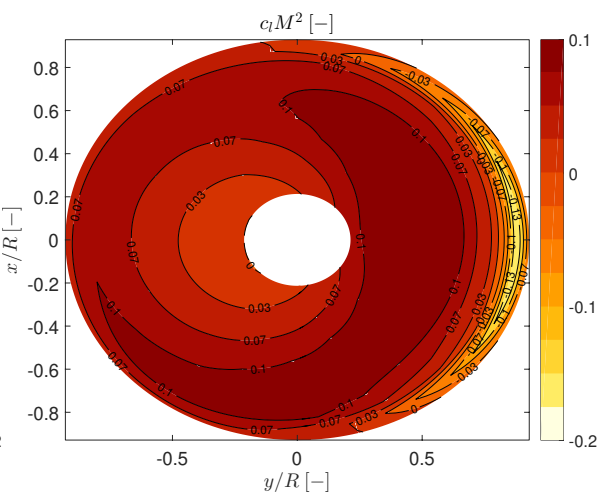
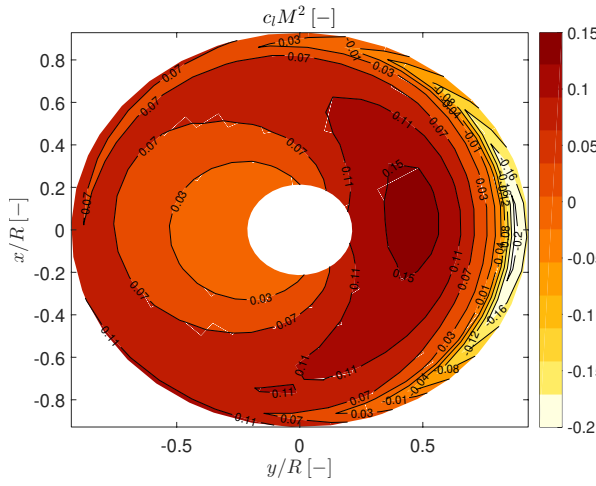
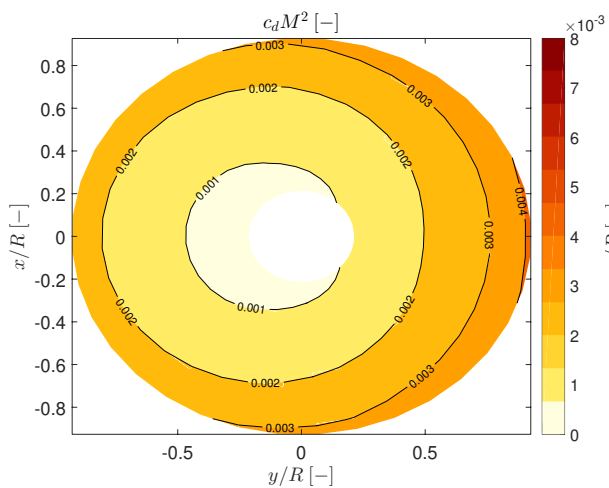
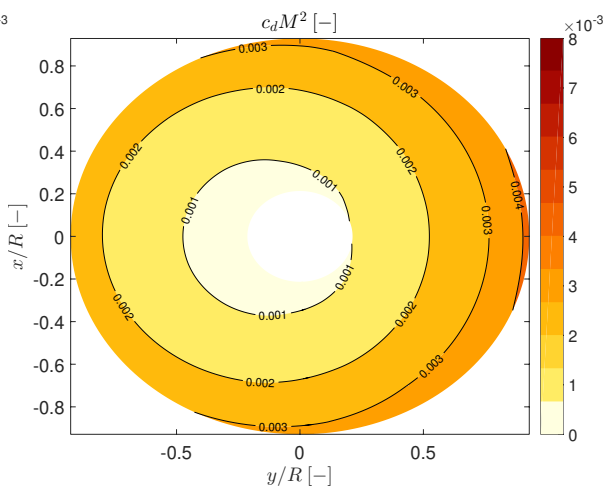
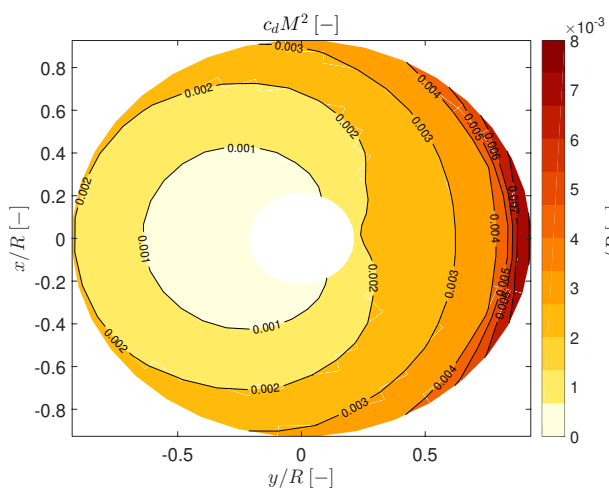
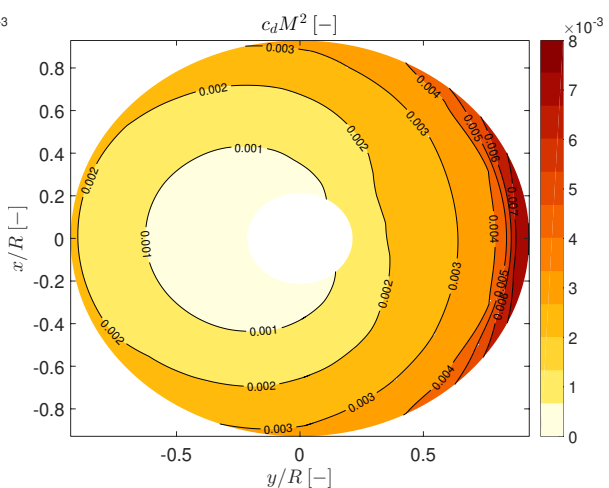
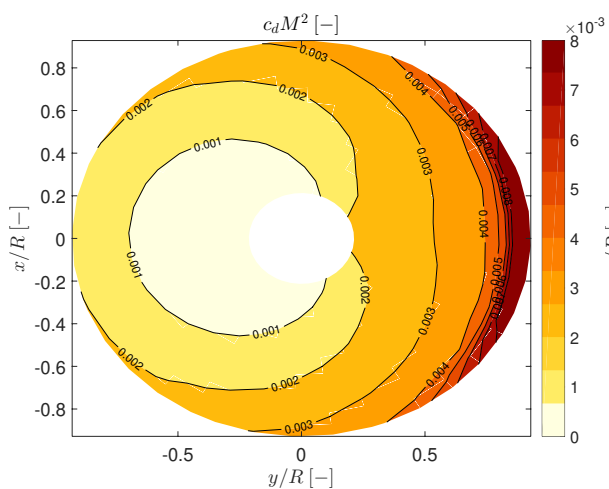
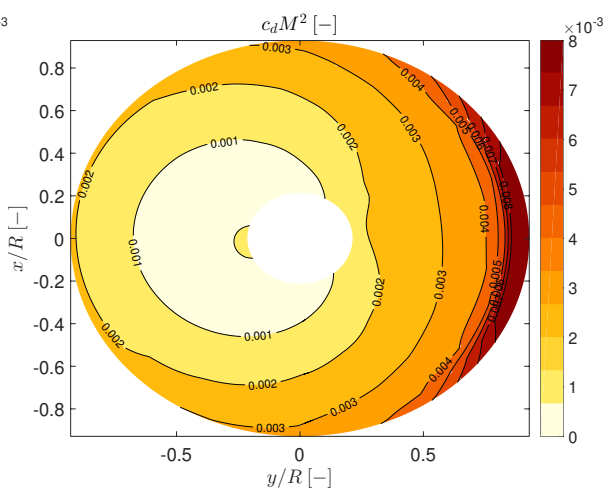


Figure B.32: $c_l M^2$ Flightlab 0 kts

Figure B.33: $c_l M^2$ SimMechanics 20 ktsFigure B.34: $c_l M^2$ Flightlab 20 ktsFigure B.35: $c_l M^2$ SimMechanics 50 ktsFigure B.36: $c_l M^2$ Flightlab 50 ktsFigure B.37: $c_l M^2$ SimMechanics 100 ktsFigure B.38: $c_l M^2$ Flightlab 100 kts



Figure B.45: $c_d M^2$ SimMechanics 50 ktsFigure B.46: $c_d M^2$ Flightlab 50 ktsFigure B.47: $c_d M^2$ SimMechanics 100 ktsFigure B.48: $c_d M^2$ Flightlab 100 ktsFigure B.49: $c_d M^2$ SimMechanics 120 ktsFigure B.50: $c_d M^2$ Flightlab 120 kts

C

Trim Validation Conventional UH-60A Model with Peters-He Inflow Model

The situation over the rotor disk is compared between the constructed model and FLIGHTLAB for α , c_l , c_d , $c_l M^2$, $c_d M^2$ and v_i at different flying speeds. Note that this validation is with the Peters-He inflow model implemented.

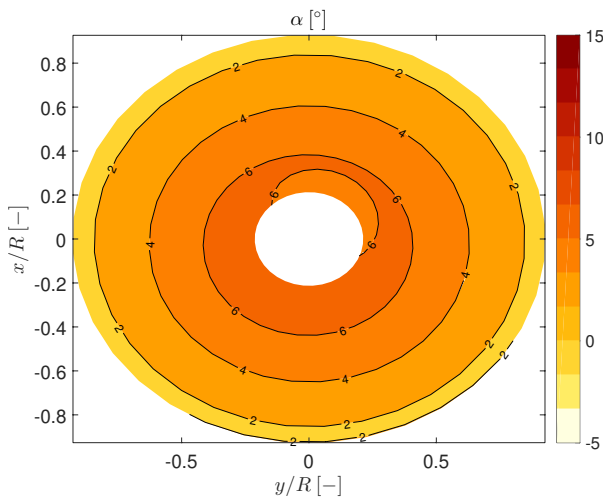


Figure C.1: α SimMechanics 0 kts

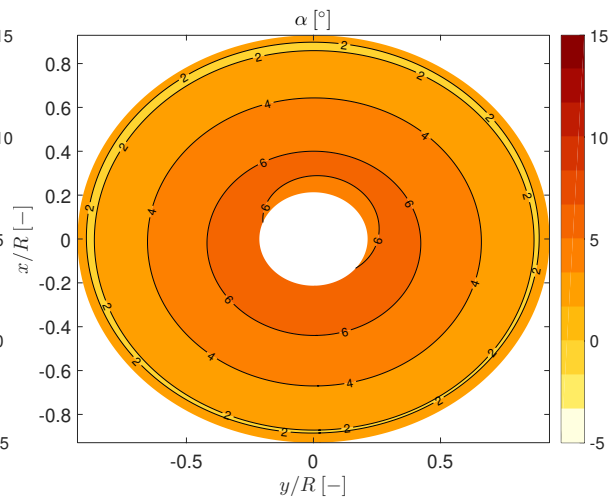


Figure C.2: α Flightlab 0 kts

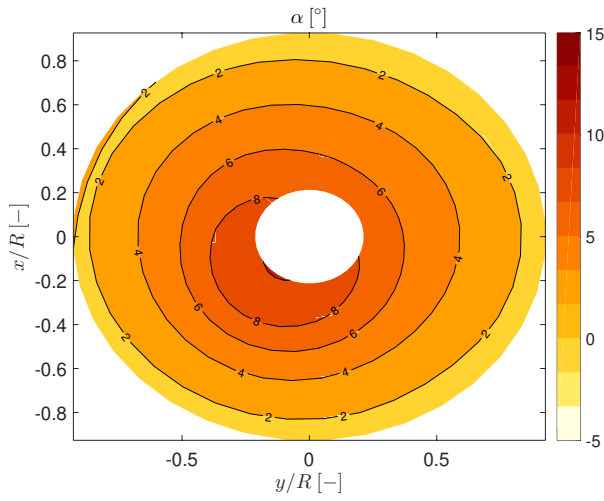


Figure C.3: α SimMechanics 20 kts

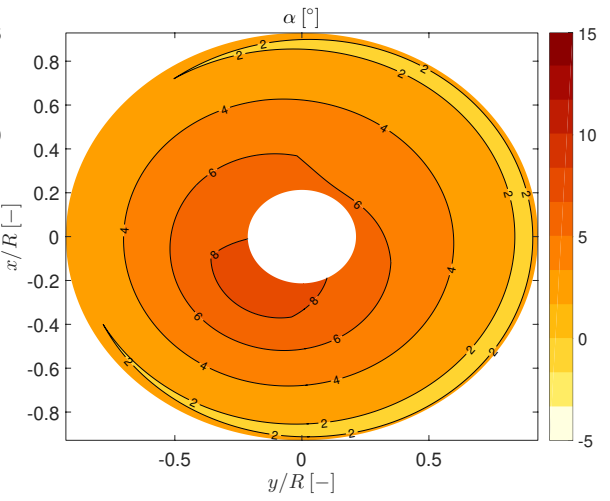


Figure C.4: α Flightlab 20 kts

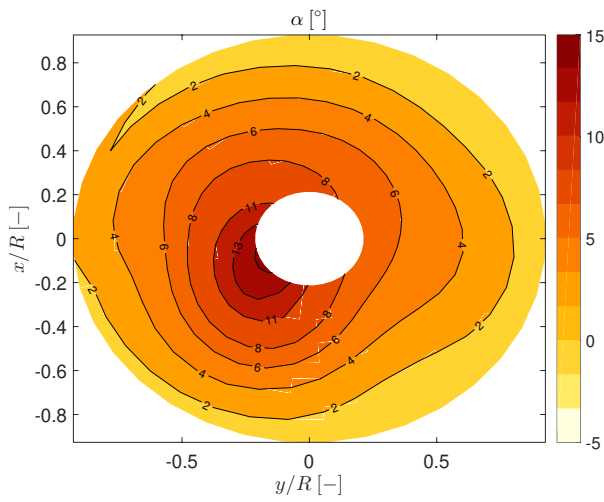


Figure C.5: α SimMechanics 50 kts

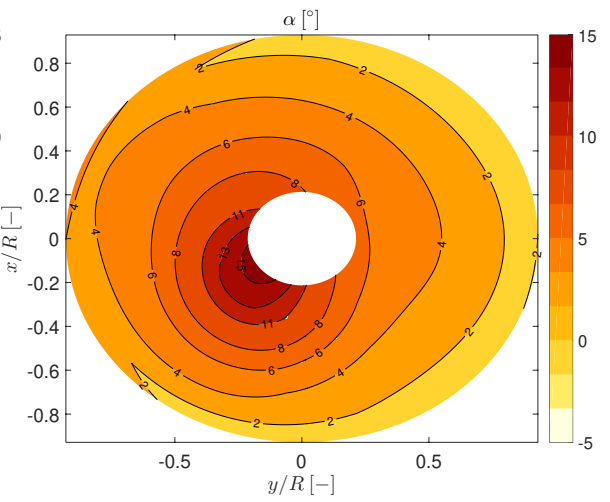


Figure C.6: α Flightlab 50 kts

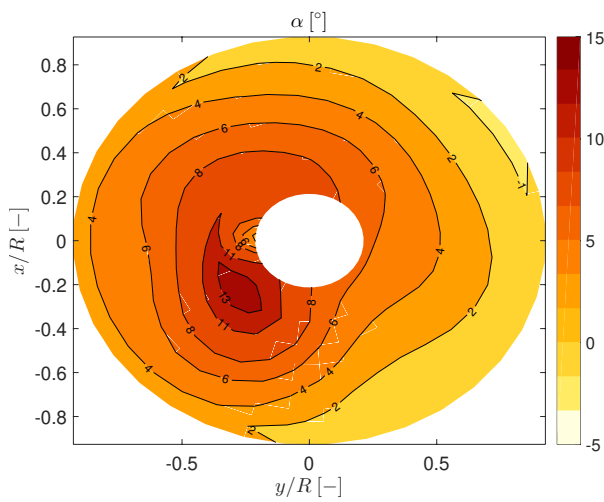


Figure C.7: α SimMechanics 100 kts

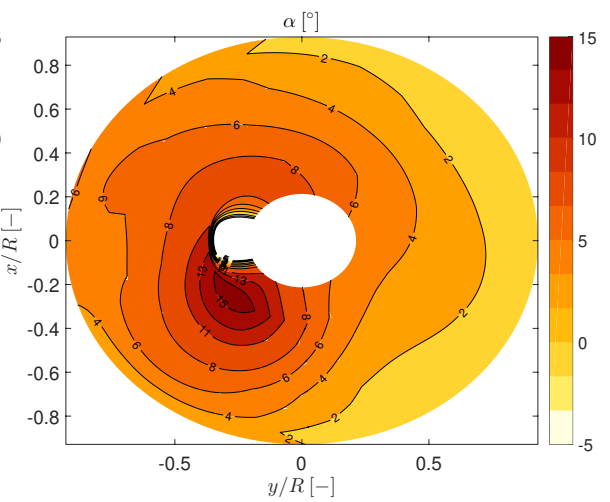


Figure C.8: α Flightlab 100 kts

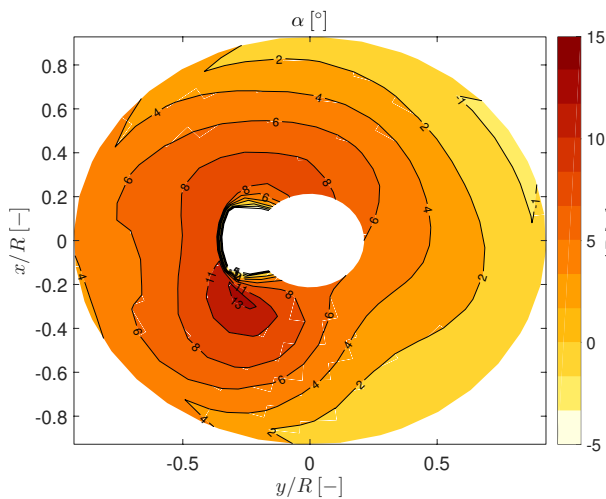


Figure C.9: α SimMechanics 120 kts

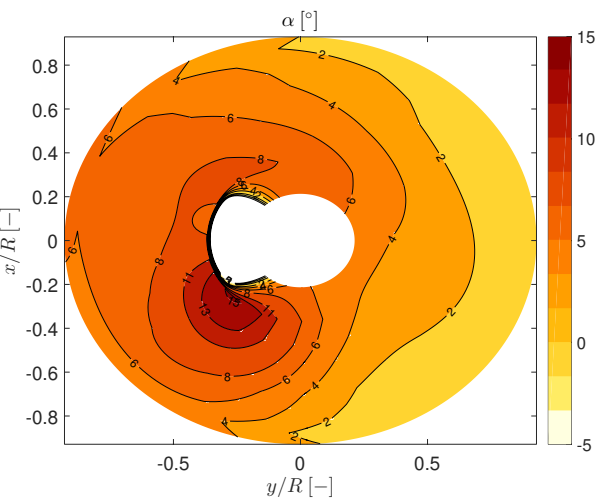


Figure C.10: α Flightlab 120 kts

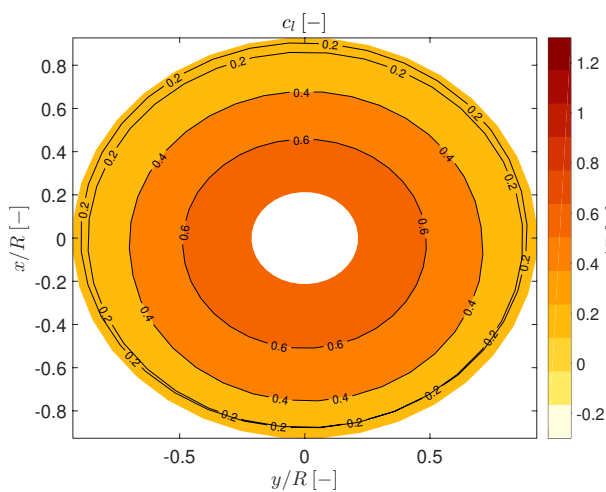


Figure C.11: c_l SimMechanics 0 kts

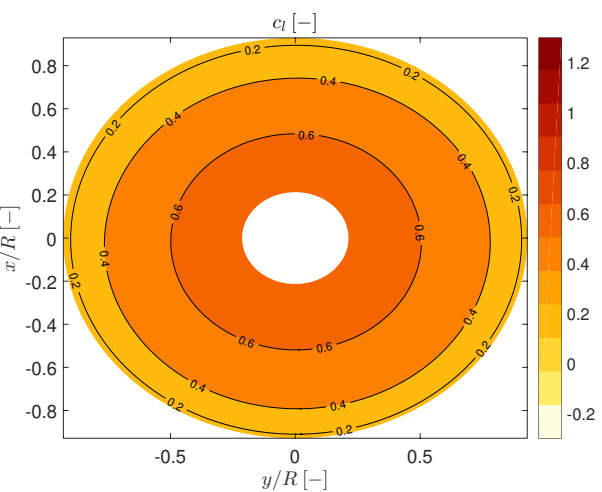


Figure C.12: c_l Flightlab 0 kts

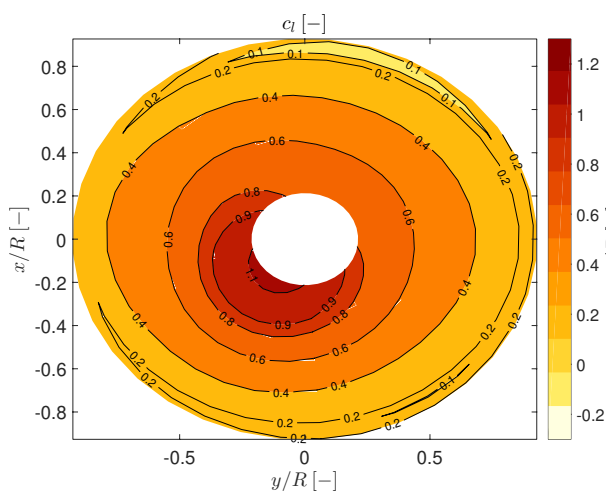


Figure C.13: c_l SimMechanics 20 kts

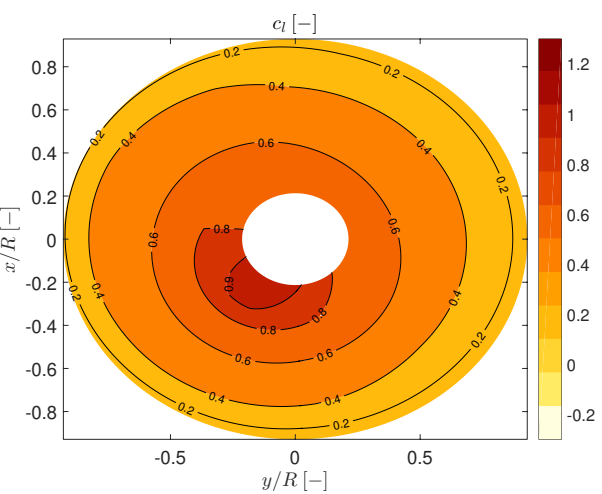


Figure C.14: c_l Flightlab 20 kts

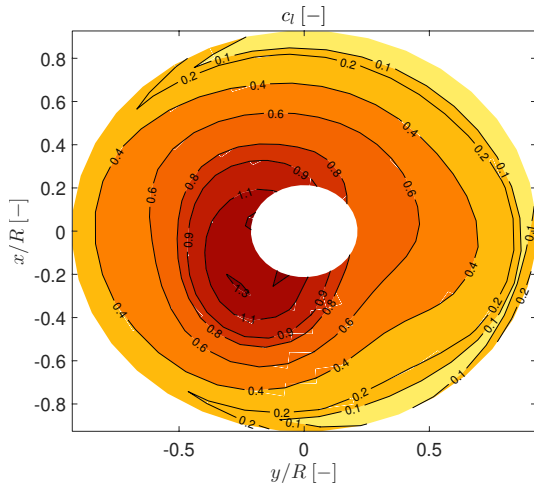


Figure C.15: c_l SimMechanics 50 kts

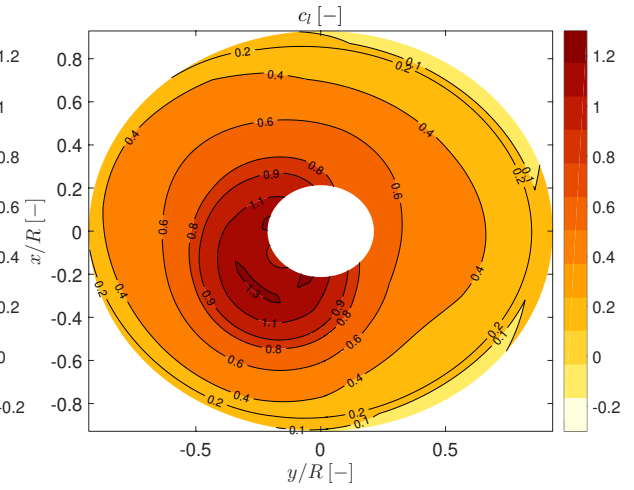


Figure C.16: c_l Flightlab 50 kts

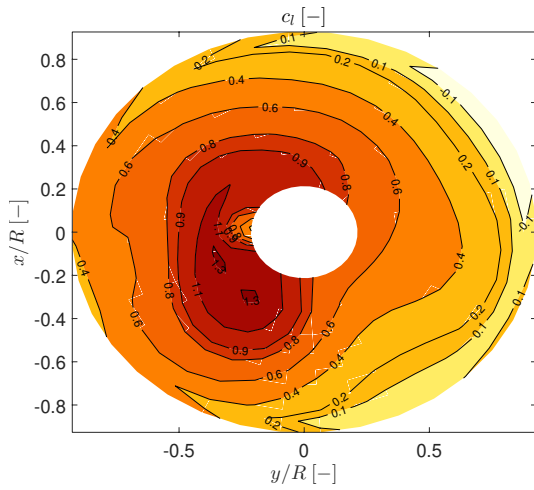


Figure C.17: c_l SimMechanics 100 kts

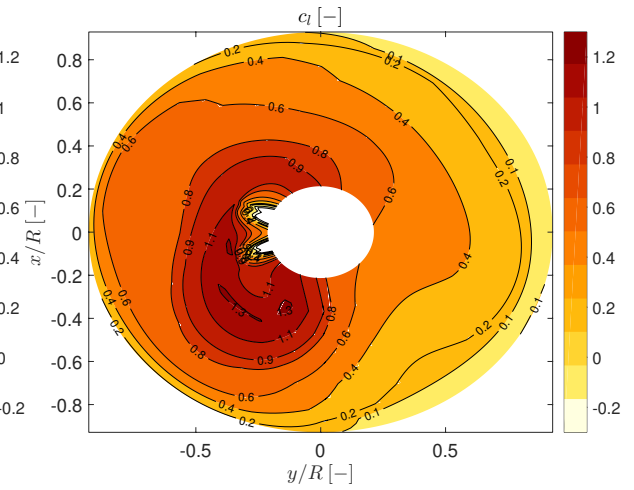


Figure C.18: c_l Flightlab 100 kts

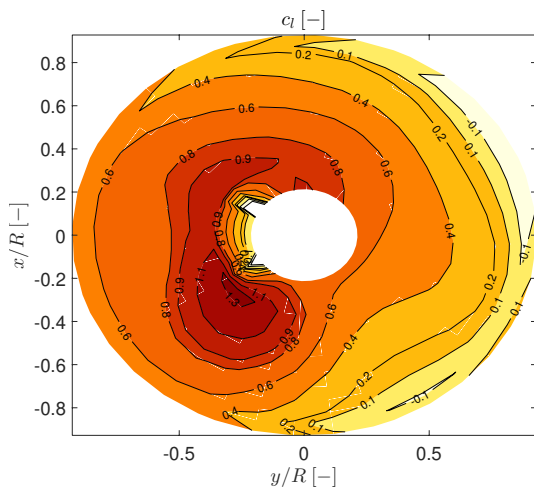


Figure C.19: c_l SimMechanics 120 kts

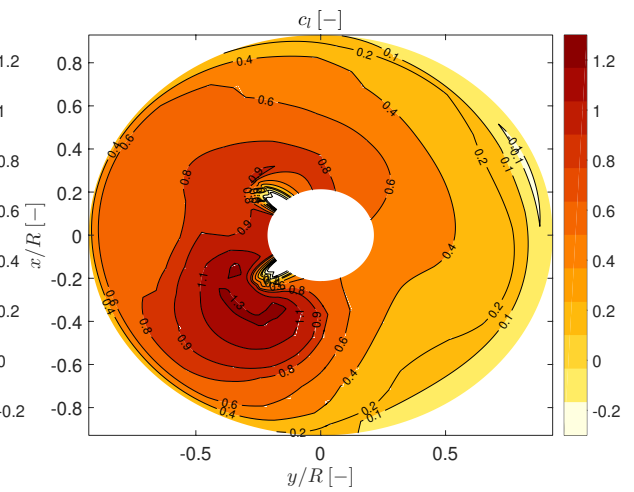
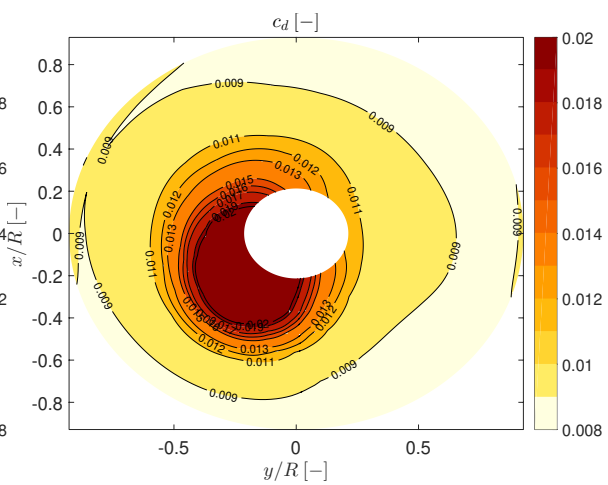
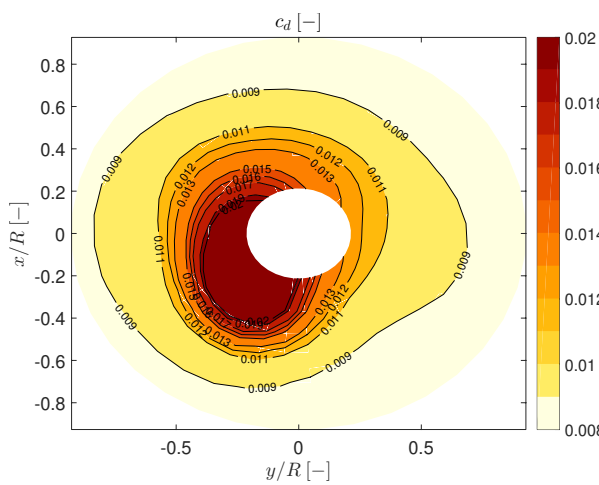
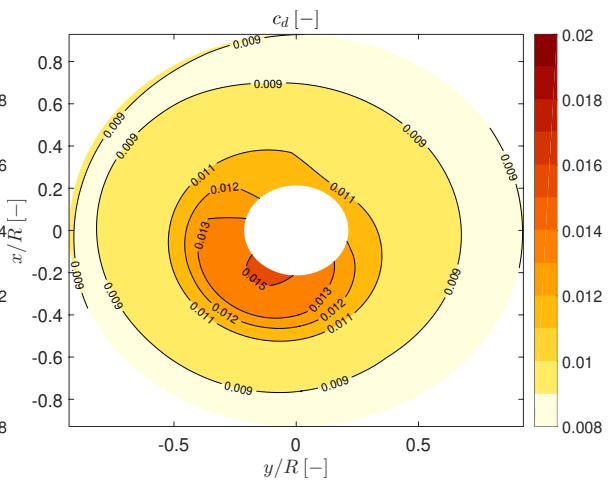
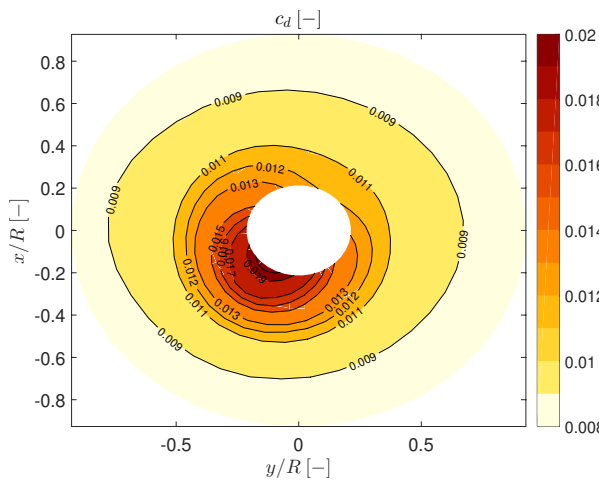
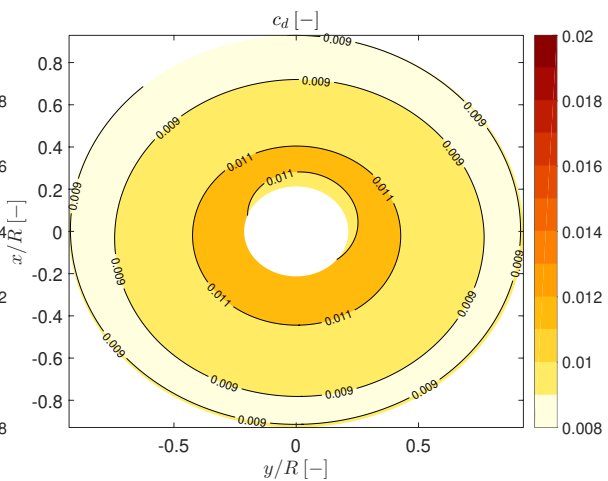
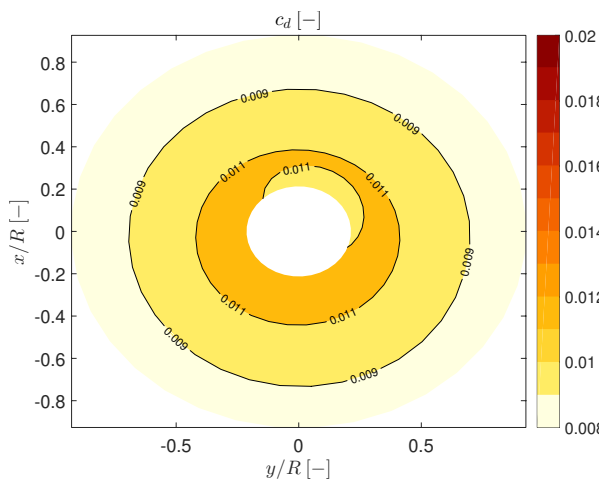


Figure C.20: c_l Flightlab 120 kts



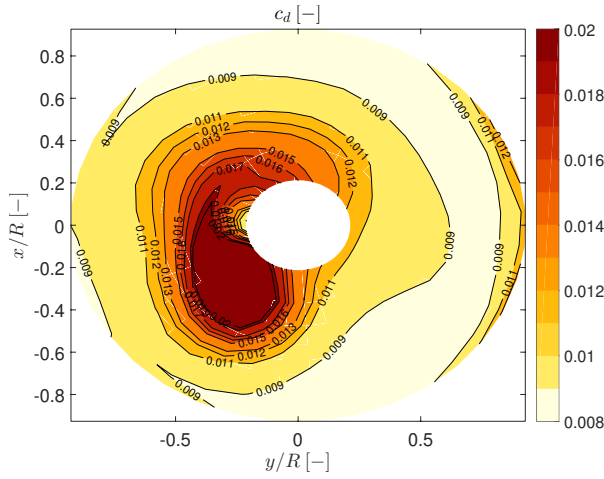
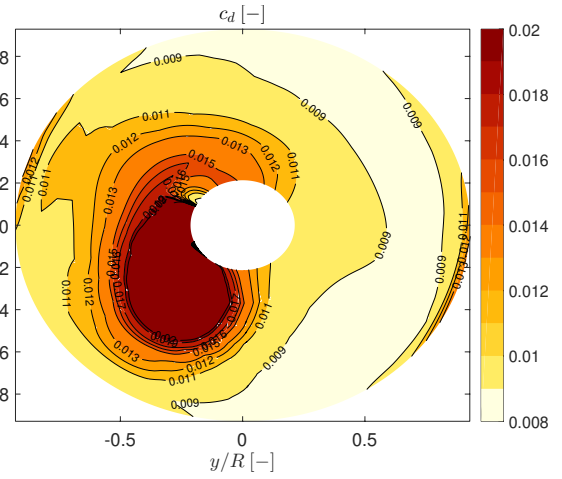


Figure C.27: c_d SimMechanics 100 kts



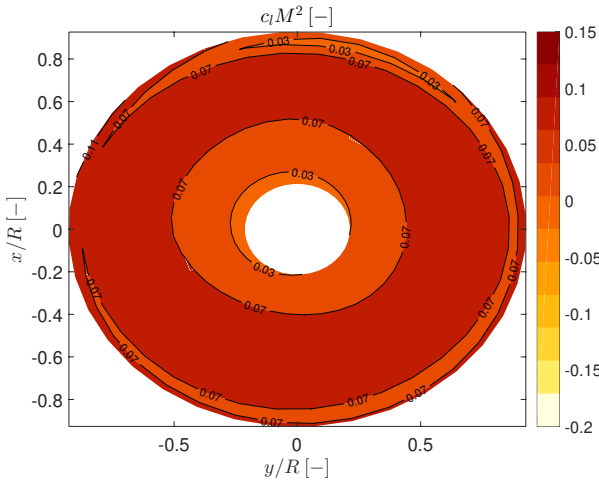


Figure C.33: $c_l M^2$ SimMechanics 20 kts

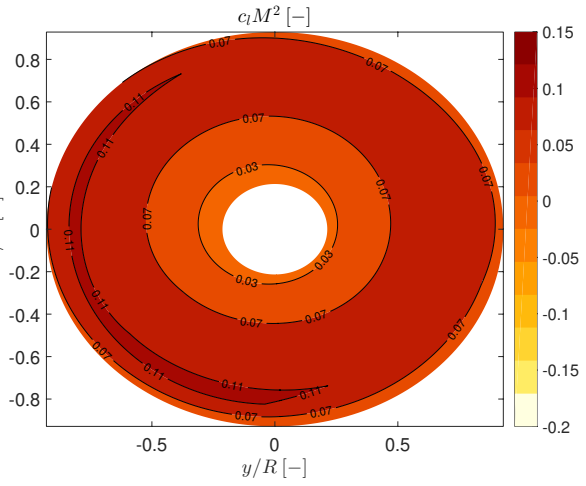


Figure C.34: $c_l M^2$ Flightlab 20 kts

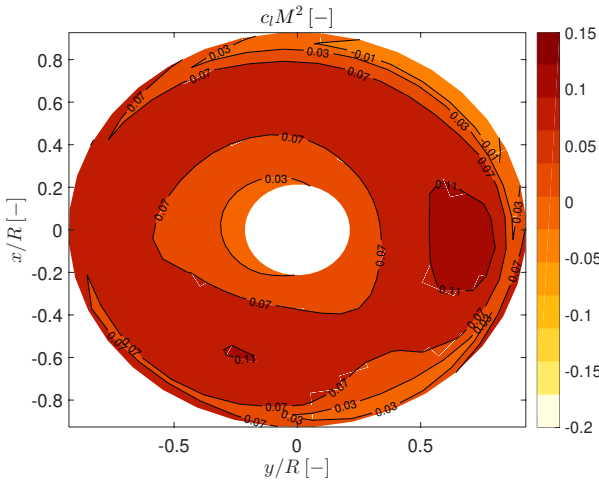


Figure C.35: $c_l M^2$ SimMechanics 50 kts

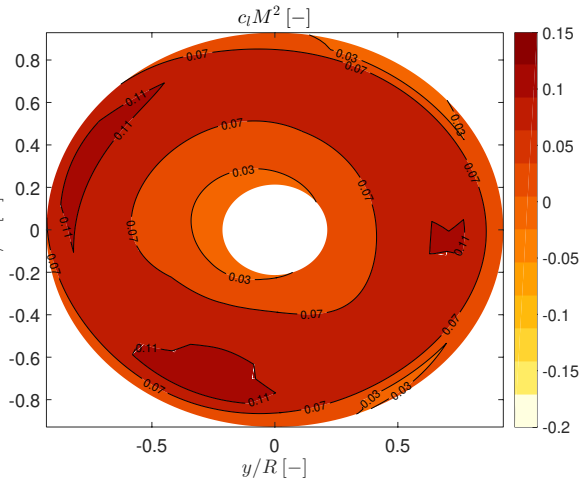


Figure C.36: $c_l M^2$ Flightlab 50 kts

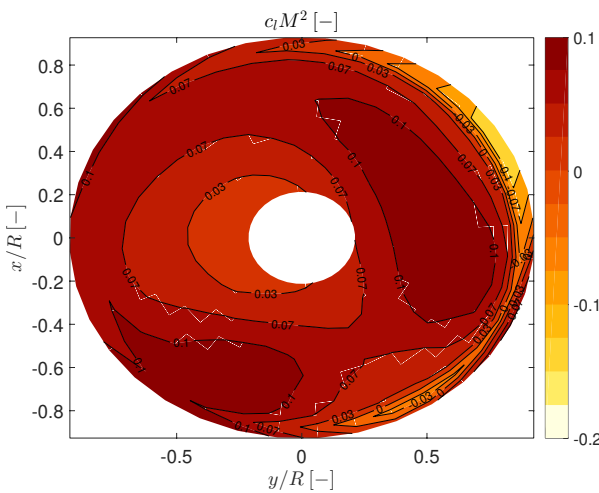


Figure C.37: $c_l M^2$ SimMechanics 100 kts

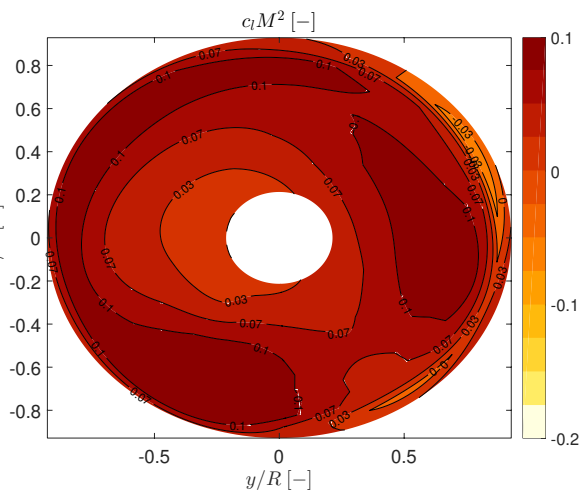


Figure C.38: $c_l M^2$ Flightlab 100 kts

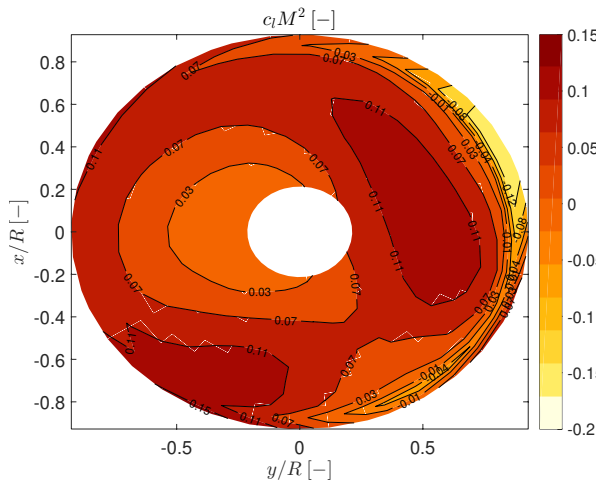


Figure C.39: $c_l M^2$ SimMechanics 120 kts

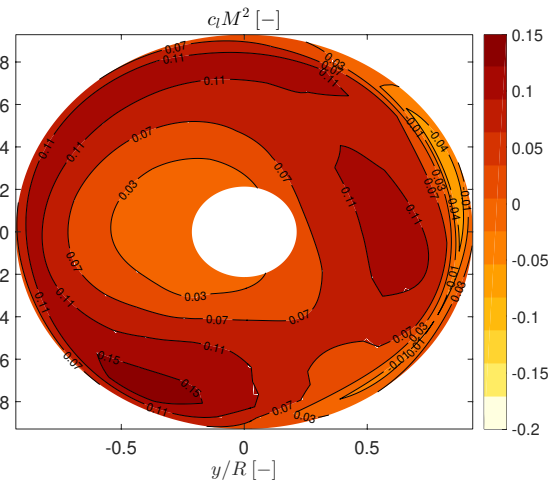


Figure C.40: $c_l M^2$ Flightlab 120 kts

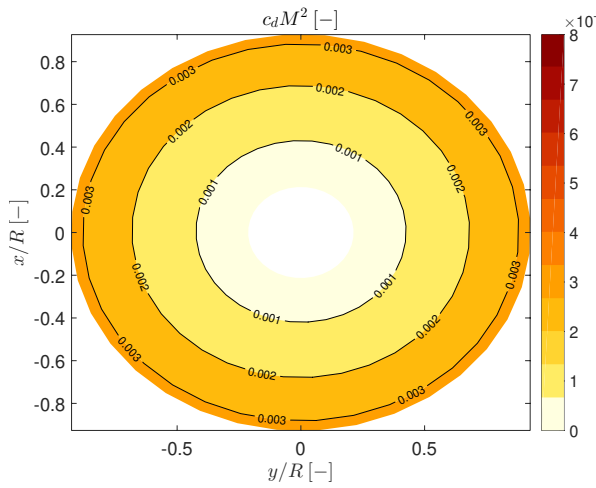


Figure C.41: $c_d M^2$ SimMechanics 0 kts

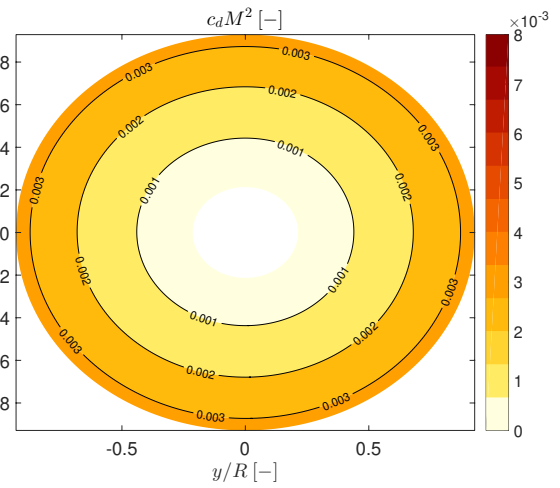


Figure C.42: $c_d M^2$ Flightlab 0 kts

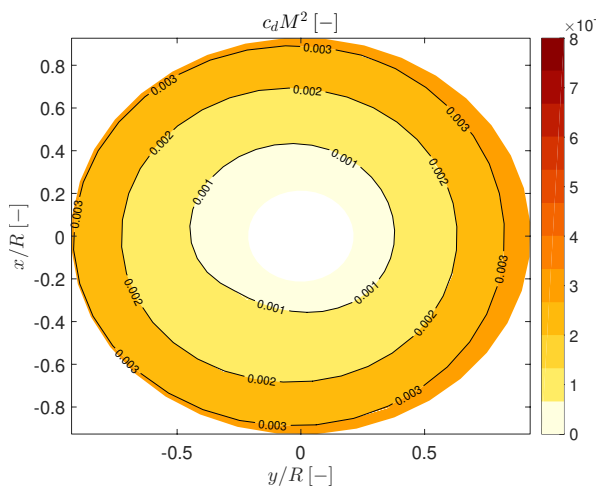


Figure C.43: $c_d M^2$ SimMechanics 20 kts

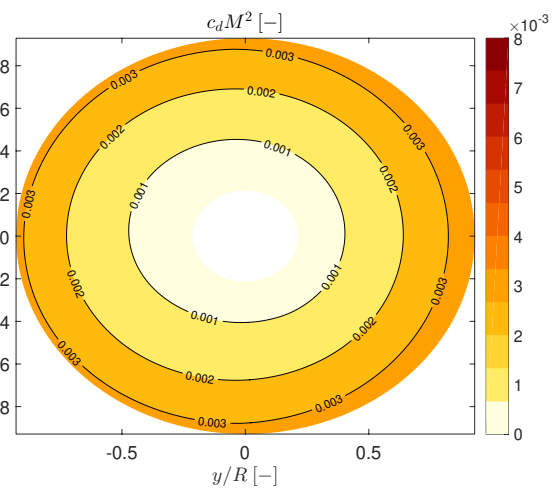


Figure C.44: $c_d M^2$ Flightlab 20 kts

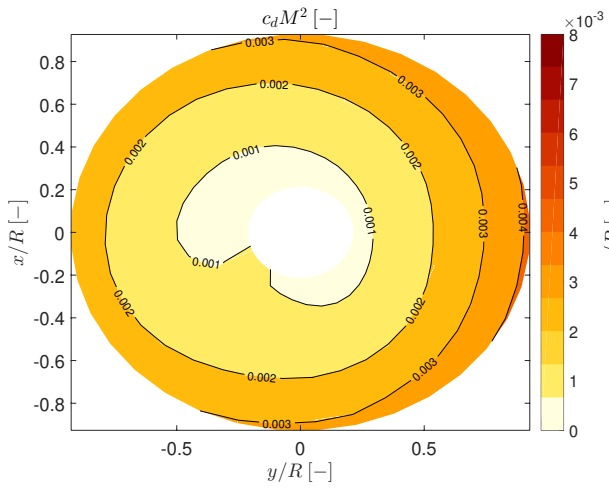


Figure C.45: $c_d M^2$ SimMechanics 50 kts

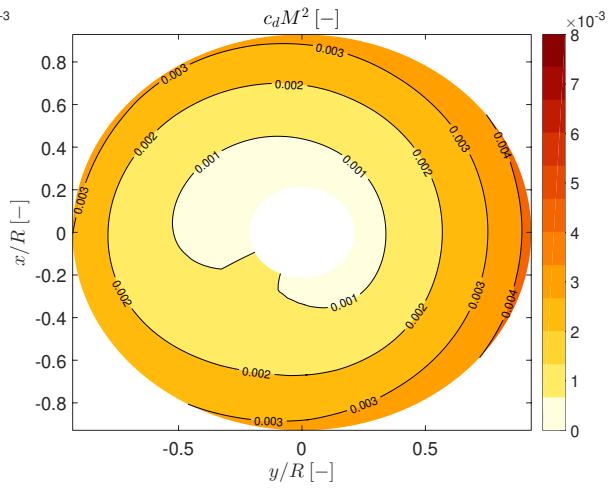


Figure C.46: $c_d M^2$ Flightlab 50 kts

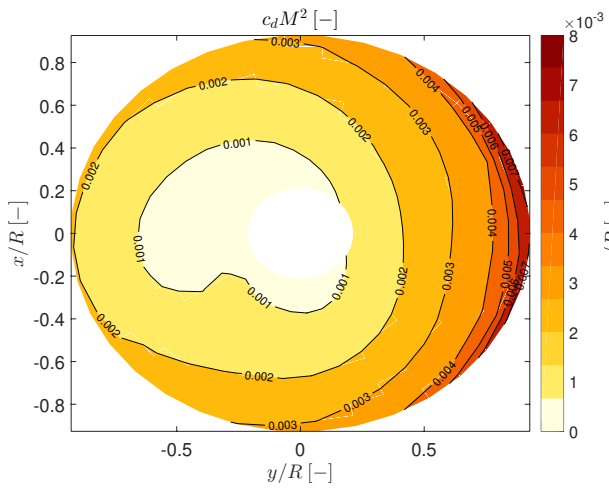


Figure C.47: $c_d M^2$ SimMechanics 100 kts

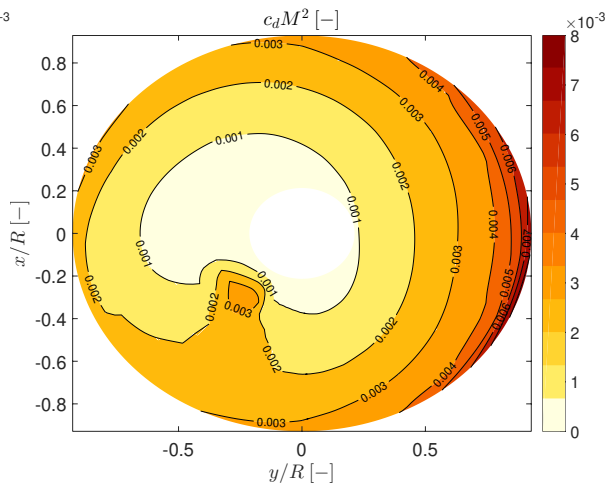


Figure C.48: $c_d M^2$ Flightlab 100 kts

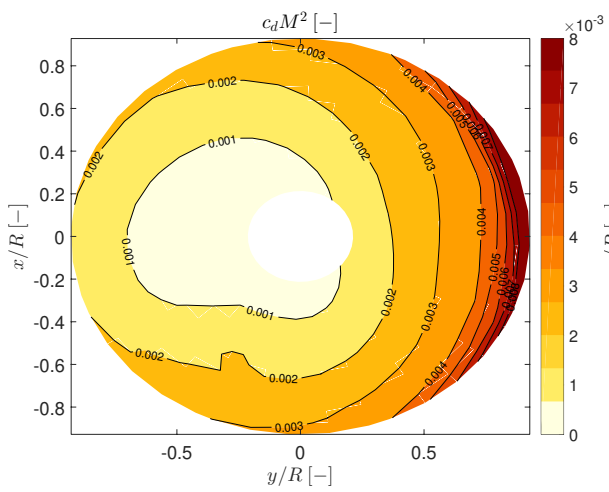


Figure C.49: $c_d M^2$ SimMechanics 120 kts

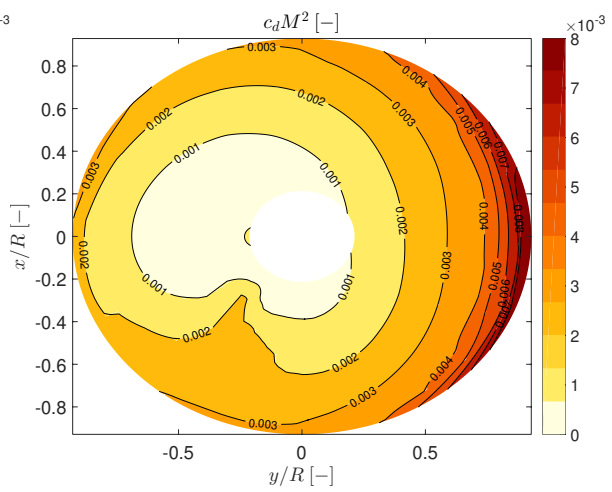


Figure C.50: $c_d M^2$ Flightlab 120 kts

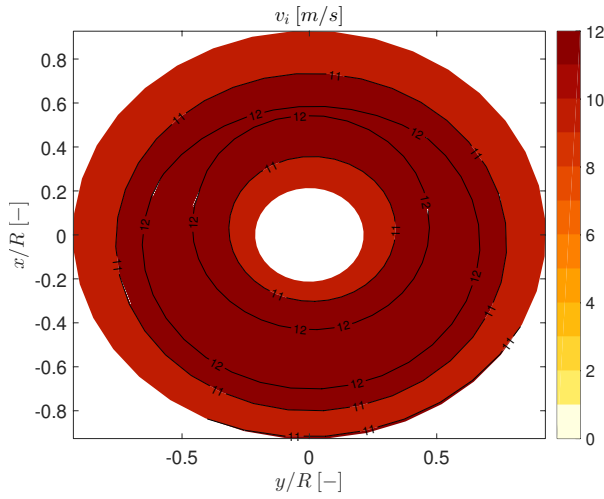


Figure C.51: v_i SimMechanics 0 kts

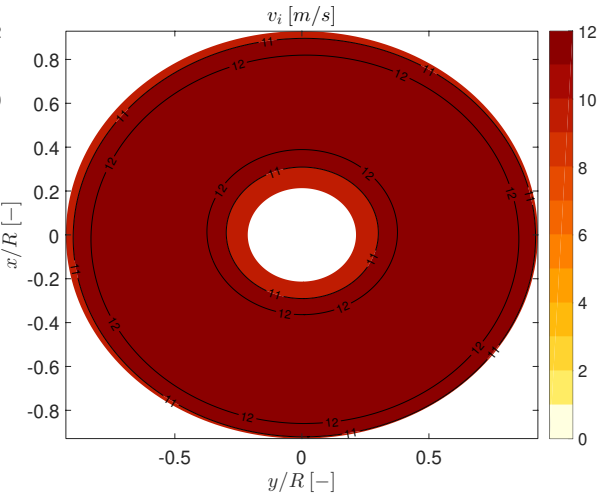


Figure C.52: v_i Flightlab 0 kts

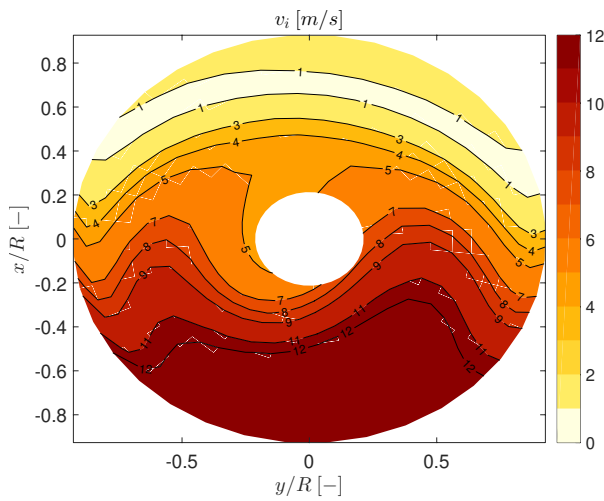


Figure C.53: v_i SimMechanics 20 kts

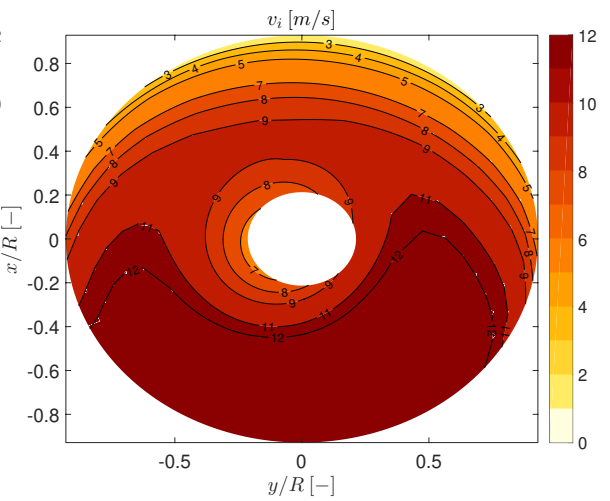


Figure C.54: v_i Flightlab 20 kts

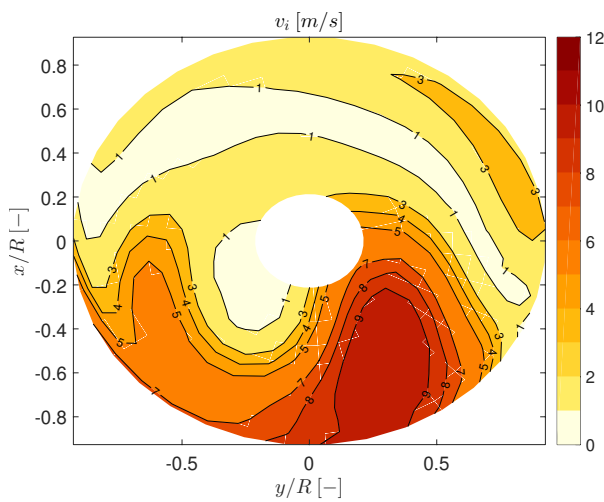


Figure C.55: v_i SimMechanics 50 kts

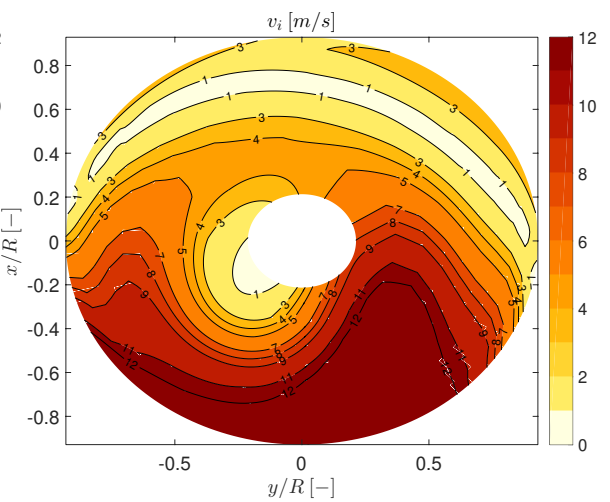
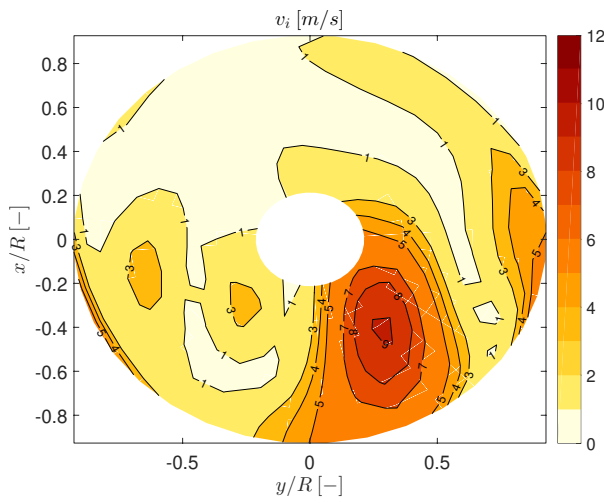
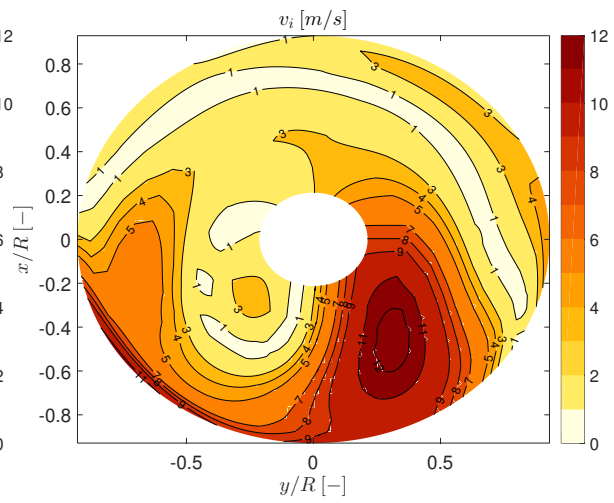
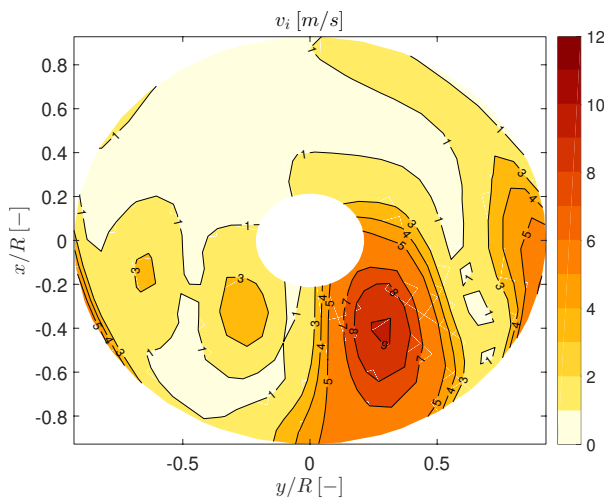
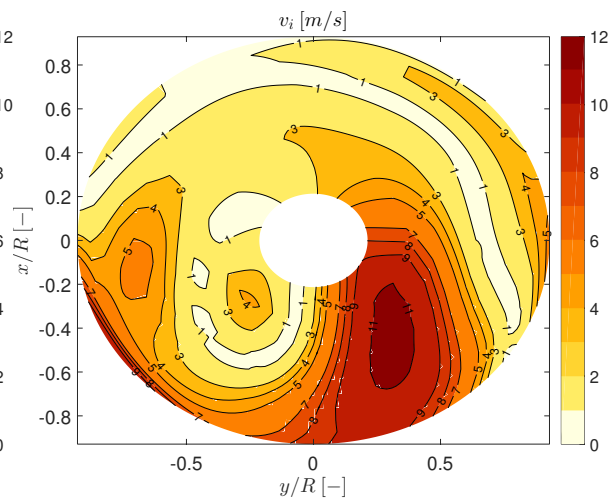


Figure C.56: v_i Flightlab 50 kts

Figure C.57: v_i SimMechanics 100 ktsFigure C.58: v_i Flightlab 100 ktsFigure C.59: v_i SimMechanics 120 ktsFigure C.60: v_i Flightlab 120 kts

D

The Effect of Different Trim Settings on Loads in the Rotor Hub

D.1. Effect of Horizontal Tail Deflection on Responses and Loads During Roll Doublet

A right roll doublet with 50% lateral cyclic and 50% aileron input at 120 kts is initiated at different trim settings. This section presents the effect of a horizontal tail deflection on loads in the main rotor hub during a roll right doublet. The baseline trim settings with $i_{tail} = 0^\circ$ and a $i_{tail} = 5^\circ$ horizontal tail deflection trim setting are defined according to Table 6.1. The trim condition is summarised in Table 6.2. This section presents a complete overview of the attitude quickness, vehicle attitude, flap angles, loads and load quickness during the roll doublet.

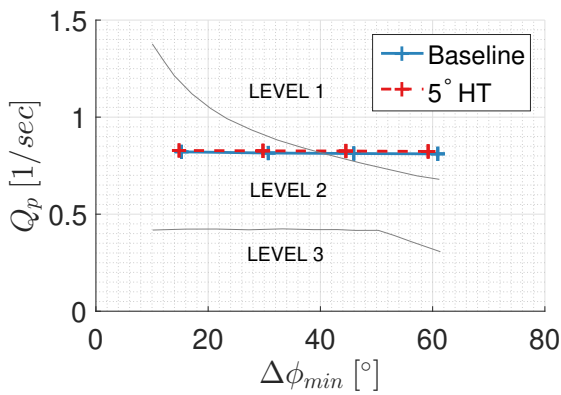


Figure D.1: Attitude quickness roll-in

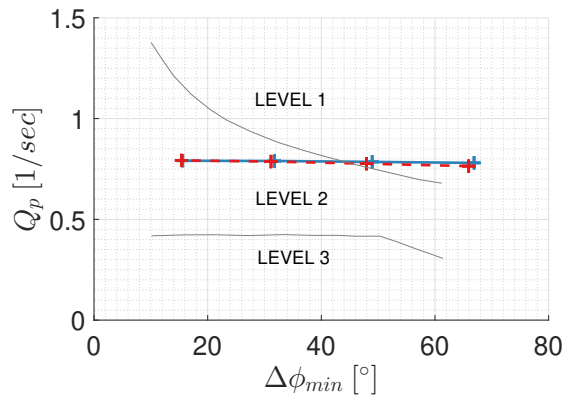
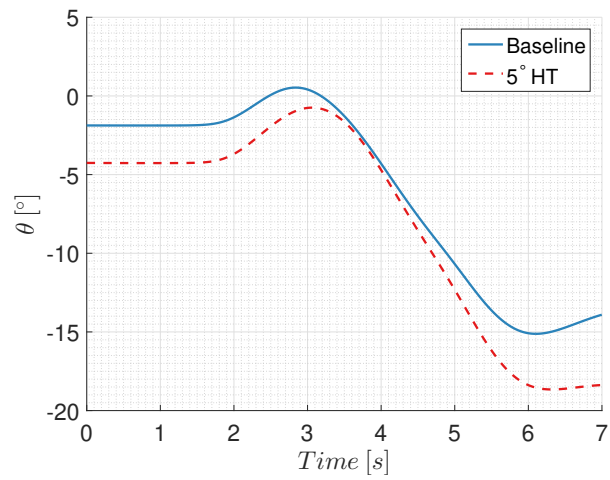
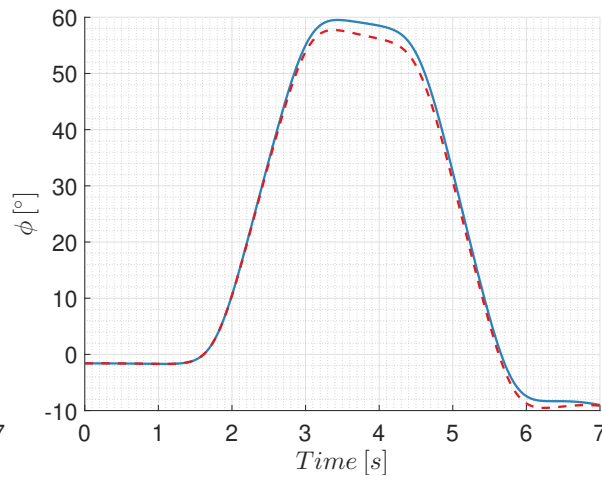
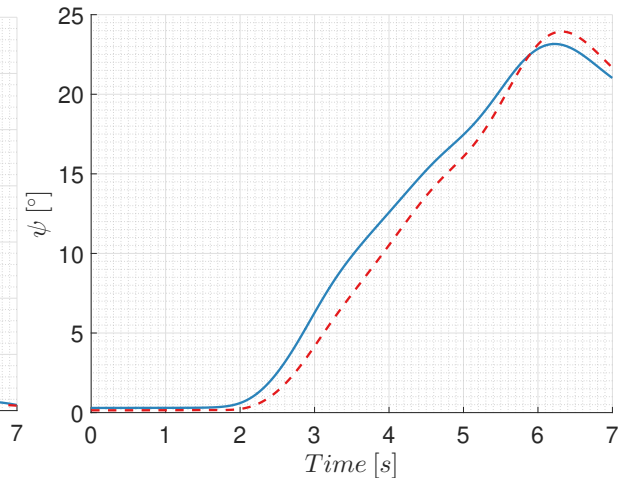
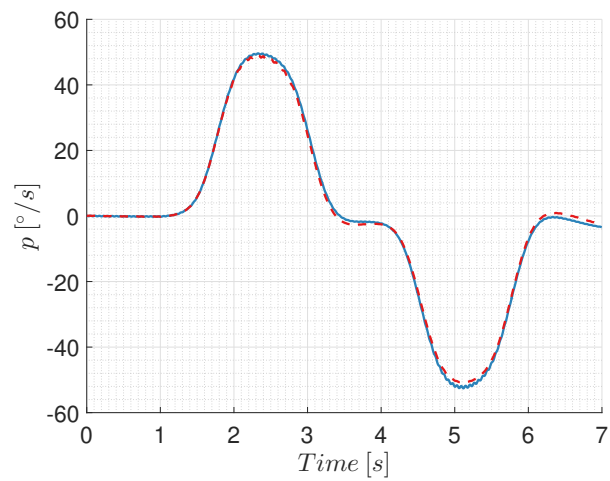
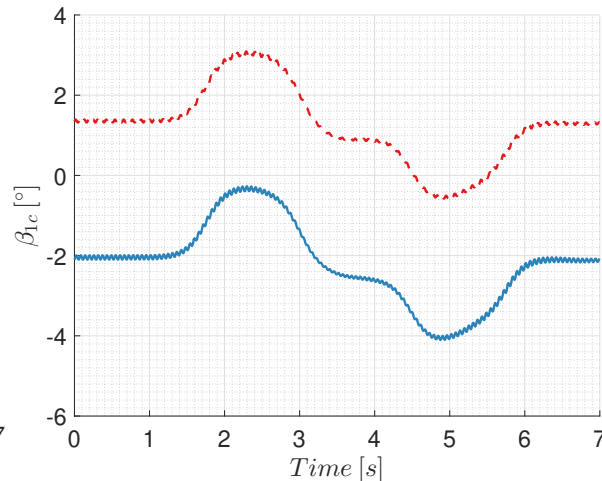
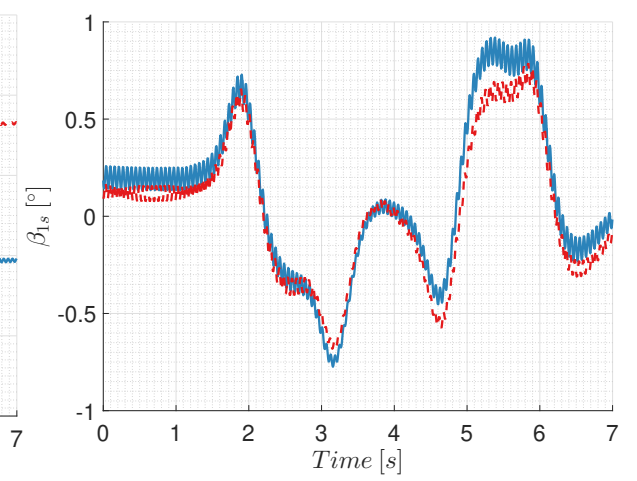


Figure D.2: Attitude quickness roll-out

Figure D.3: θ response, 50% cyclic - 50% aileronsFigure D.4: ϕ response, 50% cyclic - 50% aileronsFigure D.5: ψ response, 50% cyclic - 50% aileronsFigure D.6: p response, 50% cyclic - 50% aileronsFigure D.7: β_{1c} response, 50% cyclic - 50% aileronsFigure D.8: β_{1s} response, 50% cyclic - 50% ailerons

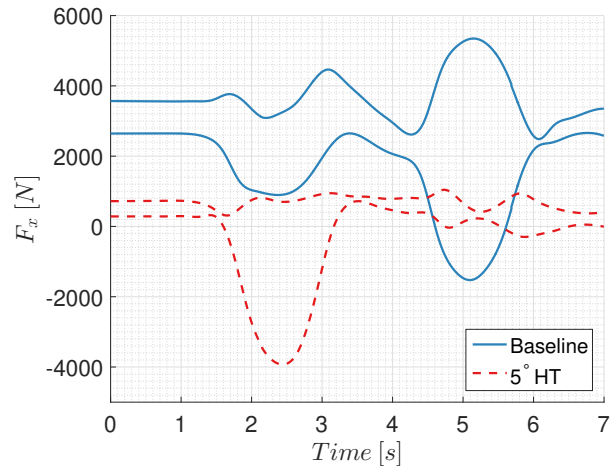


Figure D.9: F_x response, 50% cyclic - 50% ailerons

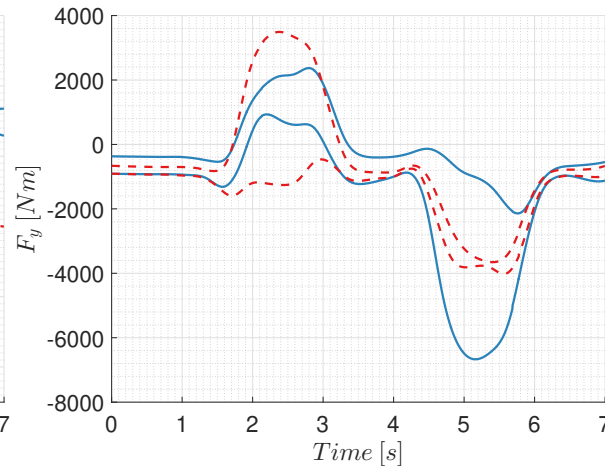


Figure D.10: F_y response, 50% cyclic - 50% ailerons

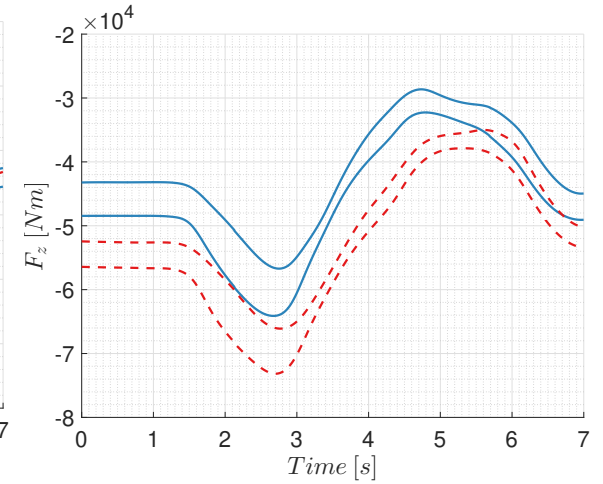


Figure D.11: F_z response, 50% cyclic - 50% ailerons

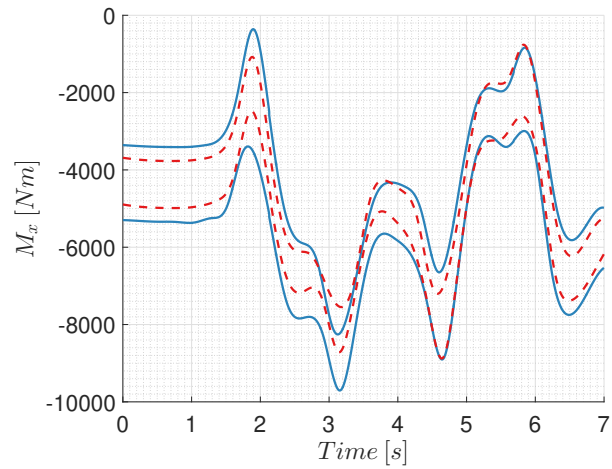


Figure D.12: M_x response, 50% cyclic - 50% ailerons

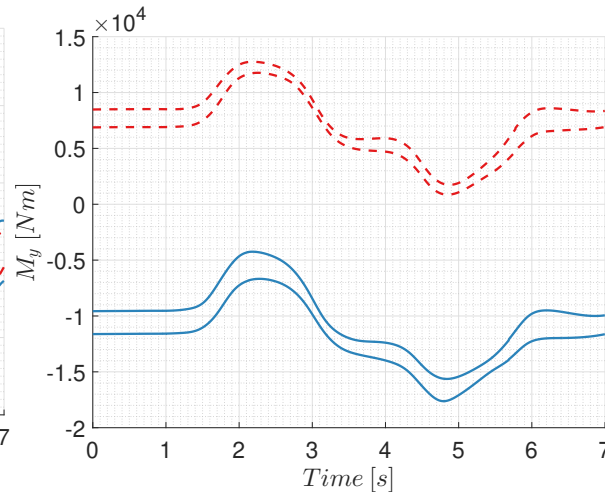


Figure D.13: M_y response, 50% cyclic - 50% ailerons

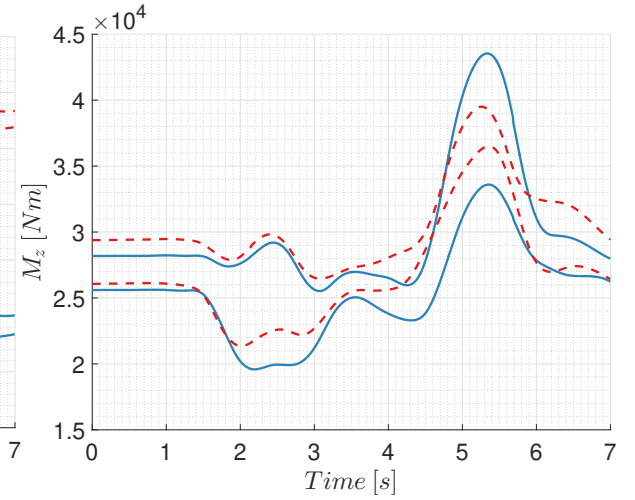


Figure D.14: M_z response, 50% cyclic - 50% ailerons

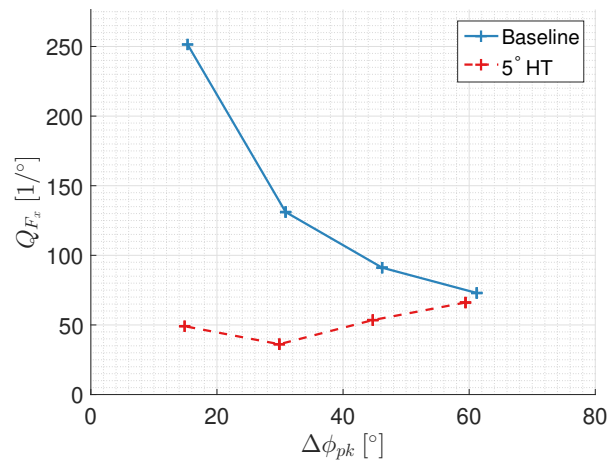


Figure D.15: F_x quickness roll-in

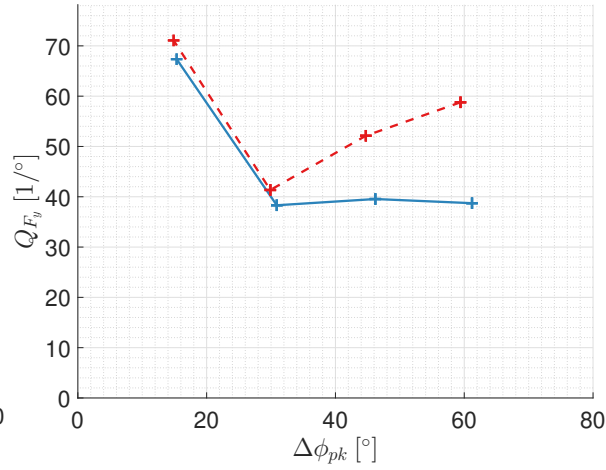


Figure D.16: F_y quickness roll-in

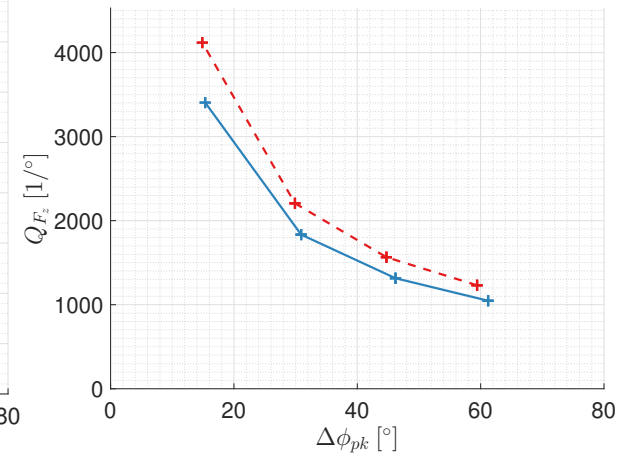


Figure D.17: F_z quickness roll-in

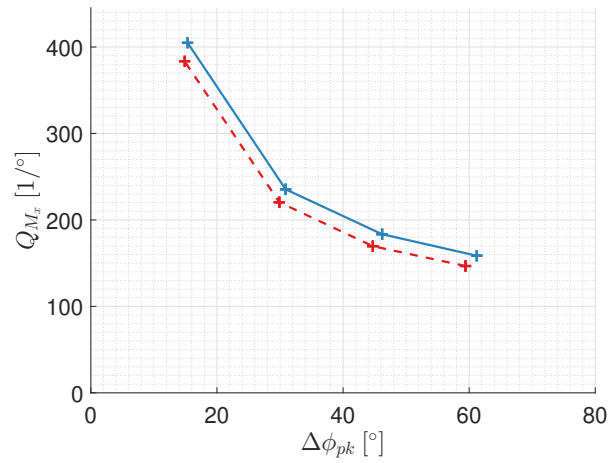


Figure D.18: M_x quickness roll-in

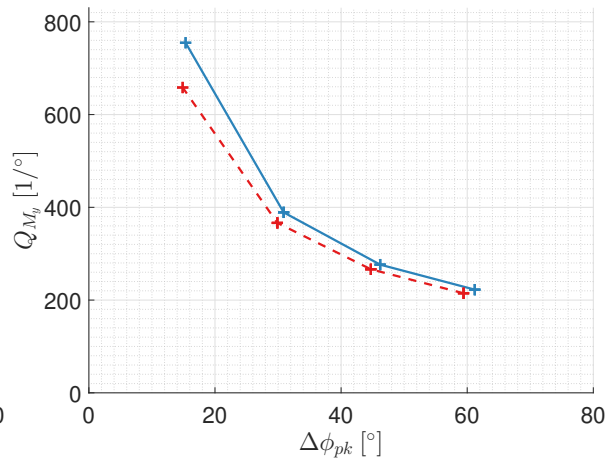


Figure D.19: M_y quickness roll-in

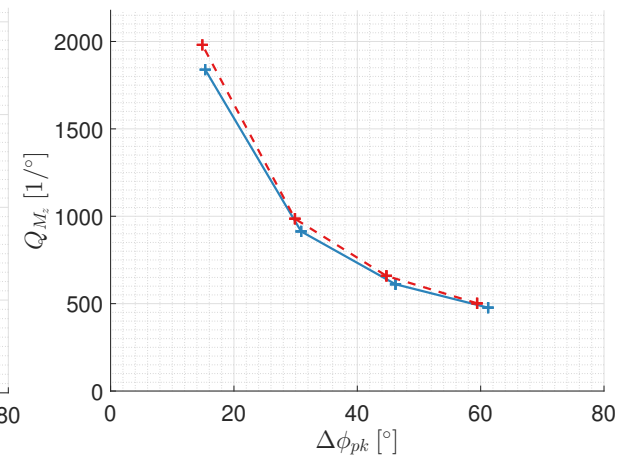


Figure D.20: M_z quickness roll-in

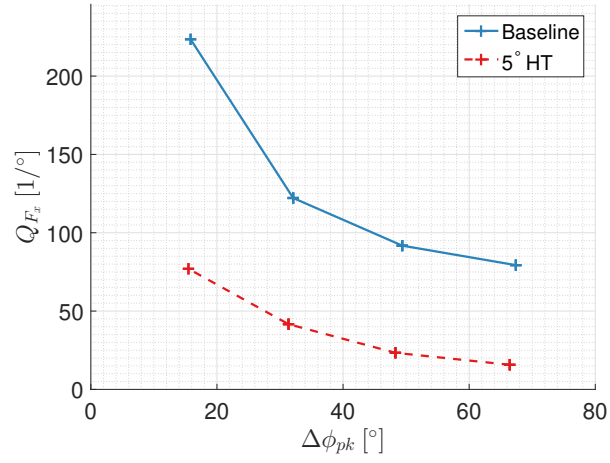


Figure D.21: F_x quickness roll-out

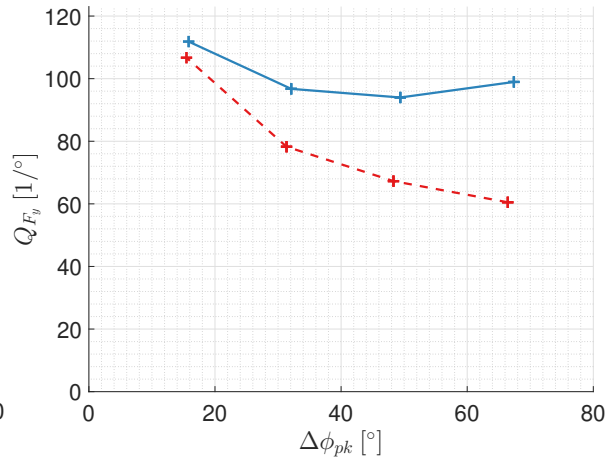


Figure D.22: F_y quickness roll-out

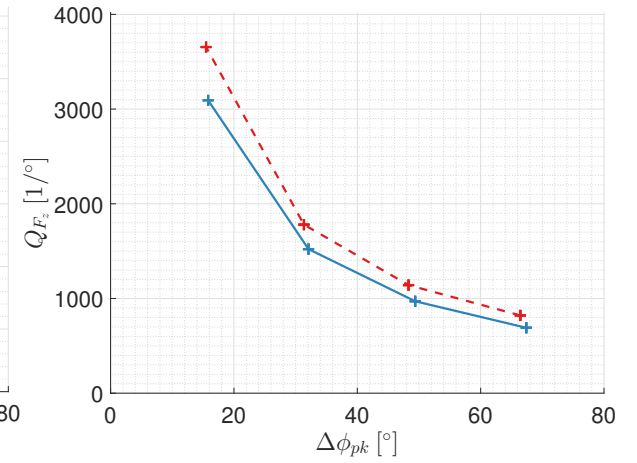


Figure D.23: F_z quickness roll-out

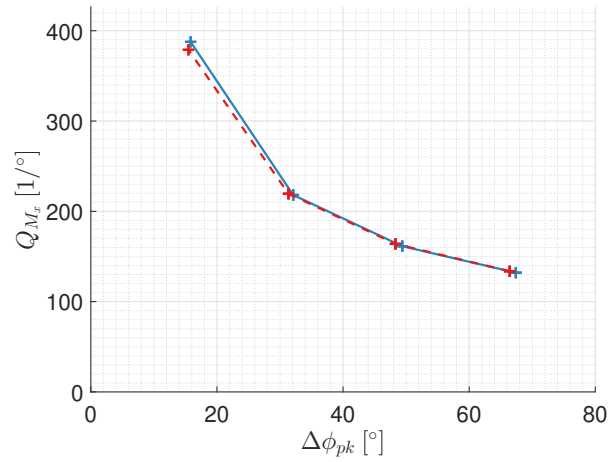


Figure D.24: M_x quickness roll-out

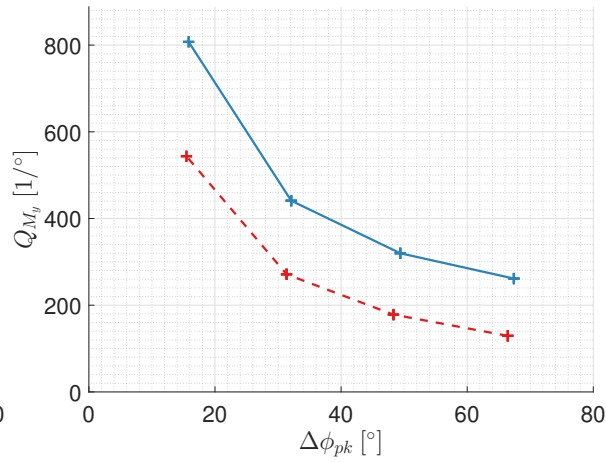


Figure D.25: M_y quickness roll-out

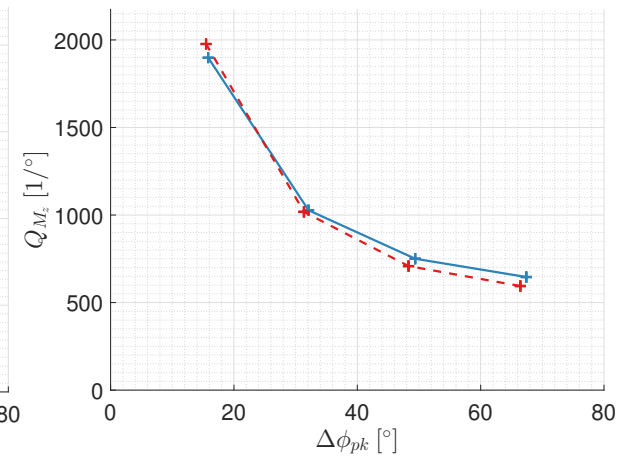


Figure D.26: M_z quickness roll-out

D.2. Effect of Compound Thrust on Responses and Loads During Roll Doublet

The helicopter is now trimmed at 120 kts with 5000 N thrust generated by the push propeller mounted near the tail of the aircraft. A roll right doublet is executed using the 50% lateral cyclic and 50% aileron control strategy. Trim settings are defined according to Table 6.1. The trim condition is summarised in Table 6.2. This section presents a complete overview of the attitude quickness, vehicle attitude, flap angles, loads and load quickness during the roll doublet.

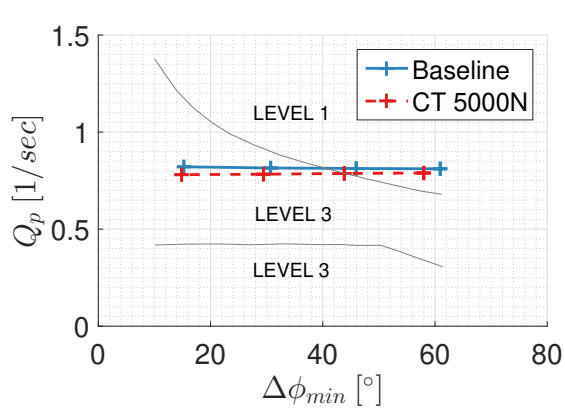


Figure D.27: Attitude quickness roll-in

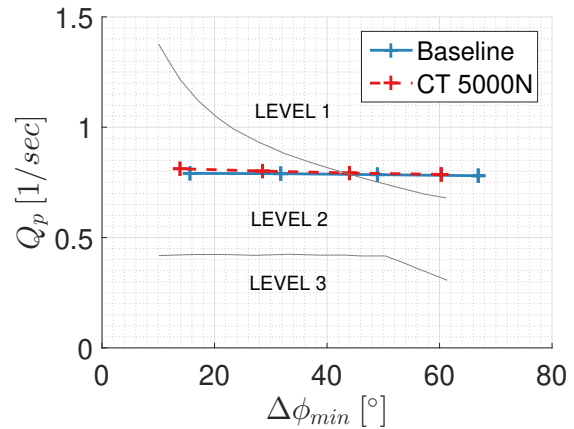


Figure D.28: Attitude quickness roll-out

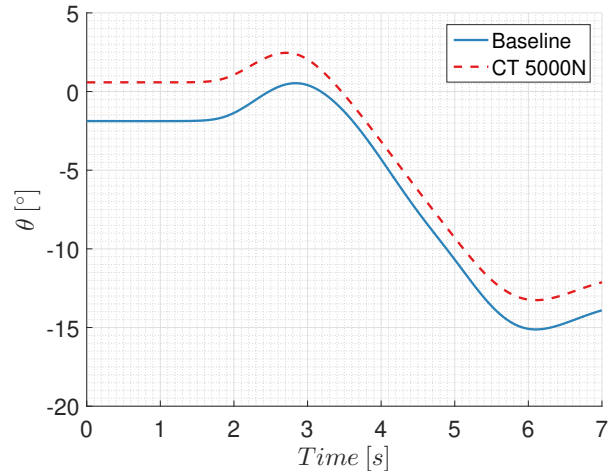


Figure D.29: θ response, 50% cyclic - 50% ailerons

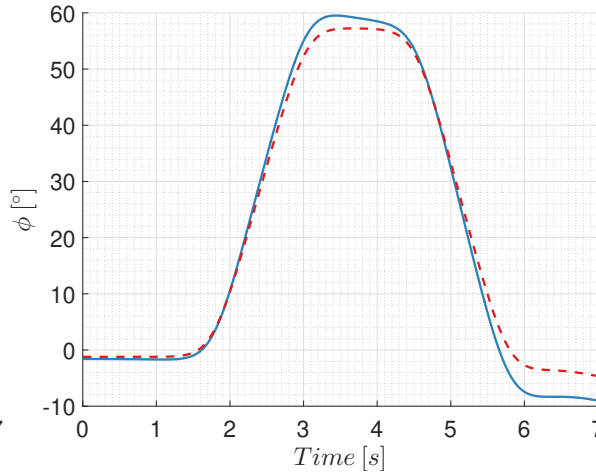


Figure D.30: ϕ response, 50% cyclic - 50% ailerons

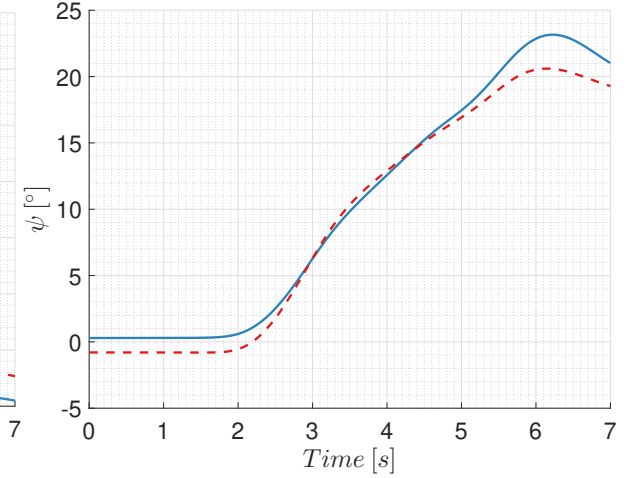


Figure D.31: ψ response, 50% cyclic - 50% ailerons

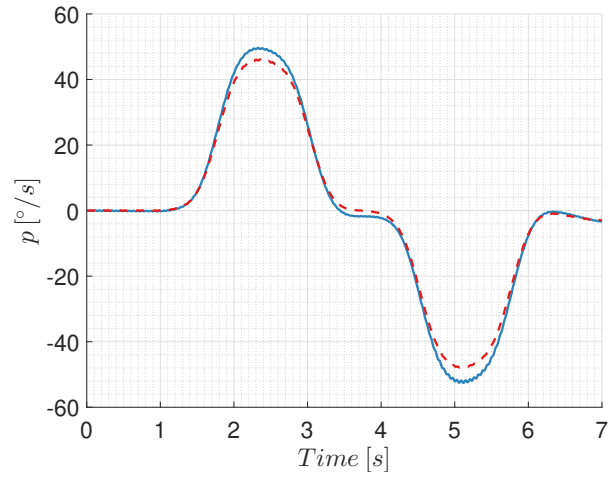


Figure D.32: p response, 50% cyclic - 50% ailerons

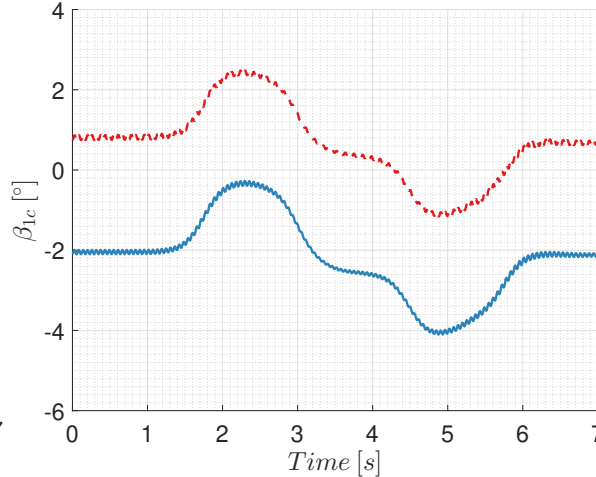


Figure D.33: β_{1c} response, 50% cyclic - 50% ailerons

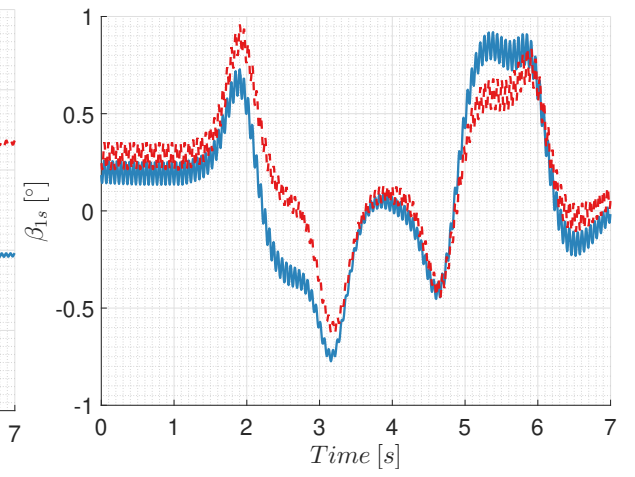


Figure D.34: β_{1s} response, 50% cyclic - 50% ailerons

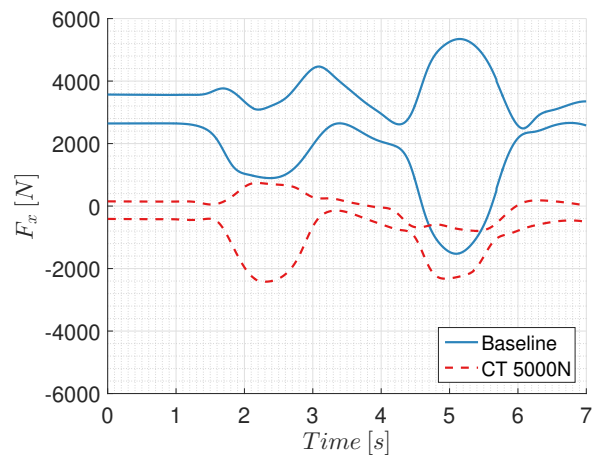


Figure D.35: F_x response, 50% cyclic - 50% ailerons

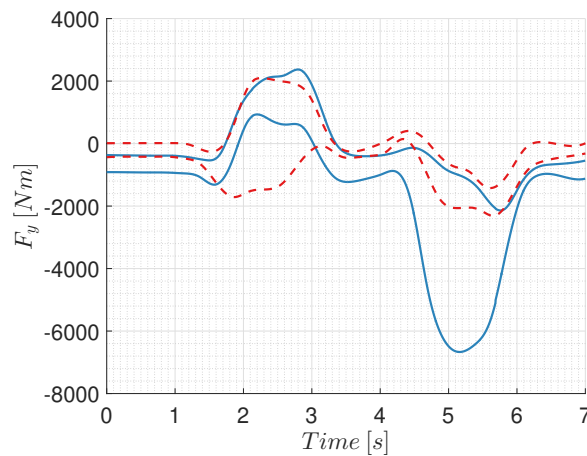


Figure D.36: F_y response, 50% cyclic - 50% ailerons

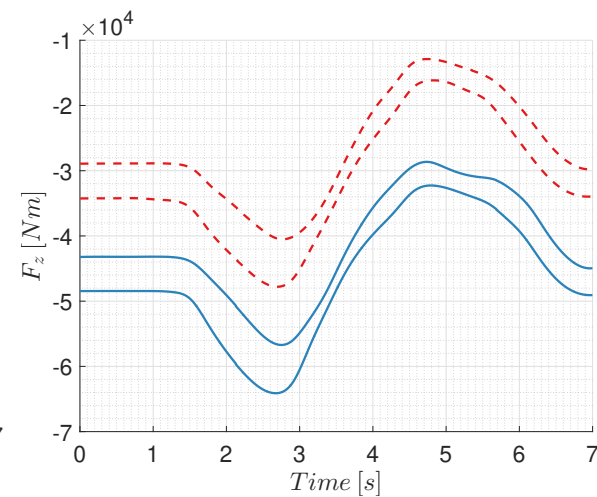


Figure D.37: F_z response, 50% cyclic - 50% ailerons

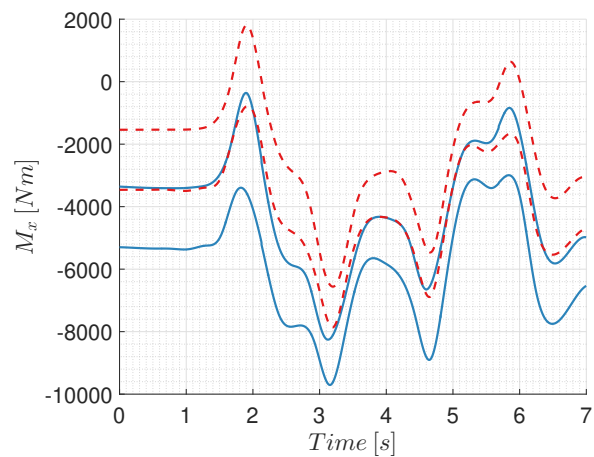


Figure D.38: M_x response, 50% cyclic - 50% ailerons

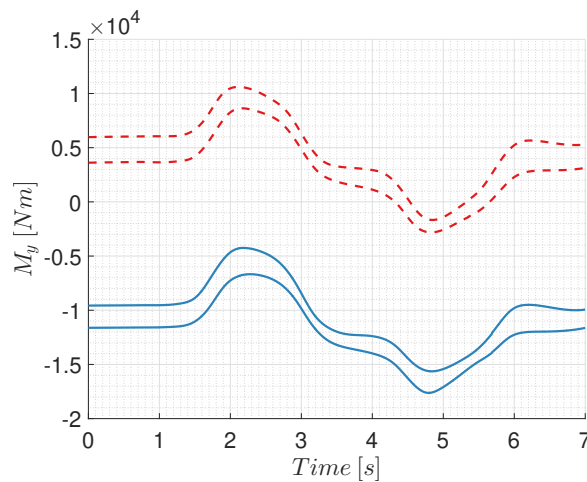


Figure D.39: M_y response, 50% cyclic - 50% ailerons

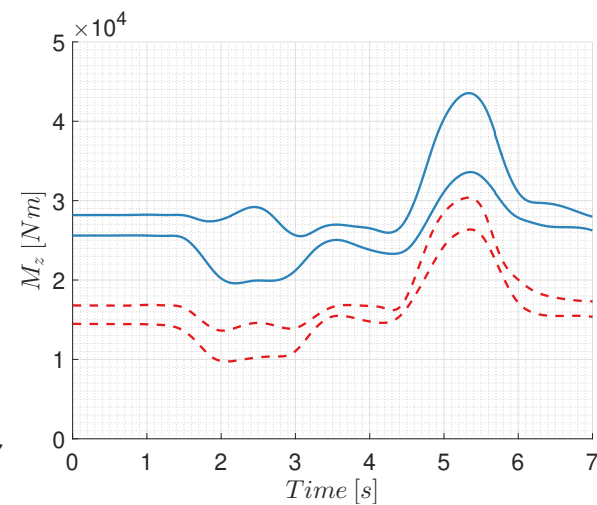


Figure D.40: M_z response, 50% cyclic - 50% ailerons

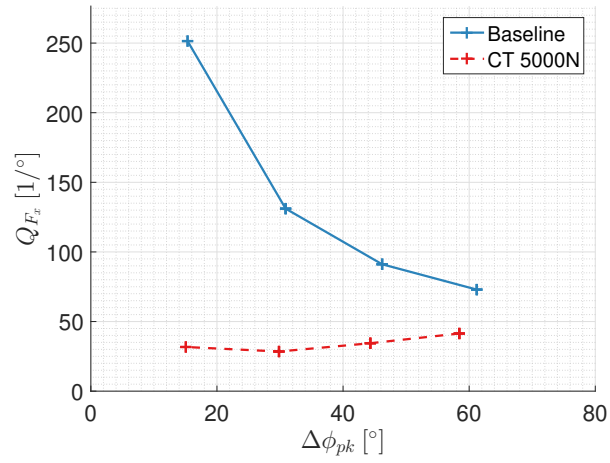


Figure D.41: F_x quickness roll-in

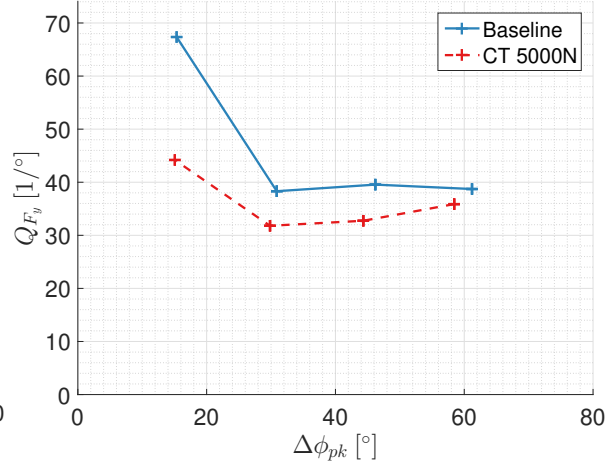


Figure D.42: F_y quickness roll-in

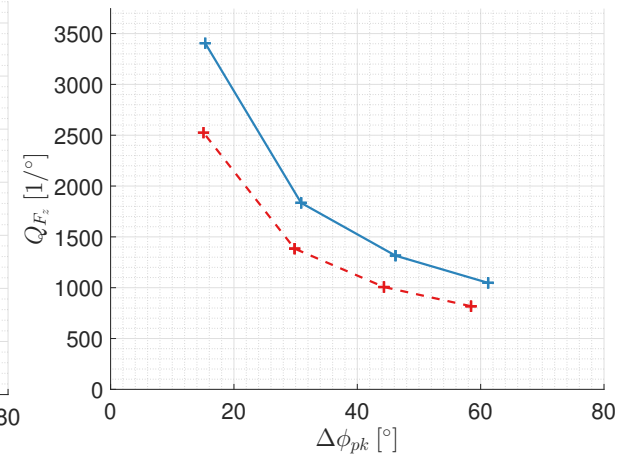


Figure D.43: F_z quickness roll-in

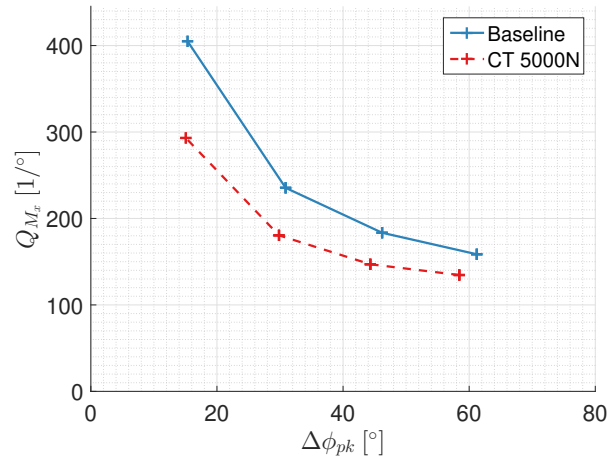


Figure D.44: M_x quickness roll-in

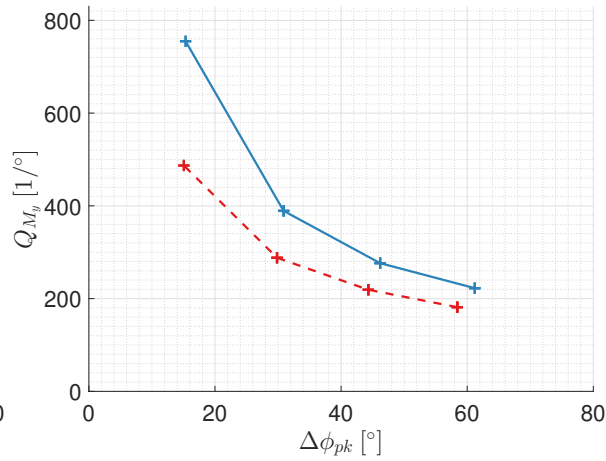


Figure D.45: M_y quickness roll-in

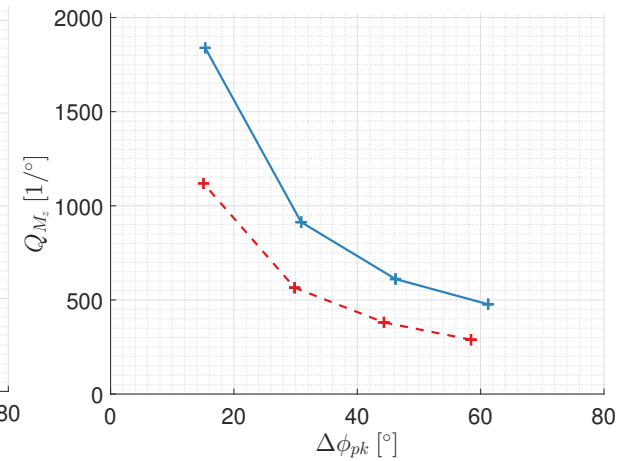


Figure D.46: M_z quickness roll-in

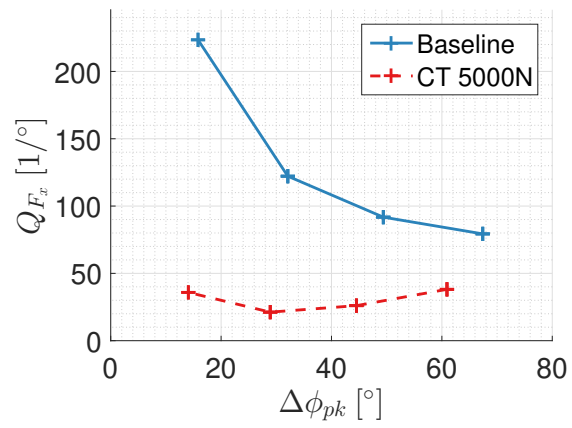


Figure D.47: F_x quickness roll-out

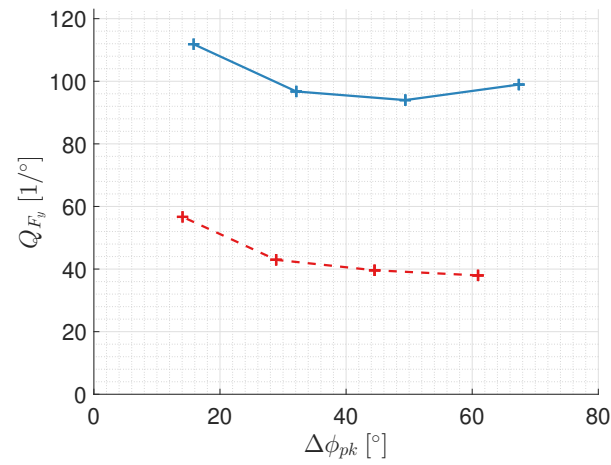


Figure D.48: F_y quickness roll-out

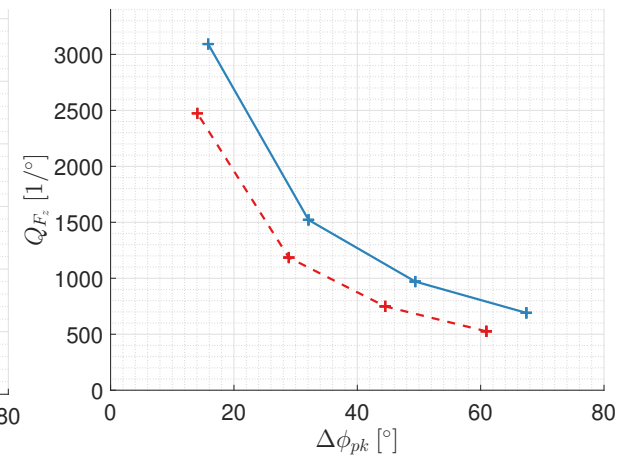


Figure D.49: F_z quickness roll-out

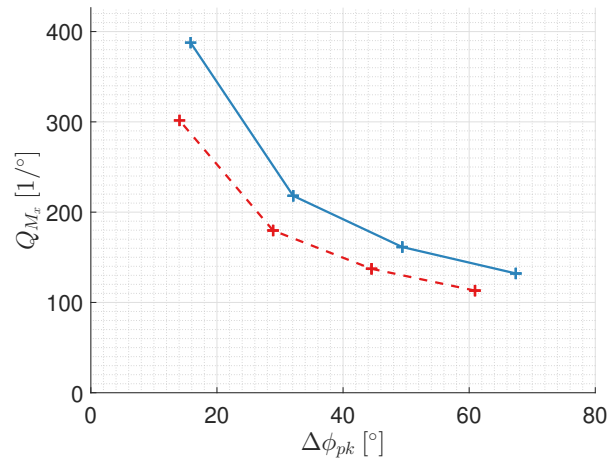


Figure D.50: M_x quickness roll-out

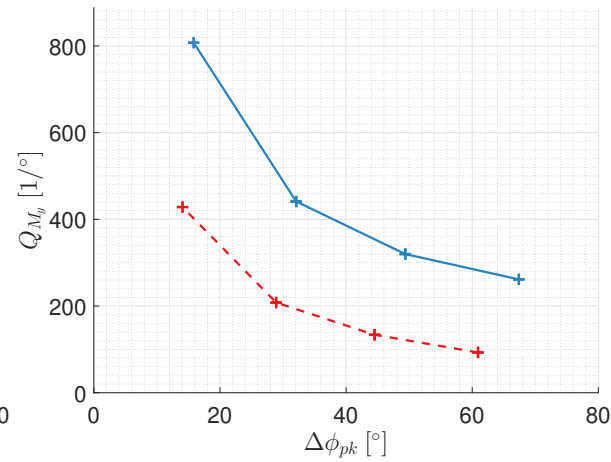


Figure D.51: M_y quickness roll-out

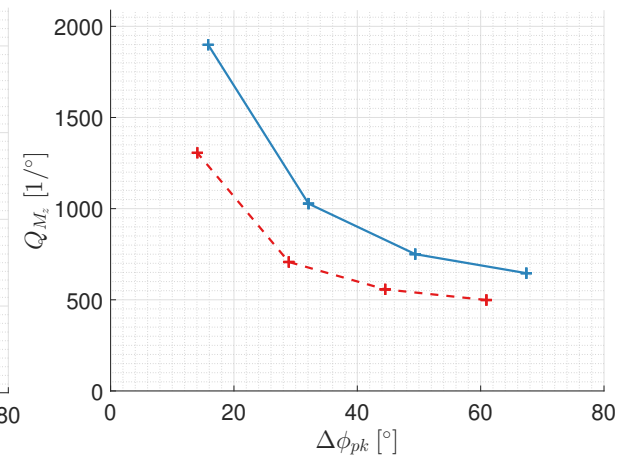


Figure D.52: M_z quickness roll-out

D.3. Effect of Lowering the Main Rotor RPM on Responses and Loads During Roll Doublet

A right roll doublet with 50% lateral cyclic and 50% aileron input at 120 kts is initiated at different trim setting. This section presents the effect of a lower main rotor rpm on loads in the main rotor hub during a roll right doublet. The baseline trim settings and a 80% reduced rotor rpm trim setting are defined according to Table 6.1. The trim condition is summarised in Table 6.2. This section presents a complete overview of the attitude quickness, vehicle attitude, flap angles, loads and load quickness during the roll doublet.

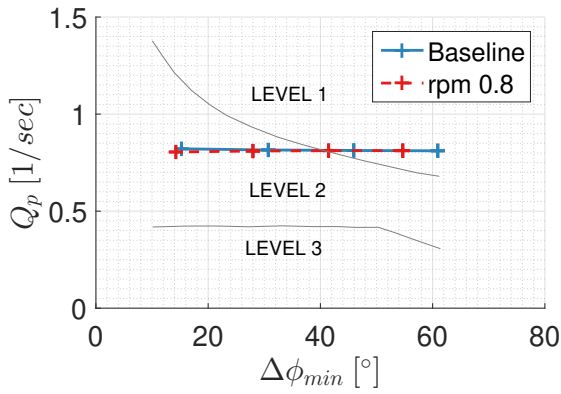


Figure D.53: Attitude quickness roll-in

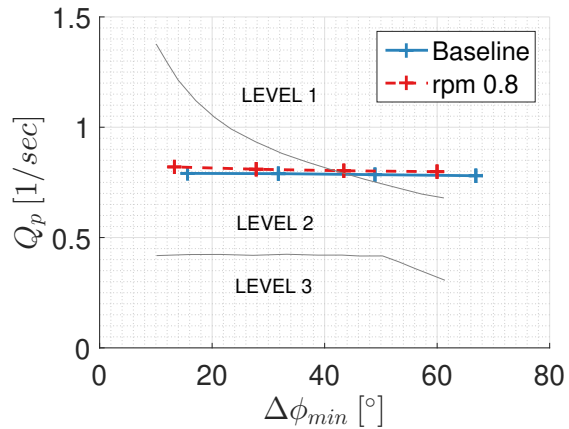
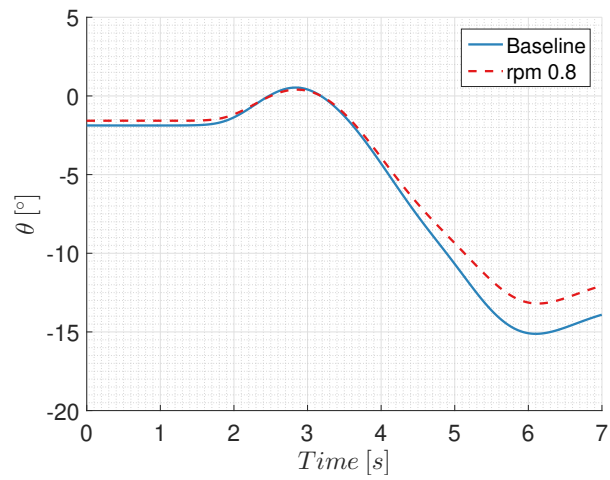
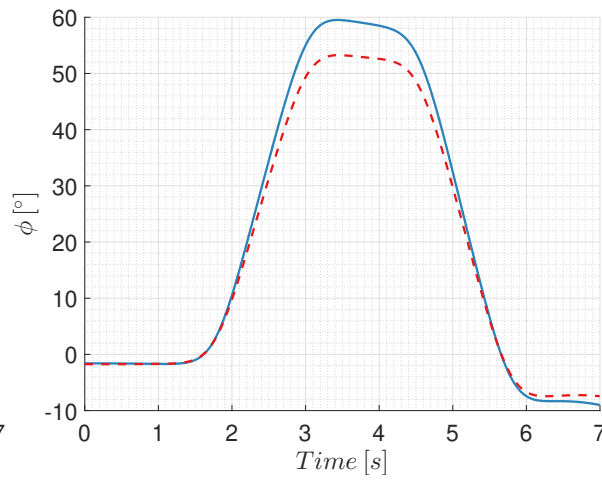
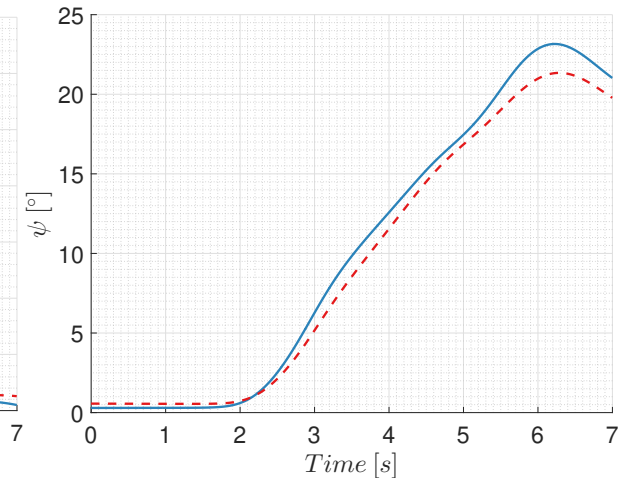
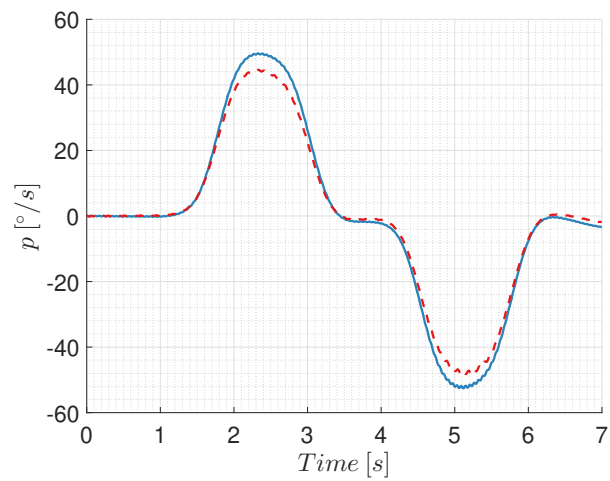
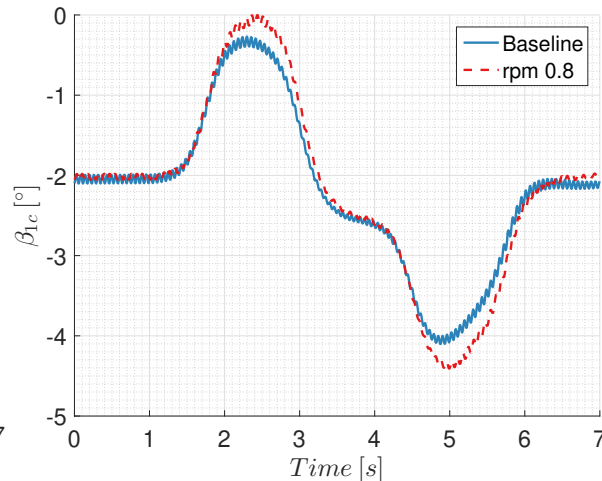
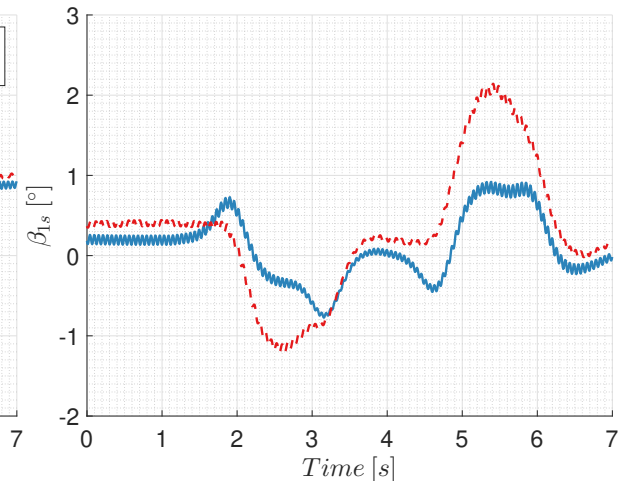


Figure D.54: Attitude quickness roll-out

Figure D.55: θ response, 50% cyclic - 50% aileronsFigure D.56: ϕ response, 50% cyclic - 50% aileronsFigure D.57: ψ response, 50% cyclic - 50% aileronsFigure D.58: p response, 50% cyclic - 50% aileronsFigure D.59: β_{1c} response, 50% cyclic - 50% aileronsFigure D.60: β_{1s} response, 50% cyclic - 50% ailerons

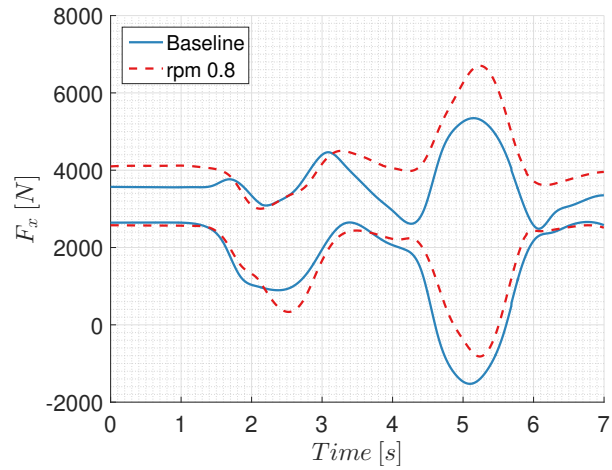


Figure D.61: F_x response, 50% cyclic - 50% ailerons

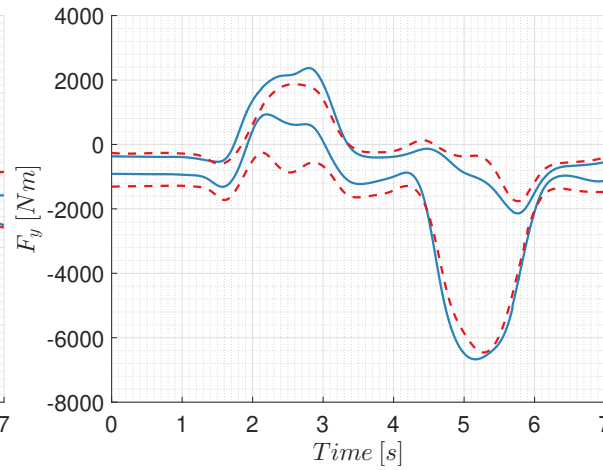


Figure D.62: F_y response, 50% cyclic - 50% ailerons

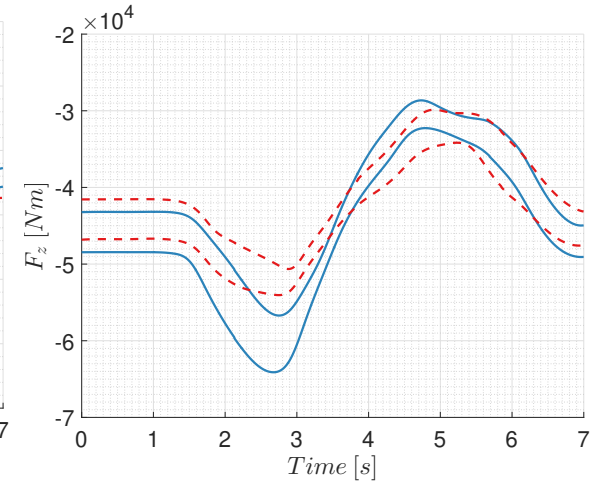


Figure D.63: F_z response, 50% cyclic - 50% ailerons

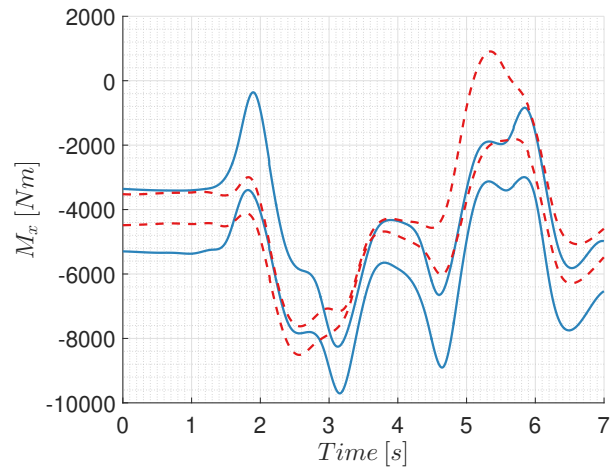


Figure D.64: M_x response, 50% cyclic - 50% ailerons

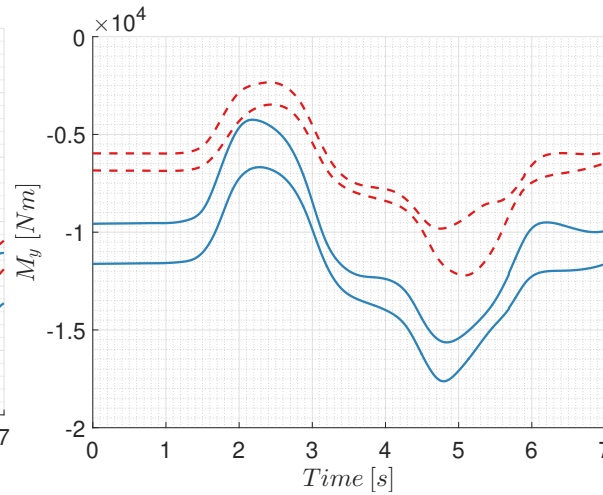


Figure D.65: M_y response, 50% cyclic - 50% ailerons

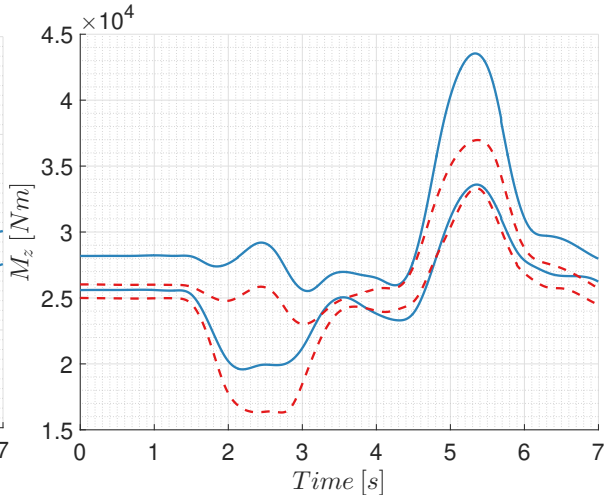


Figure D.66: M_z response, 50% cyclic - 50% ailerons

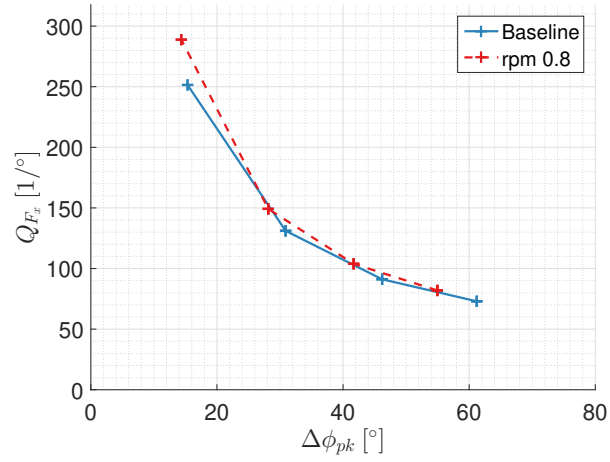


Figure D.67: F_x quickness roll-in

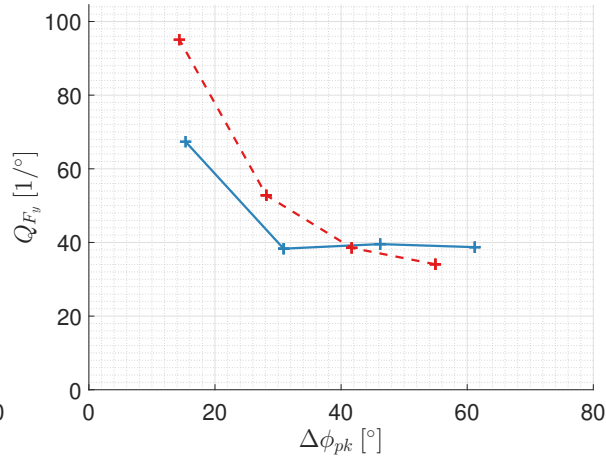


Figure D.68: F_y quickness roll-in

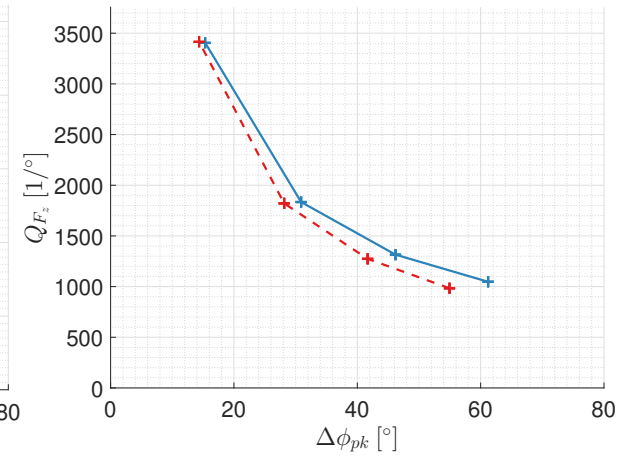


Figure D.69: F_z quickness roll-in

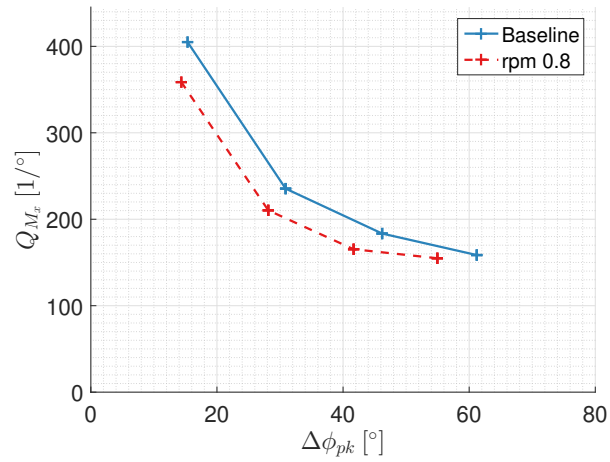


Figure D.70: M_x quickness roll-in

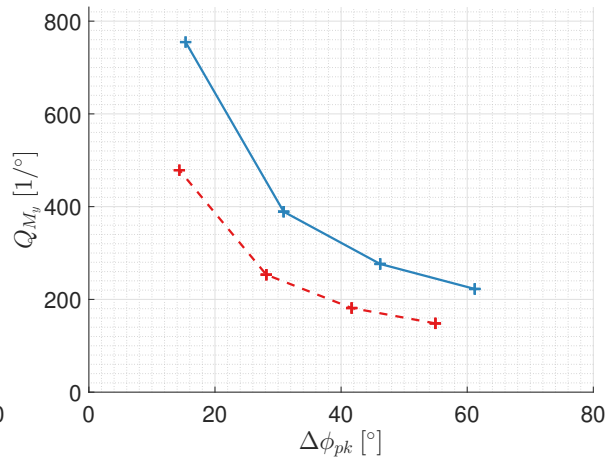


Figure D.71: M_y quickness roll-in

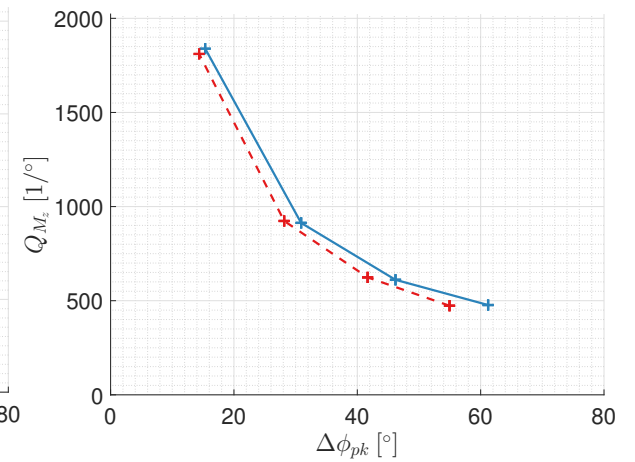


Figure D.72: M_z quickness roll-in

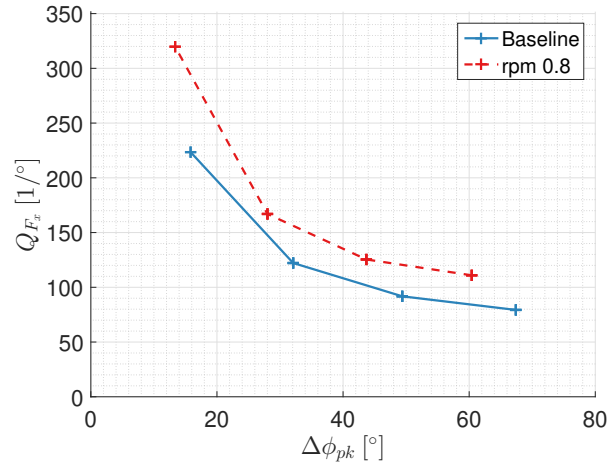


Figure D.73: F_x quickness roll-out

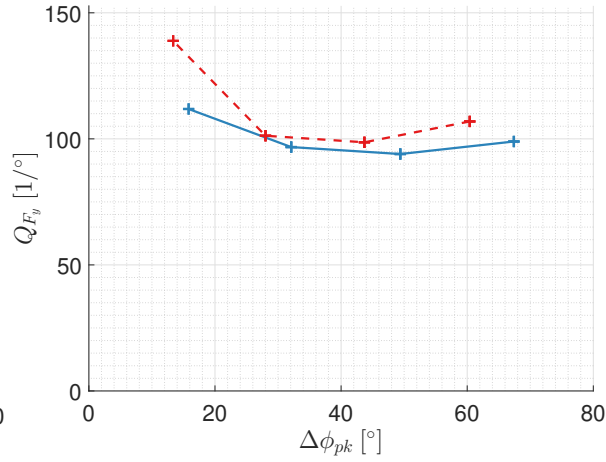


Figure D.74: F_y quickness roll-out

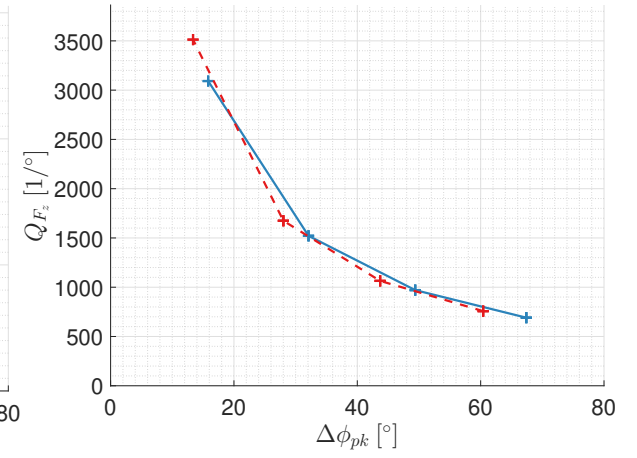


Figure D.75: F_z quickness roll-out

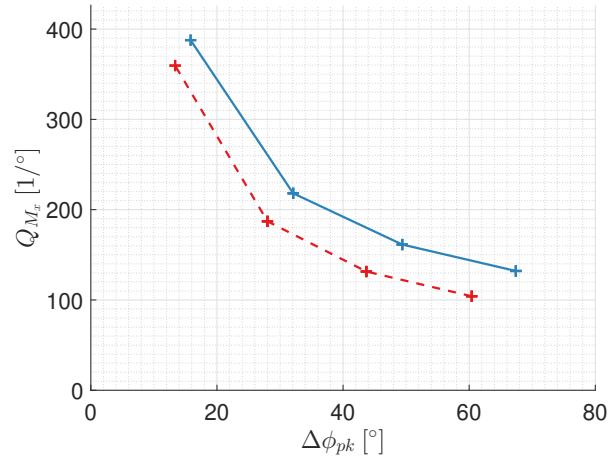


Figure D.76: M_x quickness roll-out

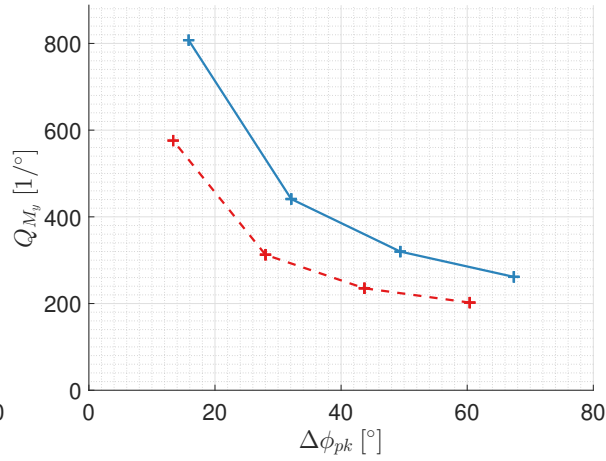


Figure D.77: M_y quickness roll-out

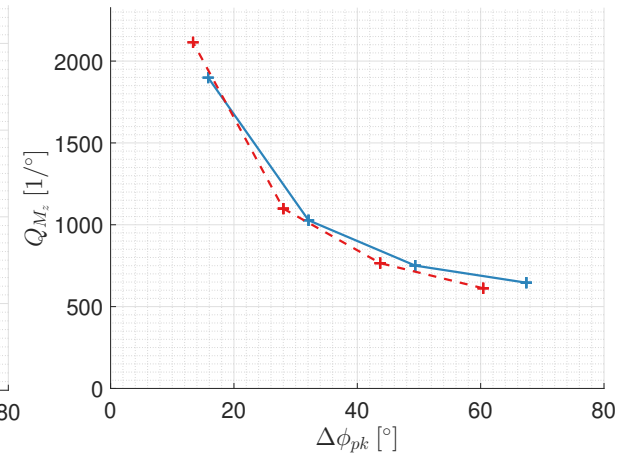


Figure D.78: M_z quickness roll-out

D.4. Effect of a Constant Aileron Input in Trim on Responses and Loads During Roll Doublet

To increase cruise performance, a constant roll right aileron input is set during trim. This shifts the lifting area more to the outboard section of the advancing blade where it operates at a higher dynamic pressure, hence increases its efficiency. This concept is similar to the advancing blade concept used in the Sikorsky X2 shown in Figure 1.2, the principle is explained in Section 2.4.3.

Again a roll right doublet is flow at 120 kts with a 50% lateral cyclic and 50% aileron control input strategy. Baseline and 3° constant roll input trim settings are defined according to Table 6.1. The effect on response and loads are presented in this section. The trim condition is summarised in Table 6.2. This section presents a complete overview of the attitude quickness, vehicle attitude, flap angles, loads and load quickness during the roll doublet.

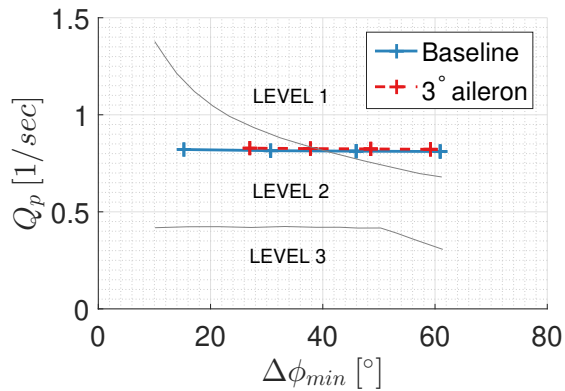


Figure D.79: Attitude quickness roll-in

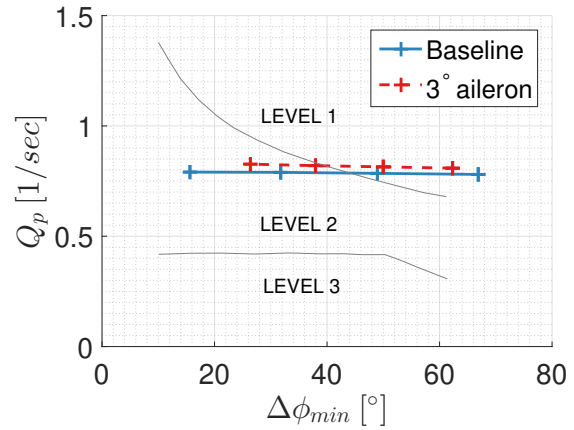


Figure D.80: Attitude quickness roll-out

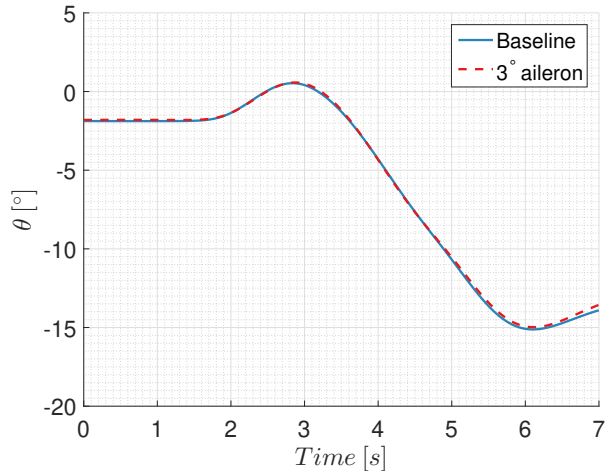


Figure D.81: θ response, 50% cyclic - 50% ailerons

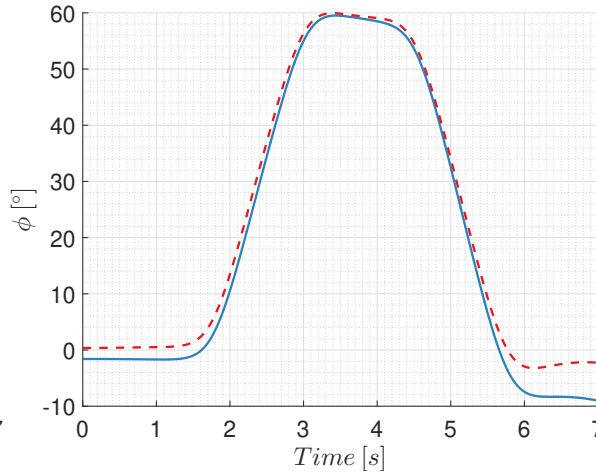


Figure D.82: ϕ response, 50% cyclic - 50% ailerons

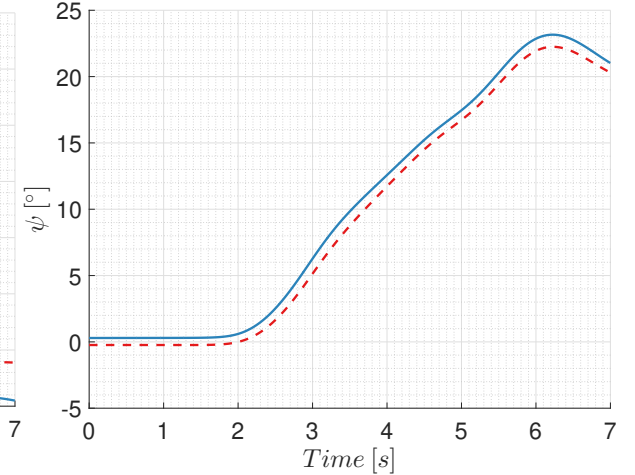


Figure D.83: ψ response, 50% cyclic - 50% ailerons

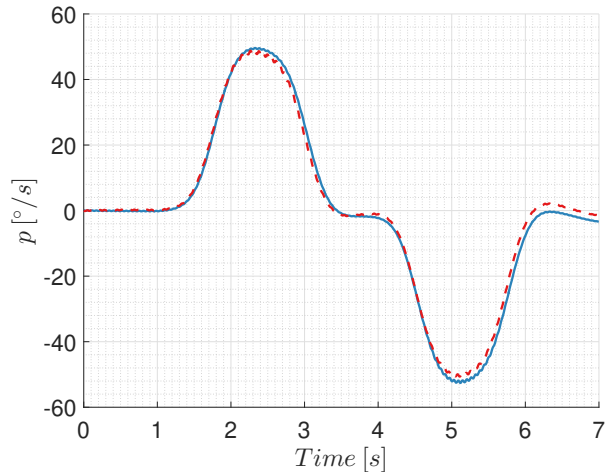


Figure D.84: p response, 50% cyclic - 50% ailerons

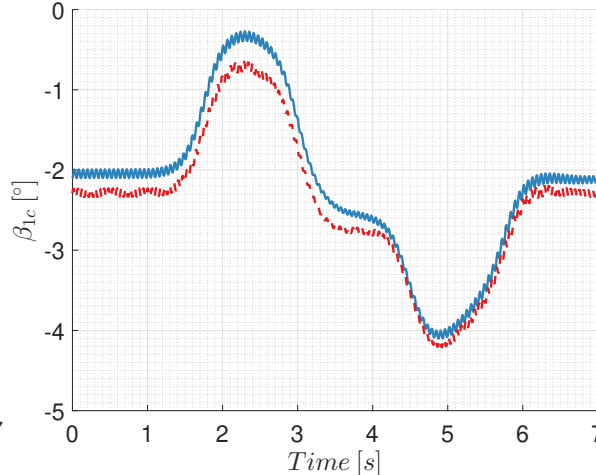


Figure D.85: β_{1c} response, 50% cyclic - 50% ailerons

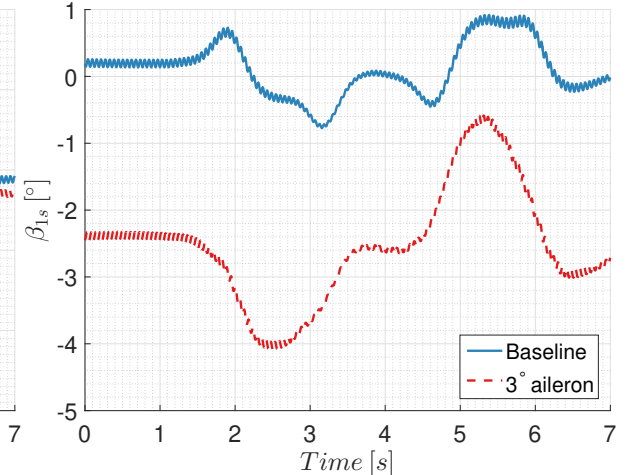
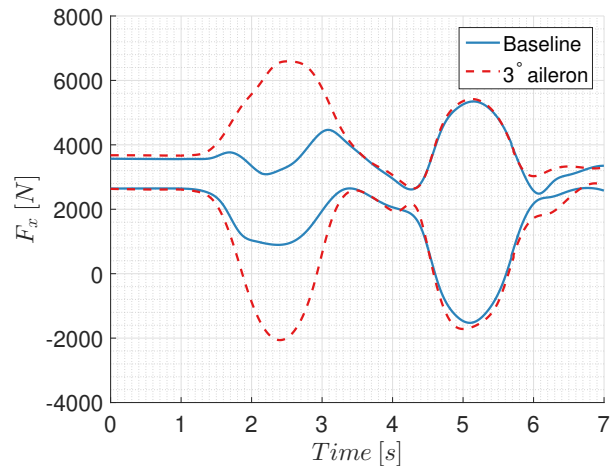
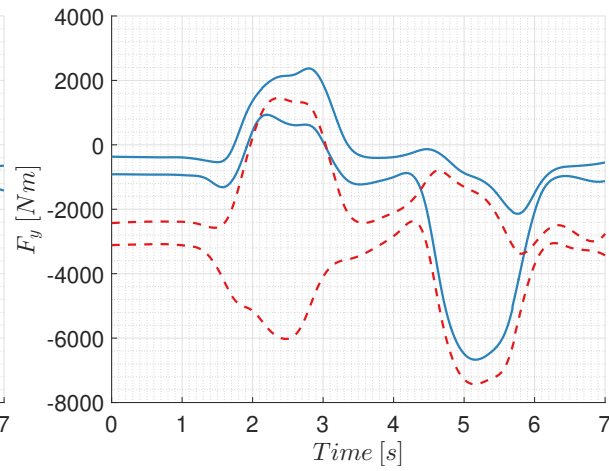
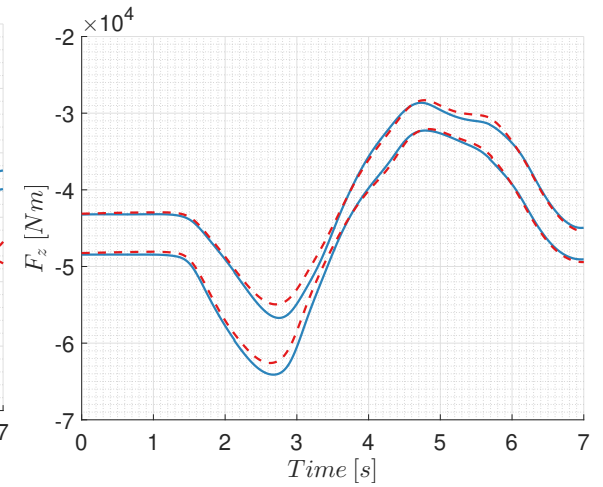
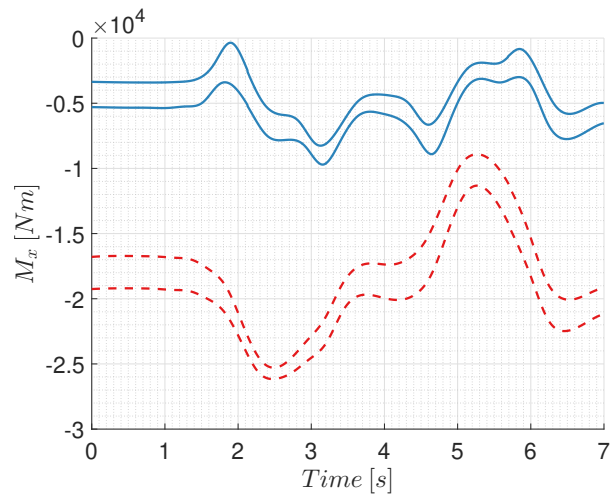
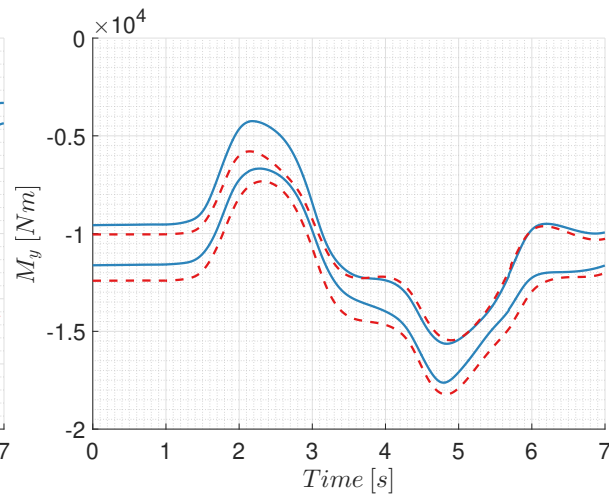
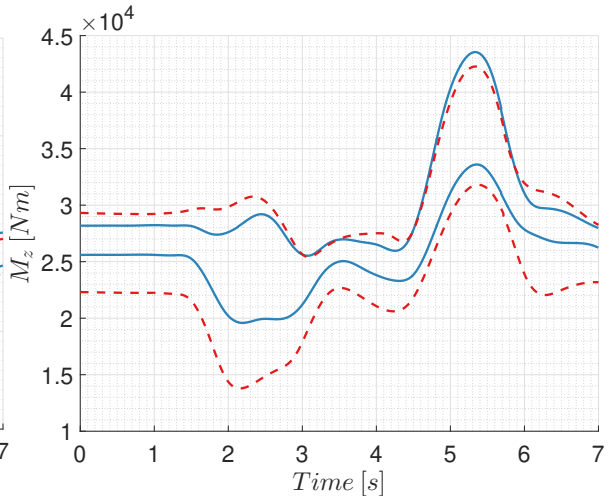


Figure D.86: β_{1s} response, 50% cyclic - 50% ailerons

Figure D.87: F_x response, 50% cyclic - 50% aileronsFigure D.88: F_y response, 50% cyclic - 50% aileronsFigure D.89: F_z response, 50% cyclic - 50% aileronsFigure D.90: M_x response, 50% cyclic - 50% aileronsFigure D.91: M_y response, 50% cyclic - 50% aileronsFigure D.92: M_z response, 50% cyclic - 50% ailerons

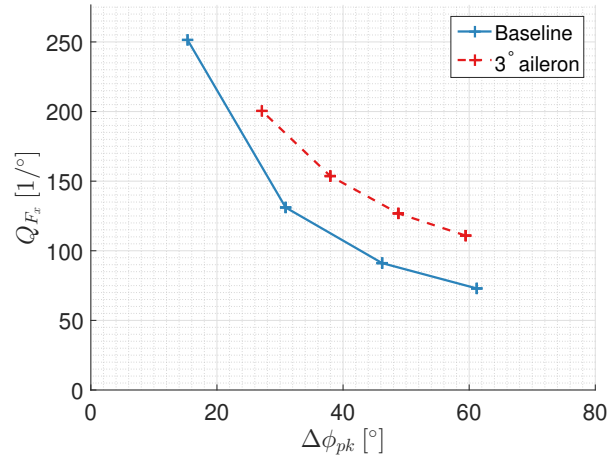


Figure D.93: F_x quickness roll-in

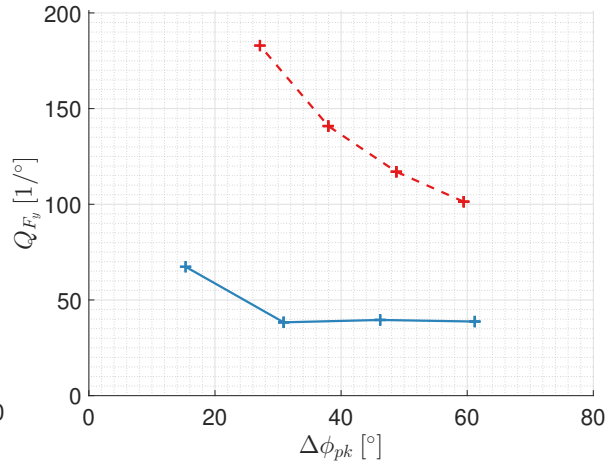


Figure D.94: F_y quickness roll-in

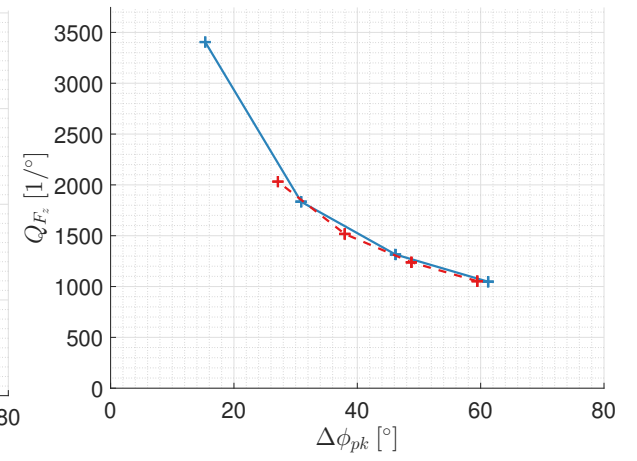


Figure D.95: F_z quickness roll-in

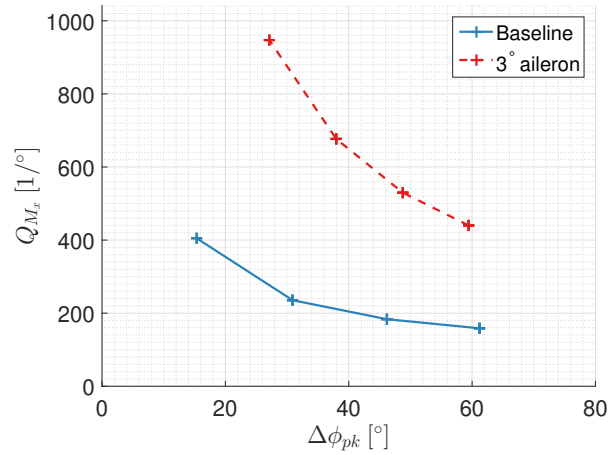


Figure D.96: M_x quickness roll-in

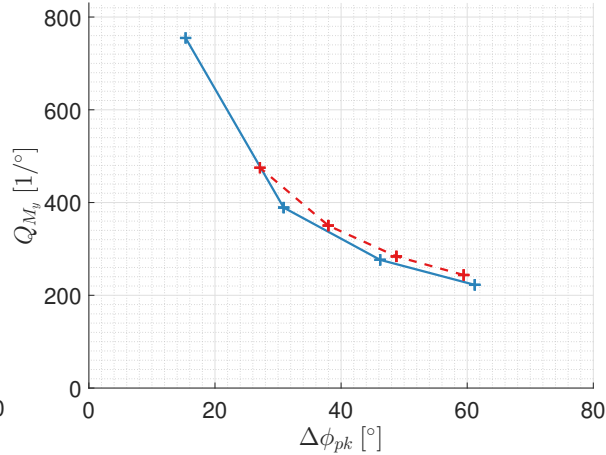


Figure D.97: M_y quickness roll-in

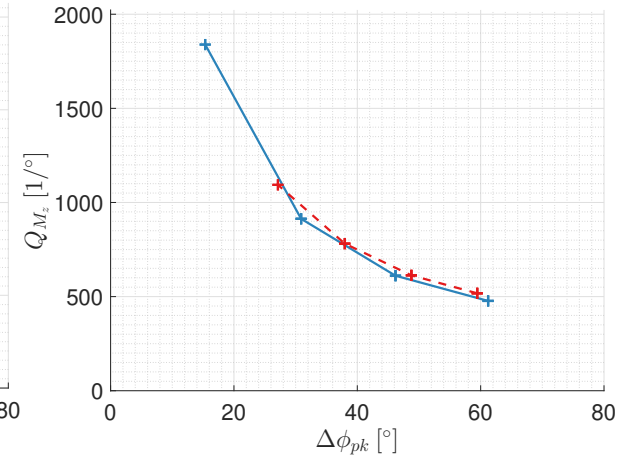
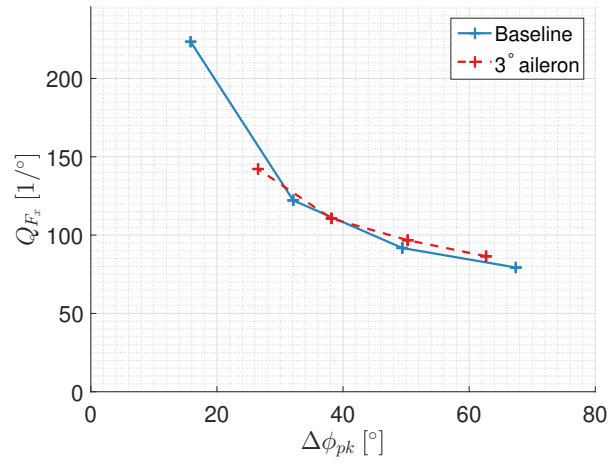
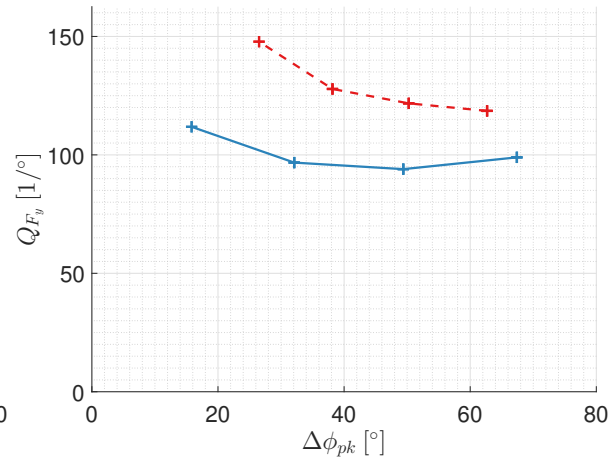
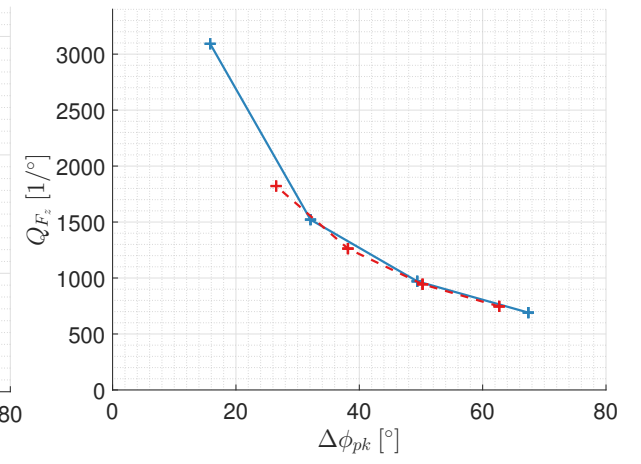
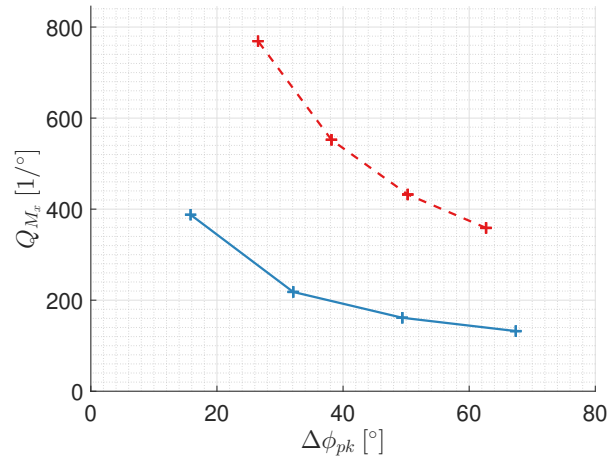
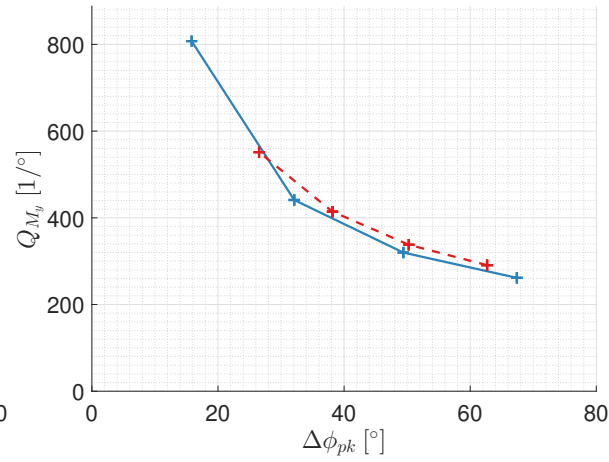
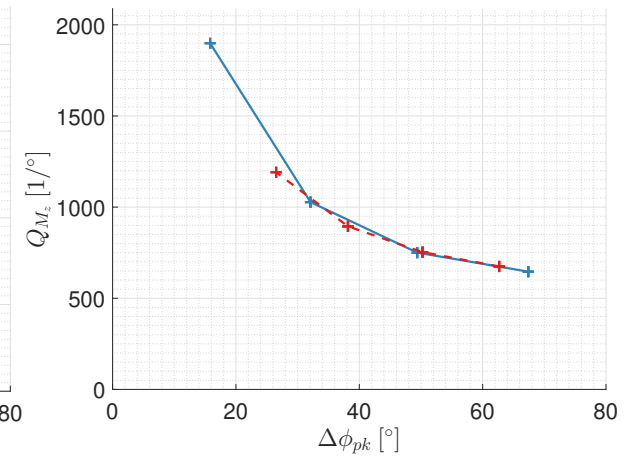


Figure D.98: M_z quickness roll-in

Figure D.99: F_x quickness roll-outFigure D.100: F_y quickness roll-outFigure D.101: F_z quickness roll-outFigure D.102: M_x quickness roll-outFigure D.103: M_y quickness roll-outFigure D.104: M_z quickness roll-out

D.5. Suboptimal Cruise Condition Responses and Loads During Roll Doublet

A suboptimal cruise setting was introduced to simulate a realistic compound helicopter trim condition. The main rotor rpm is lowered to 80% of its nominal value, 5000 N of compound thrust is added and a constant 3° roll right aileron deflection is applied.

A roll right doublet is flown at 120 kts, varying all three control strategies: either a pure lateral input, pure aileron input or a 50% cyclic - 50% aileron input. The trim condition is summarised in Table 6.2. This section presents a complete overview of the attitude quickness, vehicle attitude, flap angles, loads and load quickness during the roll doublet.

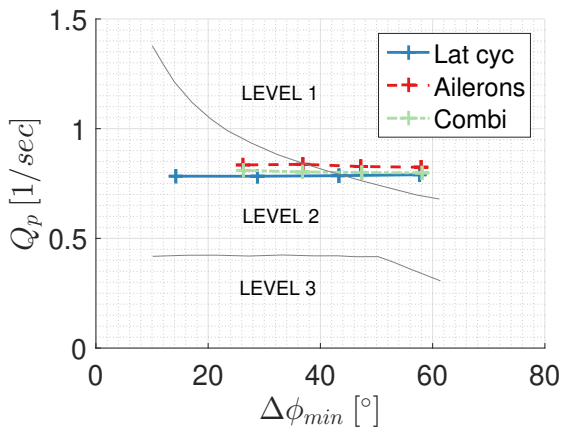


Figure D.105: Attitude quickness roll-in

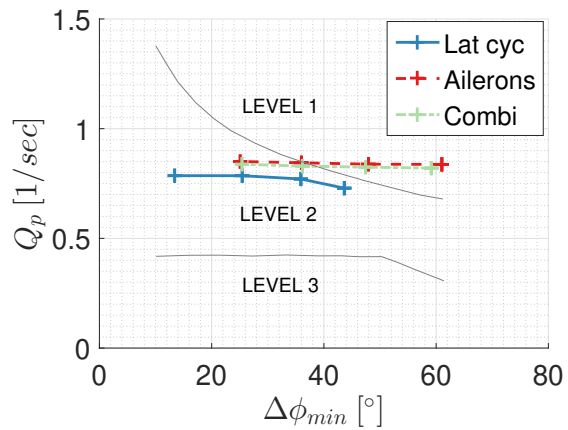
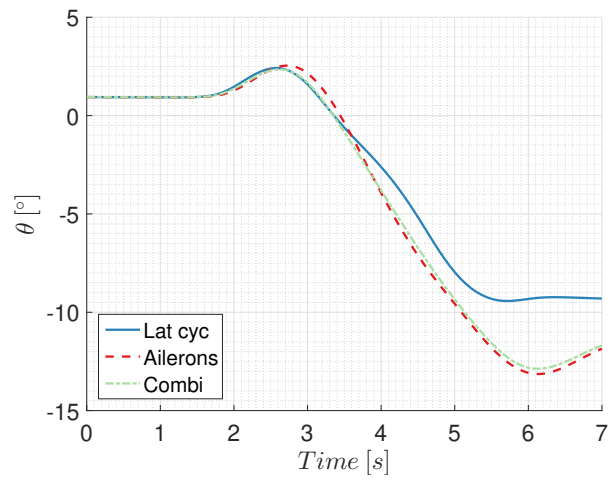
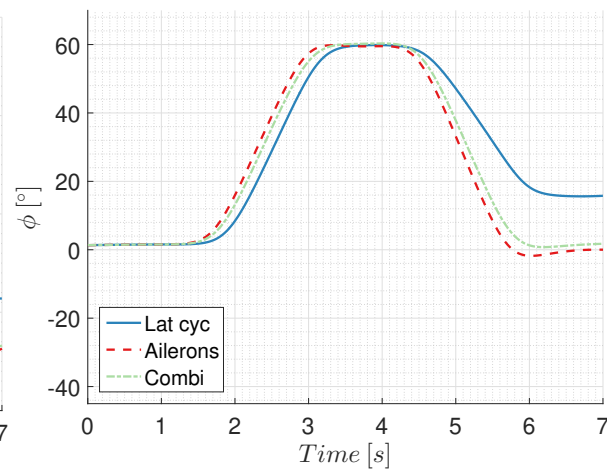
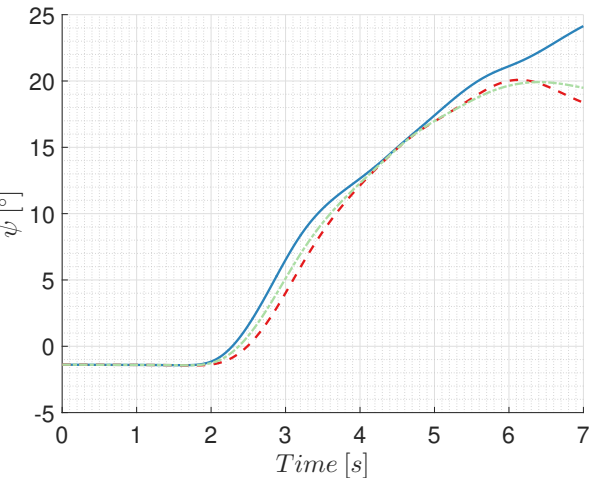
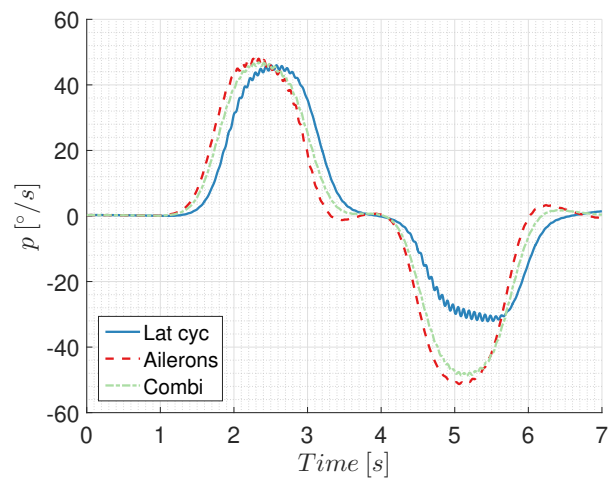
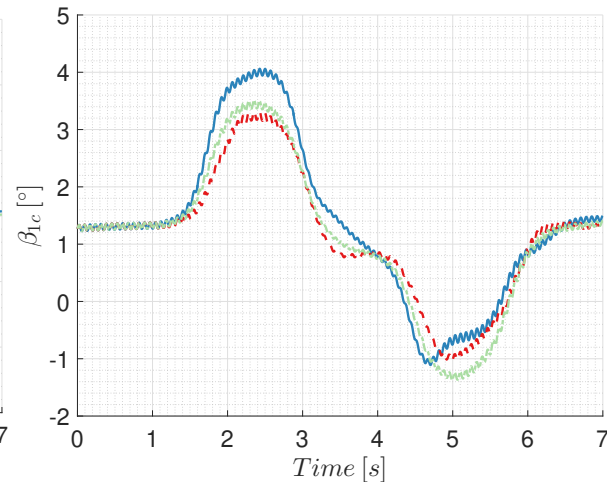
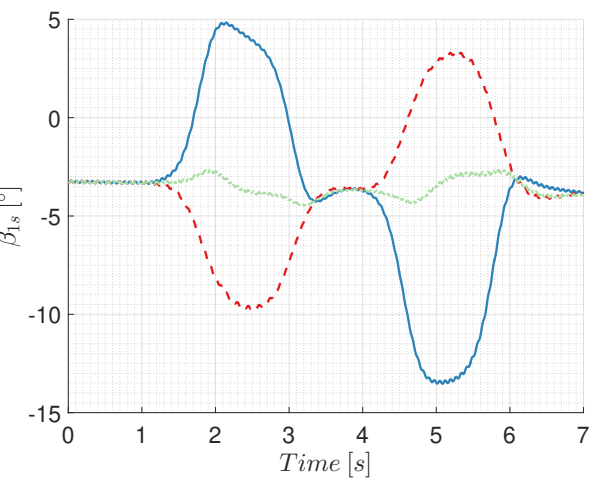


Figure D.106: Attitude quickness roll-out

Figure D.107: θ response, 50% cyclic - 50% aileronsFigure D.108: ϕ response, 50% cyclic - 50% aileronsFigure D.109: ψ response, 50% cyclic - 50% aileronsFigure D.110: p response, 50% cyclic - 50% aileronsFigure D.111: β_{1c} response, 50% cyclic - 50% aileronsFigure D.112: β_{1s} response, 50% cyclic - 50% ailerons

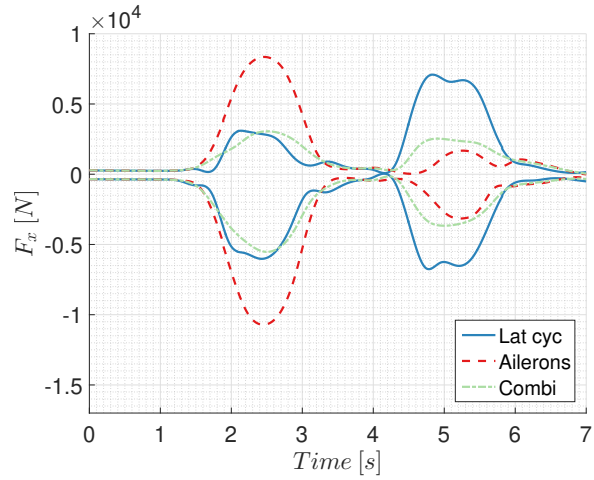


Figure D.113: F_x response, 50% cyclic - 50% ailerons

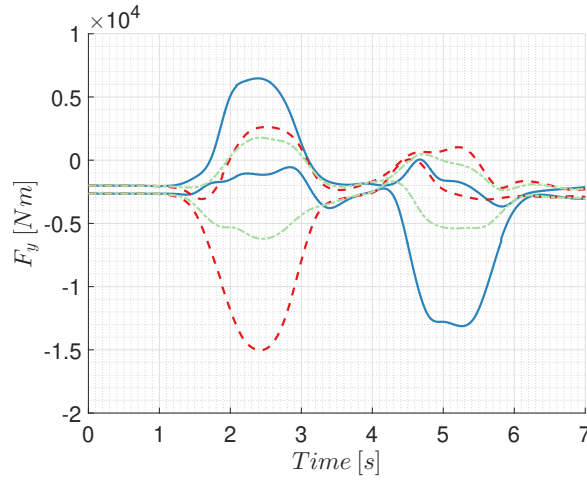


Figure D.114: F_y response, 50% cyclic - 50% ailerons

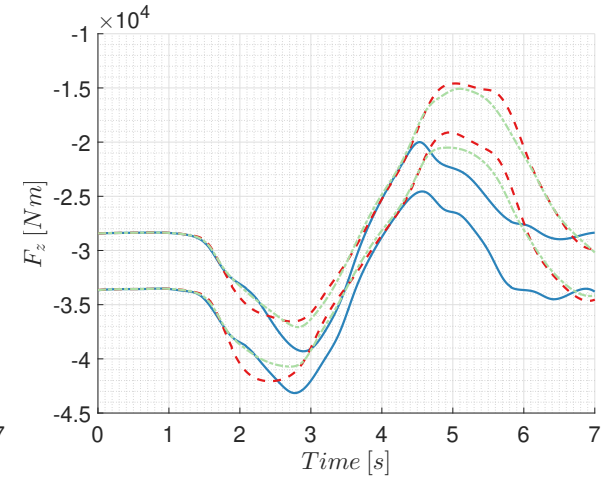


Figure D.115: F_z response, 50% cyclic - 50% ailerons

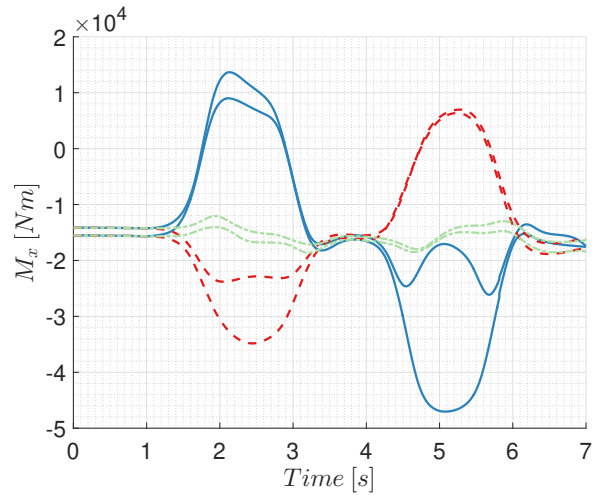


Figure D.116: M_x response, 50% cyclic - 50% ailerons

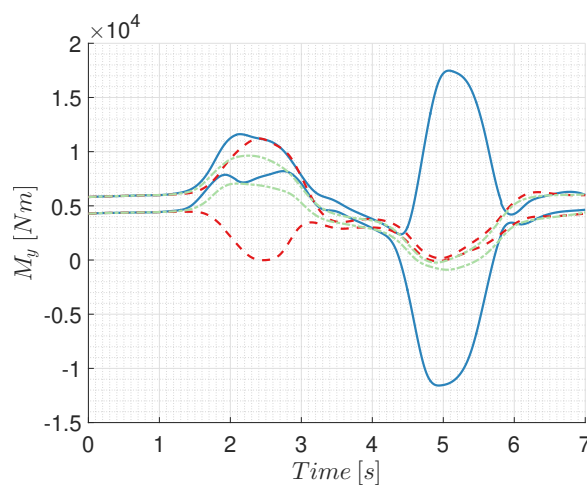


Figure D.117: M_y response, 50% cyclic - 50% ailerons

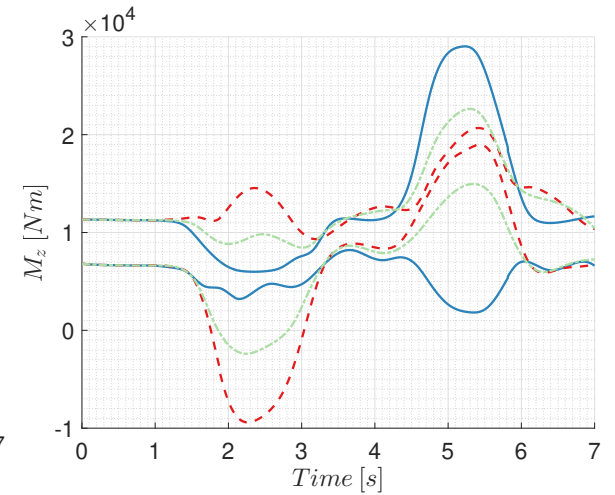


Figure D.118: M_z response, 50% cyclic - 50% ailerons

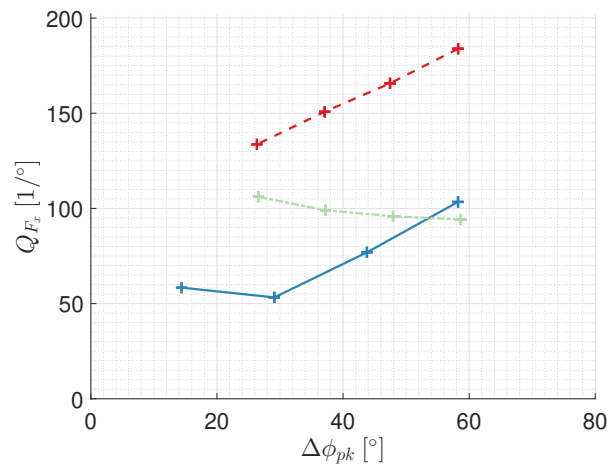


Figure D.119: F_x quickness roll-in

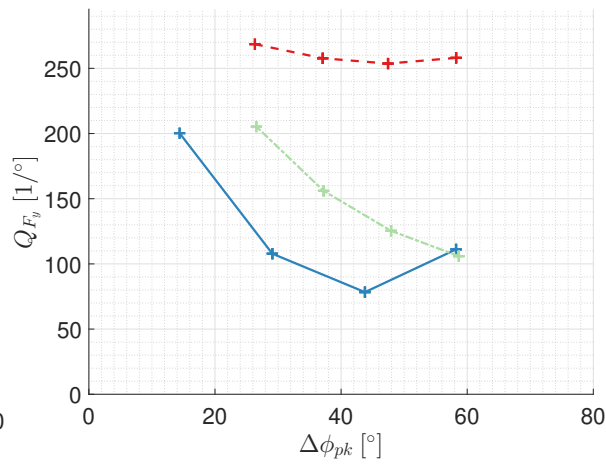


Figure D.120: F_y quickness roll-in

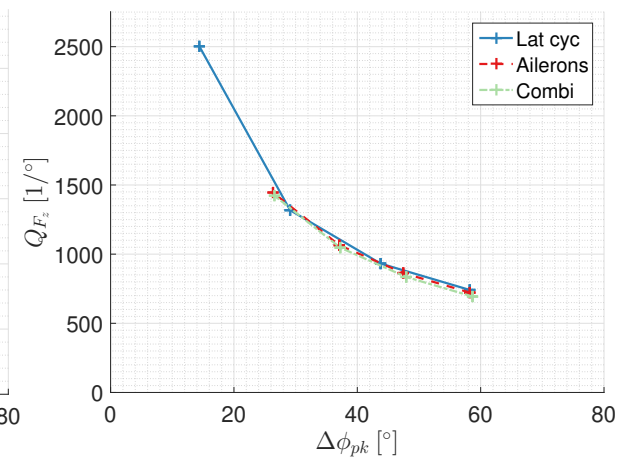


Figure D.121: F_z quickness roll-in

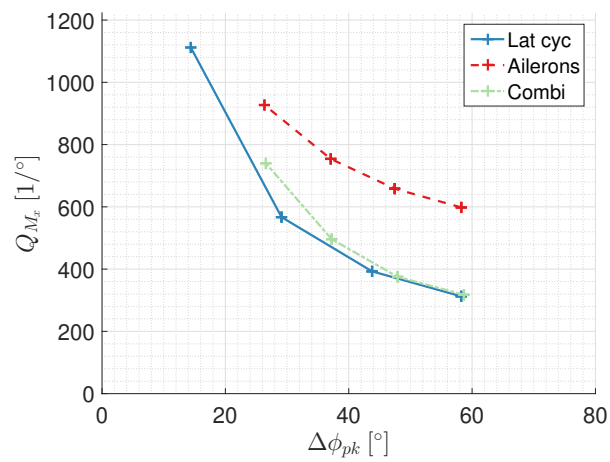


Figure D.122: M_x quickness roll-in

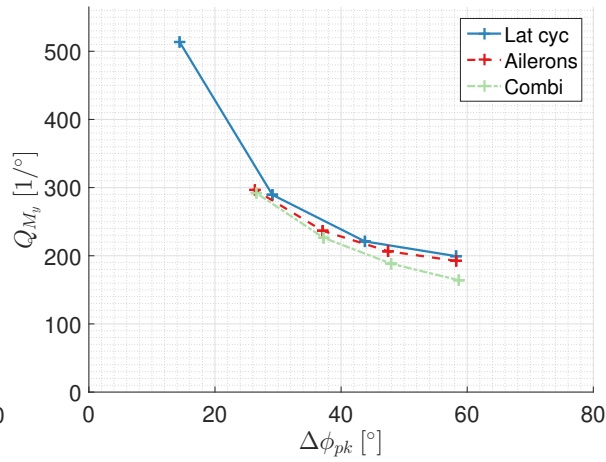


Figure D.123: M_y quickness roll-in

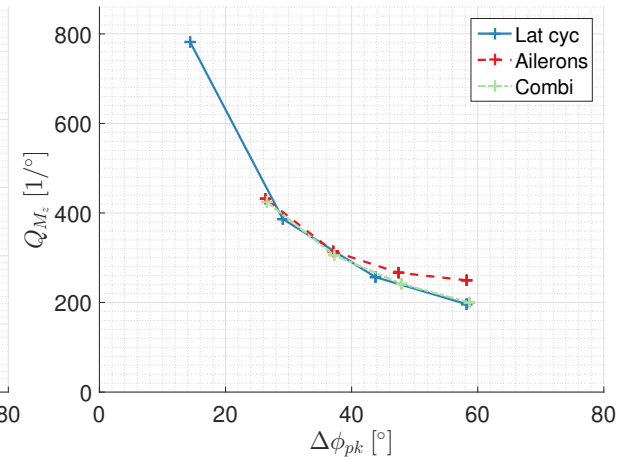


Figure D.124: M_z quickness roll-in

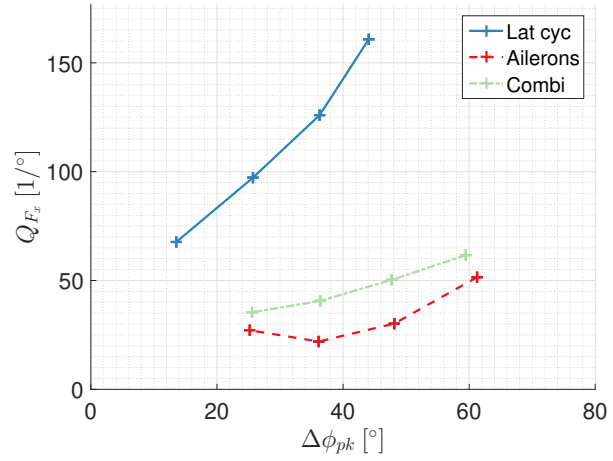


Figure D.125: F_x quickness roll-out

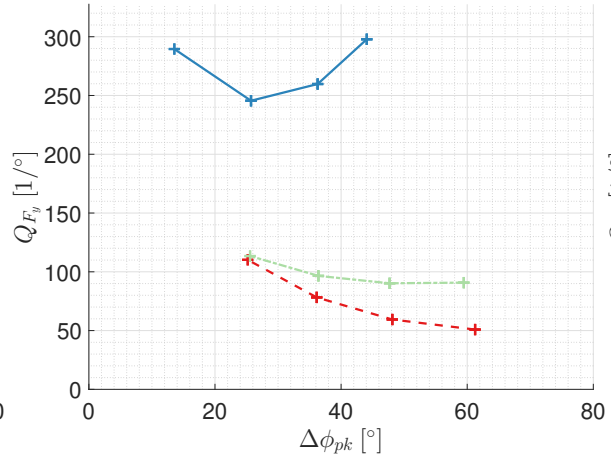


Figure D.126: F_y quickness roll-out

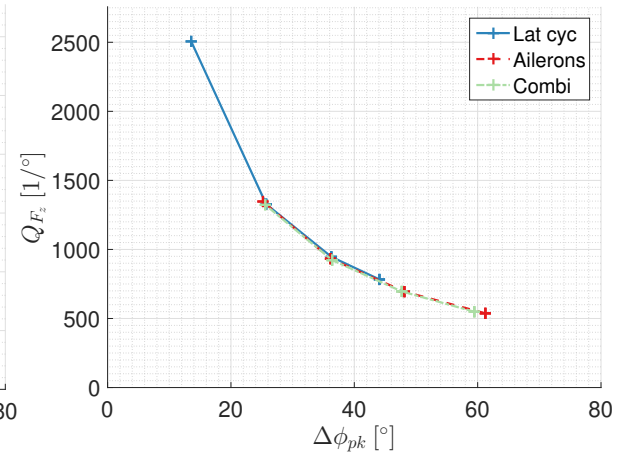


Figure D.127: F_z quickness roll-out

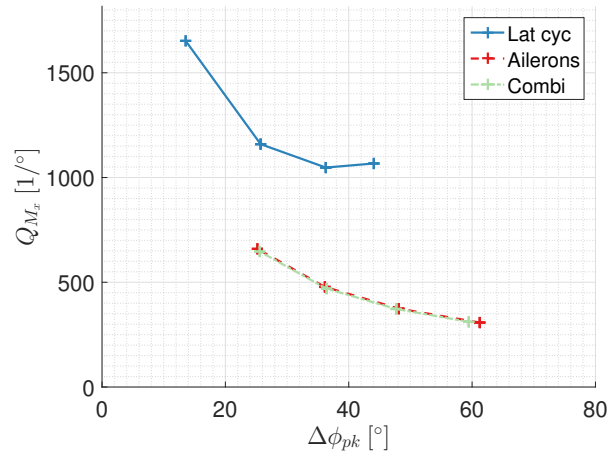


Figure D.128: M_x quickness roll-out

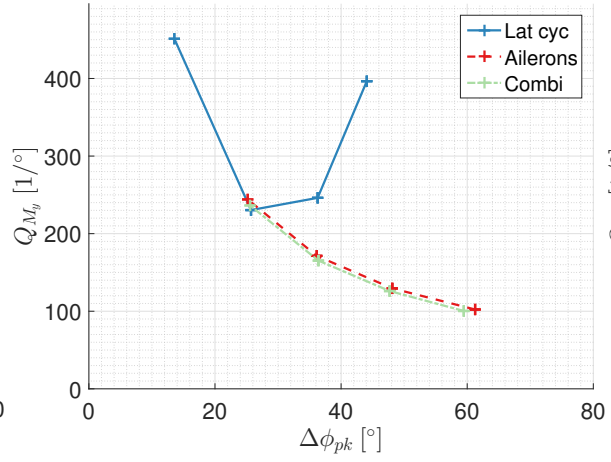


Figure D.129: M_y quickness roll-out

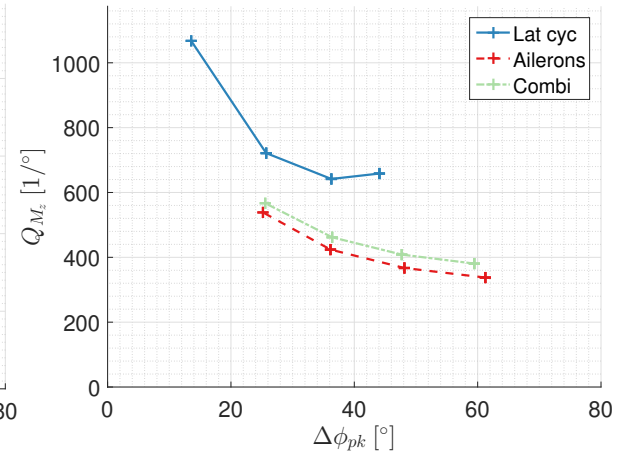


Figure D.130: M_z quickness roll-out

Bibliography

- [1] Airbus Racer, Airbus Website. URL <https://www.airbus.com/newsroom/stories/Racer-for-the-layman.html>. Accessed: 2019-11-3.
- [2] Airbus X³, Airbus Website. URL <https://www.Airbus.com>. Accessed: 2018-10-5.
- [3] Bell 360 Invictus, Bell Website. URL <https://www.bellflight.com/products/bell-360>. Accessed: 2019-11-3.
- [4] Boeing Future Vertical Lift, Boeing Website. URL <https://www.boeing.com/defense/future-vertical-lift/index.page>. Accessed: 2019-11-3.
- [5] Sikorsky X2, Lockheed Martin Website. URL <https://www.lockheedmartin.com>. Accessed: 2018-10-5.
- [6] John D Anderson. *Fundamentals of Aerodynamics*, volume 1. McGraw-Hill, New York, 5th editio edition, 2015.
- [7] Army Headquarters Department of the Army. Operator's Manual for UH-60A, UH-60L, EH-60A Helicopter. Technical report, 1996.
- [8] United States Army Aviation and Missile Command. Aeronautical Design Standard Performance Specification Handling Qualities Requirements for Military Rotorcraft. Technical report, 2000.
- [9] Jr Bailey, F J. A simplified theoretical method of determining the characteristics of a lifting rotor in forward flight. Technical report, National Advisory Committee for Aeronautics. Langley Aeronautical Lab.; Langley Field, VA, United States, 1941.
- [10] Kenneth A. Bordignon. *Constrained Control Allocation for Systems with Redundant Control Effectors*. PhD thesis, Virginia Polytechnic Institue and State University, Blacksburg, Virginia, 1996.
- [11] William G Bousman and Robert M Kufeld. UH-60A Airloads Catalog. Technical report, NASA, Moffett Field, 2005.
- [12] Roy L Brewer, Fort Worth, Joseph F Horn, L T C Carl R Ott, Ridley Park, Cody E Fegely, Paul D Ruckel, Fort Worth, Sean P Pitoniak, Ridley Park, William C Fell, West Palm Beach, James M Rigsby, Fort Worth, and P Chase Schulze. Further Development and Piloted Simulation Evaluation of the Break Turn ADS-33 Mission Task Element. *AHS International 74th Annual Forum & Technology Display*, pages 1–12, 2018.
- [13] B Bruchem. Helicopter drive train modelling for manoeuvre load alleviation. Technical report, Delft University of Technology, Delft, 2017.
- [14] Robert T N Chen. A survey of nonuniform inflow models for rotorcraft flight dynamics and control applications. *15th European Rotorcraft Forum*, pages 64–1 to 64–62, 1989.
- [15] Frank Colucci. SpeedHawk—Phase I. *Vertiflite*, 2007.
- [16] A. Datta and I. Chopra. Validation and Understanding of UH-60A Vibratory Loads in Steady Level Flight. *Journal of the American Helicopter Society*, 49(3):271–287, 2004.
- [17] A. Datta, T. R Norman, and H. Yeo. Experimental Investigation and Fundamental Understanding of a Slowed UH-60A Rotor at High Advance Ratios. *American Helicopter Society 66th Annual Forum*, 2011.
- [18] Mark E. Dreier. *Introduction to Helicopter and Tiltrotor Flight Simulation*. AIAA, Arlington, Texas, 2007.
- [19] Federal Aviation Administration (FAA). Special Conditions: Boeing 747-8/8F Airplanes, Interaction of Systems and Structures - 14 CFR Part 25 [Docket No. NM400; Special Conditions No. 25–388A–SC], 2011.

- [20] B. Geldberg, B. N. Meyers, and L.V Tempkins. 16H-1A Flight Test Research Program. Technical report, U.S. Army Aviation Materiel Laboratories for Eustis Virginia, Philadelphia.
- [21] Kurt Gtzfried. Survey of Tiger Main Rotor Loads from Design to Flight Test. *23rd European Rotorcraft Forum*, sep 1997.
- [22] Mario Hamers and Pierre-Marie Basset. Application of the Finite State Unsteady Wake Model in Helicopter Flight Dynamic Simulation. *26th European Rotorcraft Forum*, (September):27–1:16, 2000.
- [23] Kathryn B. Hilbert. A Mathematical Model of the UH-60 Helicopter. Technical report, NASA, Moffett Field.
- [24] Mike Hirschberg. JMR Technology Demonstration Update: The Road to Future Vertical Lift. *Journal of the AHS*, (Vol. 62, No. 1):22–27, 2016.
- [25] Joe Horn, Anthony J. Calise, and J. V. R. Prasad. Flight Envelope Limit Detection and Avoidance for Rotorcraft. *Journal of the American Helicopter Society*, 47(4):253, 2002.
- [26] Joseph F. Horn and Nilesh Sahani. Detection and Avoidance of Main Rotor Hub Moment Limits on Rotorcraft. *Journal of Aircraft*, 41(2):372–379, 2004.
- [27] J.J. Howlett. UH-60A Black Hawk Engineering Simulation Program: Volume I - Mathematical Model. Technical report, Sikorsky Aircraft, Stratford, 1981.
- [28] I. Chopra and A. Datta. *Helicopter Dynamics*. snu open courseware ENAE 633, 2011.
- [29] Leishman J.G. *Principles of Helicopter Aerodynamics*. Cambridge University Press, Cambridge, second edition, 2006.
- [30] J. N. Johnson. Attack Helicopter Evaluation AH-56A Cheyenne Compound Helicopter. Technical Report June, National Technical Information Service, Springfield, 1972.
- [31] Robert M. Kufeld and William G. Bousman. High Load Conditions Measured on a UH-60A in Maneuvering Flight. *Journal of the American Helicopter Society*, 43(3):202–211, 1998.
- [32] H. Youngren M. Drela. AVL, Extended Vortex Lattice Model, . URL <http://web.mit.edu/drela/Public/web/avl/>. Accessed: 2019-10-5.
- [33] H. Youngren M. Drela. XFOIL, Subsonic Airfoil Development System, . URL <https://web.mit.edu/drela/Public/web/xfoil/>. Accessed: 2019-10-5.
- [34] U.S Department of Defense. Flying Qualities of Piloted Aircraft - MIL-STD-1797B Notice 1. Technical report, 2012.
- [35] R. A. Ormiston. Realizing the Potential of the Compound Helicopter. *Journal of the AHS*, 2016.
- [36] G. D. Padfield. *Helicopter Flight Dynamics : the theory and application of flying qualities and simulation modelling. – 2nd ed.* Blackwell, Washington DC, second edition, 2007.
- [37] Marilena D. Pavel and Gareth D. Padfield. The Extension of ADS-33—Metrics for Agility Enhancement and Structural Load Alleviation. *Journal of the American Helicopter Society*, 51(4):319, 2006.
- [38] David A. Peters, David Doug Boyd, and Cheng Jian He. Finite-state induced-flow model for rotors in hover and forward flight. *Journal of the American Helicopter Society*, 34(4):5–17, 1989.
- [39] W. F. Phillips and D. O. Snyder. Modern adaptation of Prandtl’s classic lifting-line theory. *Journal of Aircraft*, 37(4):662–670, 2000.
- [40] Ray Prouty. *Helicopter Aerodynamics Volume I*. I Eagle Eye Solutions, 2009 edition.
- [41] J. Cross K. Studebaker C. Jennison R. Kufeld, D. Balough and W. Bousman. Flight Testing the UH-60A Airloads Aircraft. page pages 557–577, 2007.

- [42] Jean-Paul Reddinger and Farhan Gandhi. Physics-Based Trim Optimization of an Articulated Slowed-Rotor Compound Helicopter in High-Speed Flight. *Journal of Aircraft*, 52(6):1756–1766, 2015.
- [43] Jean-Paul Reddinger, Farhan Gandhi, and Hao Kang. Using Control Redundancy for Power and Vibration Reduction on a Compound Helicopter at High Speeds. *Journal of the American Helicopter Society*, 63(3): 1–13, 2018.
- [44] Umberto Saetti and Joseph F Horn. Load Alleviation Control Design Using Harmonic Decomposition Models, Rotor State Feedback, and Redundant Control Effectors. *AHS International 74th Annual Forum & Technology Display*, (May), 2018.
- [45] Martin K. Sekula and Farhan Gandhi. Effects of Auxiliary Lift and Propulsion on Helicopter Vibration Reduction and Trim. *Journal of Aircraft*, 41(3):645–656, 2004.
- [46] P W Theriault and D. R. Segner. XH-51A Compound Helicopter Design and Development. *AIAA/RAeS/JSASS Aircraft Design and Technology Meeting*, 1965.
- [47] Adam Thorsen. Assessment of Control Allocation Optimization on Performance and Dynamic Enhancement of a Compound Rotorcraft. Technical report, Pennsylvania State University, 2014.
- [48] Adam Thorsen. A Unified Flight Control Methodology for a Compound Rotorcraft in Fundamental Aerobic Maneuvering Flight. Technical report, Pennsylvania State University, 2016.
- [49] Mario Verhagen. Feasibility Study of a Novel Load Alleviation System on the UH-60A Blackhawk Helicopter. Technical report, Delft University of Technology, 2015.
- [50] Mark Voskuil and Mario R. Verhagen. Helicopter Main Rotor Hub Load Alleviation Using a Variable Incidence Horizontal Stabilizer. *Journal of the American Helicopter Society*, 63, 2018.
- [51] Mark Voskuil, B. Manimala, D. J. Walker, and R. Kureemun. First steps towards the design of an Active Pitch Link Loads Reduction system using novel control techniques. *31st European Rotorcraft Forum*, pages 76.1–76.15, 2005.
- [52] Mark Voskuil, D. J. Walker, and B. J. Manimala. Helicopter load alleviation using active control. *Aeronautical Journal*, 112:663–672, 2008.
- [53] Daniel J. Walker, Binoy J. Manimala, Mark Voskuil, and Arthur W. Gubbels. Multivariable Control of the Bell 412 Helicopter. *Proceedings of the 45th IEEE Conference on Decision and Control*, pages 1527–1532, 2006.
- [54] Hyeonsoo Yeo and Wayne Johnson. Prediction of Rotor Structural Loads with Comprehensive Analysis. *Journal of the American Helicopter Society*, 53(2):193–209, 2008.
- [55] Hyeonsoo Yeo, William G. Bousman, and Wayne Johnson. Performance Analysis of a Utility Helicopter with Standard and Advanced Rotors. *Journal of the American Helicopter Society*, 49(3):250–270, 2004.